Processing and Sintering of Carbonate Hydroxyapatite

Jake Barralet

A Thesis Submitted for the Degree of Doctor of Philosophy

QUEEN MARY AND WESTFIELD COLLEGE

UNIVERSITY OF LONDON

JANUARY 1995

PAGE NUMBERS ARE CUT OFF IN THE ORIGINAL

TO
MUM & DAD

"Sweet is the lore which Nature brings;
Our meddling intellect
Mis-shapes the beauteous form of things
We murder to dissect."
William Wordsworth, "The Tables Turned," 1798.

ABSTRACT

Since the early 1970's there have been a number of investigations into the preparation of dense sintered hydroxyapatite for medical applications. However, there have been few studies reporting the production of sintered carbonate apatite, which resembles more closely the composition of human bone mineral.

This work has studied the precipitation, processing and sintering of carbonate apatites. Crystallisation variables such as temperature and bicarbonate ion concentration have been investigated in order to determine some effects on the size, morphology and composition of carbonate apatite precipitates. By employing the correct conditions, nanoscale precipitates have been produced that have enabled the use of a colloidal filtration route in processing. The effect of sintering atmosphere, green density, and carbonate content were investigated isochronally over a range of temperatures. Isothermal experiments demonstrated the evolution of microstructure and changes in density with time.

Results from this study indicated that translucent 99.9% relative density carbonated hydroxyapatite could be produced by sintering in an atmosphere of carbon dioxide and water. Water was found to enhance densification in carbon dioxide furnace atmospheres. The temperature at which maximum densification occurred decreased with carbonate content. Bloating was found to be related to carbonate content as larger expansions were observed in higher carbonate content materials. The partial pressure of water did not effect the composition of the carbonate apatite, whereas the green composition did, contrary to the findings of other workers.

Acknowledgements

The author gratefully acknowledges the invaluable help, support and enthusiastic supervision of Prof. W. Bonfield and Dr. S. Best.

For their technical assistance the author wishes to acknowledge the following:

Dr. S. Puajindanetr for his kind help and guidance when at the beginning of my project, Mr. S. Adams for his assistance with analysis and problem solving, Dr. J. Knowles for his X-Ray Diffraction expertise and help, Dr. I. Abrahams for his refinements and suggestions, Mr. K. Shrapel also for his X-Ray assistance, Prof. C. Davies for his time and sintering advice, Dr. R. Stevens for his sintering and thermodynamic contributions, Mr. A. Murphy for his quality chemical analysis, Dr. M. Reece for TEM, ceramic and safety assistance, Dr. R Crookes for gas equilibrium advice, Dr. I. Rehman for his FTIR collaboration, Mr. R Whitenstall, Mr. M. Willis, Dr. Z. Lu klinska, Mr. J. Manston and Mr. K. Pell for all the superb microscopy and photographic advice and help, Dr. D. Bader for his orthopaedic, linguistic and numeric guidance, Dr. K. Tanner for her kind help and proof reading, Mrs. N. Mo for image analysis, Mr. C. Langdown for his design assistance, Mr. J. Cowley for his glass blowing skill and honey, Dr. J. Elliott, Dr. P. Marquis and Prof. H. Aoki for their apatite wisdom, Dr. F. Mahmud for his scientific support, Miss J. Hemmings micrometer, Dr. P. Tetlow for teaching me ceramics, Mrs. Y. Johnson for her expert risk analysis, Mrs S. Wells, Miss C. Belsham and Miss J. Spanton for their secretarial assistance, all the library staff especially Ms K. Abbottand Miss S. Richards, Mr. M. German typing help, Dr. S. Downes for her cell culture expertise and help, Mrs C. King, Mr. D. Bacon and Mr. R. Crundwell for their photographic assistance, Mr. K. Critoph for his electrical support, Mr. A. Bradshaw for his advice and co-operation and my sincere apologies to those I may have omitted.

For their friendship and support the author wishes to acknowledge the following:

Mr. M. Kelay, Mr. S. Nazhat, Mr. K. Whalley, Mr. M. German, Dr. Y. Tanabe, Mr. A. Cronin, Mr. D. Oddy, Mr. H. Forster, Mr. S. Simner, Dr. A. Yoosefinejad, Miss. D. Balderson, Mr J. Shaw, Dr. A. Ahmadnia, Mr. K. Akutagawa, Miss. A. Bagnall, Mr. P. Zhenpeng, Dr. K. Hemachandra, Mr. R. Alkalay, Mr. G. Blugan, Mr. V. Chohan, Mr. F. Bollet, Mr. A. Steed, Mr. J. Suwanprateeb, Mr. P. Girardin, Mr. M. Puccioni, Mr. and Mrs. Byrne, Mr. C. Myers, Mr. J. Parkinson, my Parents and all others who helped in any way, with special thanks to Miss. J. Hemmings for her patience.

Finally the author gratefully acknowledges the financial support of the S.E.R.C., the now E.P.S.R.C.

Contents

List of Figures

List of Tables

1 Introduction

Hydroxyapatite is used clinically in granular, porous and dense forms and more recently as a plasma sprayed coating on hip prostheses. Dense apatite is used as a spacer in orthopaedic applications, (Shinjo *et al.*, 1989), middle ear reconstruction (Feenstra and de Groot, 1983), or as an artificial trachea, blood vessel and as a percutaneous device, (Aoki, 1994). Hydroxyapatite's mechanical properties are not dissimilar to soda glass and so it is not used in load bearing applications. Carbonate hydroxyapatite is more similar in composition to bone mineral than hydroxyapatite.

Carbonate apatite has increased acid solubility (LeGeros and Tung, 1983) and lower sintering temperatures than hydroxyapatite, it could be expected that carbonate apatite would be resorbable *in vivo* under the action of acidic enzyme secreted by osteoclasts, but not generally soluble as is tricalcium phosphate. Carbonate apatite may therefore be a new class of "smart" biomaterial which dissolves only in response to the bone remodelling/healing process and remains intact and bonded to the interface in regions free of osteoclastic action.

There are few reports on the sintering behaviour of carbonate hydroxyapatite, possibly the first was that of Ellies *et al.* (1988), although this work was a qualitative treatment, these workers noted the effect of 'sintering temperature' being reduced with increasing carbonate content. The next report would appear to have been that of Doi *et al.* (1993). These workers also concluded that carbonate lowered the sintering temperature and put forward the proposal that this was due to a decrease in particle size. Not long after (Suwa *et al.*, 1993) compared the sintering behaviour of sodium containing and sodium free carbonate apatites. They reported that sodium containing apatites attained a higher bulk density than sodium free apatite at a given sintering temperature. The improvement in sintering behaviour for the sodium containing apatites is attributed to the formation of $NaCaPO_4$, which they suggested formed a liquid phase during sintering.

There have been a considerable number of investigations into the sintering behaviour of hydroxyapatite. The bulk of the work on carbonate apatite concerned the dissolution behaviour of dental enamel. However there have been few studies concerning the sintering and in *vivo* and *in vitro* behaviour of carbonate apatite despite its composition being close to bone mineral. Many *in vivo* and *in vitro* studies of biomaterials suffer from trying to draw comparisons between inadequately characterised materials. It is therefore essential to establish methods for the reproducible production of carbonate apatite of known carbonate content, density and grain and pore size, before biological evaluation is attempted.

2 Bone And Bioceramics

Since De Jong's (1926) early X-ray investigations demonstrated the presence of an apatite-like phase in bone and tooth, much work has been conducted on hydroxyapatite in attempts to produce a bone mineral analogue. The science of bone is vast and what follows is a brief outline.

The human skeleton primarily serves the function of supporting soft tissue. It is divided into jointed segments, to provide the flexibility required for movement. Only the vault of the skull and the ribs have a predominantly protective function. The bones also form a mineral reservoir for calcium and phosphorus ions. The morphological properties of bone have been studied on macroscopic, (visible with the naked eye), microscopic, (visible under the light microscope), and ultra structural levels, (<10μm) as defined by Thomson (1942).

Bone is a living tissue that is constantly remodelled as a result of forces exerted on it (Spengler *et al.*, 1983). In addition, metabolic genetic and nutritional factors are active in influencing variations in bone from individual to individual. However it is essentially a fibre reinforced ceramic composite with properties that vary with function.

2.1 Ultrastructure

The main ultrastructural components of bone are the mineral phase and collagen (70 wt% and 19 wt%), the two other phases are ground substance and water (8 wt% and 2 wt%), for bovine cortical bone, (Eastoe and Eastoe, 1954). These ultrastructural constituents are considered at in more detail in the following sections.

2.1.1 Collagen

Collagen is the protein constituent of bone. Three coiled collagen molecules wind together to form a tropocollagen triple helix which is 300 nm long, 1.5 nm wide. These units pack together to form a collagen fibril. The longitudinal organisation gives rise to a regular 68nm D staggered arrangement as shown in Figure 2.1. There is a 35nm separation between adjacent ends. The D period of the fibril has a densely packed 0.4 D region and a gap region 0.6 D, (Hodge and Petruska, 1963).

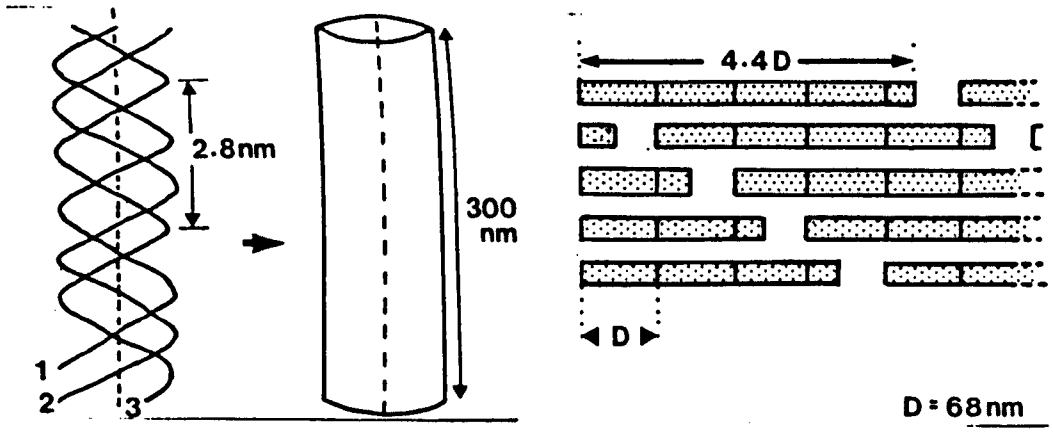

Figure 2.1. Helical arrangement of the tropocollagen molecules in the fibril and the staggered arrangement of the fibrils, after Hodge and Petruska (1963).

Collagen Mineral Relationship

The systems controlling the behaviour of bone cells is complex and has yet to be resolved. Prior to 1953 calcification was thought to involve simply precipitation dynamics and it was thought that the ionic product of Ca^{2+}, PO_4^{3-} and OH in the body fluid was below that required for saturation. However, (Neuman and Neuman, 1953) proposed the theory of epitactic nucleation whereby a nucleus is formed that mimics the structure of apatite.

Bonucci (1967) claimed that the osteoblast provided the nucleation site by means of cellular extrusions which provided an epitaxial nucleation site. Aggregation of hydroxyapatite crystals leads to the formation of bone nodules, which coalesce with the association of collagen fibres. Subsequent investigations have shown that the first site of mineralisation in the epiphyseal

cartilage (Bonnucci, 1971) and mineralised tendon (Arsenault *et al.*, 1991) is the matrix vesicle (~250 nm in diameter) this is a membranous sac within the bone forming cells. The mineral then becomes extravesicular and spreads axially and laterally with the collagen fibres. It is thought (Arsenault *et al.*, 1991) that phosphoproteins and / or osteonectin act as secondary nucleators in the presence of apatite. Support for this theory comes from earlier work by Glimcher *et al.*, (1979) who found that these proteins are present in mineralised tissue but are absent in non mineralised portions. Hodge and Petruska (1963) proposed that bone mineral crystals are located in the gap region of the collagen fibril. However recent evidence shows the mineral crystals are found in a periodic distribution along the collagen fibril, not coinciding with the gaps as was suggested by Hodge and Petruska (1963), but corresponding to the position of hydrophobic groups, which were found to be non-favoured sites, giving rise to an asymmetric but periodic distribution along the fibril (Maitland and Arsenault, 1991). This may be a contributing factor in the distribution of mineral crystal sizes observed. Particle size measurements by Wiener and Price (1987), also indicate that it is impossible for a large proportion of crystals to fit into the gap region as they are too big.

2.1.2 Ground Substance

Ground substance contains glycosaminoglycans, glucoproteins, lipids (< 0.1%) and peptides (0.55% dry weight) Vaughan (1981). Glycosaminoglycans are known to be hydrophillic, and can cross link to act as ionic filters. They are believed to perform a regulatory role in the calcification process. *In vitro* studies by Blumenthal *et al.* (1979), showed them to have a strong inhibitory affect on the formation of hydroxyapatite. Lipids in the form of calcium phospholipid complexes are associated with the initiation of calcification. They are found in calcifying cells and matrix vesicles, in largest amounts where calcification is being initiated at fracture healing sites. Irving (1963) first realised the significance of phospholipids as essential chemical complexes for mineralisation. It is suggested that apatite formation is facilitated by calcium and phosphate ions in the correct orientation and proportion for crystal formation. This process is considered to be enzyme controlled.

2.1.3 Water

The water content of bone has been reported as 15 % (Aoki, 1991) and 8.2% Eastoe and Eastoe (1954). Some of this water is thought to form a hydration shell around the mineral crystals Neuman and Neuman (1969). It may form part of crystalline structures such as octacalcium phosphate, Brown *et al.* (1962). The mechanical properties of living bone require water and Currey (1988) has shown that the changes exhibited by dehydrated bone are largely reversed on re-hydration.

2.1.4 Bone Mineral

This section briefly reviews the size and morphology of bone mineral and the problems associated with measuring small crystals that are sensitive to separation procedures. The composition of bone mineral is considered and it is seen that of all the substituted ions only carbonate is present in substantial quantities.

Mineral Size and Morphology

There has been some debate as to the morphology of bone mineral. Robinson (1952) first suggested a tabular morphology, typically 10 x 25 x 50 μm in size and since then various morphologies have been suggested, rods, (Speckman and Norris, 1957), needles (Fernandez-Moran and Engsrom, 1957), ovoids (Molnar, 1960) and plates (Johansen and Parks, 1960). These conclusions have been drawn from TEM investigations. A current view (Hodgkinson, 1991) is that bone mineral is indeed tabular. Although apatite belongs to a hexagonal class of crystal and has an acicular habit, another calcium phosphate, octacalcium phosphate (OCP), has a tabular habit and can transform to hydroxyapatite of the same morphology. This suggests that OCP may be the precursor of biological apatite, as was proposed by Eanes (1980).

Bone mineral size and aggregation are known to be sensitive to sample preparation technique. Work by Weiner and Price (1986) confirmed the existence of tabular crystals and suggested that at least some of these crystals were aggregated into larger structures, possibly bound by collagen. Sodium hypochlorite and ultrasound were used to remove the organic

component. The crystals were then graded using differences in settling rates in either water or ethanol and measured by electron microscopy. They noted that crystals prepared in ethanol did not settle, whereas those prepared in the same manner except using water, did, suggesting a smaller crystal particle size when in ethanol. The fact that alcohol groups inhibit interparticulate hydrogen bonding has been successfully used to reduce agglomeration in the preparation of ceramic powders (Shi *et al.*, 1993). Weiner and Price (1986), found that 60% of the unaggregated mineral crystals in a femoral cortical bone specimen from a 67 year old man to be greater than 45nm in length. This would suggest that a significant amount of the mineral is not associated within the collagen fibril. Hodgkinson (1991) independently found that bone mineral in plate like in shape and has an average length of 100nm. He found a weak trend of the mineral crystal length increasing with age. Unfortunately only one sample per sex per age group was investigated, making it hard to draw any definite conclusions.

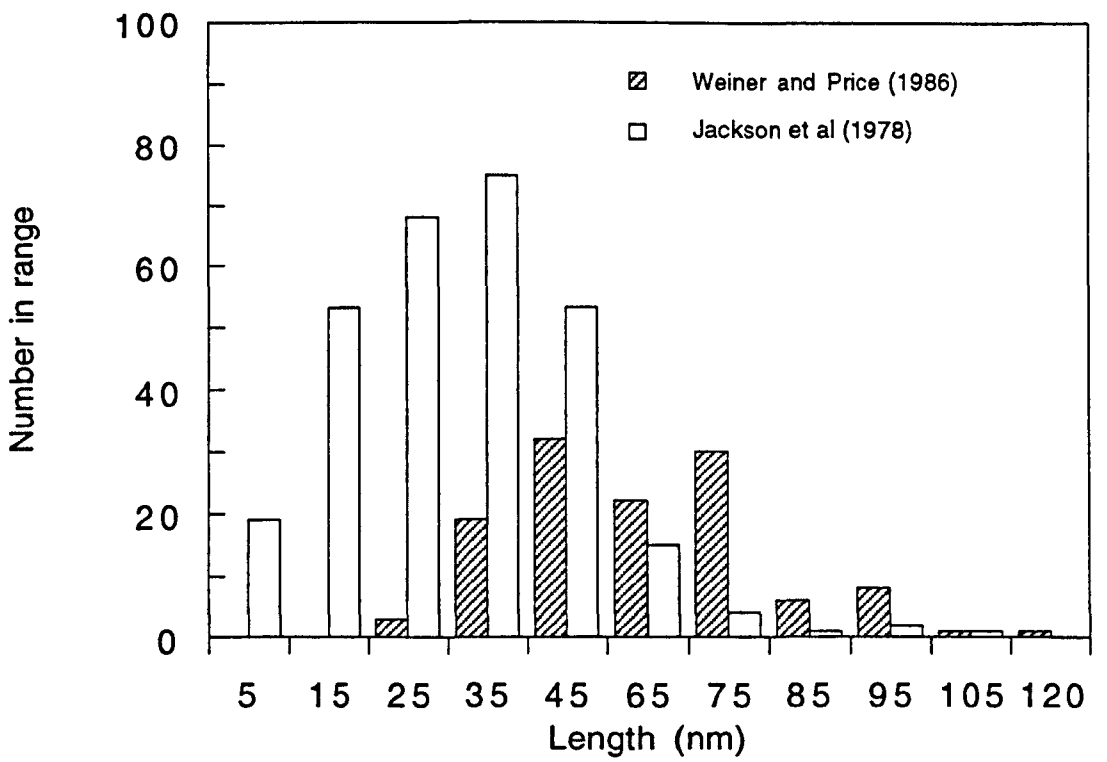

Figure 2.2. Crystal length distributions of mineral from male human femurs 65-67, by different techniques as reported by Jackson *et al.* (1978) and Weiner and Price (1986) .

Jackson *et al.* (1978) obtained a size distribution for the crystal lengths of a 65 year old male human femur by examination of thin sections of untreated bone. However these workers could only include isolated unagglomerated crystals in their measurements. Their measurements are compared with those obtained by Weiner and Price, (1986) in Figure 2.1. Both groups of workers found a similar upper limit of size, though Weiner and Price did not report any measurements in the 5-15nm range. This suggests that dissolution of small crystals may have occurred, however the precaution was taken of saturating all solutions used with respect to hydroxyapatite. A comparative study of size measurement techniques on the same bone sample would provide better information as to the superiority of a particular method.

Mineral Composition

The similarity between bone mineral and apatite was first noticed in X-ray diffraction patterns, (de Jong, 1926). Further investigations by LeGeros (1965) revealed a closer similarity to the patterns of carbonated apatites. Developing bone contains a large amount of an amorphous phase and this amount decreases on maturity to a level of not more than 10%, (Posner and Betts, 1975). Other phases are thought to exist in bone mineral, (Driessens, 1983), however evidence for these phases is based on chemical analysis. The most abundant mineral in human bone is apatite. Various ions are found in bone mineral, as shown in Table 2.1, and are thought to substitute into the crystal structure. It can be seen there is little variation in the reported values for the constituents of bone mineral. There is greater than 1wt% carbon which is thought to be present as carbonate giving values in excess of 5wt% carbonate. Bone mineral is a carbonate apatite that contains trace amounts of other ions associated with physiological fluids.

Table 2.1. Some reported weight percentages of elements found in bone mineral.

	Aoki (1991)	Driessens (1983)	Dallemange *et al.* (1966)	HA
			(bovine)	(Stoichiometric)
Ca	34	36.7	36.6	39.8
P	15	16.0	17.1	18.5
Mg	0.5	0.46	0.6	-
Na	0.8	0.77	1.0	-
K	0.2	-	0.07	-
C	1.6	1.60	1.31	-
Cl	0.2	-	0.1	-
F	0.08	0.04	0.1	-

2.2 Bone Microstructure

Two distinct forms of bone tissue exist in adults humans, namely primary and secondary bone. Primary bone is the first to be laid down in bone growth, for example the newly formed skeleton. During ageing bone is resorbed and reformed producing secondary bone.

2.2.1 Bone Cells

Although the main cells involved with bone formation, resorption and maintenance have been mentioned previously, their specific functions need to be discussed in further detail.

Osteoblasts

Osteoblasts are responsible for the synthesis of the organic constituents of bone, collagen and glycoproteins. They are located at bone surfaces and form a continuous layer. When active they are cuboid in morphology, but as their synthesising activity decreases they become flatter in shape. Osteoblasts possess cytoplasmic processes that bring them into contact with neighbouring cells. Extrusion of the synthesised proteins takes place at the cell surface in contact with the bone matrix. Mineralisation occurs primarily within membrane bound spheres (~0.1μm) known as matrix vesicles, which

are produced by the osteoblast. Within these vessels the first needle-like calcium phosphate crystallites appear. Thereafter mineralisation is thought to occur spontaneously outside the vesicle. Osteoblasts are found on the bone surfaces and are generally cuboid in morphology.

Osteoclasts

Osteoclasts are very large multinuclear (6-50 nuclei), cells. They are irregularly branched and vary in shape and thickness. Their function is bone resorption, during which portions of the cell are found to lie in enzymatically etched pits known as the resorption lacunae of Howship. A main feature of the cell is the ruffled border which acts as a high surface area interface for excretion of proteins and collagenolytic enzymes and for the absorption of decomposition products. Calcium containing crystals have been found in the folds of the ruffled border and in the vacuoles. Fragments of collagen have only been found in the ruffled border.

Osteocytes

Osteocytes are osteoblasts that have been enclosed in pockets of mineralised tissue formed when in their ex-osteoblast state, these pockets are called lacunae. The exact role of the osteocyte is unclear but is thought to be involved with lymphatic flow, take part in mineral homeostasis and respond to stresses within the bone. Within the canaliculi filamentous filopodial processes from adjacent cells are connected via gap junctions. This network provides a mechanism for the intercellular flow of ions and small molecules. Death of an osteocyte is followed by resorption of the surrounding matrix.

2.2.2 Primary Bone

Woven bone is a type of primary bone, microstructurally it appears amorphous, in this way it differs in appearance from other types of bone. It has low density due to the random packing of the collagen fibres. It is found in young bones but has normally disappeared by the age of four (Jaffe, 1929) as a result of the dynamic process whereby bone is constantly resorbed and reformed allowing changes in bone shape and structure. During growth, it is

found at the growth plate found at the end of long bones. In adults primary bone is found at healing fracture sites and in those suffering from certain diseases, e.g. osteosarcoma. It is its ability to form *de novo* that distinguishes it from other bone.

2.2.3 Secondary Bone

When bone is resorbed and replaced with new bone tissue, it is termed secondary bone. This resorption is effected by cells known as osteoclasts and the subsequent formation occurs through the action of osteoblasts, the resulting structure is a secondary osteon. A secondary osteon has a central vascular channel known as a Haversian canal. This is surrounded by a series of concentric lamellae that spiral the osteon and contain osteocytes arranged in a circular manner. The entire secondary osteon is 200-300μm in diameter and 2-3 mm in length in human bone. Secondary Haversian bone is distinguished by the presence of a cement line 1-5μm thick that separates the osteon from the other bone matrix.

Lamellar bone (primary or secondary) constitutes the majority of bone found within the body. It consists of sheets (lamellae) 3-7μm in width. These lamellae may be found as cylindrical structures making up the secondary osteons, or arranged circumferencially around the end- or periosteal surfaces as primary lamellar bone, (Figure 2.3). Haversian systems occupy ~50% of the cross sectional area of cortical bone. In long bones the Haversian systems run approximately parallel to the long axis of the bones, interconnected by oblique canals termed Volksmann's canals.

The Haversian canal contains three structures, blood vessels, nerves and bone cells. The vessels have the characteristics of capillaries, (Cooper *et al.*, 1966) and are generally paired within the canal, (Kelly and Peterson, 1963). These vessels are 15μm in diameter. They contain no smooth muscle and blood flow in them is thought to be controlled by pressures in the medullary cavity vessels. Nerves have been found to accompany 60% of Haversian vessels in adult humans (Sherman, 1963). The role of the nerves

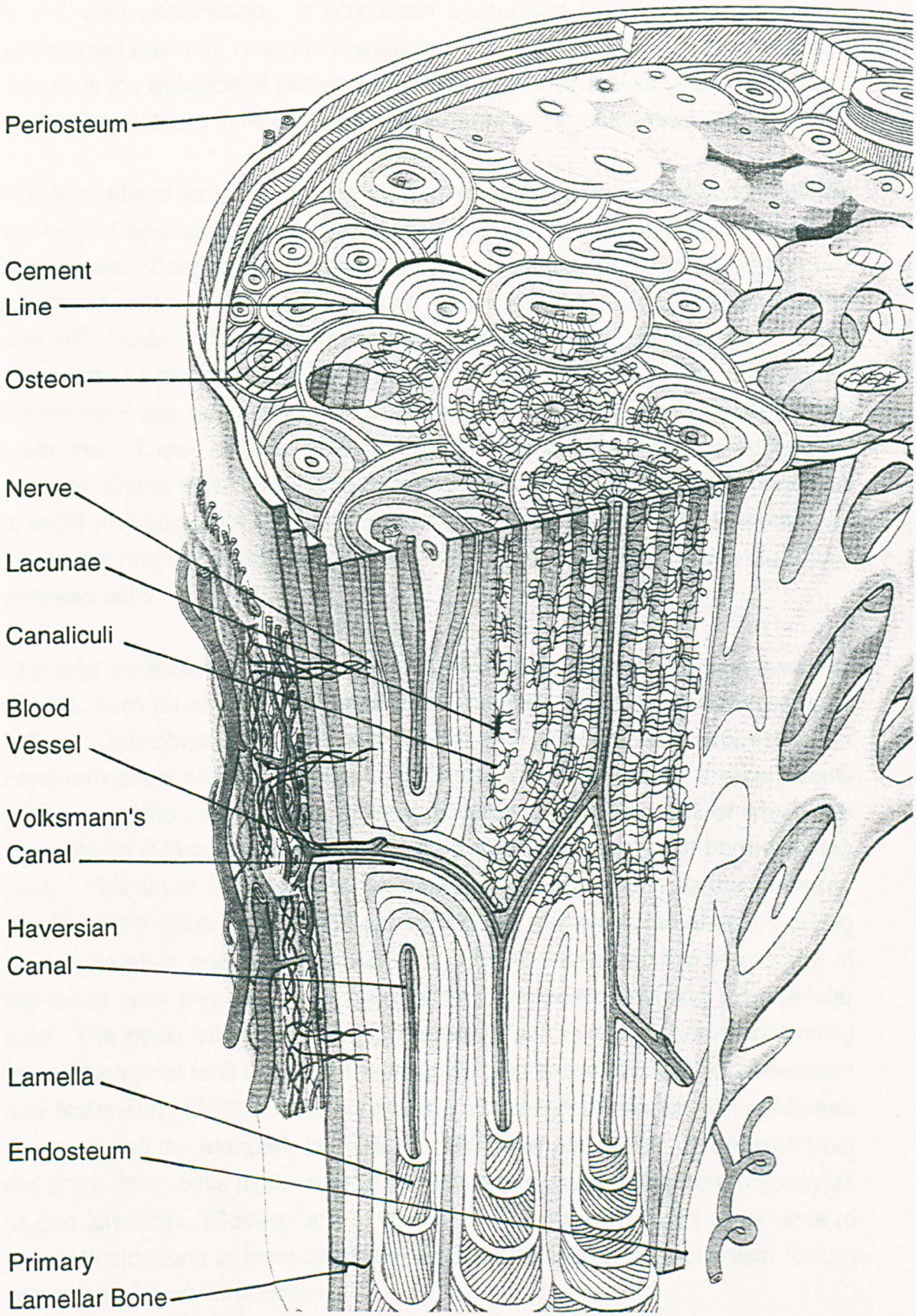

Figure 2.3. Schematic diagram showing the main structural features of bone. (Reproduced from Williams and Warwick, 1980)

is not well understood. It has been postulated that they may possess specialised pressure or stretch receptors, (Thompson, 1982), or that they can influence the diffusion of certain molecules from the vessels (Martin and Burr, 1989) though there is little evidence to confirm either of these ideas.

In the middle of lamellae or along the margins are found ovoid spaces called lacunae. Lacunae are usually occupied in life by a branched cells known as osteocytes. Connecting the lacunae and Haversian canal of an osteon are minute channels known as canaliculi. This system is filled by the osteocytes and with fluids. This system provides a massive surface area over which exchange of mineral ions can occur, (Robinson, 1964). The osteocytes themselves are connected by filamentous processes that connect at gap junctions. These connections can bridge the cement lines of secondary osteons (Curtis *et al.* 1985). Transportation of material through the canaliculi is rapid and suggests that the roles of the canaliculi are ones of metabolic, ionic and nutrient transport between the blood and extracellular fluid and between cells.

The area between the blood vessel and the canal wall may contain a variety of cells, such as osteoblasts in active and dormant states and undifferentiated cells. Osteoblasts have been found with cytoplasmic processes in communication with osteocytes in the mineralised matrix via the canaliculi. Adjacent to the canal wall is a layer of bone lining cells 10% of which are osteoblasts (Merz and Schenk, 1970) and provides a pool of bone forming cells. This layer is thought to be continuous and reports to the contrary, (Parfitt, 1973; Miller *et al.*, 1980) are considered to have come about by drying and preparation artefacts, (Menton *et al.*, 1984). Between the membrane of the lining cells and the bone matrix exists a space containing extracellular fluid. The bone lining cell layer is thought to act as a membrane controlling the exchange of ions between the vascular and extracellular fluid, (Neumann and Neumann, 1980) and to control the exchange of calcium ions between the bone and the extracellular fluid (Norimatsu *et al..*, 1978). Processes from the bone lining cells pass into the canaliculi and meet those from osteocytes at gap junctions, (Cooper *et al.*, 1966). These gap junctions allow cells to detect fluctuations in ionic concentrations, and suggest a mechanism for the activation of bone remodelling.

2.3 Macroscopic Structure of Bone

There are two distinct morphologies found in bone, cancellous or trabecular and cortical or compact, each type constitutes 20% and 80% of the human skeleton respectively.(Ackermann, 1992).

2.3.1 Trabecular Bone

Trabecular bone consists of a network of trabeculae within which there are interconnected spaces or cannceli that contain marrow. As both trabecular bone and cortical bone are highly porous the difference between them are determined by the relative solid content per unit volume and porosity, (about 87% for trabecular bone, Galante *et al.*, 1970). The architecture of the trabeculae provide a high specific strength and impact resistance. Compact bone is always found on the exterior surface of trabecular bone. It is found therefore inside short bones e.g. carpi that are subject to pressures, flat bones e.g. the cranuim that require a high strength to weight ratio and in the ends of long bones.

2.3.2 Cortical Bone

As mentioned previously forms the surface of all trabecular bones and the shaft of the long bones in which it surrounds the marrow cavity. The external surface is coated in a periosteal membrane except where cartilage is present. The internal surfaces are also coated in a connective membrane the endosteum. Cortical bone is much more dense than trabecular bone and does not contain as many cannceli.

2.3.3 Marrow

Marrow is a soft tissue found within the interior cavities of most bone of which there are two types. Yellow marrow is 96% fat and is found in the shafts of long bones. Red marrow is found in flat and short bones, the ends of long bones, the vertebrae and ribs. It contains blood forming cells which can differenciate into osteoblasts and the osteocytes, and less fat than yellow

marrow. Osteoclasts, bone resorption cells, (see Section 2.2.3) are found mainly in the red type.

2.3.4 Blood supply

The osseous blood supply is extensive, typically it consists of several discreet points of nutrient arterial inflow which feed complex sinusoidal networks within the bone. These drain into various channels which leave the bone through all non-cartilaginous surfaces. In addition to providing nutrition for the bone cells and tissue, it provides the mechanism for effecting mineral homeostasis. Lymphatic vessels are found in the periosteum only, whereas nerves accompany the blood vessels into the Haversian systems, (see Figure 2.3)

2.4 Mechanical Properties of Cortical Bone

There are a wide range of external influences that effect the mechanical properties such as age, sex, diet, specimen density, test technique and environment. Bone is anisotropic, thus the properties vary with specimen orientation.

2.4.1 Modulus

A variety of techniques have been used to measure Young's modulus including three point bend tests, tension tests and ultrasound. Reilly *et al.*, (1974) compared the elastic moduli of Haversian and primary bone derived from load deformation data, in the longitudinal and transverse directions. This method was also used to determine the elastic moduli for the more osteonal tibial bone by Knets (1978). Katz *et al.* (1984) have studied osteonal remodelling on the elastic moduli using the measurement of ultrasonic wave propagation velocities in bovine cortical bone. Table 2.2 compares the results from some of these workers.

Table 2.2. Elastic moduli (GPa) of human and bovine bone measured by mechanical deformation in tension and compression and by ultrasonic measurements.

	Primary		Haversian	
	Trans.	**Long.**	**Trans.**	**Long.**
Reilly *et al.*. (1974)				
Mechanical Test (Tension)				
Human Femur	11	27	10	18
Bovine Femur			10	23
Katz *et al.*. (1984)				
Ultrasound				
Bovine Femur	22-25	35	21	30

It can be seen from Table 2.2 that the modulus is lower in the transverse direction in all specimens due to orientation of the collagen fibres. Osteonal remodelling reduces the modulus in the longitudinal direction, but has little effect on the modulus in the transverse direction, as can be seen by comparing values for primary and haversian bone specimens. Bovine bone has similar elastic properties to human bone and thus is often used in tests.

2.4.2 Strength

This is defined as the maximum stress a sample can withstand before fracture. There are a number of possible test configurations. Tensile tests are performed on a sample of reduced cross sectional area to minimise the effect of gripping technique. Universal joints are used to hold the sample to ensure correct specimen alignment. Compressive tests are harder to perform accurately since edge effects are more dominant. Bending tests can be used but the effect of non-elastic deformation must be taken into account. Table 2.2 shows values for strengths calculated by various test methods. There is generally good agreement between the values, the tensile strength being ~130MPa and the compressive strength ~200MPa in the longitudinal direction and approximately half these values in the weaker transverse direction.

Table 2.3. Tensile and compressive strengths for human femur.

Test Type	Load Direction	Fracture Strength(MPa)	Reference
TENSILE			
	Longitudinal	122	Ko (1953)
	Longitudinal	129	Sweeny *et al.* (1965)
	Transverse	56	
	Longitudinal	138	Melick and Miller (1966)
	Longitudinal	133	Reilly and Burstein (1975)
	Transverse	51	
	Longitudinal	135	Cezaryirlioglu *et al.* (1985)
COMPRESSIVE			
	Longitudinal	193	Reilly and Burstein (1975)
	Transverse	133	
	Longitudinal	206	Cezaryirlioglu *et al.* (1985)

2.4.3 Microhardness

Carlstrom (1954) first used microhardness of bone using the Vickers hardness technique to demonstrate variations in mineral content. Weaver (1966) later confirmed this and found a power law relation to the hardness and mineral content. The same author found that hardness increases with age to the mid-twenties whereafter it remains constant, thus hardness can give an indication as to mineral content. Evans *et al.*. (1988) found a square law relation between hardness and mineral content, from a range of species and a linear relation between hardness and modulus. Comparisons with a polyethylene-hydroxyapatite composite confirmed the findings, which appeared insensitive to microstructure. This finding enabled determination of modulus from hardness values. Human bone has Vicker's hardnesses in the range of 30-60.

2.4.4 Fracture Toughness

There is limited data concerning the fracture toughness of human bone. The values vary in the longitudinal and transverse directions 3.3 and 8.1MPa.$m^{1/2}$ respectively, Charalambides (1988), being higher in the transverse direction probably due to shorter crack path parallel to the osteons. Fracture toughness is found to decrease with increasing strain rate (Bonfield and Datta, 1974) and with crack velocity (Bonfield *et al.* , 1978).

2.5 Bioceramics

When a foreign body is placed within a tissue there are a number of responses that may occur which depend to a large degree on the nature of the foreign material. Toxic death of the surrounding tissue, non-toxic resorption, formation of a fibrous capsule or the formation of an interfacial bond may occur, (Hench, 1986). Metals have the strength and toughness to be used in load bearing applications. For example corrosion resistant titanium alloys are used to manufacture artificial hip joints (Smith and Hughes, 1966). However due to the high stiffness of metals compared with bone, the dynamic modelling of bone is interrupted and resorption can result. This effect is thought to be one of the possible causes of the problem of long term loosening in artificial hip joints (Wroblewski, 1986) which currently prohibits their use in younger patients. Polymers can posses superior biocompatibility to metals and can be manufactured to degrade non toxically in service, for example degradable stitches. However polymers may degrade prematurely under the action of certain enzymes, (Williams, 1987). They also creep under the action of long term loading. Polymer wear particles in artificial joints have been known to cause irritation and subsequent bone resorption in artificial hip systems (Wroblewski, 1979). Ceramics are renowned for their inertness. As a result of this property they are widely used in crucibles, reaction vessels, kitchen ware, food storage applications, catalyst supports and as bioceramics.

2.5.1 Types of bioceramic

There are three categories of bioceramic: bioinert, bioresorbable and bioactive, (Heimke and Griss, 1983; Hench, 1990). A brief outline of the different types of bioceramic is given in the following section, hydroxyapatite, which is bioactive, is considered in more detail.

Bioinert

An inert bioceramic is non-toxic and bio- inactive. Upon implantation a fibrous non- bonding encapsulation occurs. As the fibrous capsule is non bonding, movement can occur which can be disadvantageous. Dense alumina is by far the commonest bioinert ceramic. It is used in hip and knee protheses, bone screws and maxillofacial reconstruction, (Hulbert *et al.*, 1987).

Bioresorbable

Bioresorbable ceramics need to degrade at the same rate as healing occurs. This is the main problem with resorbable ceramics because the healing process does not occur at a fixed rate and resorption is dependent on the surface area of the implant which itself varies throughout healing. It is desirable that the degrading ceramic maintains its integrity during resorption. Dense tricalcium phosphate is one of the more widespread bioresorbable ceramics that has been used in the repair of non- load bearing maxillofacial regions, (de Groot, 1988).

Bioactive Ceramics

A bioactive material is one which causes the formation of a bond at the interface of the tissue and the implant. This bond may be formed between hard or soft tissue, (Wilson *et al.*, 1981). Examples of bioactive ceramics are Bioglass® and hydroxyapatite. Bioglass® is a particular composition of sodium, calcium and phosphorus glass. In this system there exists a composition range over which bonding is demonstrated. Sintered hydroxyapatite displays excellent bonding to bone, (Dennissen *et al.* (1980), Jarcho (1981); Winter *et al.*, 1984). The reason for this is not known exactly

though evidence of epitaxial crystal growth between a hydroxyapatite implant and bone have been reported. (Luklinska and Bonfield, 1991). Resorption has been reported not to occur, (Klein *et al.*, 1984), however more recently Aoki (1994) has suggested that resorption of dense hydroxyapatite does occur at a rate of 1μm per year. Gomi *et al.* (1993) reported that partially sintered hydroxyapatite of undetermined porosity and mean grain size of 0.5μm was resorbed by osteoclasts *in vitro*. Though the authors do not mention the grain size as significant it is likely that the small grain size was responsible for the effect.

Hydroxyapatite is used clinically in granular, porous and dense forms and more recently as a plasma sprayed coating on hip prostheses (Osborn and Neweseley, 1982). The granular and porous forms are used mainly as fillers, (Oonishi (1991), whereas dense apatite is used as a spacer in orthopaedic applications, (Shinjo et al., 1989), middle ear reconstruction (Feenstra and de Groot, 1983), or as an artificial trachea, blood vessel and as a percutaneous device, (Aoki, 1994). Hydroxyapatite is not used in load bearing applications. Its mechanical properties are not dissimilar to soda glass and for this reason is unsuitable in this capacity. Best (1990) reported an in depth investigation into the mechanical properties of commercial apatites.

Carbonate hydroxyapatite is more similar in composition to bone mineral than hydroxyapatite and is more soluble than hydroxyapatite. Ellies *et al.* (1988b) reported an *in vivo* study comparing the tissue response to two sintered carbonate apatites, (3 and 6 wt%) and a sintered hydroxyapatite. Although the workers found increased marrow bone after four weeks implantation in rat femurs, ventral and dorsal bone formation was reduced in carbonate apatites compared with hydroxyapatites. There was a insufficient quantity of data, (five femurs per sample), to eliminate doubt from their findings and they concluded that a difference between the *in vivo* response of carbonate apatite and hydroxyapatite existed. As with the vast majority of reports concerning comparative data of *in vivo* response to different bioceramics, the materials were poorly characterised. It is likely that these materials varied in grain size and porosity as well as carbonate content, these differences may have hidden the effects of carbonate. Aoki *et al.* (1989) implanted single crystals, (2-5mm x 100-200μm), of A type carbonate apatite into the medullary cavity of rat femurs. They reported increased bone formation after one week, after four weeks dissolution of the crystals was observed. Again this study fell into the category of merely demonstrating biocompatibility as neither a carbonate free

apatite nor a non-apatitic control was used in order to assess the effect of carbonate.

As a consequence of the increased acid solubility and low sintering temperatures and thus small grain sizes of carbonate apatite, it is expected that carbonate apatite is resorbable *in vivo* under the action of acidic enzymes secreted by osteoclasts, and not generally soluble like tricalcium phosphate. Carbonate apatite may therefore be a new class of "smart" biomaterial which dissolves only in response to the bone remodelling /healing process and remains intact and bonded to the interface in regions free of osteoclastic action. Bone ingrowth would then follow as with porous ceramic materials. It is anticipated that remodelling would continue until the carbonate apatite was completely removed.

3 Carbonate Hydroxyapatite

3.1 Calcium Phosphates of Biological Significance

Biological calcium phosphate compounds belong to the orthophosphates, i.e. they are built around the PO_4^{3-} group. They are often found as geological minerals and thus are frequently still referred to by their mineral names Table 3.1.

Table 3.1. Calcium phosphorus ratios and formulae for the calcium phosphates

Ca/P	Formula	Name	Abbreviation
2.00	$Ca_4(PO_4)_2$	Tetracalcium Phosphate (Hilgenstockite)	TeCP
1.67	$Ca_{10}(PO_4)_6(OH)_2$	Hydroxyapatite	HA
1.5	$Ca_3(PO_4)_2$	Tricalcium Phosphate	TCP
1.33	$Ca_8H_2(PO_4)_6.5H_2O$	Octacalcium Phosphate	OCP
1.00	$CaHPO_4.2H_2O$	Hydrated Dicalcium Phosphate Brushite	DCP
1.00	$CaHPO_4$	Anhydrous Calcium Phosphate (Monetite)	DCPA
0.50	$Ca(H_2PO_4)_2H_2O$	Monocalcium Phosphate Monohydrate	MCPM

Some of these are not significant biologically, for example monocalcium phosphate is highly soluble and tetracalcium phosphate does not form under aqueous conditions, thus are unlikely to be found *in vivo*. TCP, DCP and DCPA are found in dental calculi, urinary and cartilage mineralisations and are more soluble than hydroxyapatite. Hydroxyapatite or more specifically carbonate hydroxyapatite is by far the most abundant inorganic phase in the human body, (~15 wt % of the dry mass). Carbonate apatite is the inorganic constituent of human bone and teeth (LeGeros, 1967) and more recently has been found by Bocchi and Valdre (1993) to be the inorganic constituent of mineral concretions found in the pineal gland, called pineal acervuli or "brain sand".

3.2 Structure of Hydroxyapatite

The structure of apatite (fluorapatite) was established independently by Naray-Szabo and Mehmel in 1930. Hydroxyapatite was shown to have the same crystal structure , with OH^- replacing F^-, by Posner (1958). This structure was refined by Kay *et al.* (1964) who showed the OH^- to be displaced up by 30pm from z = 0.25. The OH^- ions are thought to lie in ordered columns with possible areas of reversal of direction. Stoichiometric hydroxyapatite is hexagonal, space group $P6_3/m$ ($\mathbf{a} = \mathbf{b} \neq \mathbf{c}$, $\mathbf{a} = \mathbf{b} = 90^o \neq \gamma$, $\gamma = 120^o$) **a** = 942.1 pm, **c** = 688.0 pm, (JCPDS, 1980). The structure of the unit cell is illustrated in Figures 3.1 and Figure 3.2. Figure 3.1 d shows the position of the hydroxyl groups in the unit cell. They lie at z = 0.29, 0.79. Figure 3.1 b shows the position of what are termed the columnar calcium atoms (Ca I), of which there are four per unit cell. The remaining six calcium atoms (Ca II) are arranged in triangular co-ordinated groups, (Figure 3.1a), with successive triangles rotated 60^o with respect to one another, forming 'tunnels' parallel to the **c** axis housing the OH^- ions. The remaining volume is filled with orthophosphate tetrahedra (Figure 3.1c). The complete unit cell is shown in Figure 3.2.

If alternate hydroxyl columns are in opposite orientation (Figure 3.3) the hexagonal symmetry is lost and the unit cell is monoclinic due to a doubling in length of the **b** axis, as was found in chlorapatite by Young and Elliot (1966). Elliot (1971) went on to prepare very pure hydroxyapatite that was monoclinic. This suggests that disordered hydroxyapatite is not in its energetically most stable form and explains the preferential substitution of OH^- by F^- to form a more ordered structure.

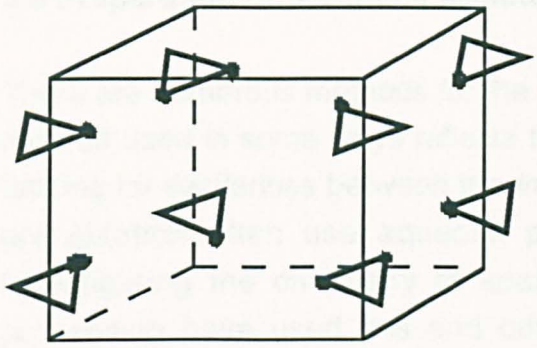

Figure 3.1a) Position of calcium(II)

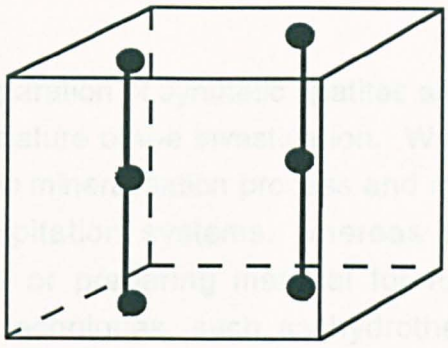

b)Position of calcium (I)

c) Position of phosphate groups

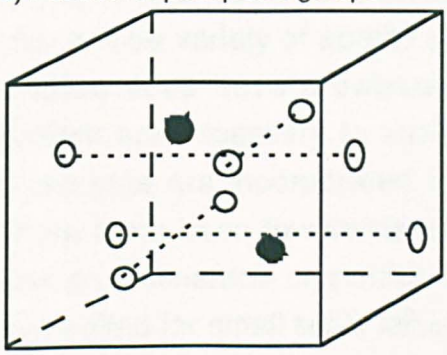

d)Position of hydroxyl groups

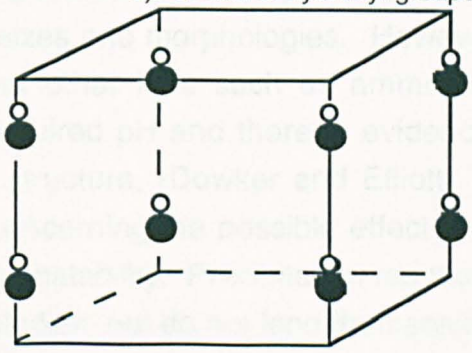

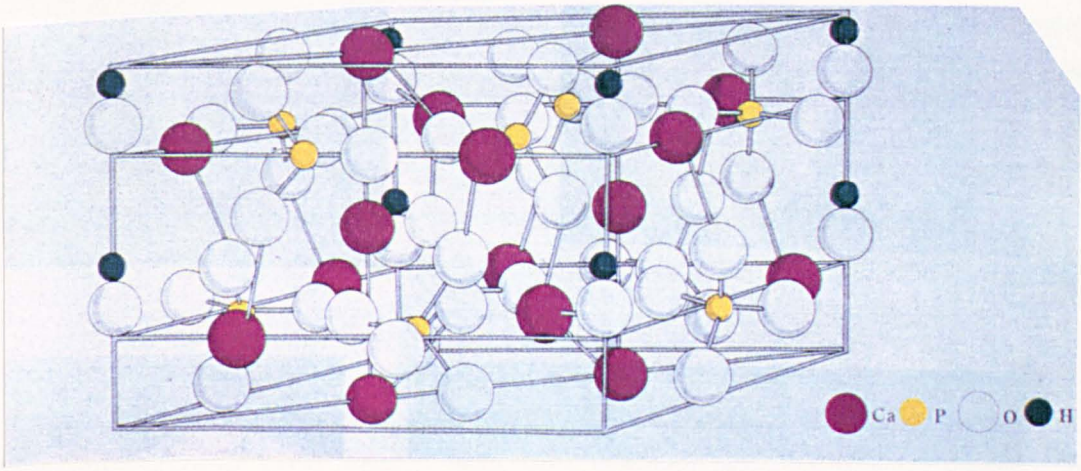

Figure 3.2 hydroxyapatite unit cell. (Reproduced from Aoki, 1991)

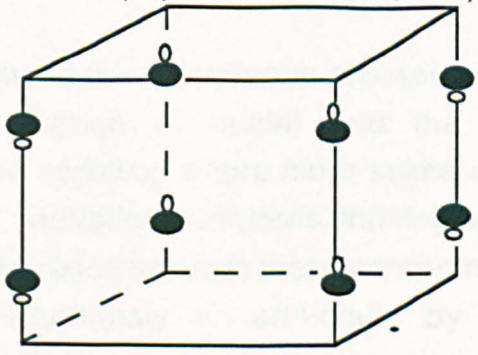

Figure 3.3. Half unit cell of monoclinic hydroxyapatite. OH group position

3.3 Preparation of Synthetic Apatites

There are numerous methods for the preparation of synthetic apatites and the method used in some ways reflects the nature of the investigation. Workers looking for similarities between the *in vivo* mineralisation process and *in vitro* precipitation often use aqueous precipitation systems, whereas those investigating the chemistry of apatites or preparing material for further processing have used this and other techniques, such as hydrothermal production, in attempts to modify characteristics under study. By far the most common method is that of aqueous precipitation, not only because it is closer to the *in vivo* case but because it is a relatively simple procedure that can give a wide variety of apatite particle sizes and morphologies. However this method does have drawbacks in that other ions such as ammonium or sodium are necessary to attain the required pH and there is evidence that these ions are incorporated into the structure, (Dowker and Elliott, 1983). There have been few investigations concerning the possible effect of these ions on mechanical properties or biocompatability. Precipitation reactions are well suited for small scale laboratory studies, but do not lend themselves well to industrial continuous production applications due to the large numbers of factors that can influence the final product. However, the lack of work clearly outlining the requirements of apatite for use as a material for sintering into a dense component and the wide variety of processes that can be used to achieve a sintered body are probably the main reasons for the wide range of quality of commercial synthetic apatites that exist (Best, 1990). As aqueous precipitation is the method used in this study a brief outline of the precipitation process and factors that can influence it is given in the following section.

3.4 Precipitation

There are three stages to the precipitation process namely, achievement of supersaturation, formation of nuclei and the growth of crystals. Supersaturation is the condition where more solute is dissolved in solution than is present under equilibrium conditions, the degree of supersaturation, s, being given by the difference between these concentrations. Nucleation can then proceed spontaneously or artificially by seeding, known as homogeneous and heterogeneous nucleation respectively. As apatite is

observed to nucleate spontaneously and impurity contamination is avoided, the case of homogeneous nucleation is considered. In regions of localised supersaturation sub-nuclei, regions of molecular order, are constantly being formed and re-dissolved. However, if a certain critical size is exceeded a stable nucleus is formed. As the free surface energy ΔG_s increases positively as the square of particle dimension r, and the free volume energy ΔG_v increases negatively as a cubic function of r, the maximum overall excess free energy ΔG is given when:

$$\Delta G = \frac{4\pi\gamma r_c^2}{3} \qquad (3.1)$$

Where γ is the surface energy and r_c is the critical particle radius below which dissolution occurs above which growth continues. This mechanism requires that material be transported to the surface of the nucleus and incorporated in the lattice. It is found that the growth rate, g is linearly related to supersaturation:

$$g \propto s \qquad (3.2)$$

as derived from Randolph and Larson (1971). The constant of proportionality consists of terms relating to reaction and diffusion.

3.4.1 Effect of Temperature

Temperature can effect precipitation reactions in a number of ways. The relation between a reaction rate constant, k and absolute temperature, T, is given by the Arrhenius equation, which can be rearranged to give:

$$\ln k = \ln A. - \left(\frac{E}{RT}\right) \qquad (3.3)$$

Where E is the activation energy of the process, R is the gas constant and A is constant for a particular system. The highest activation energy for a particular growth mechanism will determine rate controlling mechanism.

In addition to altering the dominant mechanisms of growth, temperature affects the degree of supersaturation according to Equation 3.4.

$$\ln s = \frac{2 M \gamma}{R T \rho r} \qquad (3.4)$$

Where M is the molecular weight and ρ is the density, (Mullin, 1961). It can be seen that as temperature decreases supersaturation for a given solute concentration will increase, influencing growth rate (Equation 3.2) The degree of supersaturation also affects the particle size of the crystals. It is thought that as the number of nuclei increase the average particle size will decrease as there is only a fixed mass of possible reaction product. Equation 3.4 shows the relation of particle size to supersaturation. Above what is termed the metastable limit, heterogeneous nucleation can occur. The supersaturation ratio above which homogeneous nucleation can occur yields the largest crystal size. Above this ratio, i.e. at lower temperatures, the particle size falls. This effect has been observed in many precipitates (Von Weimarn, 1925).

3.4.2 Effect of Agitation

The rate at which crystals grow at a given temperature and constant supersaturation can be altered by agitating the crystals. The growth rate increases during the initial stages as the velocity of the crystal through the liquid increases, but a constant growth rate is soon reached, after which further increases in velocity have no effect. This phenomenon is thought to be due to an increase in the concentration gradient between the solution and the crystal surface, brought about by a reduction in the distance of concentration variation. Although growth rate is independent of size, crystal size can affect the relative velocities and thus growth rates of crystals.

3.4.3 Habit Modification

The habit of a crystal is the external shape it possesses as a result of different growth rates on the various faces. Crystals of the same substance may have entirely different morphologies and still belong to the same crystal system. Among the causes of habit modification are: solvent type, pH, impurities, degree of supersaturation, cooling rate, temperature and agitation rate. At very high supersaturation the concentration gradient of solute near the crystal surface is great such that the layer of reduced concentration around the crystal is absent. This result alters the growth rate at edges relative to surfaces which can influence the habit, Parffit (1969). The alteration of habit though unpredictable is of great interest to the ceramist when producing material with better characteristics for sintering. For example, rounded particles give better green packing than acicular ones, which can be better used as a reinforcement in composites.

3.4.4 Ageing and Recrystallisation

During this process flocculation, coalescence, ripening and surface remodelling occur. Material particles of high solid-liquid surface area will tend to flocculate in order to reduce their effective surface area. Mass transfer processes such as ripening, brought about by the inverse relationship to particle radius and solubility and recrystallisation are temperature dependent. Ripening results in the growth of the larger particles at the expense of the smaller ones. Recrystallisation involves the partial dissolution of all crystals from areas of high energy e.g. edges and the subsequent deposition of material at areas of low energy e.g. dislocations. In an infinite amount of time precipitate would form a single crystal of normal habit. Although this state does not occur in practise, the system is constantly moving towards it. This can have the effect of 'locking in' impurity ions and is of special relevance in systems producing precipitates of large specific surface area from homogeneous nucleation when a pure material is required. For example, in aqueous apatite preparation, unless of course the impurity is desirable.

3.5 Aqueously Precipitated Hydroxyapatites

Aqueous precipitation techniques all involve the combination of calcium, phosphate and hydroxyl ions, usually under basic conditions. What varies from method to method are the other associated ions, concentrations, ageing times and temperatures. One of the first reports on the preparation of hydroxyapatite (Collin, 1959) describes the precipitation reaction of hot aqueous diammonium hydrogen phosphate and calcium nitrate, made basic by the addition of ethylene diamine. This method was modified by Hayeck and Newsley (1963), who replaced the ethylene diamine with sodium hydroxide and conducted the reaction at room temperature. Young and Holcombe (1982) successfully used this method at 100°C. Similar methods are reported by a number of workers, (Eanes, 1965; Posner *et al.*, 1975; Jarcho, 1976). The reaction can be described thus,

$$10Ca(NO_3)_2 + 6(NH_4)_2HPO_4 + 2H_2O \longrightarrow Ca_{10}(PO_4)_6(OH)_2 + 12NH_4NO_3 + 8HNO_3 \quad (3.5)$$

This preparation route has been used to produce fibrous hydroxyapatite up to 1cm long by reacting calcium nitrate gelled in agar, with ammonium orthophosphate (Tanahashi *et al.*, 1992).

Bonel *et al.* (1987) studied the effect of ammonia on Ca/P ratios, finding that the ratio increased with increasing ammonia concentration in the phosphate solution. This raises the question as to whether ammonium ions substitute into the structure or alter the precipitation product.

Another method reported involves the reaction of orthophosphoric acid with calcium hydroxide:

$$10\,Ca(OH)_2 + 6H_3PO_4 \longrightarrow Ca_{10}(PO_4)_6(OH)_2 + 18H_2O \quad (3.6)$$

This method was used by Boehm (1974). Hydroxyapatite made by this method was used to study the solubility of hydroxyapatite in water at a range of temperatures by McDowell *et al.* (1977). Irvine (1981) of British Charcoal McDonald patented a continuous production process which involved a similar reaction to that above, hydrated lime slurry, being reacted with steam and phosphoric acid.

Barsa *et al.* (1977) used a reaction of sodium phosphate and calcium carbonate in a basic aqueous medium. This method was used by Boistelle and Valero (1966) to study the effect of pH on reaction product. They found that at 37°C Brushite was formed at pH < 6.5, and ACP at 6.5< pH < 8. This ACP transformed to OCP in 24 hours and hydroxyapatite was formed at pH> 8 after several days ageing.

Eanes (1980) discussed the influence of factors such as pH, temperature and the presence of certain anions such as carbonate and fluoride, on the formation products of such reactions. In the case of spontaneous precipitation, the first product of reaction is thought to be amorphous calcium phosphate (ACP-$Ca_3(PO_4)_{1.87}(HPO_4)_{0.2}$. A decrease in pH or an increase in temperature increases the rate of transformation to a crystalline phase. At pH > 9.5 this phase is apatitic, at pH < 9.5 octacalcium phosphate (OCP) is the transformation product. Carbonate ions are found to have a retarding effect on this transformation whereas fluoride has a promoting effect. Concentrations of 3% fluoride were found to cause a by-passing of the OCP precursor stage, as deduced from the needle morphology of the resulting apatite.

Posner and Betts (1975) thoroughly investigated ACP and its transformation to hydroxyapatite using microscopy and X-ray diffraction data. They concluded on the basis of a lack of a correlation between calculated diffraction data for small hydroxyapatite clusters, a single hydroxyapatite unit cell and ACP, that ACP is a structural entity in its own right. Electron microscopy revealed that the ACP phase consisted of spheroidal particles 30-100nm in diameter. However, although there is a limit to the crystal size detectable by XRD, there is also an energetic limit to size, below which it is unstable or impossible for a crystal to exist in its normal form, e.g. a unit cell. It is likely that due to the extremely high surface energy of very small crystals, (Adamson, 1982) that some rearrangement would occur to minimise this surface energy, thus the particles are spheroidal and not acicular as is their normal habit. These workers also looked at the conversion rates of ACP to hydroxyapatite as a function of pH. They commented on the report that as pH decreases, i.e. as hydroxyapatite solubility increases, the conversion rate is increased. But the ACP was in contact with the mother liquor, which contained unreacted ions it seems more likely that the small crystals were able to rearrange themselves by a process of solution and reprecipitation into

the more energetically favourable acicular morphology. Determinations of ACP formulae have mainly been deduced from the results of quantitative analyses, however hydroxyapatite is known to tolerate deviations in stoichiometry. It would appear that ACP is a term that has incorrectly been used to describe a form of apatite, incorrectly assumed to be a precursor in the formation of large crystals of hydroxyapatite. The work described in this thesis is thought to be the first in knowingly studying the sintering behaviour of what has previously been termed ACP.

Although no comparative study of these and other techniques of aqueous precipitation methods on the final product and its suitability for orthopaedic purposes seems to have been carried out, examination of the problem would suggest the best method for a pure product would be that which forms the least amount of additional compounds, with the least amount of intermediate phases at the least cost.

3.6 The Carbonate Substitution

Interest in the nature of the carbonate substitution was firstly of a geological nature. This work was largely based around the carbonate apatite minerals francolite, a fluorapatite, and dahlite a carbonate apatite. Biological and geological investigations then followed with synthetic apatite investigations coming a little later. The motive for the work appeared to be to understand the mechanism of biological mineralisation. LeGeros (1967) was of the belief that carbonate in hydroxyapatite was the reason for caries susceptibility in human enamel. This stimulated work in the area of acid dissolution of hydroxyapatites and carbonate apatite was found to increase solubility of hydroxyapatite (LeGeros and Tung, 1983).

3.5.1 Mineral and Biological Carbonate Apatite Studies

Eitel (1924) expressed the results of chemical analysis of dahlite as $Ca_{10}(PO_4)_6(CO_3)$ where one carbonate group substitutes for two hydroxyls. Grunner and McConnel (1937) related lattice parameter measurements and chemical analysis of francolite and dahlite to the mode of substitution. They concluded that for dahlite the mode of substitution was the same as deduced by Eitel. For francolite they found that the carbonate for hydroxyl substitution was not possible as the 4% fluoride ions present was sufficient to replace all the hydroxyl sites. The shorter **a** axis compared to fluorapatite indicated that the carbonate ion had replaced the larger phosphate group. They proposed a carbon for calcium and a CO_4^- for phosphate substitution. Bourneman and Starinkevitch (1939) questioned Grunner and McConnel's substitution and proposed a CO_3OH ion of tetrahedral configuration. Belov (1939) agreed with Grunner and McConnel that carbonate could not substitute for fluorine and with Bourneman and Starinkevitch that a CO_3OH or CO_3F substituting ion was the most likely. Hendicks and Hill (1942 and 1950) suggested two mechanisms based on the condition of electroneutrality. Firstly that three phosphate groups replaced four carbonates and a calcium ion is replaced by a sodium. Secondly the carbonate ion in francolite is adsorbed on the surface. The first mechanism (1942) was proposed from the results of chemical analysis of bones and teeth. The second (1950) was proposed as no difference in XRD patterns of francolite and fluorapatite were observed. However the equipment available at that time was possibly unable to detect differences of that magnitude. Silverman *et al.* (1952) conducted analyses to determine the quantities of calcite associated with carbonate apatite minerals. They concluded that carbonate in francolite was present as calcite.

McConnel (1952) modified his original proposal on carbonate in francolite. He suggested that water replaced calcium and phosphorus, carbonate substituted for some phosphate and fluoride replaced a phosphate oxygen (similar to the manner of Belov, 1939). Posner and Duyckaerts (1954) compared X-ray diffraction patterns of francolite before and after some of the carbonate had been leached out and found them to be identical. Comparisons of the IR spectra of bone, enamel, francolite, and calcium and magnesium carbonate led them to conclude that bone, francolite and enamel display evidence of similar carbon-oxygen bonds as were found in calcite and magnesite. Carlstrom (1955) observed that on heating carbonate apatite at

800°C for 146 hours in carbon dioxide calcite is detected by XRD and he concluded that calcite had grown from calcite that was previously amorphous, (and therefore not detectable by XRD.) He proposed the existence of a layer of calcium carbonate 2.5 nm thick around the apatite particles. No correlation between carbonate content and lattice parameter was reported. Trautz (1955) measured the lattice constants of mineral and synthetic apatites and correlated changes in fluoride and carbonate substituents with **a** axis contractions of 1.3 and 0.9 pm per % of fluoride and carbonate respectively, the contraction being due to the smaller size of the substituents. Later Trautz and Zapanta (1960) calculated, on the basis of birefringence measurements of francolite and fluorapatite that carbonate groups are inclined at 43° to the **c** axis and proposed that they may occupy one face of the PO_4 tetrahedron.

3.5.2 Synthetic carbonate apatite studies

Bredig *et al.* (1932) boiled calcium carbonate and calcium hydroxide in a solution of sodium carbonate and sodium phosphate. The products gave XRD patterns of poorly crystallised apatite. They assumed that the product had the same characteristic as francolite. Romo (1954) reported a method for the formation of carbonate apatite by refluxing calcite and alkaline phosphate ion solution at 95°C. The product was shown to be apatitic by XRD and he concluded from IR data that carbonate had substituted for hydroxyl groups i.e. an A type (Section 3.5.3) substitution had occurred. Wallaeys (1954) reacted TCP at 900°C in dry carbon dioxide and obtained an apatite with an expanded **a** and **c** axis. On the basis of XRD and chemical analysis he concluded that an apatite was formed in which 60% of the hydroxyl groups were substituted with carbonate. Montel (1958) prepared carbonate apatite by the dropwise addition of alkaline sodium phosphate and sodium carbonate into alkaline calcium chloride. The XRD pattern was that of a poorly crystallised apatite. Ames (1959) prepared carbonate apatite by passing tri-sodium phosphate solution over a calcite column at pH 12.4. XRD patterns showed an apatitic product and that traces of calcite had disappeared after the reaction. Isotope studies of C^{14} and Ca^{45} showed that calcium was retained and the $C^{14}O_3$ content to be ~10 wt% from chemical analysis. He determined the structure to be $Ca_{9.35}Na_{1.07}(PO_4)_{5.46}(CO_3)_{1.36}(OH)_{0.67}(H_2O)_{1.33}$. Elliot (1963) varied the amount of substitution in the hydroxyl site up to 85% by passing dry carbon dioxide over hydroxyapatite for periods of up to fifteen hours. He observed that a proportional relation existed between the increase in **a** axis

and decrease in **c** axis with carbonate concentration. Gron *et al.* (1963) precipitated a series of carbonate apatites from metastable solutions of calcium and phosphorus ions containing sodium bicarbonate by seeding the solution with apatite. Chemical analysis showed that the carbonate content of the precipitated apatite phase was proportional to that in the solution. However they suggested that the carbonate was adsorbed on the surface. Kühl and Nebergal (1963) added calcium nitrate solution to an alkaline solution of potassium hydrogen phosphate and potassium carbonate. On the basis of chemical analysis they proposed the formula:

$$Ca_{10-x+u}(PO_4)_{6-x}(CO_3)_x(OH)_{2-x+2u} \qquad (3.7)$$

Where

$$0 \leq x \leq 2, \text{ and } 2u \leq x$$

This model assumes that one phosphate ion is replaced by one carbonate ion and some of the resulting calcium and hydroxyl ions are filled with some degree of calcium hydroxide.

Simpson (1964) modified Ames' reaction by suspending calcite in alkaline phosphate solutions for 105 days. The maximum carbonate content was 5.6wt%. He assumed a coupled substitution of carbonate for phosphate and sodium, potassium or H_4O_4 for calcium. However XRD was not carried out to establish whether or not a single phase product was formed.

LeGeros *et al.* (1965) formed carbonate apatite by the dropwise addition of calcium acetate to boiling solutions of phosphate and sodium bicarbonate. The product had a shorter **a** and longer **c** axis than carbonate free apatites. She concluded that on the basis of chemical analysis that a coupled substitution of the type $NaCO_3$ for $CaPO_4$ occurred (LeGeros, 1967). LeGeros (1967) also reported the effect of autoclaving amorphous type carbonate apatites. She found that this treatment resulted in an increase in crystallinity and a reduction in **a** axis. LeGeros (1969) reported two distinct carbonate substitutions that could be characterised by XRD and IR spectra, (Section 3.5.2). They are named after the crystal sites in which they are located, A (OH) and B (PO_4).

Nadal *et al.* (1970) showed by means of comparisons of IR data that a mixed AB type substitution was obtained in fluorapatite by altering the amount of fluoride in the apatite, before heating in dry carbon dioxide at 900°C. Bonel (1972a) prepared A type apatite in the manner of Wallaeys (1954). He

showed that substitution occurred in the hydroxyl site and the **a** axis increased with carbonate content in agreement with Elliot (1963). He proposed the reaction:

$$Ca_{10}(PO4)_6(OH)_2 + 0.6\,CO_2 \text{ ------>} Ca_{10}(PO4)_6(OH)_{0.8}(CO_3)_{0.6}+0.6H_2O \quad (3.8)$$

Bonel (1972b) prepared AB type carbonate apatite by slowly pouring a mixture of phosphate, carbonate and sodium fluoride into an alkaline calcium chloride solution. The precipitate was then heated in dry carbon dioxide for one hour at 900°C. Pure B type fluorapatites were obtained by replacing the apatite above with fluorapatite. Bonel found that by heating hydroxyapatite and calcium fluoride in dry carbon dioxide for three hours a B type fluorapatite was obtained. The thermal behaviour of carbonate apatites produced in a similar way to that of LeGeros (1967) were also investigated. The precipitates were heated at 900°C in air, dry nitrogen and dry carbon dioxide. On the basis of density measurements and chemical analysis, Bonel proposed a substitution based on:

$$Ca_{10-x}(PO_4)_{6-2x}\,(CO_3OH)_{2x}(OH)_{2(1-x)} \quad (3.9)$$

This mechanism is in agreement with that originally proposed by Bourneman and Starinkevitch (1939)

Labarthe *et al.* (1973) prepared carbonate apatite by the same method as LeGeros (1967) except the sodium salts were replaced by ammonium salts and no alkaline ions were added. The product was weakly carbonated and he noticed the formation of ammonium carbonate. In an attempt to prevent this Labarthe changed round the way in which reagents were added to each other. I.e. the phosphate and carbonate was added to the calcium solution instead of the calcium solution added to the other. These two methods were termed the inverse and direct respectively. Table 3.2. shows the products of the Direct and Inverse Methods as reported by Vignoles (1973).

Table 3.2. Effect of precipitation procedures, times, pH, temperature and carbonate / phosphate molar ratio on the phase and crystallinity of precipitates produced by the method of LeGeros (1965), Vignoles (1973).

Method	Precipitation Time	pH	Temperature	$\frac{(CO_3^{2-})}{(PO_4^{3-})}$ (c/p)
Direct	$t \leq 2h$ apatite + calcite $t \geq 3h$ well crystallised apatite	$pH \leq 7.5$ apatite + calcite $7.5 < pH < 11.5$ apatite $pH \geq 11.5$ apatite and chalk	$T \leq 60°C$ No XRD pattern $T \geq 80°C$ well crystallised apatite	< 10 apatite + calcite $10 \leq c/p \leq 50$ apatite > 50 apatite + calcite
Inverse	$t < 2h$ apatite + calcite $t \geq 3h$ well crystallised apatite	$pH \leq 9$ apatite + calcite $9 < pH < 11.5$ apatite $pH \geq 11.5$ apatite + chalk	$T \leq 60°C$ No XRD pattern $T \geq 80°C$ well crystallised apatite	>2 apatite and calcite $0 < c/p < 2$ apatite >0.5 and pH 11 apatite and calcite

Labarthe *et al.* (1973) precipitated carbonate hydroxyapatites at 20, 40, 60, 80°C and boiling point. By the Direct Method they found that at a fixed carbonate phosphorus ratio of 20 the amount of carbonate in the precipitate produced at 20°C was high and that produced at 40°C was low, (the actual amounts being unspecified). IR spectra of the precipitates produced by the Inverse Method showed an increase in the intensity of the carbonate bands at a fixed carbonate phosphorus ratio of 0.8, (equivalent to 90mM $[HCO_3^{2-}]$ in this study). Carbonate apatite prepared at 20°C decomposed to form TCP and apatite at 1000°C, they hypothesised that these precipitates contained HPO_4^{2-} ions. On the basis of XRD patterns, only precipitates formed at

boiling point were well crystallised. On the basis of this observation only this temperature (unspecified in the report) was used for further investigations. The results of chemical analysis led the authors to propose the following general formula:

$$Ca_{10-x+u}(PO_4)_{6-x}(CO_3)_x(OH)_{2-x+2u} \qquad (3.10)$$

Where

$$0 \leq x \leq 2, \quad 0 \leq u \leq \frac{x}{2}$$

This model is essentially the same as that proposed ten years earlier by Kühl and Nebergal (1963).

Chickener *et al.* (1980) prepared carbonate apatite by the hydrolysis of OCP in the presence of sodium and carbonate ions. They calculated the contraction of the **a** axis and compared it with that of LeGeros (1965) and found approximately double the contraction for a given carbonate content. On the basis of this observation they concluded that some of the carbonate in LeGeros' sample was present in another form.

Doi *et al.* (1982) prepared a mixed AB type apatite in the presence of sodium ions and a B type in the presence of ammonium ions. These precipitates were investigated using electron spin resonance, IR and X-ray diffraction using the direct precipitation method of LeGeros (1965). Their data clearly showed a diminishing of the OH IR band with increasing carbonate content, together with an **a** axis decrease and **c** axis increase with increasing carbonate content. However the sodium carbonate apatite **a** axis was found to contract more drastically than the sodium free product. They proposed that either the ammonium ion inhibits carbonate substitution, it substitutes in the lattice or sodium enhances A type substitution.

Nelson and Featherstone (1982) prepared aqueous and high temperature hydroxy- and carbonate apatites. High temperature apatite was made by the method proposed by Lehr *et al.* (1967). Aqueous hydroxyapatite was made by the method used by Hayeck and Newesely (1963) with the added precaution of conducting the precipitation under nitrogen to prevent the substitution of carbonate formed by atmospheric carbon dioxide. Aqueous carbonate apatite was made by the same method as hydroxyapatite except sodium bicarbonate was added to the phosphate solution. High temperature

carbonate apatite was formed by the heat treatment of aqueous carbonate apatite in wet carbon dioxide for four hours at 900-950°C. Unlike LeGeros (1967) weak correlation was found between sodium and carbonate content but a strong relation was found between phosphorus content and carbonate content for the aqueous and high temperature carbonate apatites. Aqueous carbonate apatite showed an increase in the **a** axis at low carbonate contents. This was attributed to water in the hydroxyapatite lattice. Nelson and Featherstone (1982) also observed that high temperature and aqueous apatites displayed the same spectra except aqueous carbonate apatites displayed an extra peak at 1550 cm-1. Despite the weak link between sodium contents and carbonate contents they agreed with LeGeros' mechanism of sodium for calcium carbonate for phosphorus substitution. Three phosphates being replaced by four carbonate ions with sodium compensating for electronic deficiency. They derived the general formula:

$$Ca_{10-x}\,Na_x(PO_4)_{6-x}(CO_3)_{4x/3}\,(OH)_{2-2x/3} \qquad (3.11)$$

Hydroxyl substitution was discounted as a possibility as the corresponding IR peaks were not observed, and no **a** axis expansion was detected. However these workers did not appear to have considered the possibility of a substitution mechanism similar to that suggested by Bourneman and Starinkevitch (1939). Neither did they present any data concerning partial pressures of carbon dioxide or water. Driessens *et al.* (1983 a) prepared an AB type apatite by the reaction of DCPA and calcium carbonate at 870°C in an atmosphere of carbon dioxide and 5mmHg water. They proposed, on the basis of chemical analysis, a mechanism whereby three carbonate groups substitute for three phosphate ions with the formation of two calcium and one hydroxyl vacancies.

The same group (1983b) investigated the high temperature behaviour of a sodium containing apatite made by the reaction of DCPA and sodium and calcium carbonate at 870°C in dry carbon dioxide for one to five days, until equilibrium was reached. However, they reported that when no sodium was present and at high calcium / phosphorus ratios it took up to six months heating before equilibrium was reached. At low sodium / calcium ratios IR peaks characteristic of the A type substitution were observed, at higher sodium levels these peaks disappeared and B type peaks remained. The

workers defined a region of sodium and calcium phosphorus ratios within which a single phase product was formed as shown in Figure 3.4.

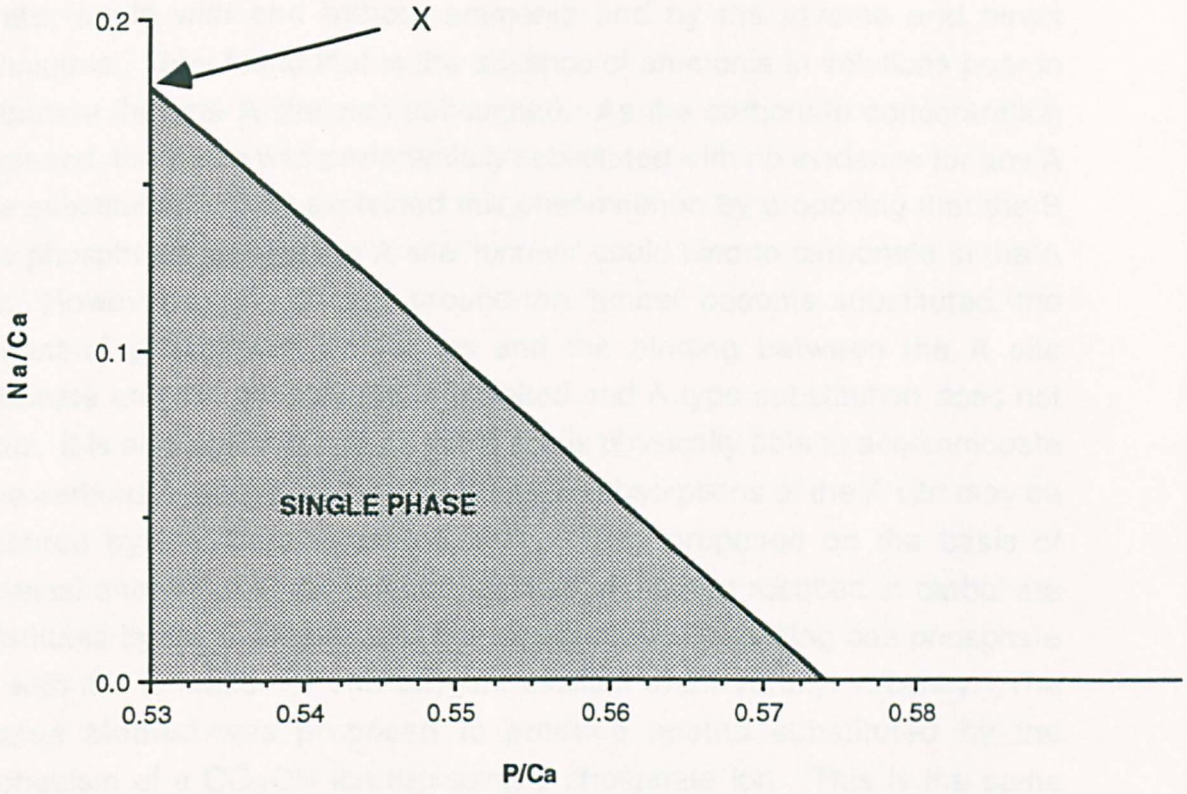

Figure 3.4. Single phase apatite field in the system CaO P_2O_5-Na_2O- CO_2-H_2O at 870°C. (Driessens *et al.* (1983b)

The point X in Figure 3.4 was reported to refer to the composition $Ca_{8.5}Na_{1.5}[(PO_4)_{4.5}(CO_3)_{1.5}]$ CO_3. The reason why Driessens *et al.* (1983a and b) chose 870°C for their experiments is not clear. In light of the long times required for equilibrium to be reached in some cases, a higher temperature may have made compositional effects clearer.

Vignoles *et al.* (1987) precipitated carbonate apatites by the direct and Inverse Methods with and without the addition of alkaline ions (aqueous ammonia). Carbonation was effected by the addition of ammonium carbonate, the products were therefore sodium free. They concluded that in the absence of alkaline ions that the ammonium ion substituted for calcium as part of the mechanism for carbonate substitution. At temperatures greater than 400°C these ions react with carbon to form cyanate and cyanide ions as

determined by IR spectroscopy. However after heating to 700°C in air it appeared that these ions were no longer present, presumably as a result of a volatisation process. When the heat treatment was carried out in helium, these ions persisted. Vignoles (1984) and Vignoles *et al.* (1988) prepared carbonate apatite by the reaction between ammonium salts and calcium nitrate, again with and without ammonia and by the inverse and direct techniques. They found that in the absence of ammonia in solutions poor in carbonate that the A site was substituted. As the carbonate concentration increased, the B site was preferentially substituted with no evidence for any A type substitution. They explained this phenomenon by proposing that the B type phosphorus around the A site 'tunnels' could bind to carbonate in the A site. However as the B sites around the 'tunnel' become substituted, the amount of phosphorus decreases and the binding between the A site carbonate and the phosphorus is inhibited and A type substitution does not occur. It is also possible that as the B site is physically able to accommodate more carbonate ions relative to the A site, IR absorptions of the A site may be obscured by the more intense B type. They proposed on the basis of chemical analysis that the direct precipitation method resulted in carbonate substituted by the mechanism of one carbonate ion replacing one phosphate ion with the formation of one oxygen, calcium and hydroxyl vacancy. The Inverse Method was proposed to produce apatite substituted by the mechanism of a CO_3OH ion replacing a phosphate ion. This is the same mechanism as that proposed by Bourneman and Starinkevitch (1939). The carbonate apatite produced by the Direct Method is calcium deficient, this was reported as being due to the calcium being added to the phosphate solution i.e. in a calcium deficient medium. They proposed the general formula:

$$Ca_{10-x+u}\ \square_{x-u}\ (PO_4)_{6-x}(CO_3\ \square)_{x-u}\ (CO_3\ OH)_u(OH)_{2-x+u}\ \square_{x-u} \qquad (3.12)$$

where $0 \leq x \leq 2$, $\square$ is a vacancy and u depends on the preparation conditions.

This is essentially the same mechanism as that reported by Labarthe *et al.* (1973) except the Inverse preparation method substitution mechanism is accounted for.

Shimoda *et al.* (1990) precipitated carbonate apatite in neutral (pH 7.5) and alkaline (pH 10.5) conditions by a precipitation reaction of calcium nitrate and ammonium salts. They found that in neutral conditions an AB type carbonate

apatite was formed and as the carbonate content increased the amount of A type substitution decreased. In alkaline conditions a purely B type carbonate apatite is formed. They found that as the concentration of reactants was decreased the particle size increased and the workers reasoned that as the supersaturation increased the nuclei number increased and therefore the size decreased. In alkaline conditions the crystal morphology was acicular, in neutral conditions a more rod like habit was developed. The crystal size decreased with carbonate content, the smallest being for an 11.5 wt % carbonate apatite (~0.5μm). Nordström and Karlsson (1990) soaked sintered hydroxyapatite in mineral water for 1-2 months. They showed that a B type substitution occurred. Unfortunately they did not measure the carbonate content of the mineral water. They suggested that implanted hydroxyapatite could become carbonated *in vivo*.

For the purposes of studying the effect of carbonate on the sintering, a pure carbonate hydroxy calcium apatite is required so that carbonate effects are not masked by other effects e.g. sodium ions. It would appear from the preceding work that the Inverse Method is preferable to the Direct Method as the product is not calcium deficient. Alkaline conditions would seem to be desirable for the formation of a B type product. As alkaline conditions are required for the precipitation of hydroxyapatite (e.g. Posner and Betts, 1975), it is reasonable to assume that these conditions are ideal for carbonate apatites. The use of ammonium salts would appear to be preferable to sodium salts as it would appear that sodium is incorporated into the lattice as part of the carbonate substitution mechanism. Large degrees of supersaturation would be expected to increase the number of nuclei and thus result in a small particle size, which would increase the driving force for sintering. Supersaturation is increased by reducing the temperature and increasing the concentration of the reactants.

3.5.3 Characterisation of Carbonate Location

As stated previously, carbonate may occupy either the hydroxyl (A) site or the phosphate (B) site in hydroxyapatite. Location of the carbonate groups in hydroxyapatite may be determined by IR spectroscopy since changes in the environment of an ion will alter its vibrational frequency. Assignment of the peaks has been based on the studies of fluorapatites in which the A site is assumed to be completely occupied by the fluoride ion. A type substitutions

are often thought as being a result of high temperature reaction, though some studies have shown that weakly carbonated precipitated apatites are A type in some precipitation conditions. Table 3.3 shows reported peak assignments for various carbonated apatites.

Table 3.3. Reported infra red and raman peak assignments for the carbonate ion in hydroxyapatite.

	CO_3^{2-}				CO_3^{2-}
	v3				v2
Activity	IR+R				IR
SAMPLE					
Le Geros *et al.* (1969)					
A type	1550,	1525,	1460		877
B type (ppt)	1540,	1450,		1410	870
Nadel *et al.* (1970)					
A type	1534,	1465			884
B type(fluorapatite heated on CO2)		1455,		1430	864
AB type (ppt)	1534,	1465,		1430	
Bonel (1972)					
A type	1534,	1465			883
B type		1455		1430	864
Francolite		1455		1430	864
AB type fluorapatite	1552,1534,	1465,1457		1429	
Nelson+Featherstone (1982)					
AB Type (From heating B type in CO_2 at 900°C) 8 wt%	1500,	1469,	1454,	1415	879,873
AB Type (Aqueous ppt) 2 wt%	1555,	1462,		1415	878,872
Shimoda *et al* (1990)					
From neutral precipitation	1546,	1498,	1471,1455,	1416	874
From alkaline precipitation	1484,	1457,	1420		875
Herzburg (1945)					
Undistorted carbonate ion				1415	879

The bands corresponding to a given vibration mode are not easily resolved and are found over a narrow range of wavenumbers. However the most easily distinguishable difference would appear to be the presence of a peak at around 1550 cm^{-1} for an A type apatite and a peak at 1430 cm^{-1} for a B type substitution. On the basis of IR spectra, changes in lattice parameter have been attributed to different types of substitution location, namely the **a** axis expands and the **c** axis contracts as a result of an A type carbonate substitution and the reverse trend is observed for a B type substitution. Shimoda *et al.* (1990) used this effect to quantify the amount of carbonate in each site. However in light of the reported phenomenon of mixed AB type substitutions and the differences in lattice parameter changes reported, the results of such a technique are questionable.

3.5.4 Effects of Carbonate On Apatite Dissolution

Okazaki *et al.* (1981) demonstrated that the dissolution rate of hydroxyapatite in acid (pH 4) conditions was greatly reduced (~50%) by small amounts of fluoride, (6% in the hydroxyl site). Nelson (1981) showed that carbonate increased the rate of acid dissolution in both precipitated and high temperature hydroxyapatites and was not a size effect. He correlated this effect with the lattice disorder observed in high resolution TEM lattice images. LeGeros and Tung (1983) showed that the extent of acid (pH 5.2) dissolution was directly proportional to the carbonate content. However if fluoride was present at levels of ~2 wt% the effect of carbonate was minimised. After an initial acid exposure, dissolution rates on a second exposure were reduced, the workers inferred that recrystallisation of a carbonate free layer had occurred. Simultaneously Nelson *et al.* (1983) reported a similar increase in acid dissolution with carbonate content. Structurally incorporated fluoride was found to have little effect on dissolution rate at levels of 0.1 wt%, however fluoride levels of 1μg ml^{-1} in the dissolution solution were found to reduce dissolution rates by up to 30%. The recrystallisation of a fluorapatite may have caused this effect.

3.5.5 Effects of Carbonate On Apatite Morphology

Perhaps the first report of a change in morphology due to the presence of carbonate was that of LeGeros *et al.* (1967). At carbonate contents of 0.5

wt% the precipitate of an aqueous reaction at 95°C consists of needles in the order of ~ 1μm in length. At carbonate levels of 15.5 wt % the precipitate was spheroidal and were ~ 100nm in diameter. At 37 and 25°C LeGeros (1967) reported the precipitation product as being very amorphous. This description was made on the basis of XRD patterns that did not display any sharply defined peaks. However no TEM investigations were carried out to discover if the characteristics of the patterns were due to broadening of reflections due to the small size of the crystals. On the basis of high resolution TEM Nelson (1981) described carbonate apatites as having a domain structure that decreased in size to 8nm with increasing carbonate content. It was not clear whether these domains were in fact individual crystals, though he described the presence of what he termed grain boundaries between them. Shimoda *et al.* (1990) found that in neutral conditions the morphology changed from thin ribbons to rods with increasing carbonate content. The authors proposed that carbonate inhibits the **c** axis growth. Cross sections of these rods showed them to be hexagonal but elongated. Though it is tempting to propose that this implies that $\mathbf{a} \neq \mathbf{b}$, this effect could be a due to the section not being perpendicular to the **c** axis, giving the impression that the hexagonal symmetry is non regular. In alkaline conditions the morphology remained acicular with increasing carbonate content. Reducing the concentration of the reactants by a factor of three had the effect of increasing the crystal size by a factor of approximately five. Carbonate had the effect of increasing the thickness of the needles and the aspect ratio tended to one.

Most of the previous investigations on the precipitation of apatites have either been attempting to elucidate a possible mechanism for *in vivo* calcification or to attempt to show evidence for a particular substitution mechanism. This work has to some extent been successful in that the effect of various variables are known to some degree. It would seem unlikely that *in vitro* studies will reveal the complete process as the number of possible variables is so large. With the exception of perhaps only Puajindanetr (1992), no one has looked at the effect of precipitation conditions with a view to improving the precipitate's characteristics for sintering.

4 Processing

Ceramic particles produced from a precipitation route are formed in a liquid. Often this liquid contains unreacted or by product ions in solution. It is usually desirable to remove these ions by washing the precipitate before further processing occurs. Some salts such as ammonium nitrate will sublime and can be removed during a calcination stage, Hayek and Newesely (1963). Removal of superfluous salts by heat treatment during a sintering process is undesirable as bloating may occur as a consequence of volatisation. Precipitation products may be extremely fine and have specific surface areas in the order of 10^3 m^2 g^{-1}. Assuming dissolved ions are likely to interact with the surface of the precipitate, some of the reported washing treatments would appear to be unlikely to remove the majority of the ions present (e.g. Royer *et al.*,1993).

4.1 Ceramic Suspensions

Particles in suspension are subject to various interactions namely: Van der Waals forces, electrostatic repulsion, steric interactions and Brownian motion, of these interactions the first three are more commonly manipulated by the ceramist and are considered in more detail in the following sections. These interactions can result in either particle dispersion called deflocculation or agglomeration or flocculation. Small particles usually <500 nm, (i.e. those kept in suspension by Brownian motion), dispersed in liquids may form colloidal suspensions. Solid dispersions in liquids or solids are termed sols.

4.1.1 Van der Waals Forces

These are attractive forces that exist between molecules. There are three types of Van der Waals forces: between two molecules having permanent electric dipoles, between a molecule with a permanent electric dipole that induces a dipole in a second non polar molecule and induced dipole-induced dipole interactions. It can be shown (Atkins, 1978) for two molecules the interaction energy V is:

$$V = C R^{-6} kT^{-1} \quad (4.1)$$

Where C is a constant, R is the separation distance, k is Boltzman's constant and T is the absolute temperature. It can be seen from Equation (4.1) that the interaction energy decreases as the temperature increases. This equation refers to the theoretical case of an isolated pair of molecules. For a system of molecules the interaction energy decreases as a function of R^2.

4.1.2 Electrostatic Forces

Electrostatic interactions are attractive between unlike charges and repulsive between like charges. The Coulombic potential ø at a distance r from a charge ze is:

$$ø\ (r) = \frac{ze}{4\pi\varepsilon}\frac{1}{r} \quad (4.2)$$

where z is the number of the charge, e is the charge of an electron, and ε is the permittivity of the medium :

$$\varepsilon = \varepsilon_0 \varepsilon_r \quad (4.3)$$

where ε_0 is the permittivity of a vacuum and ε_r is the relative permittivity. For water at 25°C ε_r is 78.5, so Coulombic interactions are reduced in aqueous solution. In an ionic liquid ions of the opposite charge are attracted towards a charged particle so the potential in the vicinity of the particle is shielded by the attracted ionic atmosphere. In this situation the r^{-1} term in Equation (4.2) is replaced by:

$$\frac{1}{r} \exp\frac{-r}{r_d} \quad (4.5)$$

where r_d is the Debye length. When r_d is large, the exponential term tends to 1. The charges around a positively charged particle in an ionic liquid are shown schematically in Figure 4.1.

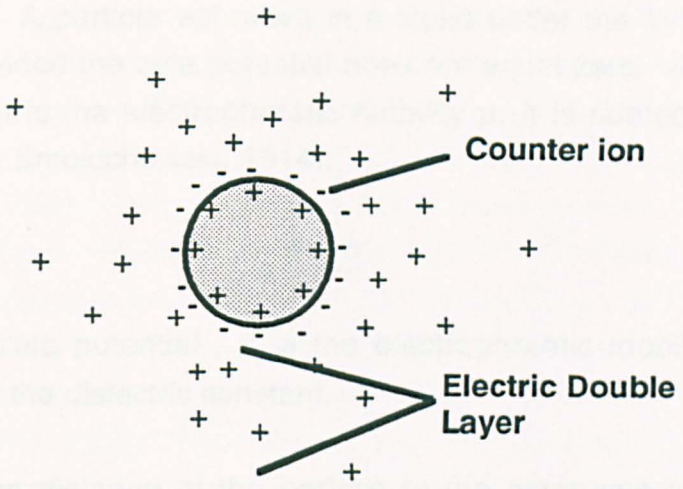

Figure 4.1. Charges around a positively charged particle in an ionic liquid.

In an aqueous solution protons and hydroxyl ions are present. At a particular pH for each system an overall zero charge is obtained known as the zero point of charge (zpc). An increase in pH from the zero point of charge results in a net negative charge and a decrease in pH results in a net positive charge. There are two regions in the double layer, one that is tightly bound and one that is free to move. A slip plane exists at the boundary of these two regions, the potential at this boundary is the zeta potential ζ.

The net interaction energy as a function of separation distance R is shown in Figure 4.2.

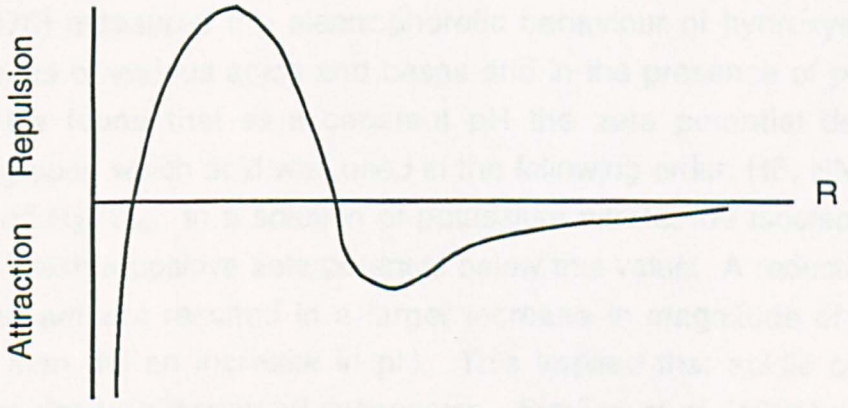

Figure 4.2. Schematic diagram of the net interaction energy as a function of separation distance R.

The pH at which the zeta potential is equal to zero is termed the isoelectric point and is often indistinguishable from the zpc. A double layer is required to effect dispersion. If the double layer is small repulsive interactions are reduced and flocculation occurs. A large zeta potential is often indicative of

a dispersed sol. A particle will move in a liquid under the influence of an electric field provided the zeta potential does not equal zero. A measure of this phenomenon is the electrophoretic mobility μ, it is related to the zeta potential by (Von Smoluchowski, 1914):

$$\zeta = \frac{4\pi\mu\eta}{\varepsilon} \tag{4.6}$$

Where ζ is the zeta potential , μ is the electrophoretic mobility, η is the viscosity and e is the dielectric constant.

A measure of the distance of the particle to the point where the electric double layer becomes negligible is K^{-1}:

$$K^{-1} = \left(\frac{2e\ n_o{}^2\ z^2}{\varepsilon_r\ kT}\right)^{-1/2} \tag{4.7}$$

where e is the charge of an electron, n_o is the concentration of the solution at an infinite distance from the particle, z is the charge number, ε_r is the relative permittivity, k is Boltzman's constant and T is the absolute temperature. At small K the repulsion energy ø is given by:

$$ø = 2\pi ez^2 \exp(-KR) \tag{4.8}$$

where R is the particle separation.

Doss (1976) measured the electrophoretic behaviour of hydroxyapatite in the presence of various acids and bases and in the presence of potassium nitrate. He found that at a constant pH the zeta potential decreased depending upon which acid was used in the following order: HF, HNO_3, HCl, H_2SO_4 and H_3PO_4. In a solution of potassium nitrate, the isoelectric point was ~pH 7 with a positive zeta potential below this value. A reduction of pH by a given amount resulted in a larger increase in magnitude of the zeta potential than did an increase in pH. This implied that acidic conditions would give rise to a dispersed suspension. Simões *et al.* (1991) measured the viscosity of hydroxyapatite slips as a function of pH and found a minimum viscosity at pH8. However, the electrophoretic mobility increased between pH from 5 to 12, implying, from Equation 4.5, that the zeta potential increased in this pH range and this would imply that the viscosity too would decrease with increasing pH. The viscosity is perhaps the best measure of

interparticulate forces as theoretical predictions can often be influenced by overlooked variables. The zeta potential of stoichiometric and calcium deficient apatites was measured over various time periods by Ducheyne *et al.* (1992). They found that the zeta potential varied both as a function of pH and time. The calcium deficient apatite had a large negative zeta potential at high pH, yet the potential approached zeta within one week. At pH 6 the zeta potential was positive and small for short times, but it increased significantly within a day. There was a clear trend of the isoelectric point increasing with time. However for stoichiometric hydroxyapatite the zeta potential reached a steady value within a day and there was no systematic change in ζ with pH. This result was explained in terms of dissolution affecting the characteristics of the counter and electric double layer atmosphere.

The work on the electrical properties does not appear to reveal any obvious trend. It is reasonable to assume that the conditions for dispersion depend on a number of factors that are hard to predict. Dispersion in a given apatite system is probably best determined by experiment.

4.1.3 Steric Interactions

Polymeric molecules with ionic heads, (e.g. 1-alcohols) can cluster around a particle as shown in Figure 4.3.

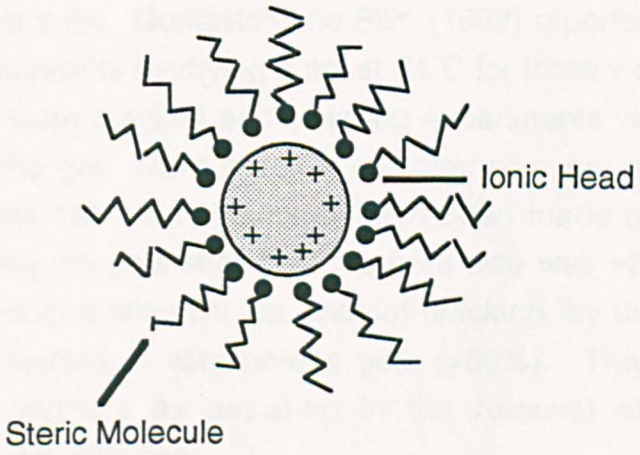

Figure 4.3. Configuration of steric molecules around a charged particle.

The polymeric chains perform the role of the electric double layer as in the aqueous ionic case and repel other particles. It is assumed that during

sintering these organic molecules volatise and no chemical interactions occur either during processing or sintering.

4.2 Monolith Formation

If a liquid is removed from a sol the particles experience changing interactive forces as the separation between them decreases as shown in Figure 4.2. Eventually the stage is reached where the repulsive forces are overcome and attractive Van der Waals forces dominate. The particles then touch one another, this point is termed the gelation point. Liquid loss continues until the gel is dry. If this process occurs in air the product is an xerogel. Aerogels are the product of hypercritical drying, where the liquid and gas phases have the same density. Liquid removal can be effected by a number of methods including: evaporation, dialysis (Scherrer, 1992), evaporation and filtration. Filtration is an attractive route to small monolith formation because formation and gelation can occur simultaneously. The sol-gel process can give rise to powders that are easier to handle than very fine primary particles. Gel monoliths can be formed which are the same shape as the final product. Monoliths are massive homogeneous agglomerates that have sufficient strength to hold their shape before being fired. One of the main problems with the sol-monolith processing route is that monolith geometries are limited by the methods used to form them, additionally monolith size is limited by poor strength and cracking. Klein and Gamey (1982) reported the successful production of alumina monoliths 50mm in diameter and 5mm thick. Gurkovich and Blim (1982) reported the formation of lead titanate monoliths by drying a sol at 34°C for three weeks. However these 'monoliths' were cracked and sintering experiments were carried out on fragments of the gel. More recently complex near net shape silica gel optical components 100mm in diameter have been made by Hench *et al.* (1992). By forming the gels such that the pore size was >200nm the gels could be dried within a few minutes, without cracking, by using microwave warming. This resulted in very porous gels (>80%). These pores were reported by the authors as assisting in the removal of chemisorbed impurities prior to densification.

4.2.1 Filtration

Filtration is the separation of a solid from a liquid phase by means of a membrane permeable to the liquid but not the solid. In the laboratory the Buchner funnel is often used to separate a filtrate from a precipitate and has been used in the preparation of gel fragments of hydroxyapatite by Jarcho *et al.* (1976). Filtration may be effected by slip casting, vacuum and pressure filtration. All these methods work by means of a pressure difference between the slip and the filtration medium.

The pressure difference, Δp, in slip casting occurs by means of the capillary suction of the pores given by:

$$\Delta p = \frac{2\gamma}{r} \tag{4.9}$$

where r is the radius of curvature and γ is the surface energy.

Often the mould is plaster of Paris as this porous material is readily available and easily formed. Plaster of Paris has been estimated as giving suctions of 100-200kPa. The mould must be large relative to the volume of the cast since the capillary phenomenon relies on the condition of non saturation.

Pressure filtration enables the application of a wide range of pressures up to ~ 100MPa (Lange and Miller, 1987). However special equipment is required to contain the slurry at these high pressures. Vacuum filtration provides a pressure difference by the reduction of vapour pressure beneath the filtrate. This is equivalent to the application of a positive pressure above the filtrate. The maximum theoretical pressure difference attainable by vacuum filtration is atmospheric pressure (~ 100kPa).

Filtration behaviour is described by Darcy's law (Darcy, 1856), for fluid flow through a permeable medium:

$$J = \frac{k}{\eta}\,\frac{dP}{dx} \tag{4.10}$$

where J is the fluid flux (volume area^{-1} time^{-1}), k is the permeability (m^2), η is the viscosity of the liquid (1×10^{-3} Pa s for water), dP is the change in pressure over a distance dx. Darcy's law can be rewrittten in terms of the easily measurable fall in liquid level, h, (Philipse *et al* .,1990):

$$\frac{dh}{dt} = \frac{K\Delta P}{\eta\ l\ t} \tag{4.11}$$

where t is time and l is the filter cake thickness. If the slip is homogeneous then the drop in liquid level is proportional to the increase in thickness of the filter cake, i.e. :

$$l_t = C\ h_t \tag{4.12}$$

where C is a constant given by (Lange and Miller, 1987):

$$C = \left(\frac{V_o}{V_l - V_o} \right) \tag{4.13}$$

where V_l, is the particle volume fraction in the filter cake and V_o is the particle volume fraction in the slurry. By integration of Darcy's law it can be shown that:

$$h^2 = \frac{2K}{\eta} \left(\frac{V_l}{V_o} - 1 \right) Pt \tag{4.14}$$

i.e. :

$$h^2 \propto t \tag{4.15}$$

This is known as the Square Law for filtration. If V_l and V_o are known then an estimate for K can be determined from the slope of a graph of h against $\sqrt{t}$. The parabolic relation between time and the thickness of the filter cake limits the usefulness of filtration as a processing route.

A theoretical model used to predict the permeability K is the Kozeny-Carman relation, which models the consolidated layer as a bundle of tortuous capillary tubes with hydraulic diameters resembling slits (Carman, 1948):

$$K = \frac{d^2\ (1-V_l)}{36\ c\ V_l^2} \tag{4.16}$$

where d is the radius of a spherical particle, V_l is the volume fraction of solids in the filter cake and c is a constant (c= 5 for most cases) (Lange, 1989).

Aksay and Shilling (1984) showed that the zeta potential for alumina was a maximum at ~ pH3 and zero at ~pH 9. Slurries of pH 3, 5 and 8 showed the microstructure to consist of domains with a void space between these domains that increased with flocculation, i.e. pH. They reported that linearity of a plot of cake thickness squared against filtration time implied homogeneity in the filter cake. Dispersed slurries resulted in a high packing

efficiency of the filter cake, flocced slurries resulted in an open but homogeneous microstructure. However both compacts sintered to >99% density at 1550°C for thirty minutes.

Compression of the filter cake arises from drag exerted on the particles by the flowing liquid. This drag can result in the break up of agglomerates to some degree. Drag force accumulates by particle contact from a minimum at the slurry / cake interface to a maximum at the cake / filtration medium interface. Filter cakes have a pressure gradient across them that is required for liquid flow, as described in Darcy's law. Incompressible cakes possess a linear gradient and have a homogeneous density distribution. Compressible cakes (i.e. from flocced slurries) have a dense skin at the filtration medium interface, because here the drag force is sufficient to compress the agglomerates. This results in homogeneity in the density distribution and hence in the linear shrinkage during drying, which in turn can cause cracking. Tiller and Tsai (1986) showed that for both compressible and incompressible alumina filter cakes, filtration obeyed the Square Law (Equation 4.15). However this was in contradiction to the previous work of Aksay and Schilling (1984) who reported that only homogeneous microstuctures were obtained from filtration systems obeying the Square Law.

Lange and Miller (1987) reported the pressure filtration behaviour of dispersed and flocculated alumina slurries. They found that the density of filter cakes formed from dispersed slurries was 70± 2% for pressures in the range 0.7 - 80MPa. Flocced slurries showed a linear relation between density and log of the applied pressure, from 45% at 50 kPa, 54% at 1MPa and 62% at 200MPa. Only monoliths formed from flocced slurries at pressures below 1MPa displayed appreciable shrinkage and increased their densities to 54±1%. The authors inferred from this result that the capillary pressure responsible for further consolidation was of the order of 1MPa since this was the pressure required to consolidate the slurry to this density. They found for the flocced slurries that plots of cake thickness squared against time increased in linearity with filtration pressure, which would seem to be in disagreement with Tiller and Tsai (1986). The authors point out that an advantage of pressure filtration is that at an applied pressure of 70MPa the filtration time is reduced by a factor of 500 compared to slip casting filtration periods.

Philpse *et al.* (1990) compared the slip casting behaviour of flocced and dispersed silica and alumina particles. They found that the porosity increased with agglomeration in alumina monoliths but not in silica. Dispersed silica suspensions obeyed the Square Law and the solid fraction of the wet filtercake was 64%, however the agglomerated slurry only obeyed the Square Law at small time periods. At longer times linearity was found between the drop in liquid level, which is proportional to the cake thickness (Equation 4.14). Strangely the solid fraction of the filtercake was the same as for the dispersed case. Dispersed alumina also obeyed the Square Law during slip casting and gave a solid volume fraction of 65%. Aggregated alumina slurries also obey the Square Law in agreement with Tiller and Tsai (1986), and form as expected, a more porous (48% volume fraction) filter cake. Only this filter cake showed any increase in density during drying, (56%), which is very similar to the density obtained by Lange and Miller (1987) for agglomerated alumina slips that displayed shrinkage during drying, (54±1%).

Smith *et al.* (1994) used both mercury porosimetry and small angle and multiple scattering angle neutron scattering (SANS and MSANS respectively) to investigate the pore sizes of filter cakes produced by two alumina slips in different states of dispersion. No information was provided as to how the filter cakes were dried. The SANS data was used to provide a value for specific surface area, from which the authors claim a pore radius can be determined using the equation :

$$SSA = \frac{3}{\rho \; r} \qquad (4.17)$$

where (SSA) is specific surface area, ρ is density and r is radius. This equation assumes the particles to be spherical.

The authors assumed spherical geometry which would be valid for closed final stage or intergranular porosity encountered in sintered ceramics, but not the clearly interconnected pores formed during the drying of a ceramic particle filter cake. Large differences were found between the pore sizes of the green bodies from dispersed and flocculated slurries from SANS data but not in the mercury porosimetry or MSANS results. The SANS and MSANS data were in agreement for the cakes made from dispersed slurries. The authors claimed that this meant that the dispersed slurry gave a green body with a unimodal pore size distribution and the flocced slurry gave a

bimodally distributed pore population which was only detectable using SANS neutron scattering data. However the mercury porosimetry clearly showed the 'flocced' cake to have a bimodal pore size distribution, apparently the authors failed to notice this and concluded that mercury porosimetry does not provide information about the degree of dispersion from which the slip a green body was fabricated. The authors described MSANS as being suitable for pore sizes in the range 80nm - 10μm. As the average pore size detected by mercury porosimetry was > 80nm it is strange that the authors should consider the results from the method to be valid. SANS was reported to be suitable for the detection of features in the range 1nm - 1μm. The only case where the scattering data agreed, within an order of magnitude of the porosimetry data was for the filter cake made from a flocced slurry, porosimetry data was not presented for the other pore sizes determined by neutron scattering, (which coincidentally were in agreement with the particle size to within ± 10%). It is perhaps significant that the 'flocculated' sample showed a higher volume fraction (~30%) and narrower distribution for the major modal pore radius than the broader distribution of the unimodal 'dispersed' case, (~10%). This would tend to suggest that neutron scattering suffers from a low degree of sensitivity, is unable to provide porosimetry information over the full range of interest, (1nm - > 10μm), is complex, relies on very approximate geometrical assumptions and is of dubious benefit to the understanding of the microstucture of gel and filter cake green microstructures.

Nordström *et al.* (1990) reported the slip casting behaviours of a non-specified commercial hydroxyapatite powder and a stoichiometric mixture of calcium hydroxide, water and tricalcium phosphate, which they described as being hydroxyapatite. Monma *et al.* (1981) described the formation of hydroxyapatite from the hydrolysis of TCP as occurring at 80°C in slightly acidic media after two to three hours. Nordström *et al.* (1990) neither referenced this production method nor characterised the product as being apatitic. Perhaps not surprisingly they reported different zeta potentials for the different slips, -17.6mV for the commercial apatite and -9.97 mV for the TCP and calcium hydroxide mixture. They reported that ageing a slip for three day resulted in a 75% decrease in viscosity. The workers did not specify whether this phenomenon occurred in both slips. It would seem probable that if a slow hydrolysis reaction occurred in the TCP calcium hydroxide mixture, then more of the reactants would be converted to hydroxyapatite after longer ageing times. The viscosity would be expected

to increase as the zeta potential approached the larger value for hydroxyapatite. Time dependent zeta potential changes were also reported by Ducheyne *et al.* (1992) and the differences may have been due to dissolution. Deflocculants increased the maximum solid weight percent from 50% with just water to 63% with 1% of polyvinylpyrrolidinone and 2% glycerol. This represents an increase in volume fraction from 16 to 20 %. A typical shrinkage on drying was reported as being 3.6%. This gives an increase in density of around only 2%. However calculations from their linear shrinkage and final density data indicate a green density of 35%. A linear change in sintered density is reported for vacuum sintering for one hour between 1050 and 1300°C, yet a non-linear variation in linear shrinkage is displayed over the same temperature range. Having gone to some effort to determine the effect of some factors on the nature of the slips, the authors do not report any influence of the slip characteristics on the sintering behaviour of the apatites.

Simões *et al.* (1991) slip cast apatite made by the method of Jarcho *et al.* (1976). The viscosity of the slip was a minimum at pH 8. By performing the slip casting with two slips of different pH, pellets were formed with a denser layer. However these pellets are likely to be unsuitable for sintering due to the porosity variation and no possible advantage of differential porosity is presented by the authors.

4.2.2 Drying

Drying is perhaps one of the more overlooked stages of ceramic processing, yet it can have profound effects on the characteristics and structural integrity of a ceramic monolith. Both fluid flow and diffusion occur during drying. Fluid flow in the porous monolith obeys Darcy's law (Equation 4.10). Fick's law states the diffusive flux J is proportional to the concentration gradient of the diffusing species. I.e. (Crank, 1975):

$$J = -D\frac{dC}{dx} \tag{4.17}$$

where D is the diffusion coefficient and $\frac{dC}{dx}$ is the concentration gradient.

Drying can be roughly divided into two stages: the constant rate weight loss and falling rate periods.

Shrinkage

Often during drying shrinkage occurs as the volume of the system decreases as liquid is lost. During this process the liquid meniscus is situated at the surface of the monolith and the rate of water loss is constant. The stresses that result in shrinkage are capillary pressure, disjoining pressure, moisture stress and osmotic pressure.

Capillary pressure:

The decrease in pressure P above a concave surface of a liquid is:

$$P = \frac{2\gamma_{LV}}{r} \tag{4.18}$$

where γ_{LV} is the liquid / vapour surface energy and r is the radius of curvature. The maximum pressure difference occurs when the meniscus of a liquid can fit inside a pore. For a cylindrical pore of radius a, the minimum meniscus radius is:

$$r = \frac{a}{\cos\theta} \tag{4.19}$$

where θ is the contact angle. It can be shown (White, 1982), that the maximum tension is related to the surface area to volume ratio of the pore space, Sp / Vp.

$$Pmax = \gamma_{LV} \cos\theta \frac{Sp}{Vp} \tag{4.20}$$

Disjoining Pressure

Disjoining forces are short range electrostatic forces formed at a solid / liquid interface and the electrostatic repulsion between the electric double layer. These repulsive forces tend to occur as evaporation results in solid surfaces being brought together and liquid is transported from the centre of the monolith to the drying surfaces to prevent solid contact.

Osmotic Pressure

If the pores of a drying body contain an electrolyte, as is often the case with dispersed sols, evaporation of solvent near the surface causes an increase in salt concentration. As a result of the ensuing chemical potential gradient liquid diffuses to the surface, causing a reduction in the pressure of the liquid remaining in the interior, if the pores are small enough to inhibit counter flow.

Moisture Stress

The moisture potential of a liquid in a porous medium Ø is given by (Packard, 1967):

$$\text{Ø} = \left(\frac{RT}{\rho_L \, Vm}\right) \ln\left(\frac{p_v}{p_o}\right) \tag{4.21}$$

where R is the gas constant, T is the absolute temperature, ρ_L is the density of the liquid, Vm is the molar volume of the liquid, p_v is the vapour pressure of the liquid in the system and p_o is the vapour pressure of the liquid over a flat surface. This parameter includes all the driving forces for shrinkage and may be determined by measuring the vapour pressure of liquid ion the system. However it does not distinguish between pressure gradients which induce flow and concentration gradients that induce diffusion.

Constant rate period

During this period the system behaves like a free surface. The evaporation rate E is proportional to the difference betweeen the ambient vapour pressure p_a and the vapour pressure of the liquid in the monolith p_v.

$$E = k(p_v - p_a) \tag{4.22}$$

where k is a constant.

Thus evaporation will continue for as long as $p_v > p_a$. As a result of the tensile forces in the liquid, the solid phase is put in compression and if the network is compliant shrinkage will occur and the menisci will remain at the surface, minimising the creation of higher energy solid / vapour interfaces. As this process continues the solid network becomes increasingly stiff as more solid contacts are formed. This continues until the average radius of

the menisci is small enough to enter the pores, at which point the liquid is exerting the maximum compressive force, and the stiffness of the solid network cannot be overcome.

First falling rate period

During this period the evaporation rate decreases. The liquid enters the pores and is in the funicular condition and so there are continuous pathways through which flow occurs. Simultaneously evaporation occurs and the vapour transport is diffusion controlled.

Second falling rate period

The funicular condition persists for as long as the flow rate is comparable to the evaporation rate. As the distance from the surface to the drying front increases the capillary pressure gradient decreases as does the flux, as described by Darcy's law (Equation 4.10). Eventually the evaporation rate is greater than the flow rate and the liquid near the surface becomes pendicular. At this point the liquid is removed only by evaporation and is known as the second rate falling period. The pore vapour is in equilibrium with the pendicular liquid and the principle transport process is vapour diffusion. As the saturated region recedes inside the monolith the solid network expands slightly due to the removal of the compressive force of the liquid. At the same time the saturated interface tends to contract, as the saturated region becomes thinner, its contraction is inhibited more by the unsaturated region. Simpkins *et al.* (1989) observed that drying cracks in silica gels originated near the saturated interface.

4.2.3 Cracking

As the moisture distribution changes during drying so the stress distribution changes. It can be shown, Scherrer (1989), that the stress in a drying plate is:

$$s_z \approx \left(\frac{L\,\eta E}{2K}\right)\left(\frac{z^2}{L^2} - \frac{1}{3}\right) \qquad (4.23)$$

where L is the half plate thickness, η is the liquid viscosity, E is the evaporation rate, K is the permeability and z is the fractional distance from the centre. The stress increases with the plate thickness and the evaporation rate and a stress will be reached that is in excess of the fracture stress of the network and cracking will occur.

It has been observed experimentally that cracking occurs at the point where shrinkage stops e.g. Classen (1987). A possible explanation for this phenomenon (Hench, 1986) is that wide pore size distributions result in large pores emptying first and the compressive stress in the drying smaller pores causing cracking in the empty large pores.

Cracking can be avoided by increasing the pore size or by decreasing γ_{LV} cos (θ). Surfactants have been shown by Zarzycki *et al.* (1982) to reduce cracking by both lowering the surface energy and by increasing the permeability which in turn reduces the stress (Equation 4.24). The same workers demonstrated that ageing strengthens the network prior to drying. Aggressive environments have been found to accelerate this process. Mizuno *et al.* (1988) found that silica gels could be dried up to five times faster after soaking for twenty four hours in 4M hydrochloric acid or 2M ammonium hydroxide. This method is thought to work by means of a dissolution-reprecipitation mechanism, resulting in larger pores. Hypercritical drying avoids the problems caused by capillary pressures however it is time consuming and requires specialised equipment. The resulting aerogels are often of low density making sintering to full density more difficult.

5 Sintering

Sintering is the densification of a porous green compact at a temperature less than the decomposition or melting temperature of the major phase. During sintering, changes occur to the grain size and shape and the pore size and shape. Two processes may occur during sintering; namely grain growth and densification. The driving force for these processes is a result of the differences in chemical potential of a curved surface compared to one of infinite radius, i.e. a flat surface. This difference can be described by the equation:

$$\Delta\mu = RT \ln a \tag{5.1}$$

Where $\Delta\mu$ is the difference in chemical potential of a material and one in pure standard state, R is the gas constant, T is the absolute temperature and a is the activity. This equation is variously known as the Gibbs-Thompson, Thompson-Freundlich or Kelvin equation.

For vapours a is given by:

$$a = \frac{p}{p^*} \tag{5.2}$$

where p is the pressure of a gaseous component and p^* is the total pressure.

For solutions a is given by:

$$a = \gamma x \tag{5.3}$$

where γ is the activity coefficient and x is the concentration.

It can be shown that for a drop or bubble there exists a pressure difference between the inside and the outside. This pressure difference is given by the Laplace relation:

$$\Delta p = \frac{2\gamma}{r} \tag{5.4}$$

where Δp is the pressure difference, γ is the surface energy and r is the radius and r is positive for a convex surface.

Since $\Delta\mu = \Delta p V_m$, where V_m is the molar volume, from (5.1) and (5.4):

$$\Delta\mu = \frac{2\gamma V_m}{r} = RT \ln a \tag{5.5}$$

$$\Rightarrow a = \exp\left(\frac{2\gamma V_m}{RTr}\right) \tag{5.6}$$

Thus it can be seen that the radius of curvature of a solid or liquid, affects the concentration of a species, such as an impurity or vacancy and the vapour pressure above the surface. In the sintering process this exists as the

negative curvature of a neck formed between two particles, on the particles themselves, as the curvature of a grain boundary or a pore (positive), Figure (5.1).

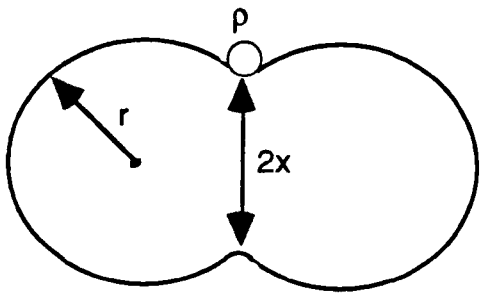

Figure 5.1. Neck geometry between two grains. 2X is the boundary width, r is the radius of curvature of the particle and ρ is the radius of curvature of the neck.

5.1 The Stages of Sintering

A powder compact consists of particles randomly co-ordinated with other particles and a connected network of porosity between them. When heated, necks form at the points of contact. Due to pressure differences at the neck and the particle surfaces, rearrangement of the particles occurs and often this results in a reduction in porosity, as particle packing efficiency is improved. This is termed the initial stage of sintering. As a result of this geometry, a vacancy concentration gradient exists between the neck surface (high) and the particle bulk (lower) and the particle surface (lowest). This results in the approach of particle centres, and a change in geometry. Pores are located along three grain edges and four grain corners and form a continuous network. This is termed the intermediate stage of sintering. As densification proceeds pores become pinched off at four grain corners and form closed porosity. From this geometry until the final density is reached, is termed the final stage of sintering. The various stages are considered in more detail below.

5.1.1 Initial Stage

Studies of model sintering systems were initiated by Kuczynski (1949). Who studied the rate of change in geometry of glass and copper spheres on glass or copper plates as shown in Figure 5.2.

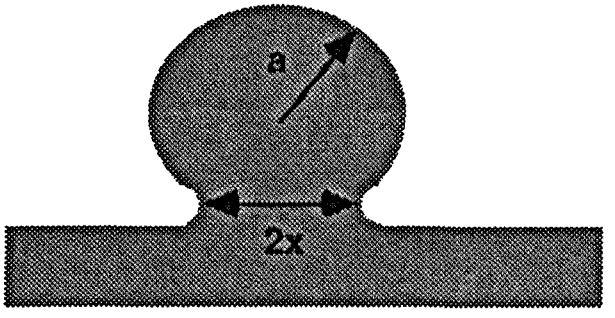

Figure 5.2. Geometry of the Kuczynski experiment.

The following relation was observed:

$$\frac{x^n}{a^m} = kt \qquad (5.7)$$

Where n and m vary for the transport mechanism, as shown in Table 5.1. Only mechanisms 1 and 3 cause densification. Results from such models are of limited value as the Kuczynski model is applicable only to the early stages of sintering, i.e. neck formation.

Table 5.1 Values of the exponents m and n for various mass transport mechanisms.

Mechanism	**n**	**m**
1) Viscous/Plastic Flow	2	1
2) Evaporation Condensation	3	2
3) Volume Diffusion	5	3
4)Surface Diffusion	7	4

Herring (1950) went on to refine the Kuczynski model to include an effect for particle size. He observed that the difference in time taken for a given change in neck geometry for particles t_2 and t_1, Δt was related to the ratio of particle radii (r_2 / r_1), termed λ, by:

$$\Delta t = \lambda^n t \qquad (5.8)$$

Where n=3 for diffusion processes and n= 2 for viscous flow.
The observed neck growth was attributed to the increased vacancy concentration at the convex edge of the neck. It can be approximated from the Gibbs Thompson equation that the vacancy concentration C is given by:

$$C = \frac{C_o 2\gamma\Omega}{akT} \qquad (5.9)$$

where C_o is the vacancy concentration of a surface of infinite radius, γ is the surface energy, Ω is the atomic volume, a is the grain radius, k is Boltzman's constant and T is the absolute temperature.

Role of grain boundaries

Kingery and Berg (1955) proposed the concept of grain boundaries acting as vacancy sinks, connecting the vacancy source to the external atmosphere. They observed that single crystal wires deformed at one hundredth of the rate of polycrystalline wires. Coble and Burke (1963) put forward a model for the first stage of sintering, based on vacancy diffusion, relating shrinkage, to time, temperature and particle size.

$$A\left(\frac{\Delta L}{L}\right) = \frac{BD\gamma\Omega t}{a^m kT} \qquad (5.10)$$

Where ΔL is the change in linear dimension, L is the original length, a is the particle radius, t is the time, T is absolute temperature Ω is the volume of the diffusing species, D is the diffusion coefficient, m, A and B are constants.

Usually the purpose of sintering is to achieve a high density ceramic, so interest has focused more on the intermediate and final stages of sintering.

5.1.2 Second Stage

As pore elimination occurs, the second stage of sintering is reached, where pores are located along 3 grain edges, as shown in Figure 5.3

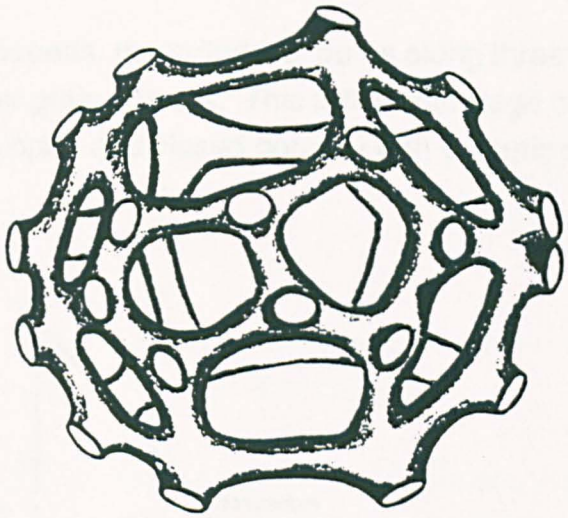

Figure 5.3. Pores around a grain during the second stage of sintering.(Rhines and DeHoff, 1983)

In this stage the porosity is often assumed to be connected and is formed by the system adopting the minimum energy configuration. Coble (1961) constructed models for the second and third stages of sintering, by using the respective geometries of each stage the Gibbs-Thompson relation. He obtained an equation for the rate of change of porosity, P assuming grain boundary diffusion:

$$\frac{dP}{dt} = \left(\frac{2DW\gamma\,\Omega}{kT\,G^4}\right)^{2/3} \qquad (5.11)$$

Where Ω is atomic volume, W is the boundary width and G is the grain size. For the general case of lattice diffusion, another model has been derived recently, by Zhao and Harmer (1991), which is similar to Coble's original model:

$$\frac{dP}{dt} \propto \frac{DN_g\gamma W^{m}\Omega}{kT\,G^n} \qquad (5.12)$$

Where N_g is the number of pores per grain, n and m are constants that vary with the operating mechanism. For grain boundary diffusion control n = 4, m= 1 and for lattice diffusion control m=0 and n =3.

5.1.3 Final Stage of Sintering and Related Phenomena

As densification proceeds, the cylindrical pores along three grain edges close, leaving pores at four grain corners. This is the final stage of sintering.
A typical change in open and closed porosity with ceramic density is shown in Figure 5.4

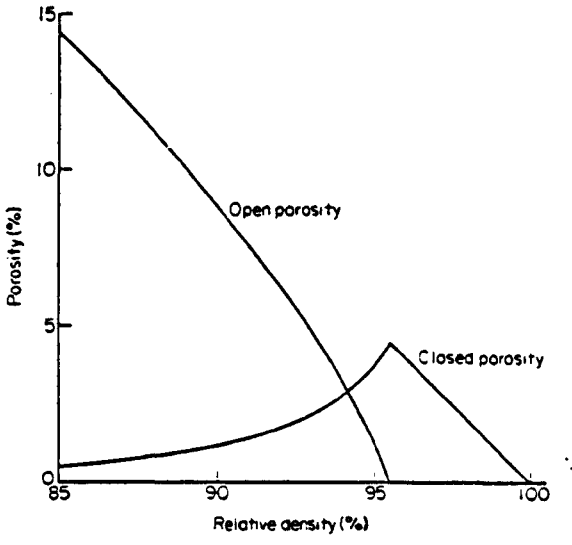

Figure 5.4. Typical changes in open and closed porosity with sintering. (Waldron and Daniell, 1978)

By altering the geometrical assumptions made in his model for the intermediate stage of sintering Coble (1961) derived a model for the final stage of densification (<2% porosity):

$$\Delta P = \frac{6\pi\, DW\gamma\, \Omega t}{\sqrt{2}kT\, G^3} \qquad (5.13)$$

Where ΔP is the change in porosity.

Pore Removal

The ratio of pore size to grain size would be expected to alter the curvature of a pore. When a pore is larger than a grain, concave pore surfaces are formed, and the surface is convex when the reverse is the case, Figure 5.5.

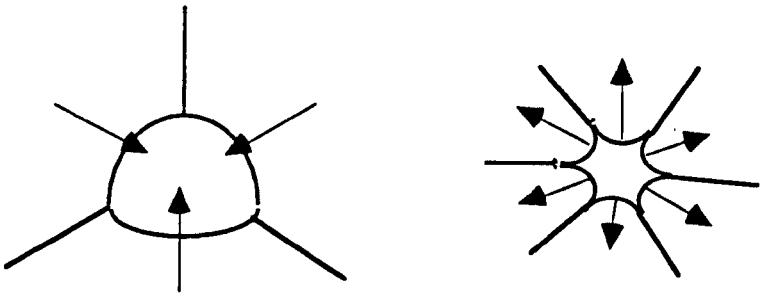

Figure 5.5. Pore geometry dependence on pore size. Pores with convex edges are expected to shrink and pores with concave edges grow.

As grains tend to grow towards their radius of curvature pores smaller than the surrounding grains shrink and those larger tend to grow. This implies that grain growth is necessary for pore elimination. Xue and Brook (1989) observed an increase in densification rate in $BaTiO_3$ during rapid grain growth. They hypothesised that grain growth resulted in a change of pore geometry causing convex pores. However Slamovich and Lange (1992) investigated densification and grain growth in stabilised zirconia powders. Porosity was introduced with diameters between 0.5 and 2μm. Two formulations were used that were known to exhibit rapid and slow grain growth (Lange, 1986). They found that pores of equal size densified faster in the fine grained material, despite having a concave curvature. It was also found that the greater the porosity the greater the densification rate and also the pore number density did not remain constant during sintering implying that shrinkage did not occur uniformly. The authors interpreted this finding in terms of pore coalescence.

Bloating

A phenomenon that may occur during final stage is bloating or volume increase. As the volume of a closed pore decreases, the pressure of non-soluble gases in the pore will increase. Eventually, the equilibrium condition:

$$P = \frac{2\gamma}{r} \qquad (5.14)$$

will be reached. It can be seen from Equation 5.14, that small pores contain gas at a higher pressure than large pores. It is energetically favourable for

gas to be transferred from small to large pores. If pore radii r_1 r_2 r_3 are such that $r_1 < r_2$, and r_1 diffuses to r_2 to form r_3 and have pressures P_1, P_2, P_3 respectively then:

$$\frac{4}{3}\pi r_1^3 P_1 + \frac{4}{3}\pi r_2^3 P_2 = \frac{4}{3}\pi r_3^3 P_3 \qquad (5.15)$$

Substituting 5.14:

$$r_1^2 + r_2^2 = r_3^2 \qquad (5.16)$$

Therefore the total pore volume increases, resulting in the expansion of the ceramic. The mechanism by which this occurs may well be grain growth. Since a small grain is consumed, the pores at its corners coalesce and no gas transport is required. If this process is not active, then the gas must be soluble in either the material or the boundary, leading to the pore growth relation (Greenwood and Boltax, 1962):

$$r_t^2 - r_o^2 = Kt \qquad (5.17)$$

where K is a constant and t is time. K depends on the solubility and diffusivity of the gas. The solubility of a gas in a solid depends upon the pressure and temperature of the gas. Thus a concentration gradient of concentration exists between pores of different sizes. However this assumes that the pore reaches equilibrium state. Pores contain gas molecules and vacancies, since both could be expected to be soluble to some degree in both the lattice and boundary, pore size is likely to be affected by the kinetics of gas solution. In order for a pore to be eliminated, both the vacancies and gas molecules must diffuse, the ratio being of the order of 1000:1. In reality, both the grain growth and gas diffusion mechanisms operate simultaneously. However, Greenwood and Boltax (1962) found that Equation 5.17 described the observed phenomenon of bubble growth observed in irradiated urania after heating at temperatures of between 880°C and 1120°C. Irridation is thought to give rise to increased vacancy concentrations and during heating the vacancies condense to form pores (Tucker, 1979).

Another process by which bloating may occur is by the evolution of gas. If closed porosity has formed at the temperature at which a gaseous phase is formed, then the pressure of the gas may be such that the pores expand until connected porosity is formed, enabling the pressure to be released. Gas may

be formed by decomposition of the solid phase, changes in temperature affecting gas solubility, decomposition of organic residue or by the oxidation or reduction of solid phases in the sample (Wang and Kröger, 1980). Bennison and Harmer (1985) reported the swelling of hot pressed fully dense alumina after annealing in air, but not in a reducing atmosphere of 236 ppm CO_2 in CO at a pressure of 0.1MPa. This gave a partial pressure of oxygen of 10^{-7} Pa. They found that the density increase followed the relation:

$$\rho_o - \rho = K \log t \qquad (5.18)$$

Where ρ_o is the density at time t = 0, and K is a constant. Swelling was attributed to the formation of CO_2 and SO_2 from the oxidation of impurities by oxygen that had diffused down the grain boundaries. The rate of swelling was enhanced by the presence of MgO. Table 5.2 shows some examples of ceramics that have been reported as displaying swelling.

Table 5.2. Examples of ceramics that have undergone swelling reactions, after Bennison and Harmer (1985).

Material	Environment	Density Loss(%)	Mechanism	Reference
Al_2O_3	1900°C /H_2 or O_2	1	Trapped N_2 Grain growth	Warman and Budworth(1967)
Al_2O_3	1600°C /O_2	4	Phase Change	Wang and Kröger (1980)
Al_2O_3	1850°C/ Air	<7	Volatisation of trapped H_20, CO, H_2S	Rice (1969)
UO_2	1700°C/H_2 or H_2O	<10	Reduction of UO_2 by C to form CO_2	Francois and Kingery (1967)
UO_2	1600-1800°C H_2	<6	Decomposition of binder	Amato and Colombo(1964)
CoO	1250°C in air	<17	Trapped gas	Howlett and Brook(1984)
ThO_2	1800°C in air	<12	Oxidation. of C+S	Morgan *et al.* (1976)
ZnO_2	1120°C pO_2 50MPa	<11	Trapped gas	Soloman and Hsu (1980)
CaO	1650°C hot pressed	--	Decomposition of carbonates causing cracking / explosions	Rice (1969)

More recently, Thompson and Harmer (1992) studied the phenomenon of 'microstructural deterioration' in alumina. They found that annealing alumina at 1850°C in reducing atmospheres caused the formation of a cracklike interconnected porosity. They sintered alumina, alumina with introduced porosity and magnesia doped alumina in hydrogen, nitrogen and argon atmospheres. These gases had oxygen contents of 5, 10 and 2 ppm respectively, at room temperature. They found that deterioration occurred in the samples that were not magnesia doped, in hydrogen and in argon and nitrogen atmospheres when carbon powder was placed near the pellet during sintering, to further reduce the oxygen partial pressure. On the basis of microstructural observation they concluded that deterioration was promoted when the ratio of coarsening rate to densification rate was enhanced. Magnesia inhibited deterioration by lowering the coarsening rate. It was concluded that the effect of atmosphere was to control the densification/coarsening rate.

5.2 Grain Growth

Grain growth is a temperature activated process and the driving force for comes from the difference in vacancy concentration either side of a curved boundary as described by the Gibbs-Thompson equation (Equation 5.1). The grain on the convex side would be expected to have a higher concentration of vacancies than the concave side. As a result of vacancy diffusion across the boundary the boundary tends to migrate towards the centre of curvature of the grain. Burke and Turnbull (1952) made a number of experimental observations from hot stage microscopy: a) grain growth occurs by the migration of boundaries, not by the coalescence of grains, b) it is a discontinuous process that may change direction, c) grains can grow, while at the same time being consumed, d) curved boundaries migrate towards its centre of curvature. Grain growth behaviour can be affected by the presence of other phases such as pores and inclusions. The single phase case is considered first.

5.2.1 Single Phase Grain Growth

A grain boundary has a free energy associated with it and so a polycrystalline material will tend towards the reduction of boundary area by means of grain growth. Grain growth occurs by the diffusion of atoms across a boundary and results in the reduction of the total number of grains. The chemical potential can be described:

$$\Delta\mu = \gamma V_m\left(\frac{1}{r_1}+\frac{1}{r_2}\right) \tag{5.19}$$

$$\text{and } \Delta\mu = RT \ln a \tag{5.20}$$

where $\Delta\mu$ is the chemical potential difference between two curved surfaces of radii r_1 and r_2 respectively, γ is the interfacial energy, V_m is the molar volume, R is the gas constant, T is the absolute temperature and a is the activity.

The difference in vacancy concentration is therefore proportional to the curvature of the boundary. Since the diffusion of vacancies can be considered to be a thermally activated process displaying Arrhenius behaviour, it can be shown that the grain growth rate U is given by a relation of the form:

$$U = C\left(\frac{1}{r_1}+\frac{1}{r_2}\right)\exp\left(-\frac{Q}{RT}\right) \tag{5.21}$$

where C is a constant, and Q is the activation energy for diffusion. At a fixed temperature, the exponential term is constant and the growth rate is inversely dependent on the radius of curvature. Beck *et al.* (1948) observed a linear relation between log grain size and log time, implying:

$$D = K t^n \tag{5.22}$$

where D is the grain size, K is a constant, t is time and n is a constant. If the initial grain size was not small then:

$$D^{1/n} - D_o^{1/n} = C t \tag{5.23}$$

better described grain growth, where D_o is the starting grain size and C is a constant. It can be shown geometrically, that n= 0.5 for single phase materials i.e. grain growth is dependent on grain area. Fisher and Fullman (1952) found that the analogous case of the growth of soap bubbles in partial vacuum followed

this behaviour. Grain growth proceeds until a limiting size is reached, the exact size depending upon the system in question.

5.2.2 Impurity Effects

Experimental observation has shown that the exponent of D in 5.23 is often less than 0.5 (Kingery, 1976). So far, it has been assumed that only grains are present. However, a second phase is invariably present and in many cases this may be porosity. Considering the force on a second phase particle (e.g. a pore) exerted by a boundary in Figure. 5.3:

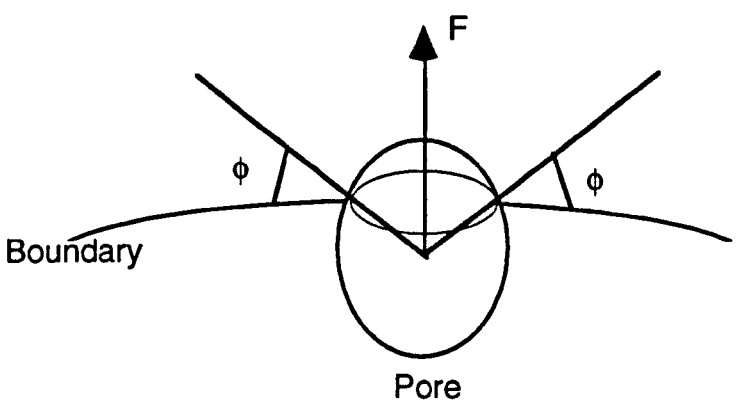

Figure 5.6. Forces acting on a pore on a migrating boundary.

The force on a pore, F, is :

$$F = \pi r \gamma \sin 2\phi. \qquad (5.24)$$

where r is the radius of the pore and γ is the surface energy, ϕ is the angle between the boundary and the conical plane with its apex at the pore centre which passes through the boundary / pore contact line, shown in twodimensions in Figure 5.6.
The force is a maximum when $\phi = 45^{\circ}$.

$$F_{max} = \pi r \gamma \qquad (5.25).$$

Using the stereology relation :

$$Sv = 2 P_L \qquad (5.26)$$

where Sv is the area of surface which intersects of a line cut by this surface P_L times. If f is the fraction of pores per unit volume then the area of spheroidal pores per unit area of grain boundary n, is :

$$n = \frac{3f}{2\pi r^2} \tag{5.27}$$

Assuming each pore exerts its total force then: the total force per unit area of grain boundary F_A is:

$$F_A = \frac{3f\gamma}{2r} \tag{5.28}$$

If equilibrium is reached and the boundary is held by the pores, then by making assumptions about the grain geometry it is found that

$$G \approx \frac{r}{10f} \tag{5.29}$$

where G is the grain size. At this point, grain growth is stopped as the boundaries are pinned by the inclusions. Where an impurity on the boundary controls boundary mobility it has been observed experimentally (Budworth, 1970) that:

$$G - G_o = 2k^{1/3}\ t^{1/3}. \tag{5.30}$$

where k is a constant and t is time.
In other words the grain growth is proportional to grain volume. Grain boundary migration is hindered by porosity, so the time for a given amount of grain growth is increased.

When grain growth is controlled by pore drag, the rate of grain growth at a given temperature can be expressed in the general form (Brook, 1968):

$$\frac{dG}{dt} \propto \frac{N_g}{q\, G^n\, (1-\rho)^m} \tag{5.31}$$

Where G is the grain size, Ng is the number of pores per grain and ρ is the relative density and q, n, and m are constants that are dependent on the diffusion mechanism. For surface diffusion controlled pore drag $q = \frac{1}{3}$, n = 3, $m = \frac{4}{3}$. For lattice and vapour phase diffusion controlled pore drag, q = 0, n = 2, m = 1. For evaporation condensation $q = \frac{-1}{3}$, n = 1, and $m = \frac{2}{3}$.

When grain boundary mobility alone limits grain growth:

$$\frac{dG}{dt} \propto \frac{1}{G^n} \tag{5.32}$$

Where n = 1 for a single phase and n = 2 for grain boundary mobility controlled by solute drag. These relations have been used recently (Thompson and Harmer, 1993) to show that grain growth of alumina in wet and dry hydrogen is effected by surface diffusion control pore drag.

Large inclusions

Large inclusions have been found to retard shrinkage in a number of composite systems e.g. SiC whiskers in Al_2O_3 , (Lee and Sacks, 1990). Sudre and Lange (1992) studied the effect of zirconia inclusions in alumina filter cakes made by pressure filtration of flocced and dispersed slurries. It was found that as the inclusion concentration increased as the shrinkage rate decreased. Cracks and pores were observed to appear between particles during sintering. This effect was attributed to heterogeneity in the green compact and stresses induced by the incompressibility of the inclusions.

5.2.3 Discontinuous Grain Growth

In real systems, grains are not monosized. If larger grains exist, they will grow at the expense of those grains whose growth has been pinned by inclusions. This results in an increase in the driving force for growth of these larger grains and discontinuous grain growth occurs. These larger grains can sweep past pores, resulting in intergranular porosity, which, as a result the increased gas diffusion path length, are not eliminated.

5.3 ATMOSPHERE

Coble (1962a) was the first person to report sintering a polycrystalline ceramic to theoretical density. In order that a ceramic obeys Equation 5.13, two conditions must be satisfied. Firstly, the pores must remain intergranular, therefore no rapid grain growth should occur. Secondly, pores must contain either no gas or a gas that can diffuse freely. Coble (1962b) found that for alumina the appropriate gas can be oxygen or hydrogen.

Vacuum sintering would appear to eliminate this problem in theory. In practise however, it is not only expensive, but also very difficult to eliminate gases. This is because much gas remains adsorbed on the surface of the particles, even after long periods of evacuation. Atmospheric nitrogen is insoluble in alumina and carbon dioxide is even less soluble. Therefore vacuum and air are unsuitable sintering atmospheres. There are two important effects of atmosphere on the sintering of ceramics: it may change the densification rate or the limiting density.

5.3.1 Densfication rate

Onsagar's (1931) relation states:

$$D_V n = D_L N \tag{5.33}$$

where n is the number of vacant lattice sites per unit volume, D_V is the vacancy diffusion coefficient, D_L is the diffusion coefficient of lattice atoms, N is the number of lattice sites per unit volume, D_V and N are constants. Therefore the lattice diffusion constant is proportional to the number of vacancies. Atmosphere can affect the concentration of both species forming Schottky vacancy pairs. From Equation 5.11, the shrinkage rate increases as D increases as the vacancy concentration increases. Kuczynski *et al.* (1959) reported no effect of oxygen partial pressure for the sintering of single crystal sapphire spheres, except in dry hydrogen. Roberts *et al.* (1957) noted different effects in ZnO with oxygen partial pressure with nine nominally pure materials from different sources.

5.3.2 Limiting Density

The effect of atmosphere on limiting density is only observed in the final stage of sintering. At the transition between the second and third stages of sintering, the pores become sealed off at the ambient pressure and the gas becomes compressed as further shrinkage occurs until the condition in Equation 5.4 is satisfied. Shrinkage stops if no gas diffusion occurs. At a slightly higher diffusivity, bloating occurs by pore agglomeration. At even higher diffusivities the pores continue to shrink and shrinkage rate is controlled by the kinetics of gas diffusion. At a sufficiently high diffusivity, the shrinkage is independent of the gas but may depend on its pressure in that it may affect the defect structure.

Coble (1962b) found that shrinkage rates of alumina did not vary in hydrogen or oxygen atmospheres in which 99.5% dense alumina was produced. He found that air, nitrogen, helium and argon did not diffuse out of alumina and resulted in 98% dense ceramics. Mocellin and Kingery (1973) observed that in dry hydrogen, pores were confined to the grain boundaries but in nitrogen and oxygen they were located intergranularly. They concluded that a reducing atmosphere prevented pore/boundary breakaway. In oxide systems a reducing atmosphere has been found to raise the rate of grain growth. In a reducing atmosphere (dry hydrogen) , the particle coarsening rate of ZnO is increased so much that densification is effectively inhibited and a coarse porous compact is produced (Quadir *et al.*, 1989). Thompson and Harmer (1993) found that densification of alumina in wet and dry hydrogen is controlled by grain boundary diffusion and grain growth is by means of surface diffusion controlled pore drag. At an oxygen partial pressure of 3×10^{-17} atm, (3×10^{-12} Pa), (dry hydrogen) the coarsening densification ratio was 2.5 times that in a oxygen partial pressure of 10^{-10} atm, (10^{-5} Pa), (wet hydrogen) and resulted in a ceramic with a limiting density of 96.5% compared with 99% in the wet atmosphere, i.e. th less reducing atmosphere. The oxidizing nature of atmospheres have been shown to influence the final density of urania. Urania containing excess oxygen e.g. $UO_{2.14}$ sinters to a higher density than a more stoichiometric material (Burke, 1962).

Water vapour pressure was found to increase the rate of shrinkage of BeO by Aitken (1960). He concluded that a competition exists between vapour transport and diffusion. Vapour transport occured by means of the formation of $Be(OH_2)_{(g)}$ and the neck between the particles could grow by either diffusion (and shrinkage occurs) or by vapour transport (where no transport occurs). As the neck grows

the driving force for material transport is decreased. The dominating mechanism was dependent on temperature and water partial pressure.

ZnO is a non stoichiometric oxide with an excess of zinc ions and the densification rate of sintering is dependent upon the partial pressure of oxygen, below a certain upper limit. Water vapour enhances the densification, and nitrogen retards it (Dollimore and Spooner, 1971). More recently experiments on the effect of wet and dry CO_2 and O_2 atmospheres showed that carbon dioxide retards sintering. It was postulated that surface adsorbed carbon dioxide formed ZnO_3 (Yasumoto, 1984). The presence of water vapour increases the densification rate even in the presence of carbon dioxide. Results of a molecular modelling study by Vila *et al.* (1994) suggest that both water and carbon dioxide are surface adsorbed. The workers claimed that sintering was enhanced due to the formation of $Zn(OH)CO_3H$., though they did not state the mechanism by which this species enhances densification rate.

5.4 GREEN DENSITY

Coble (1961b) found that in the range 42 -47% green density there was no difference in observed grain sizes during sintering experiments. Bruch (1962) studied the effect of green density on the isothermal intermediate and final stage densification rate of alumina. He found that densification rate was highly dependent on green density and decreased with increasing green density. Greskovich (1972) studied the initial stage sintering behaviour of alumina during isothermal experiments and he found that at green relative densities of between 0.42 and 0.50 there was no difference in densification rates, but it decreased between 0.31 and 0.40. Occionero and Halloran (1984) found that the shrinkage rate of alumina between 1-10% during isothermal sintering was independent of green density between 0.49-0.55, but the pore size distribution and the density at which grain growth commenced were affected. They concluded that as the green density increased, the density at which grain growth commenced was increased. Mohamed and Rahaman (1991) conducted constant heating rate experiments on ZnO at 4°C min^{-1} up to temperatures of 1100°C and measured shrinkage using loaded dilatometry. They found that the densification rate at any temperature increased with increasing green density. The effect was more noticeable at relative densities of below 0.8 and above 0.8 the densification rate was only weakly dependent on green density.

5.5 EFFECT OF TEMPERATURE ON HYDROXYAPATITES

During heat treatment of hydroxyapatite, a number of changes may occur, e.g. decomposition, the reaction with other phases present and of particular interest any carbonate present may decompose or change location in the lattice.

5.5.1Phase Changes

It is important that after sintering the ceramic consists solely of hydroxyapatite. A number of factors may influence the decomposition behaviour of apatite and they are examined in more detail.

Effect of stoichiometry

The amounts of calcium and phosphorus in hydroxyapatite can deviate significantly from the stoichiometric molar ratio of 1.67. Values as low as 1.62, (deWith *et al.*, 1981), and as high as 1.69 (Akao *et al.*, 1981) have been reported. However calcium phosphorus ratios alone can be misleading. Driessens *et al.* (1983) reported a calcium phosphorus ratio of 2 for an AB type carbonate apatite. As the occupancy of the B site was diminished, higher values were obtained. Ratios in terms of Ca'/P' where Ca' = Ca+X where X is a metal ion substituent, and P' = P+ CO_3 were given by Nelson and Featherstone (1982) for carbonate apatites and are a more informative indication of stoichiometry.

When non-stoichiometric hydroxyapatite is heated it tends to form a mixture of stoichiometric apatite and another phase, for example, tri-calcium phosphate (TCP) in calcium deficient cases (Ishikawa *et al.*, 1993) and calcium oxide in the calcium excess case (Royer *et al.*, 1993). The reasons for non stoichiometry in the starting material are unclear as different variables are reported to be responsible. Jarcho *et al.* (1976) reported that ageing time is critical and must be longer than seven hours at room temperature for a stoichiometric product. Royer *et al.* (1993) and Jarcho (1978) indicated that the calcium phosphorus ratio of the starting solutions will influence the ratio in the precipitate. A decrease in precipitation temperature was reported to decrease the calcium phosphorus ratio by Ishikawa *et al.* (1993). This effect is more likely to be related to the rapid reduction in ageing times as temperature

is increased, from 7 hours at room temperature to 10 minutes at boiling point Jarcho (1978). The uncertainty of the effect of various preparation variables makes a comparison of the different methods futile.

Phase Transformation Temperature

Calcium phosphorus ratio is thought to affect the temperature at which decomposition occurs. For a ratio of 1.65 Young *et al.* (1981) observed decomposition at 1000°C. At a higher ratio (1.69) a higher decomposition temperature (1100°C) was recorded by Wang and Chaki. (1993). These workers also noted that, in vacuum, the temperature of decomposition was decreased to 1000°C, in water vapour decomposition did not occur at 1300°C. Monma *et al.* (1981) showed a linear relation between the amount of TCP produced after one hour at 1000°C and the calcium phosphorus ratio, from 100% at 1.5 and 0% at 1.67.

Effect of atmosphere

TCP conversion has been reported (Wu and Yeh, 1988) as occurring by means of a reaction whereby stoichiometry is restored by the formation of tricalcium phosphate and water. If this reaction does occur then the presence of water would be expected to inhibit the formation of TCP from LeChatelier's principle. Some degree of bloating would be expected if the compact had developed closed porosity before decomposition was complete and water was not soluble in apatite. De With *et al.* (1981) sintered a Merck powder in wet oxygen for 6 hours and found TCP at 1150°C where the compact was 82% dense and no bloating occurred. Wang and Chaki. (1993) observed bloating in the vacuum and air atmospheres. Jarcho *et al.* (1976) reported a decrease in translucency above 1150°C which they attributed to the decomposition of the apatite. In other work either the decomposition temperature was not measured e.g. Royer *et al.* (1993) or the density was not given as a function of time or temperature e.g. Fang (1993).

5.5.2 Effect of other phases

The presence of other ions has been shown to decrease the temperature and degree of transformation of hydroxyapatite in glass composites (Knowles *et al.*, 1993: Knowles and Bonfield, 1993). Wu and Yeh (1988) reported the effect of the lowering of the transformation temperature in zirconia composites. They detected the presence of both TCP and a mixed oxide of calcium and zircon ($CaZrO_3$) and proposed this reaction to require the formation of water. They explained the low densities attained for their composites (50-70%) in terms of bloating due to water evolution. They also found that by increasing the particle size of the ZrO_2 relative to the apatite in the green compact, higher densities were obtained. This would suggest that different sintering mechanisms were responsible rather than water vapour as these compacts were likely to have had mainly open porosity. Knowles *et al.* (1993) did not measure the density of their composites. On the basis of the reports of these workers it can be concluded that certain cations can promote the formation of TCP.

The effect of the HPO_4^{2-} ion.

The phenomenon of TCP formation is further complicated by the effect of the HPO_4^{2-} ion, which has been observed to be present in calcium deficient apatites (Monma *et al.*, 1981 and Yubao *et al.*, 1994). This ion can be detected by an infra red (IR) band at 860 cm^{-1}. Above 200°C a change in the position of the band to 720 - 750 cm^{-1} has been attributed to formation of the pyrophosphate ion $P_2O_7^{2-}$. Between 800 and 900°C this ion reacts with the apatite to form TCP. Monma *et al.* (1981) and Nelson and Featherstone (1982) are among the few workers who have indicated whether the presence of this ion was checked during their characterisation.

5.5.3 Formation of oxyapatite

Hydroxyapatite is reported to remain hydrated at temperatures greater than 900°C (Kijima and Tsutsumi, 1979) and above 1200°C (Zhou *et al.*, 1993). The evidence for the existence of oxyapatite is largely based on the decrease in intensity of the hydroxyl IR band at 3570cm^{-1} and a decrease in the unit cell

parameter **a**, (Trombe and Montel, 1978). The reaction for the dehydration is thought to be:

$$Ca_{10}(PO_4)_6(OH)_2 \text{ <-------> } Ca_{10}(PO_4)_6(OH)_{2-x}O_x + xH_2O \qquad (5.34)$$

This reaction requires the formation of water, thus one would expect bloating to occur if closed porosity were present and the rate of diffusion of water in hydroxyapatite was sufficiently low. This reaction ought to lie more to the side of the reactant, if water were present in the atmosphere. Kijima and Tsutsumi (1979) observed a decrease in density between 1250 and 1350°C. Wang and Chaki (1993) noted a decrease in the temperature at which bloating commences as the water content of the gas decreases. However the results of Wang and Chaki seem inconsistent with other workers e.g. Jarcho *et al.* (1976) and Akao *et al.* (1981) who report maximum densities over 90%, in that their maximum density was only 78%. This implies that perhaps their density measurement was inaccurate as bloating would not be expected to occur in compacts of such low density. It is perhaps noteworthy that these workers report the theoretical density of hydroxyapatite as being 3.08 Mg m^{-3}, 98% of the value normally reported, (Appendix 2).

5.5.4 Effect of heat and atmosphere on the carbonate ion in apatite.

A Type

Young *et al.* (1981) have shown that the hydroxyl and carbonate group are interchangeable at 1000°C by means of the mechanism:

$$CO_2 + 2(OH^-) \text{ <--------> } CO_3^{2-} + H_2O \qquad (5.35)$$

Carbonation of this site may reach a maximum of 85% after which a separate phase is produced (Elliot,964). Driessens *et al.* (1983) formed mixed AB type apatites by heating a mixture of calcium carbonate and calcium hydrogen phosphate in a mixture of gasses that was 99.4% carbon dioxide 0.6% water at 870°C. It is not clear whether this was the gas composition at the furnace temperature or at room temperature. These mixtures were heated until a constant composition was obtained. On the basis of chemical analysis a mechanism for substitution was derived whereby three carbonate ions substitute for three phosphates forming vacancies at two calcium sites and

one hydroxyl site. By assuming this model to be correct, the workers determined a value for the equilibrium constant of Equation (5.35) at 870°C:

$$Kp = \frac{[CO_3^{2-}][Vac^*]}{[OH]^2}\frac{pH_2O}{pCO_2} = 1.4 \times 10^{-4} \qquad (5.36)$$

* As not all workers subscribe to the model proposed by Driessens *et al.* (1983) e.g. Nelson and Featherstone(1982), Labarthe *et al.* (1973) the term [Vac] refers to the overall vacancy concentration affected by the substitution.

From (5.36) it can be seen that at a given temperature, assuming [OH] is large compared to the extent of substitution:

$$\frac{pCO_2}{pH_2O} = C\,[CO_3^{2-}]\,[Vac^*] \propto [CO_3^{2-}]^2 \propto [Vac^*]^2 \qquad (5.37)$$

Where C is a constant.

Thus the ratio of carbon dioxide and water in the atmosphere will affect the extrinsic vacancy concentration of the apatite. This fact is the basis of the use of porous hydroxyapatite as a carbon dioxide sensor by Nagai *et al.* (1990).

B Type

The loss of B type carbonate in apatite on heating is thought to occur by means of the ion changing site to the A position. The ion would then be lost or exchanged in a mechanism as for an A type carbonate apatite. Evidence for this mechanism has been the change in relative intensities of the characteristic A and B type IR peaks on heating a B type apatite in air, followed by a diminishing of the intensity of the A peak (Holcombe and Young, 1980; Vignoles *et al.*, 1987). Young *et al.* (1981) reported the increase in intensity of the B type peak after heating a B type apatite in dry carbon dioxide at 1000°C. Stoichiometric HA does not develop B type carbonate during heating in carbon dioxide.

The equilibrium carbonate content of both A and B type apatites would be expected to depend upon the ratio of the partial pressures of water and carbon dioxide present in the atmosphere and the value of the equilibrium constant in 5.36. Assuming that the loss of carbonate is essentially a thermally activated diffusion process, then the rate R, at which equilibrium is achieved may given by the relationship :

$$R \propto \exp\left(\frac{-E}{RT}\right). \qquad (5.38)$$

Where E = Ex, the activation energy of A site carbonate loss. For B type loss E = Ex + Eab, where Eab is the activation energy of carbonate diffusion from a B to an A site. From 5.38 an estimate for the value of E can be determined for an AB type apatite from:

$$\text{Ln } K = -E/RT \qquad \therefore \qquad E = 84 \text{ kJ mol}^{-1}. \qquad (5.39)$$

Where K is the equilibrium constant, R is the gas constant and T is the temperature. At extreme temperature ranges the rate of carbonate exchange would appear either imperceptible or instantaneous. At intermediate temperatures carbonate loss or gain would be time dependent. The actual situation is perhaps a little more complex than is suggested. Tooth enamel is a mixed AB type apatite. When it is heated at 400°C in water vapour no carbonate is lost from either site yet it is lost from both sites when heated in dry nitrogen at 100°C (Holcombe and Young, 1980). Lopes *et al.* (1990) found that Merck powder contained carbonate ions, (the actual quantity was not determined), when calcined at 1150°C for sixteen hours. Carbonate was not substituted in the calcined powder after being heated in wet carbon dioxide at 1150°C for sixteen hours. The moisture content of the carbon dioxide was reported as being 91kPa. Presumably this is the partial pressure at room temperature. This result would imply that water vapour inhibits the substitution of carbonate.

Carbonate Contents During Sintering

During the sintering of a porous compact the rate of carbonate exchange may also be dependent upon the rate of gaseous diffusion through the compact. In the final stage of sintering the rate of lattice or boundary diffusion may alter the rate of carbonate loss. Suwa *et al.* (1993) found a 60% loss in the carbonate content of a carbonate hydroxyapatite powder heated in air for three hours at 900°C, whereas a compact which was 60% dense having bloated from a higher density at a lower temperature showed only a 26% loss. As the compact was highly porous, it is expected that the difference in loss is attributable to the difference in surface area. Ellies *et al.* (1988) reported three carbonate losses after sintering in carbon dioxide and nitrogen at three different temperatures with an unspecified amount of water vapour present.

This data is for only three samples each with different carbonate contents and is in no way comparative. Doi *et al.* (1993) clearly showed the time dependence of carbonate loss during heating in dry argon. For an 8wt% carbonate apatite differences in mass loss with heating rate become apparent at 600°C, whereas for an 11.8 wt% carbonate apatite compact of similar density (~90%) the difference occurred at the higher temperature of 700°C. This implies that the carbonate content has a dominant effect upon the rate of carbonate loss at temperatures in the range 600-700°C.

5.6 Sintering Hydroxyapatites

Probably the first worker to sinter a dense apatitic ceramic body were Levitt *et al.* (1969), who hot pressed powdered fluorapatite mineral. Monroe *et al.* (1971) successfully sintered a synthetic commercial apatite, Tribasic Powder (J.T. Baker and Co. Phillipsburg N.J.). The Ca/P ratio was reported as being 1.54, and the powder had an XRD pattern characteristic of hydroxyapatite. Pellets were sintered for 15 hours at 1300°C and formed white translucent ceramic that was a mixture of hydroxyapatite and TCP. Hydroxyapatite ceramics can be prepared by the sintering of dried slurries and compacted powders, (de Groot, 1983). The former method is more often used for the production of macroporous ceramics.

This section is a review of the various preparation methods used for the production of sintered hydroxyapatite. Different green states and green densities are reviewed. Reported effects of sintering atmospheres and grain growth experiments are examined. Finally methods for the formation of translucent apatites are reported and a brief introduction to the optical properties of polycrystalline ceramics is included.

5.6.1 Preparation Method

The preparation method of hydroxyapatite powders will affect their subsequent properties by influencing impurity concentrations and the size and morphology of the apatite crystals. Accepting a general requirement for sintering to be a pure starting material of narrow size distribution and small particle size, the various preparation routes can be evaluated as to whether or not these criteria would be expected to be met.

Solid state reactions would appear unsuitable as the degree of reaction depends upon the homogeneity of mixing and crystal growth would be expected at the temperatures used (~1000°C). The method of Lehr *et al.* (1967) is the reaction of TCP and calcite in an atmosphere of equal volumes of water and nitrogen at 1200°C for three hours. Rootare *et al.* (1978) reported the presence of carbonate and unreacted TCP after following this reaction route. Nelson and Featherstone (1982) also employed this method and washed unreacted calcium oxide away with triammonium citrate as described in the original report by Lehr *et al.* (1967). At best, these procedures are time consuming and unsuitable for the production of hydroxyapatite for sintering.

Methods involving apatites used in sintering studies tend either to be based on the hydrolysis of TCP (Monma *et al.*, 1981), or brushite (Monma and Kamiya, 1987), or the addition of phosphoric acid to calcium hydroxide, as used by Wu and Yeh (1988), Akao *et al.* (1981) or the method of Hayeck and Newesely (1963).

Products from the hydrolysis of TCP form a mixture of TCP and hydroxyapatite at 800°C while above 1000°C 100% TCP is formed. The hydrolysis of brushite is a two stage process. The first product is a calcium deficient apatite that is "matured" or made stoichiometric by the addition of calcium chloride. Haye k and Newesely (1963) specifically stated that the use of chloride salts is not advisable due to the formation of chlorapatite. This method has been employed by Fang and Agrawal (1993).

Many reports of the production of translucent, (implying low porosity), apatite have a precipitation method in common, e.g. Jarcho *et al.* (1976), Uematsu (1989), Wakai *et al.* (1990), Agrawal *et al.* (1992), Fang and Agrawal (1992), namely those based on that by Hayeck and Newsley (1963). The reason for this is not clear and although the difference in translucency of sintered apatites from different routes has been remarked upon by Agrawal *et al.* (1992), no explanation has been reported. Fang (1994) attributed this phenomenon to the stoichiometry, purity and thermal stability of hydroxyapatite produced by this method. Another precipitation method often used is the reaction between calcium hydroxide and phosphoric acid. Although there are no reports of a translucent ceramic being produced by this method, there is no reason to suspect this method of being in any way inferior to the Hayek and Newesely method. As this reaction is an acid base reaction

no additional ions are present in solution and one might expect a purer product.

5.6.2 The Green State

Many workers conducting sintering studies of hydroxyapatite have calcined their precipitates before sintering, (Kijima and Tsutsumi, 1979; Fang *et al.*, 1991; Akao *et al.*, 1981; Wu and Yeh, 1988; Hermansson, 1990), at temperatures between 600 and 900°C. One would expect this treatment to increase the particle size prior to sintering. Although the effect of particle size on the densification rate of hydroxyapatite has not been reported, it would be reasonable to expect its densification behaviour in the second and third stages of sintering to follow that proposed by Coble (1963), as described by Equations 5.11 and 5.13. This relation effectively predicts a decrease in densification rate with an increase in particle size. If high density is desirable, it is necessary to maximise the densification rate relative to the coarsening rate (Wu *et al.*, 1984). Both of these mechanisms are sensitive to particle size, the actual effect depending upon the densification and coarsening mechanisms in operation in hydroxyapatite. As no-one has reported even a tentative proof for the mechanism of either process, calcining merely introduces a unquantified variable of unknown effect into the reported studies, though has the obvious practical advantage of improving the ease of handling of the material.

Doi *et al.* (1993) were among the few workers who used freeze dried hydroxyapatite powders. However their work did not include a powder dried by any other method for comparison, so no particular advantage of this processing method was apparent in the report.

The sol gel method was reported indirectly by Jarcho *et al.* (1976) and again by Jarcho (1978). Although the name sol gel is not used to describe their method, the precipitate is described as gelatinous. The term filter cake is used to describe what is presumably a gel monolith. Uematsu *et al.* (1989), compared the sintering behaviour of a gel formed by centrifuging a suspension at 2000 r.p.m. and that of a powder compact formed by pressing the gel at 100MPa. Sintering was by hot isostatic pressing (HIP) at 100MPa for two hours at temperatures between 700°C and 1000°C. They found that the powder compact sintered to full density at 800°C whereas the gel still

contained residual porosity. This difference is attributed to a reduction in agglomeration of the powder compact. However, since no comparison of green density between the gel and powder compact was made, this conclusion was by no means proven.

5.6.3 Green Density of Powder Compacts

Most workers reported details of the pressure used in powder pressing. However few gave details of the resulting green density. Figure 5.7 shows some of the reported green densities attained for various compaction pressures. The results of Fang *et al.* (1992) are of particular interest as they demonstrate an effect of particle size on green density.

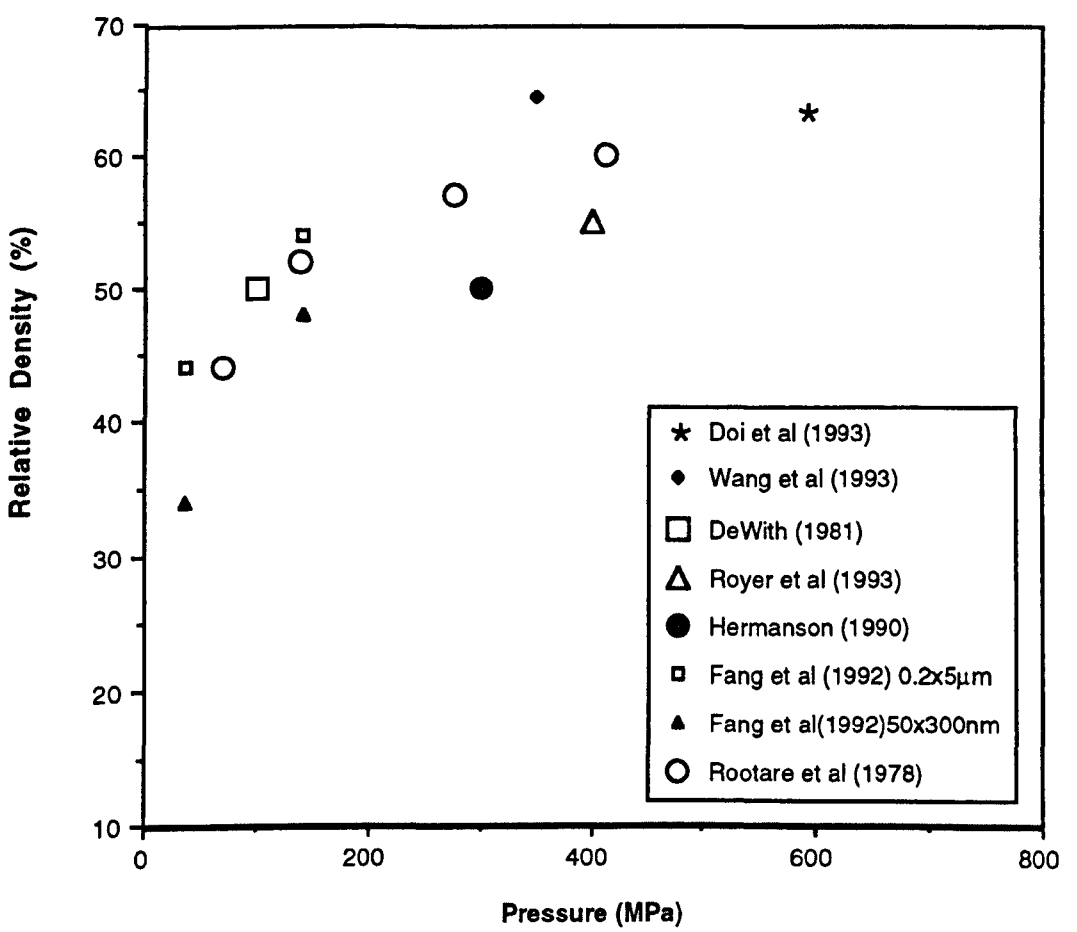

Figure 5.7. Effect of compaction pressure on green density of apatite compacts.

It would appear that a smaller particle size results in a lower green density, though this effect diminishes with increasing pressure. The spread in the results is therefore attributed to variations in particle size. The increase in green density is less pronounced at higher pressures (>300MPa) than at lower pressures.

5.6.4 Sintering Methods

By far the most common method used for the sintering of hydroxyapatites is heating by means of an electric furnace in air at atmospheric pressure. Heating rates using this method are usually up to 5°C min^{-1}, and is limited by the maximum rate at which heat can be transferred from the element to the sample. Aoki (1991) claimed to have been the first person to have sintered hydroxyapatite without decomposition using hot pressing, as described by Aoki *et al.* (1973). The workers found that the temperature at which sintering commenced was not affected by pressure, but the temperature at which densification terminated was decreased from 1225°C at 0Pa, to 900°C at 70MPa. A variation on this technique is HIP. Transparent hydroxyapatite can be produced by sintering at 160 MPa at 1100°C, Aoki (1994). With the exception of microwave sintering, and the work of Jarcho *et al.* (1976), translucent or transparent hydroxyapatite has been produced by hot isostatic pressing, (Section 5.8). Microwave sintering of hydroxyapatite has been carried out by a group at Pennsylvania State University, mainly Fang, Agrawal Roy and Roy,(1990, 1991). The first report of successful microwave sintering of hydroxyapatite was by Fang *et al.* (1990). The advantage of microwave sintering is that sintering times are reduced to tens of minutes, instead of hundreds of minutes. The disadvantage is that only small samples can be produced and the equipment is complex. Fang *et al.* (1991) reported the effect of green density, powder morphology and sintering temperature. The results obtained, discussed in other sections, were compared with conventional heating with a heating rate of 5°C min^{-1} with a two hour dwell and lower densities were obtained. Agrawal *et al.* (1992) produced powders by means of the hydrolysis of TCP, brushite and from a method similar to that of Jarcho *et al.* (1976). Only material produced by this method resulted in a translucent ceramic. Grain sizes of conventionally heated apatite were up to twice those of the microwaved material.

5.6.5 Effect of atmosphere

The effect of atmosphere on chemical changes of apatites has been reported in Section 5.3. Despite the quantity of work describing chemical effects, few workers have compared the effect of different atmospheres upon the sintering behaviour of apatites. Lopes *et al.* (1990) noted an enhanced densification for pellets, 50% green relative density, of Merck powder sintered in wet carbon dioxide (85%), compared with material sintered in air (75%), at 1050°C. These workers reported a partial pressure of water of 91kPa for the moist carbon dioxide atmosphere. Carbonate groups were substituted into the structure as determined from infrared data.

5.6.6 Effect of Green Density

The effect of green density on sintering behaviour has been investigated by some workers e.g. Fang *et al.* (1991). However due to differences in preparation method, heating rates, times and temperatures results from one report to another are rarely comparable. Generally one might reasonably expect an increase in green density to reduce the time required for a given relative density to be reached at a given temperature. As the vast majority of sintering experiments on hydroxyapatite have been isochronal, the effect of a decrease in green density is more likely to manifest itself as a reduction in the temperature at which a given relative density is attained.

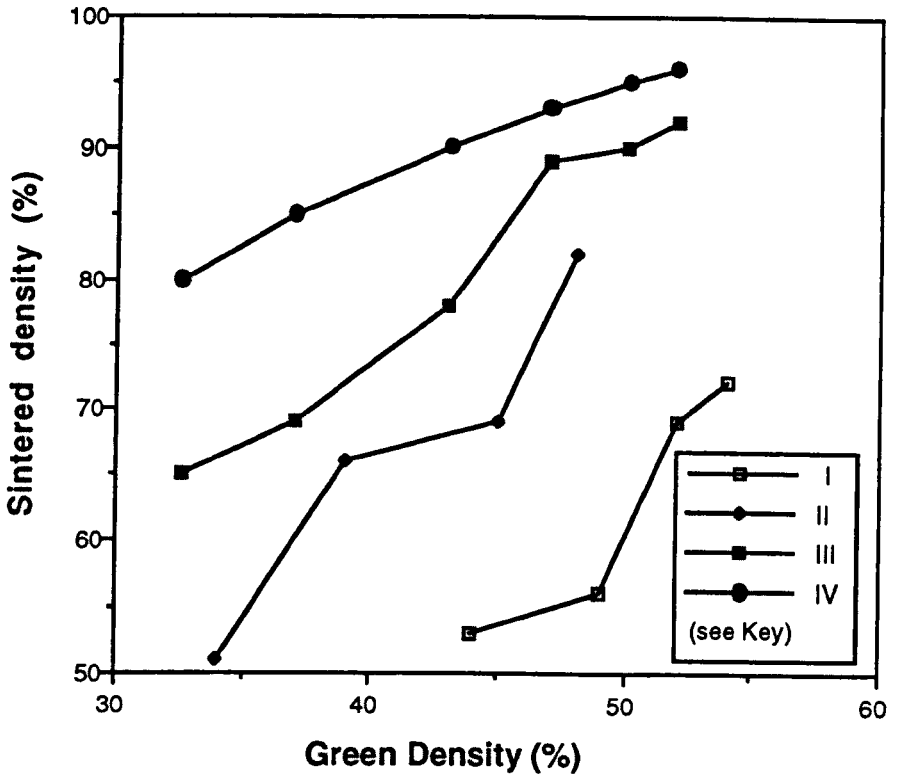

KEY

	Reference	Preparation Method	Temperature(°C)	Time(min)
I	Agrawal *et al.* (1992)	Hydrolysis TCP	1150	1
II	"	" Brushite	1150	1
III	Fang *et al.* (1994)	" Brushite	1200	10
IV	"	" "	1300	10

Figure 5.8. The effect of green density on sintered density for apatites from different preparation routes sintered by microwave heating at different times and temperatures.

Figure 5.8 clearly shows that green density has a significant effect upon the sintered density within a given time. This effect is less apparent at high temperatures, presumably because the rate of densification is increased. Differences may be seen between powders derived from different routes and this is may be attributed to the differences in the particle size. Hydroxyapatite derived from TCP being approximately ten times the linear dimension of that derived from Brushite, i.e. one thousand times the volume. This implies that a decrease in particle size results in an increase in densification rate.

5.6.7 Grain Growth Experiments

Isochronal

Since hydroxyapatite was first sintered to produce a dense material for biomedical applications (Aoki, 1973; Jarcho *et al.*, 1976), a number of workers have studied its sintering behaviour, e.g. deWith *et al.* (1979), Best (1990), Fang *et al.* (1993). The Hall-Petch relation between strength and grain size has been observed in polycrystalline ceramics (Knudsen, 1959) A knowledge of grain growth behaviour is therefore desirable if mechanical properties are to be optimised.

The rate of grain growth can be described by an Equation of the form :

$$\frac{dG}{dt} = C \exp(-\Delta H/RT) \qquad (5.40)$$

where G is the grain size, C is a constant, R is the gas constant, T is the absolute temperature, t is time and ΔH is the activation energy for grain growth. Grain size data from isochronal experiments conducted at various temperatures can be used to determine a value for ΔH. The grain size is considered to be large compared with the size before grain growth occurs, so $dG \approx G$. A graph of the natural logarithm of grain size against the inverse of temperature will yield a slope of $-\Delta H/R$.

Possibly the first workers to calculate a value of the activation energy for grain growth (Jarcho *et al.*, 1976) calculated a value of 235 kJ mol^{-1}, which they noted as being similar to the activation energy for diffusion of oxygen in many different oxides. However, a recalculation of this data yields a value approximately half that of the reported value. This implies that either the wrong logarithms were used or an error was made in the conversion of Joules to Calories.

This value has subsequently been quoted by other workers (deWith *et al.*, 1981; Wakai *et al.*, 1990). DeWith *et al.* (1981) compared the activation energy obtained from data for the sintering of a commercial powder (Merck A.G., Darmstadt, Germany) with the activation energy value after Jarcho *et al.* and that determined from grain size data of Kijima and Tsutsumi (1979). These two groups both employed stoichiometric hydroxyapatite precipitated from slightly different methods in their sintering studies. Jarcho *et al.* sintered

gel fragments whereas the Merck powder and that of Kijima and Tsutsumi were pressed compacts. The results obtained were 143 kJ mol^{-1} for the Merck powder, 239 kJ mol^{-1} for that of Kijima and Tsutsumi compared with the original value of Jarcho *et al.* of 235 kJ mol^{-1}. The lower value for the commercial powder was attributed to a higher impurity content or a lower calcium phosphorus ratio (DeWith *et al.*, 1981).

The grain size data, where grain growth occurred, for the workers mentioned is plotted in Figure 5.8. Data calculated from a study, (Royer *et al.*, 1993) of hydroxyapatite, precipitated in a similar way to Jarcho *et al.* is included as a comparison. This material was calcined prior to being compacted.

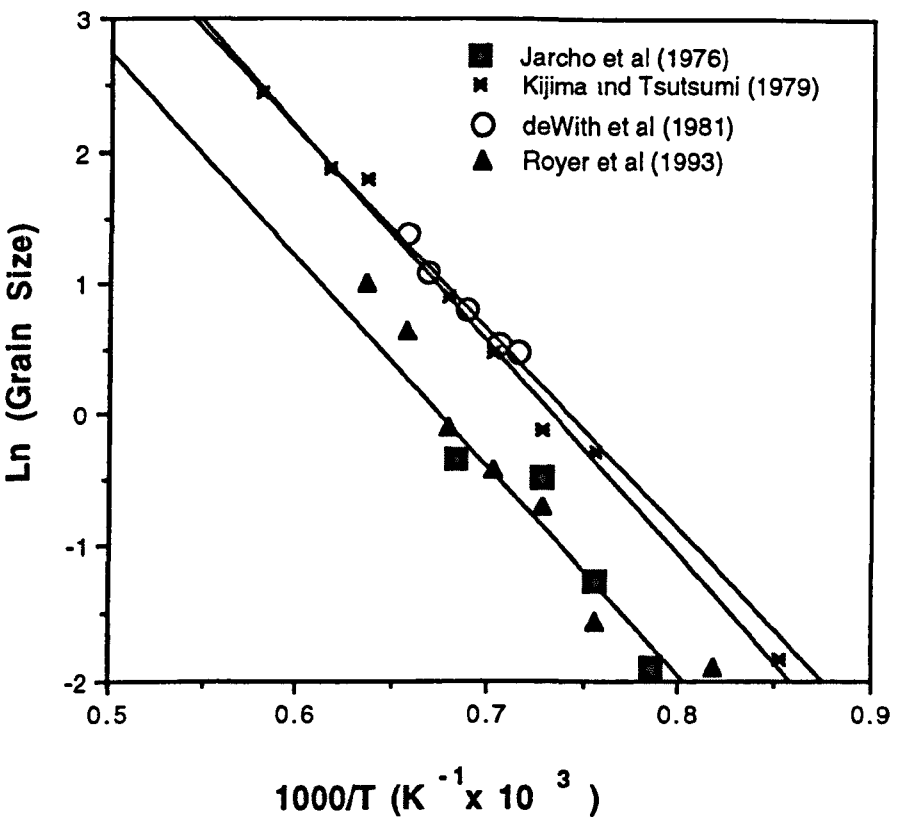

Figure 5.9. Graphs of Ln (grain size) as a function of T^{-1} for hydroxyapatite calculated from reported data. The slope of the least squares fit is ($-\Delta H/R$).

A linear regression analysis was used to fit the lines. It is apparent from Figure 5.9 that there is very little difference in the slope of any of the graphs. The calculated activation energies are shown in Table 5.3.

The mean activation energy (± s.d.) calculated from the data in Table 5.3 is 132 ± 5 kJ mol $^{-1}$. It would appear that neither differences in green compact state nor in the preparation method of these hydroxyapatites affect the activation energy for grain growth. This value is not in agreement with those previously reported. The activation energy for grain growth is a material property that describes the ease of grain growth, a high value indicates that grain growth is more likely to occur at higher temperatures than a material with a lower activation energy. The linearity of the graphs in Figure 5.9 suggest that it does not vary appreciably over the temperature ranges investigated, i.e. grain growth occurs by the same mechanism over these temperatures. One would not expect it to vary with green state, particle size or shape.

Table 5.3. Grain growth activation energy and correlation coefficient (R^2) measured from Figure 5.9 and from Best (1990).

Reference	ΔH (kJ mol^{-1}) *	R^2
Jarcho *et al.* (1976)	130	0.87
DeWith *et al.* (1981)	126	0.97
Kijima and Tsutsumi (1979)	133	0.99
Royer *et al.* (1993)	138	0.95

* Recalculated from the published data.

Isothermal

Lopes *et al.* (1990) conducted isothermal grain growth experiments for Merck powder in air, and wet carbon dioxide. At a constant temperature grain size can be related to time by an equation of the form:

$$G^m = K t \qquad (5.41)$$

where m is a constant that relates to the mechanism of grain growth. A log/log plot of grain size against time should then have a slope of m^{-1}. Lopes *et al*. found a value of 4 for all atmospheres and concluded that atmosphere did not alter the kinetics of grain growth. A mechanism of surface diffusion was deduced from the value of m. However, as the difference in slope between 1/3 and 1/4 is small and these workers had only three points per data set, the evidence presented is by no means conclusive.

5.7 Sintering Carbonate Apatites

There are few reports on the sintering behaviour of carbonate hydroxyapatite. Possibly the first was that of Ellies *et al.* (1988). Although this paper did not contain much quantitative information, these workers noted the effect of 'sintering temperature' being reduced with increasing carbonate content. The next report would appear to have been that of Doi *et al.* (1993). These workers also concluded that carbonate lowered the sintering temperature and put forward the proposal that this was due to a decrease in particle size. Not long after, the same group (Suwa *et al.*, 1993) compared the sintering behaviour of sodium containing and sodium free carbonate apatites. They reported that sodium containing apatites attained a higher bulk density than sodium free apatite at a given sintering temperature. A range of carbonate concentrations was investigated for the sodium containing apatites (1.3 - 16.9 wt%), but only one carbonate content for the sodium free material, (12.9%). However, no sintering data is given for the sodium apatite with 16.9 wt % carbonate. This would tend to suggest that the results are not comparative. The improvement in sintering behaviour for the sodium containing apatites is attributed to the formation of $NaCaPO_4$, which they suggest forms a liquid phase during sintering.

5.7.1 Effect of carbonate on densification rate

Ellies *et al.* (1988) assessed the state of maximum densification (referred to by the authors as 'sintering temperature'), by the condition where a pellet could not be easily broken in the fingers. Although this was an extremely crude measure, one might expect it to give some indication. They reported a linear relation between carbonate content and 'sintering temperature'. Doi *et al.* (1993), used thermal mechanical analysis to measure shrinkage during a heating cycle from ambient temperature to 1100°C at 5°C min^{-1}. By determining the temperature of maximum densification by extrapolation of the curve, they found a similar trend to that of Ellies *et al.* (1988) though the relation was not linear. An 8 wt % carbonate apatite attained maximum density at approximately 580°C, Ellies *et al.* reported a Figure of 780°C. Suwa *et al.* (1993) present isochronal (3 hours) density data as a function of sintering temperature. For an 11 wt% carbonate sodium containing apatite, maximum density, (~95%), is attained at 700°C. Below 4.35 wt % carbonate

very little densification appears to have occurred. The lowest density at all temperatures was observed in the sodium free material.

5.7.2 Bloating

Ellies *et al.* (1988), Doi *et al.* (1993) and Suwa *et al.* (1993) reported a decrease in density at temperatures above that where maximum density occurred, i.e. bloating occurred. This phenomenon appeared to be independent of sintering atmosphere. Ellies *et al.* (1988) sintered pellets in wet nitrogen and wet carbon dioxide. They reported that overheating resulted in pellets with roughened surfaces or warping. They did not specify whether any difference was observed in the two atmospheres, neither did they state whether the effect was temperature dependent. Doi *et al.* (1993), measured shrinkage of carbonate apatite pellets, (green density 63%, compaction pressure 600MPa), during heating at a rate of 1-5°C min^{-1} in dry argon. They observed a rapid expansion of pellets containing more than 2.5 wt% carbonate, once maximum shrinkage had occurred. For example, an 8 wt % carbonate apatite pellet exhibited an expansion of 4% of its original dimension before sintering, when heated to 1000°C. This represents an expansion of 17% during heating from 800 to 1000°C. In this temperature range, a weight loss of only 2% is observed, However at a lower heating rate of 1°C min^{-1}, a loss of nearly 5% is reported. This implies that the compact heated at 5°C min^{-1} contained more than half of the gas which was evolved at 1000°C. Suwa *et al.* (1993), carried out similar experiments with carbonate apatite pellets pressed at 300MPa, (Doi *et al.*, 1993) They too observed an expansion after maximum shrinkage was attained, during heating at a rate of 1-2 °C min^{-1}. A 7 wt % carbonate apatite attained maximum shrinkage between 850 -950°C. Between 950 and 1050°C approximately 8% expansion was measured, compared with 17% measured by Doi *et al.*. Reasons for this difference could be that the green density was lower for this material, as inferred from the differences in compaction pressure, or the heating rate was lower, thus enabling gas to escape before all the porosity became closed.

5.7.3 Atmosphere

Ellies *et al.* (1988) sintered in wet carbon dioxide and wet nitrogen. No difference in sintering behaviour was mentioned and more carbon dioxide was lost in the nitrogen atmosphere than in the carbon dioxide. The presence of carbonate was confirmed by infra-red spectroscopy. Doi *et al.* (1993) sintered only in dry argon and presented data for carbonate loss for two different carbonate contents at temperatures between 600 - 750°C for two hours. Suwa *et al.* (1993) gave similar data for one specimen heated for three hours in an unspecified atmosphere, presumably air. Figure 5.10 shows the reported carbonate contents for these materials.

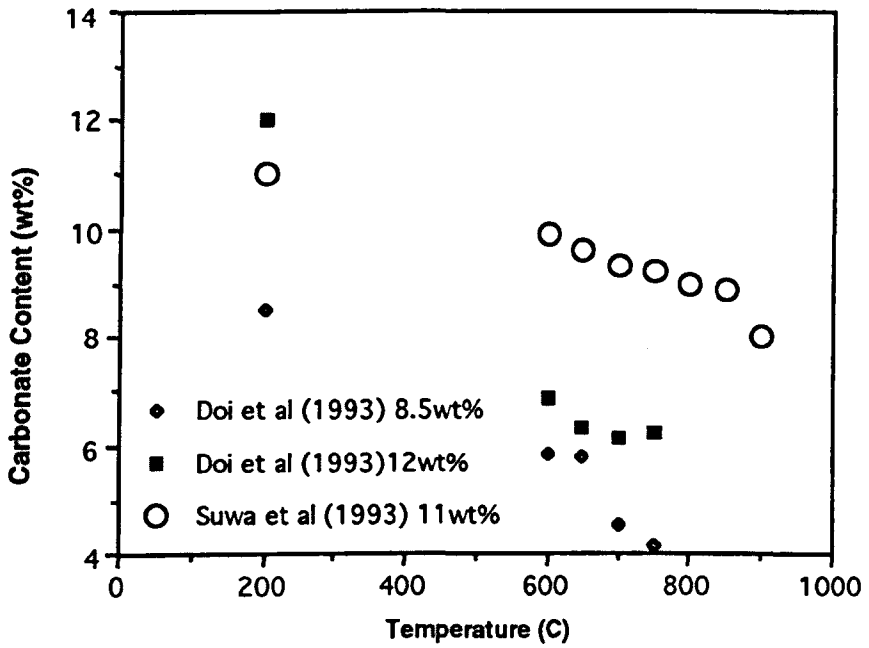

Figure 5.10. Reported effects of temperature on carbonate content of carbonate apatite pellets.

All the samples were powder compacts. Those of Suwa *et al.* were pressed at a lower pressure and were sintered for longer than those of Doi *et al.*. One would therefore expect the degree of carbonate loss to be higher for Suwa *et al.*'s material. It can be seen from Figure 5.10 that, assuming air was used by Suwa *et al.*, sintering atmosphere has a dramatic effect upon the loss of carbonate.

5.8 Translucent Apatites

There is a close correlation between optical transmission of polycrystalline ceramics and porosity. Translucent ceramics are considered to be pore free. It can be said that the purpose of sintering is to produce a dense ceramic, as mechanical properties approach their optimum in the pore free state, Knudsen (1959). For this reason the various routes that have been employed to produce translucent hydroxyapatites are reviewed.

5.8.1 Translucent Hydroxyapatite.

Hydroxyapatite has been prepared as a translucent ceramic by means of a number of methods. One of the first reports in the literature was by Aoki *et al.* (1973), describes the formation of transparent hydroxyapatite by means of hot isostatically pressing a green powder compact at 160MPa using argon at 1100°C for one hour. Jarcho first applied for a U.S. patent concerning this process in 1974, which was finally published in 1978. Jarcho *et al.* (1976) employed a sol gel monolith route to produce a translucent material after sintering in air for one hour, only sols aged for more than 24 hours produced translucent ceramics. However in the same work they indicate that under the same sintering conditions but a much less translucent ceramic is formed. No explanation for this discrepancy in the results is offered. In 1989 transparent hydroxyapatite was produced by hot isostatically sintering a filter cake at between 800 and 1000°C at a pressure of 200 MPa for two hours by Uematsu *et al.* (1989). Simultaneously Yoshimura *et al.* (1989) succeeded using cold isostatic pressing followed by hot isostatic pressing at 200 MPa for one hour. A year later Li and Hermansson (1990) reported the perhaps least commercially viable method, namely the use of conventional sintering at 1050°C for three hours followed by hot isostatic pressing at 1000°C at 200 MPa in Argon. Agrawal *et al.* (1992) describe the use of microwave sintering of cold pressed (70 - 350 MPa) powder formed by a hydrothermal route at temperatures of 1100 - 1175°C, for between 5 to 10 minutes. Translucency was observed to increase with increasing die pressure. These workers also stated that translucency is obtained to a lesser degree by conventional sintering.

5.8.2 Optical properties of polycrystalline ceramics

Opacity in polycrystalline ceramics is caused mainly by the scattering caused by pores and to a lesser degree by grain boundaries. Reflectance and absorbency also contribute to the effect. Ignoring these latter effects:

$$\frac{I}{I_0} = \exp(-Sx) \tag{5.42}$$

where I is the transmitted intensity, I_0 is the incident intensity, x is the thickness of the ceramic, and S is the scattering factor given by.

$$S = \frac{3}{4}\frac{K V}{r} \tag{5.43}$$

where V is the volume fraction of scattering particles, (e.g. pores), r is the particle radius and K is the scattering factor which depends on the ratio:

$$\frac{2\pi r}{\lambda} \tag{5.44}$$

where λ is the wavelength of the transmitted radiation. In addition, the relative refractive index, m, strongly affects K. For the case of hydroxyapatite and air it has a constant value of 0.61 for precipitated hydroxyapatite, (McDowell *et al.*, 1977). The maximum scattering for a given volume fraction of pores occurs when the pore size is of an equivalent magnitude to the wavelength of the incident radiation, (400-750nm for visible light). Below this size the scattering factor decreases with decreasing pore size, and at pore sizes greater than these, the scattering factor decreases. At pore sizes greater than approximately five times λ, a constant value of scattering factor is obtained and the scattering coefficient becomes inversely proportional to particle size as indicated in Equation 5.43. Figure 5.11 shows data for the transmission of 0.5mm thick polycrystalline alumina as a function of pore volume fraction and pore size.

It is clear from Figure 5.11 that where small (0.7μm) pores are present the optical translucency is extremely sensitive to the presence of pores. It can be seen from Equation 5.43 that as the grain size increases, the volume fraction of the boundaries decreases, which in turn leads to a reduction of the grain boundary scattering factor resulting in an increase in translucency.

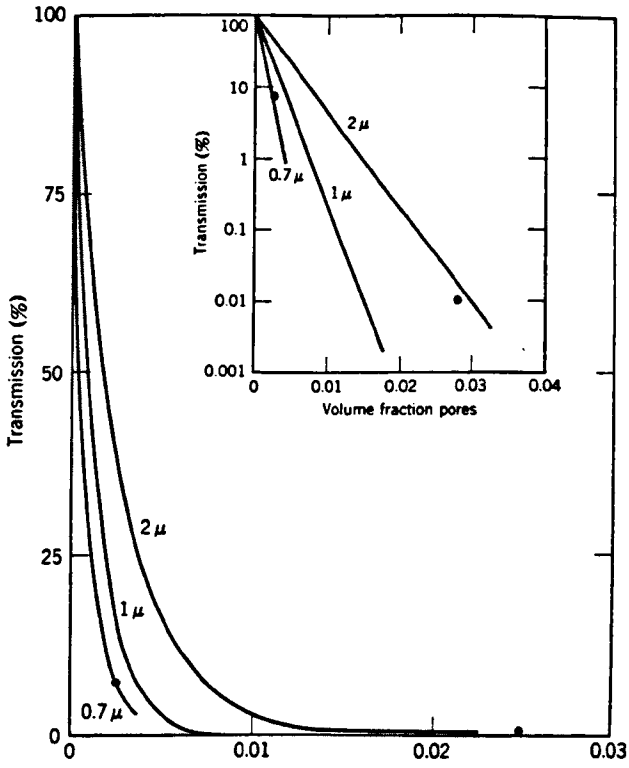

Figure 5.11. Optical transmission of 0.5 mm thick alumina as a function of pore size and pore volume fraction, (Reproduced from Kingery, 1976).

5.8.3 Techniques for translucent apatite production

The methods described to produce translucent hydroxyapatites fall into one or more of the following categories: mechanical, physical and chemical. Isostatic pressing is a mechanical method that increases the pressure of gas trapped in the pores, this has the effect of increasing the solubility of the gas in the apatite. Physical methods are those that rely on extremely high specific surface areas to promote rapid densification before grain and pore growth occur, e.g. microwave sintering or sol gel processes. Pores below 100nm diameter are unlikely to make large contributions to opacity at low volume fractions. Chemical methods are those that alter the densification rates or

increase the limiting density of the apatite such as that employed by Agrawal *et al.* (1992) who used of hydrothermally prepared apatite in preference to that formed by decomposition of brushite, Presumably the structure of the apatite prepared in this way was modified such that densification is enhanced. Fang (1994) reported that hydrothermally treated hydroxyapatite has higher thermal stability than that produced by any other method. He hypothesised that decomposition products were responsible for opacity in non-translucent apatites.

5.8.4 Desirability of translucency in hydroxyapatites

Translucency in a ceramic is usually mechanically desirable as strength σ is dependent upon the porosity by (Knudsen, 1959):

$$\sigma = \sigma_0 \exp(-nP) \tag{5.45}$$

By comparing ceramics with zero porosity a true comparison of other properties can be determined. Aesthetically translucent hydroxyapatite is of enormous potential interest as enamel is itself translucent and suitable replacements for it often lack the long term colour matching requirements demanded. Another dental application its use as part of a composite in UV setting matrices. There is also great possibility in the use of transparent hydroxyapatite enabling the observation of cellular activity using transmission light microscopy without removing the apatite from the culture medium.

6 X-Ray Diffraction, Electron Microscopy and IR Spectroscopy

6.1 X-Ray Diffraction (XRD)

XRD is a versatile technique may be used to determine d spacings within a crystal structure and thus identify the phase or phases present. In addition, it can be used to calculate precise lattice parameters, approximate particle size, preferred orientation and lattice microstrain. In addition, the structure of a polycrystalline sample may be determined by means of Reitveld structure refinement. Quantitative evaluation of phases present can be performed and atomic positions within a unit cell may be found. These applications are based on the Bragg Equation (6.1), which describes the conditions for constructive interference.

$$n\lambda=2d\sin\theta \qquad (6.1)$$

where n is an integer, λ is the wavelength of the X-rays, d is the planar spacing and θ is the angle of incidence between the X-ray beam and the lattice plane.

6.1.1 Principles

Monochromatic X-rays are incident on a flat sample of compact powder. As the powder orientation is assumed to be random, reflections are obtained with constructive interference occurring from all planes in all directions at angles ($0< \theta<180$), the exact angular range being set by the operator. A detector scans the intensity of reflection over the set range and so provides the count rate variation with 2θ (Figure 6.1) giving a trace of peaks of varying intensity at certain angles determined by Equation 6.1.

The d spacing is calculated from Equation 6.1 and after various corrections have been made the lattice parameters can be determined. For a hexagonal structure the relationship is:

$$\frac{1}{d_{(hkl)^2}} = \frac{4}{3}\left(\frac{h^2+hk+k^2}{a^2}\right)+\frac{l^2}{c^2} \qquad (6.2)$$

where $d_{(hkl)}$ is the planar spacing of a plane of indices h,k,l and a and c are the lattice parameters.

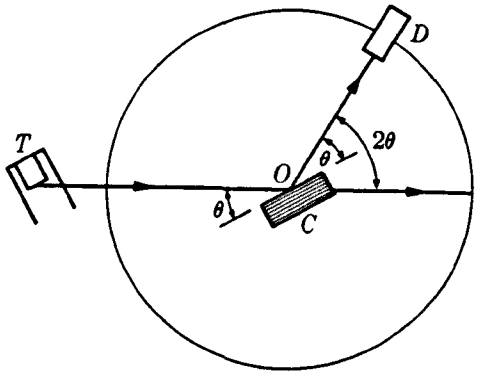

Figure 6.1. Typical X-ray source (T), detector (D) and sample (C) arrangement. (Reproduced from Cullity, 1978)

6.1.2 Crystal Size Determination

If the path difference between rays gathered by two adjacent planes differs slightly from $n\lambda$ then the two rays will interfere to produce constructive interference. If the crystal was 'infinite' (in practice ~100nm,) then at some depth from the surface there would be a plane scattering a ray exactly out of phase with the first one and so on with each consecutive plane. However if the crystal is so small (< ~100μm) that this does not occur, then reflections will be obtained at angles greater and lesser than those that satisfy exactly the Bragg equation, θ_b. This causes a broadening of the peaks observed and there is a direct relationship between the broadening measured as the breadth of the peak at half intensity, B (in radians) and the particle size, t, known as the Scherrer formula:

$$t = \frac{0.9\,\lambda}{B\cos\theta_b} \qquad (6.3)$$

where λ is the wavelength.

However, as the X-ray beam is not perfectly parallel and monochromatic, there is a broadening effect due to measured 2θ angles slightly different from those that satisfy the Bragg relation giving rise to constructively interfering reflections. This reflection can be accounted for by measuring the breadth of peaks from a pure sample, B_{ST}, with peaks near those of

interest. The true breadth, B, then being:

$$B^2 = B_{\theta b}{}^2 - B_{ST}{}^2. \qquad (6.4)$$

6.1.4 Atomic Position

Atomic position is usually found by a combination of techniques, however the principle lies in the application of the structure factor relationship by complex computer algorithms. The derivation will not be dealt with here:

$$F_{hkl} = \Sigma f_n \, e^{2\pi i(hu_n + kv_n + lw_n)} \qquad (6.5)$$

$$I \propto |F| \qquad (6.6)$$

where h,k,l are planar indices, f_n is the atomic scattering factor, u,v,w are the atomic coordinates F is the structure factor and I is the intensity.

Since some planes have equivalent spacing for example {111} in a cubic system and the amount of each equivalent planes contribute to the intensity of the reflection at that angle. This effect varies depending on the crystal system. The relative proportion of these planes is termed the multiplicity factor, p. For a hexagonal system p is given by the following relations.

$$\frac{hkl}{24}, \frac{h0l}{12}, \frac{0kl}{12}, \frac{hk0}{12}, \frac{h00}{6}, \frac{0k0}{6}, \frac{00l}{2} \qquad (6.7)$$

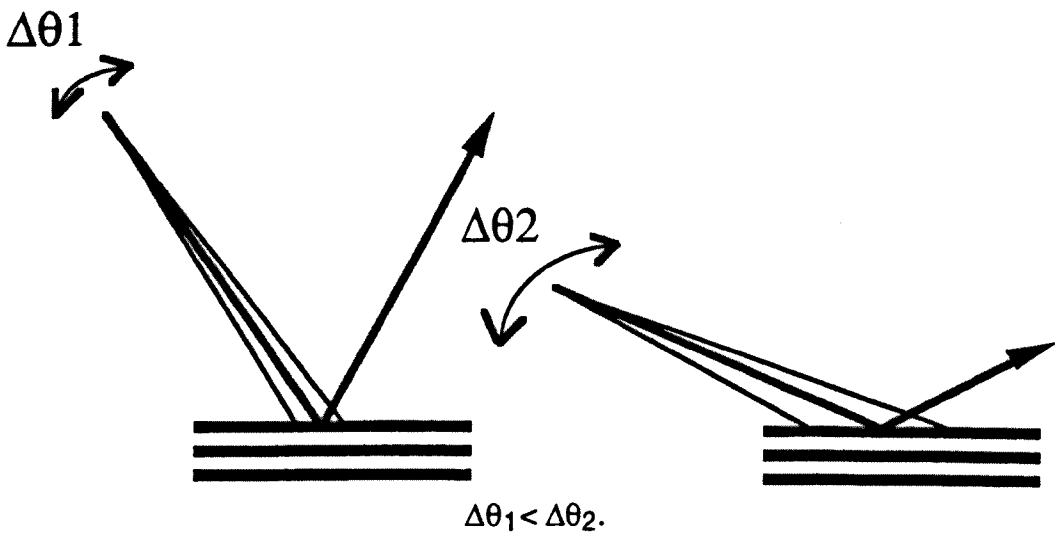

$\Delta\theta_1 < \Delta\theta_2$.

Figure 6.2. Schematic diagram showing the effect of width of X-ray beam on the reflected intensity with incident angle. Lower angles giving rise to a reduction in intensity

due to the energy being spread over a larger angular range, $(\theta_2-\theta_1)$.

As mentioned above, observed peaks always have a measurable breadth and the observed intensity depends on the angle over which energy is reflected. The larger the angle the greater the value of I_{max} (Figure 6.2)

6.1.5 Reitweld Refinement.

Reitveld refinement, developed by Hugo Reitweld (1969), involves refinement of crystal structures by approximation to the whole powder pattern. Reitveld refinement is carried out by computer and relies on a starting model, which is input by the operator and then is refined by the least squares analysis. Peak shapes are assumed to be Pseudo Voigt in nature. A five parameter polynomial is refined for the background. Minimisation of the least squares is by the R factors described in Table 6.1.

Table 6.1. Some criteria of fit for Reitveld refinement.

$$R_{WP} = \sqrt{\left(\frac{\Sigma\, w_i\, (y_i(obs) - y_i(calc))^2}{\Sigma\, w_i\, (y_i(obs))^2}\right)}$$ R-weighted pattern

$$R_p = \frac{\Sigma\, |\, y_i(obs) - y_i(calc)|}{\Sigma y_i(obs)}$$ R -pattern

where y_i is the intensity at the ith step and w_i is y_i^{-1}, (obs and calc refer to obnserved and calculated resp[ecrtively).

Perdikatis (1991) conducted a Reitveld study of Francolite heated for five hours at 530, 750 and 1200°C. He concluded that the unit cell volume of Francolite was smaller than for fluorapatite. The P occupancy tended towards 6 with increasing temperature. This was interpreted in terms of the loss of carbon dioxide between 750 and 855°C and the formation of calcium oxide.

6.2 Transmission Electron Microscopy

Transmission electron microscopy (TEM) enables the imaging of thin (<0.5μm) specimens such as films and small crystals and gives an image containing 2D information. Direct size measurements may be made and morphological information may be obtained. It has the advantage over other microscopic methods in that extremely high resolutions may be obtained (<1nm) under suitable conditions. In addition imaging of the diffraction pattern can provide information as to crystal symmetry and lattice spacings. By selecting electrons diffracted by a particular lattice plane, additional contrast may be obtained, revealing only parts of the image formed by that particular plane.

Electrons are used to image the samples because the resolving power, R, of a microscope, is related to the wave length λ, of the imaging radiation by the equation:

$$R = \frac{0.61\,\lambda}{N.A.} \tag{6.8}$$

where NA is the numerical aperture and is characteristic of the design of the lens and imaging medium. Thus a decrease in wavelength results in an increased resolution. The wavelength and thus resolution can be altered by means of the accelerating voltage:

$$p = \frac{h}{\lambda}, \qquad \frac{1}{2}mv^2 = eV \tag{6.9}$$

$$\therefore \quad \lambda = \frac{h}{\sqrt{2emV}} \quad \equiv \quad \lambda = \sqrt{\frac{150}{V}} \ (\lambda \text{ in Å.}) \tag{6.10}$$

where p is momentum of an electron, h is Plank's constant, λ is wavelength, m is the mass of an electron, e is the charge on an electron and V is the accelerating voltage.

Thus 100kV accelerating voltage produces electrons of wavelength 4pm. However in reality the resolution achievable is in the order of two orders of magnitude less than this. This degradation of resolution is due to spherical and chromatic alteration, astigmatism and diffraction effects.

6.2.1 Specimen and Electron Interactions

The most important interaction is perhaps elastic scattering in that it is responsible for the creation of contrast in the image. Electrons are scattered elastically by the nuclei of the specimen by Coulomb forces. For small scattering angles (Figure 6.3a) negligible amount of energy is transferred to the nuclei, large scattering angles (Figure 6.3b) can result in large amounts of energy being transferred to the nuclei and this can be sufficient to displace some of the specimen atoms to interstitial sites.

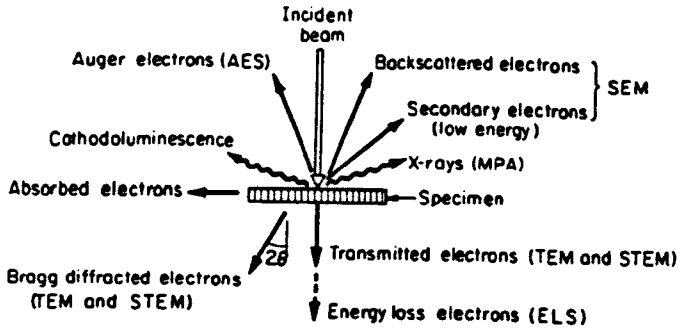

Figure 6.3a) Primary electron b) atom and c) primary electron - specimen interactions. (Reproduced from Thomas and Goirne, 1979).

Small angle scattering contributes greatly to the contrast of the image, the scattered electrons are intercepted by the objective aperture. The Coulomb potential of an atom has the effect of shifting an electron wave (Figure 6.3c), giving rise to the concept of an electron-optical refractive index. This effect gives rise to phase contrast as an interference effect between the primary and scattered electrons. An electron wave passing through the periodic potential of the crystal lattice can be diffracted in a manner described by the Bragg relation for constructive interference. This approach however is an approximation, as it neglects the effects of crystal thickness on primary and scattered wave amplitudes. If the objective aperture is large enough to allow the primary beam and one or more Bragg reflections to pass the waves interfere in the image plane and form a diffraction pattern. In addition inelastic scattering can occur which results in the emission of either X-rays or Auger electrons.

6.2.2 Imaging Modes of the TEM

The first intermediate image is formed by the objective lens, magnification M ~ 20-50 X. Resolution limiting factors such as chromatic and spherical aberration are most important in this lens as the magnification of it reduces the diameter of the apertures of the following lenses by a factor of M. In these lenses the main aberration is distortion. Diaphragms (20-200μm) in diameter are inserted into the focal plane of the objective lens, thus permitting the aperture to be decreased. A diaphragm selects all electrons scattered through angles $\theta \geq a_o$. Decreasing the aperture increases the contrast. For high resolutions the aperture is as large as possible so that high spatial frequencies can contribute to the image and contamination and charging of the aperture do not disturb the image.

The imaging system of the microscope contains at least three lenses as shown in Figure 6.4. The intermediate lens can magnify the first intermediate image which is formed in front of the lens or the first diffraction pattern that is formed in the plane of the objective lens (Figures 6.4a and b respectively,) by reducing the excitation. In many microscopes, an additional lens is inserted between the objective and intermediate lenses to image the diffraction pattern and to enable magnification to be varied in the range 10^2-10^6.

Bright Field (BF) Mode

BF is the typical TEM mode and is achieved by placing a centred aperture in the plane of the first diffraction image. This is normally between ~5-20 mrad and for high resolution work >~20 mrad, in this mode the only function of the aperture is to increase the contrast by reducing the background.

Selected Area Electron Diffraction

The cone of diffracted electrons with an aperture in the order of a few 10 mrad can pass through the small pole piece bores of the final lenses only if the back focal plane of the objective lens that contains the first diffraction

pattern is focused on the screen (Figure 6.4b).

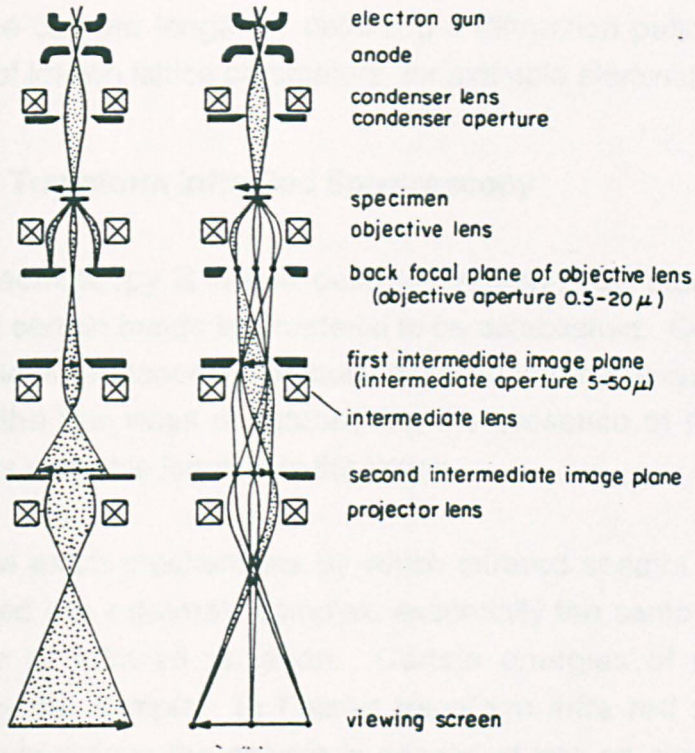

Figure 6.4. TEM lens and aperture configurations giving rise to a) bright field imaging and b) selected area diffraction modes. (Reproduced from Thomas and Goirne, 1979)

A selector aperture situated in the intermediate image plane selects an area of the specimen. This area can be selected in the BF mode. The excitation of the intermediate lens is decreased thus increasing the focal length and the diffraction pattern in the focal plane of the objective lens can be focused on the final image screen, after removing the objective aperture. The diameter of the selected area cannot be decreased below 1μm owing to spherical aberration of the objective lens. This aberration causes a distortion of less than 1% in a typical pattern. The most severe distortion is caused by the projector lens that can generate pincushion or barrel distortions. Single crystal samples produce a series of spots, the distance of the spots from the primary beam spot being related to the planar spacings (Equation. 6.11). Polycrystalline samples produce a series of rings making measurement of the parameter r more accurate (assuming a homogeneous sample).

$$\frac{\lambda}{d} = 2 \sin \theta_b \approx \tan (2\theta_b) = \frac{r}{L} \; ; \qquad d \approx \frac{\lambda L}{r} \tag{6.11}$$

where r is the distance of the diffraction spot, or ring from the primary

beam, θ_b) is the Bragg angle and L is the diffraction (or camera) length. However due to the distortions mentioned above it is necessary to calibrate the camera length by obtaining a diffraction pattern for a pure substance of known lattice parameters, for example aluminium.

6.3 Fourier Transform Infra Red Spectroscopy

Infrared spectroscopy is a non destructive technique that enables the presence of certain bonds in a material to be established. Consequently it is of particular importance in the study of carbonate hydroxyapatite as it is the one of the few ways of establishing the presence of the carbonate group and its probable location in the lattice.

Although the exact mechanisms by which infrared spectra are detected and displayed are extremely complex, essentially the sample is exposed to a source of infrared radiation. Certain energies of radiation are absorbed by the sample. In Fourier transform infra red spectroscopy (FTIR) the signal from the sample is converted into an electronic signal which can be interpreted in terms of signal intensity and frequency. A broad band radiation source is collimated onto a beam splitter. One part of the beam is transmitted to a moving mirror, the other to a fixed mirror. The two beams are recombined and because of the path difference between the beams, constructive and destructive interference occurs at frequencies determined by the difference in path length, (mirror position). This occurs at all frequencies simultaneously and the resulting signal is called an interferogram and varies in intensity with time of mirror scan. By application of Fourier transform algorithms the intensity with frequency can be computed for the signal from the specimen. Because all frequencies under investigation are scanned simultaneously the average signal from multiple scans can be used to eliminate noise. The position of the mirror is determined by using a single wavelength laser and so extremely high resolution (0.01 cm^{-1}) can be obtained.

6.3.1 Principles

Molecules possess various modes of vibration and rotation. When a molecule is supplied with energy, it can alter its energy state and in doing

so some energy is absorbed, the frequency ν, of absorption is given by the Bohr relation:

$$\nu = \frac{\Delta E}{hc} \qquad (6.12)$$

where ΔE is the energy change, h is Plank's constant and c is the velocity of light. Often the contribution to a vibration at a particular frequency comes from two atoms with a bond between them. The frequency of vibration is determined mainly by the masses of the atoms and the strength of the bond between them. The frequency of vibration is only slightly altered by other atoms in the vicinity, thus vibrational modes at a particular frequency are characteristic of a particular group. The band positions are designated in units of wavenumber (cm^{-1}), which are proportional to the energy. A non linear molecule of n atoms has 3n degrees of freedom: three translational, three rotational and 3n-6 vibrational. Infrared absorption only occurs when a periodic change in dipole results, hence some symmetrical movements result in a zero net dipole change.

Vibrations may be either stretching or bending types. Sometimes a group of symmetrical atoms may have equivalent vibrational frequencies and only one absorption is observed when in fact several vibrations are contributing. This effect is called degeneracy. When the molecular environment distorts a group so that its symmetry is lost, degeneracy is removed and several peaks are observed.

6.3.2 Infrared Spectra of Carbonate Hydroxyapatite

In the range 400 - 4000cm^{-1} the infrared spectra of carbonate hydroxyapatite have bands due to hydroxyl, carbonate and phosphate ions. The vibrations of these ions are influenced by the neighbouring atoms in the lattice. Consequently there is a loss of degeneracy.

The carbonate ion is a trigonal planar in its uncombined form, and has four normal modes of vibration of which υ_2 (out of plane bending), υ_3 (asymmetric stretching) and υ_4 (planar bending) are infrared active (Figure 6.5).

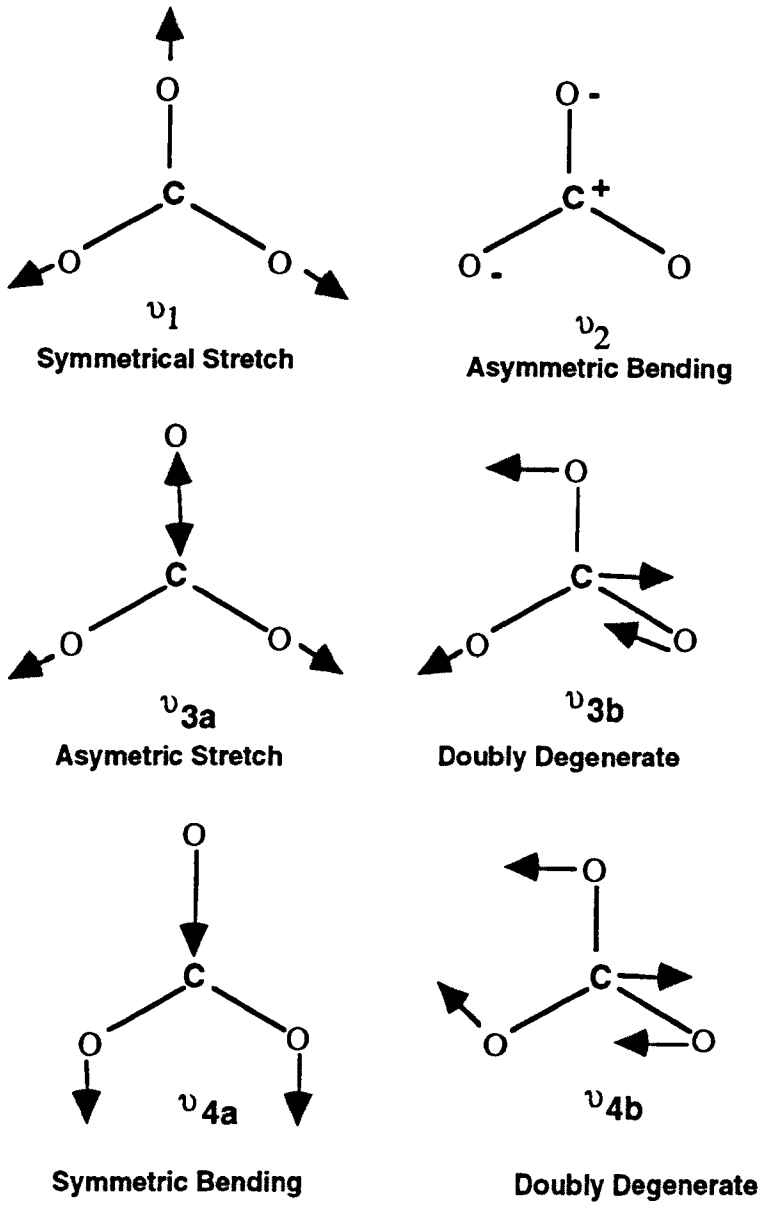

Figure 6.5. Vibrational mode of the carbonate ion, after Herzburg (1945).

The symmetric υ_1 is not infrared active. Studies on the dimorphic forms of calcium carbonate, aragonite and calcite showed that splitting of the degenerate modes into doublets was due to the calcium ions around the carbonate (Alder and Kerr, 1962).

The phosphate ion has nine vibrational degrees of freedom. Of the four modes two are triply degenerate and one is doubly degenerate (Figure 6.6).

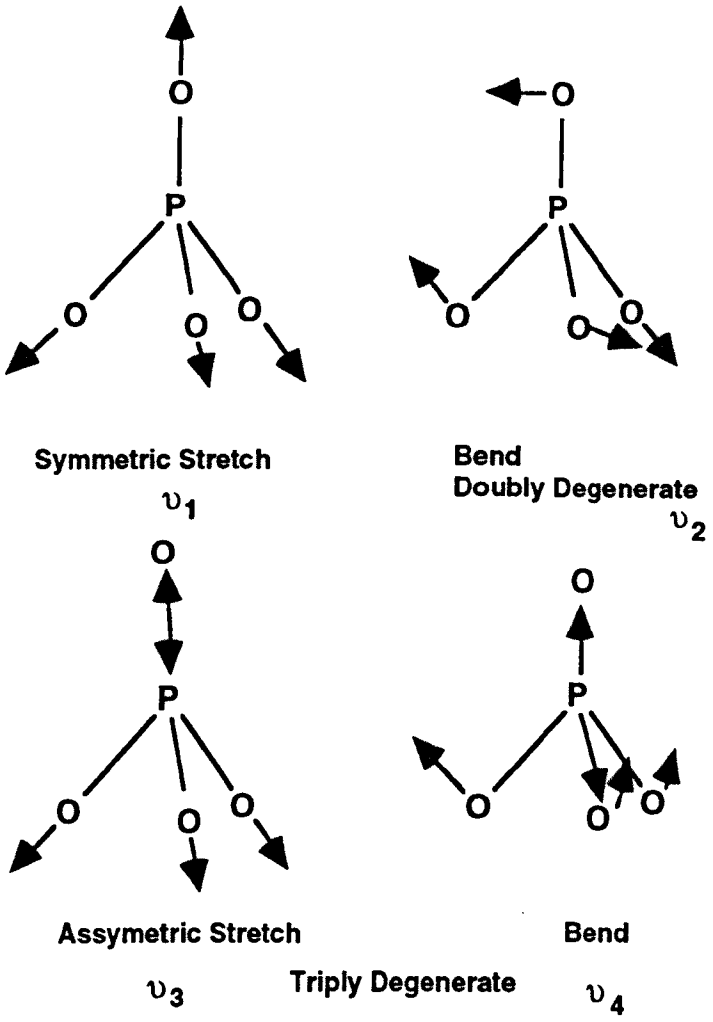

Figure 6.6. Vibrational modes of the phosphate ion, after Herzburg (1945).

As a result of symmetry effects, in the free state only the υ_3 and υ_4 are observed. However if the symmetry is lowered by incorporation into a compound the υ_1 and υ_2 adsorbtions are also observed. In apatite the triple degeneracies are lost indicating the phosphate ion in hydroxyapatite is distorted to some degree, (Alder, 1964).

The hydroxyl group exhibits a linear stretching vibration (Herzburg, 1945) and a liberational motion parallel to the **c** axis. Cant *et al.* (1971) observed the appearance of an additional hydroxyl peak at temperatures above 485°C. The intensity of this peak was found to increase with temperature and the effect was found to be fully reversible. These workers attributed this peak to the high temperature ordering of the hydroxyl groups. Reisner and Klee (1982) also observed this phenomenon and proposed in addition to Cant *et al.* 's model the

possibility of the formation of water and oxide ions at high temperature.Some previously reported peak assignments are shown in Table 6.2.

One of the first workers to observe that the bands in carbonate were different to simple carbonates were Hunt *et al.* (1950). The differences were attributed to the fact that the carbonate was incorporated in the lattice. Emerson and Fisher (1962) were perhaps the first workers to report the presence of the carbonate doublet at 873 - 880 cm^{-1} in calcified tissues. They interpreted these bands as being due to the non degeneracy of the υ_2 vibrational mode as a consequence of there being two different environments, the adsorbed on the surface and in the lattice.

Dowker and Elliott (1979) observed the appearance of bands in the region 2010 to 2340cm^{-1} in heat treated precipitated carbonate apatites. They were attributed them to the formation of cyanate and cyanamide groups due to the products of a reaction between nitrogen present from the ammonium salt preparation reagent and the carbonate present at temperatures in the range 450 and 650°C.

Dowker and Elliott (1983), carried out an infrared study on trapped carbon dioxide in heated carbonate apatites in the range 120-900°C in air, carbon dioxide, nitrogen and under vacuum. A band at 2340 cm^{-1} that had been attributed to carbon dioxide trapped in the lattice was observed after heating in air. During heating in air at 370°C the intensity of this peak decreased with time. Atmosphere did not make an appreciable difference to the carbon dioxide peaks observed. It was concluded that the carbon dioxide originated from the samples and not from the atmospheres, though the exact mechanism of evolution was not clear.

A resolution enhanced FTIR study of the υ_2 carbonate bands of pig enamel by Rey *et al.* (1991a) indicated the possible existence of four carbonate locations, one principally in the B site, two in the A site and a fourth unstable location. They also noted a decrease in the amount of A type substitution with increasing carbonate content which would seem to agree with other workers e.g. Vignoles *et al.* (1988). In bone mineral however the second A type site is not observed, (Rey *et al.*, 1991b). Investigations of the previously poorly defined υ_4 carbonate bands of synthetic apatites by El Feki *et al.* (1991) showed the presence of five

Table 6.2. Reported peak assignments of carbonate hydroxyapatites, phosphates and carbonate ion.

	OH^-	CO_3^{2-}	PO_4^{3-}	PO_4^{3-}	CO_3^{2-}	OH^-	PO_4^{3-}	PO_4^{3-}
	υ_3	υ_3	υ_3	υ_1	υ_2		υ_4	υ_2
Nelson and Featherstone (1982) Hydroxyapatite	3571		1088, 1065, 1035	962		631	602, 574 565	474,462
A Type (From heating B type in CO_2 at 900°C) 8 wt%	3572	1500,1469,1454 1415	1090, 1060, 1032	961	879,873	634	605, 575 568	474,424
B Type (Aqueous ppt) 2 wt%		1555,1462,1415			878,872			
Le Geros *et al.* (1969) A type		1550,1525,1460	1045, 1025	950	877		602, 572	
B type (ppt)		1540,1450,1410	1090, 1040	957	870		602, 562	
Nadel *et al.* (1970) A type	3566	1534,1465			884	633		
B type (Fluorapatite heated in CO2)		1455,1430			864			
AB type (ppt)		1534,1430,1465						
Herzburg (1945) Undistorted carbonate ion		1415			879	680		
Fowler (1974) Hydroxyapatite	3752		1087-72 shoulder : 1046-32	962		630	601,571	474,462

bands. Owing to the loss of double degeneracy two bands would be expected in this region. Two peaks were assigned to two different B type environments, two to one A type site and one unspecified site, possibly an A B intermediate. The positions of the peaks are shown in Table 6.3.

Table 6.3. IR bands in the υ_4 carbonate domain of precipitated carbonate apatites as reported by El Feki *et al.* (1991).

Band Position (cm^{-1})	Assignment	Observation
716-718	B	Broad, two peaks at low concentrations.
692-695	B	
757	A	766cm^{-1} in pure A type
670	A	675cm^{-1} in pure A type
740	?	Intensity increases with heating

7 Methods

7.1 PRECIPITATION

A precipitation reaction based on that used by Nelson and Featherstone (1988) was used for the preparation of hydroxyapatite and carbonate hydroxyapatites with varying degrees of substitution. This method was selected as it has been reported that a well defined product was formed in which the carbonate content could easily and predictably be varied. In addition the reagents used are freely available and a similar system has been investigated in our laboratory (Puajindanetr, 1991). Although many methods for the formation of aqueous precipitated carbonate apatites have been reported (Bredig *et al.* ,1932; LeGeros *et al.* ,1965; Bonel, 1972b), Nelson and Featherstone first characterised and sintered this material.

7.1.1 Method and Yield Measurement

A 130mM solution of AR (analytical grade) tri-ammonium orthophosphate at pH ≥9 was dripped into a continuously stirred 210mM solution of AR calcium nitrate 4-hydrate over a period of approximately two hours. In order to avoid contamination, the solutions were filtered to remove insoluble impurities. Double distilled water (DDW) and analytical grade reagents were used throughout the preparation and the pH of the DDW used to make up the solutions was measured Care was taken to ensure that all apparatus was clean. Dust contamination was kept to a minimum and at all times the reagents or precipitates were only handled with thoroughly cleaned utensils. All apparatus was washed with detergent, rinsed in tap water, washed in dilute hydrochloric acid, rinsed in tap water and then finally rinsed in DDW. The experimental apparatus is shown in Figure 7.1. The resulting precipitates were aged for 24 hours and then filtered in a Buchner funnel, boiled in approximately a litre of water and filtered again. This treatment was intended to remove soluble ammonium nitrate, which is a by-product of the precipitation. A portion of precipitate was kept in water for characteriation,

while the remainder was air dried. The reaction yield was calculated by measuring the mass of the dried precipitate.

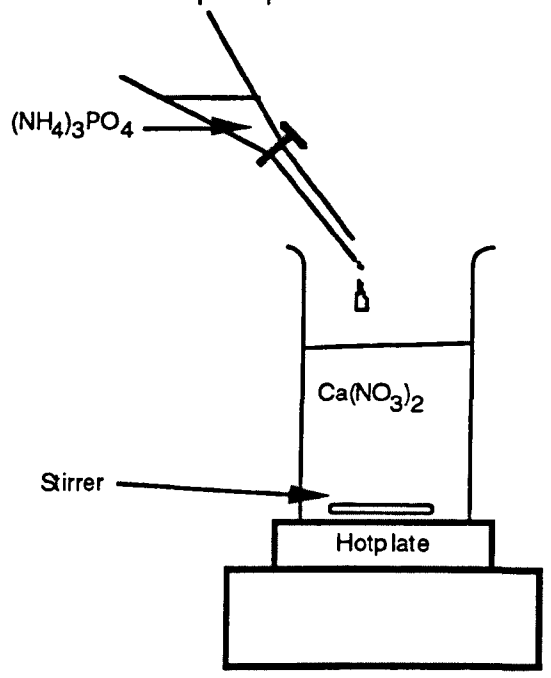

Figure 7.1. Schematic diagram of apparatus for aqueous precipitation of carbonate hydroxyapatite.

7.1.2 Precipitation Variables

Six temperature ranges were used for reactions, 3°C, 25°C, 37°C, 45°C, 60°C, 70°C, and 90°C. The temperature variation at each temperature was ±3°C. The 3°C temperature range was achieved by immersing the reaction vessel in an ice bath, while other temperatures were maintained by use of a thermostat controlled hot plate. Up to nine concentrations of AR sodium bicarbonate were added to the phosphate solution at each temperature, between 10mM, and 640mM, (Table 7.1). The samples were classified with the notation, **X**C **Y**M, where **X** is the reaction temperature and **Y** is the molarity of the sodium hydrogen carbonate solution ($x10^{-2}$). The range of bicarbonate concentrations used produced phosphate / carbonate ratios as shown in Table (7.2). For subsequent processing the precipitates 3C9M and 3C16M were used.

Table 7.1. Temperature and bicarbonate concentration ranges at which reactions were initially conducted. (**X** denotes prepared in precipitate and powder form).

	HCO_3^- CONCENTRATION (mM)									
Temp (°C)	0	10	40	90	160	240	320	480	560	640
3	X	X	X	X	X		X	X	X	X
25	X		X				X	X		
37	X		X		X		X	X		
45	X		X		X		X			
60	X									
70	X	X	X		X	X	X	X		X
90	X	X	X							

7.2 Precipitate Characterisation.

7.2.1 Transmission electron microscopy.

Particle size and shape of the precipitate were determined with transmission electron microscopy. The microscope used was a JEOL 1200 EX2. Carbon coated 200 mesh copper grids were dipped in a dilute suspension of the precipitate. The excess suspension on the grid was carefully removed using absorbent paper before being left to dry in air prior to insertion into the microscope. The precipitates were examined in bright field mode at magnifications typically up to 50,000x, using an accelerating voltage of 100kV, selected area electron diffraction patterns were obtained for each of the precipitates. From representative area micrographs, primary particle size measurements were determined. The camera length of the microscope was calibrated using a diffraction pattern from an evaporated aluminium standard sample. By knowing the camera length, ring or dot spacing and electron wavelength the patterns could be indexed by reference to JCPDS (1980) data.

A 5.8 wt% carbonate apatite sintered at 1300°C in wet carbon dioxide for four hours was ion beam thinned until a hole was formed, the sample was carbon

coated. The region around the hole was examined in bright field mode using an accelerating voltage of 200kV on a JEOL JEM 2010.

Table 7.2. Concentration of bicarbonate ions and carbonate: phosphate ratios used in the carbonate hydroxyapatite precipitation.

$[HCO_3]^-$ (mM)	$\frac{PO_4^{3-}}{CO_3^{2-}}$	$\frac{CO_3^{2-}}{(PO_4^{3-}+CO_3^{2-})}$
10	11.52	0.08
40	2.88	0.26
90	1.31	0.44
160	0.72	0.58
240	0.48	0.66
320	0.36	0.72
480	0.24	0.79
560	0.21	0.81
640	0.18	0.83

7.2.2 Light scattering

A Malvern Mastersizer particle size analyser was used to measure the particle size distribution of the precipitates. The software allowed the refractive index and reflectance of the material being analysed to be taken into account during calculation of the size distribution. The value of refractive index was taken to be 1.6, (McDowell *et al.*, 1977), the suspension medium used was tap water. Prior to any measurements, the water was degassed by applying ultrasound in the dispersion chamber, followed by vigorous stirring to remove the adhered bubbles. This procedure reduced the possibility of bubbles being produced, which would interfere with the analysis. Ultrasound was applied until a stable minimum mode value of particle size ($d_{0.5}$) was observed and a measurement was taken. By comparing the light scattering results with the primary particle size measurements obtained by microscopy an indication as to the extent of agglomeration was derived.

7.3 Processing

A number of routes were investigated before the final method was developed. Initially the powders were produced by air drying at different temperatures, although this method showed some promise it was not effective for processing precipitates of small (<50nm) particle size. For this reason the gelation route was adopted on the basis of previous results.

7.3.1 Gelation

Initially filtration was carried out in a Buchner funnel (50mmø), using Whatman No. 1 filter paper. Approximately 300ml of suspension was slowly added to the funnel over a period of one to two hours. Filtration proceeded until the gel cracked, thus it was necessary to remove the vacuum before cracking occurred. As a consequence of the sudden and unpredictable manner in which cracking occurred, inevitably material had to be scrapped. The next step prior to drying was the removal of the gelled monolith or 'cake' from the funnel. This often resulted in breakage as the wet monolith adhered to the sides of the funnel and was extremely fragile. A removable mould was designed that fitted the funnel and facilitated removal, (Figure 7.2).

A number of designs that were based on biaxial vacuum filtering were tried before the equipment shown in Figure 7.3 was found to work successfully. As pH is known to influence gel packing (Tiller and Tsai, 1986) the pH of the sol was measured for reference. The pH was not altered by the addition of bases or acids as this could have interfered with the sintering behaviour. Polymeric deflocculants were not employed as these may only partially decompose during sintering and mask the presence of carbonate.

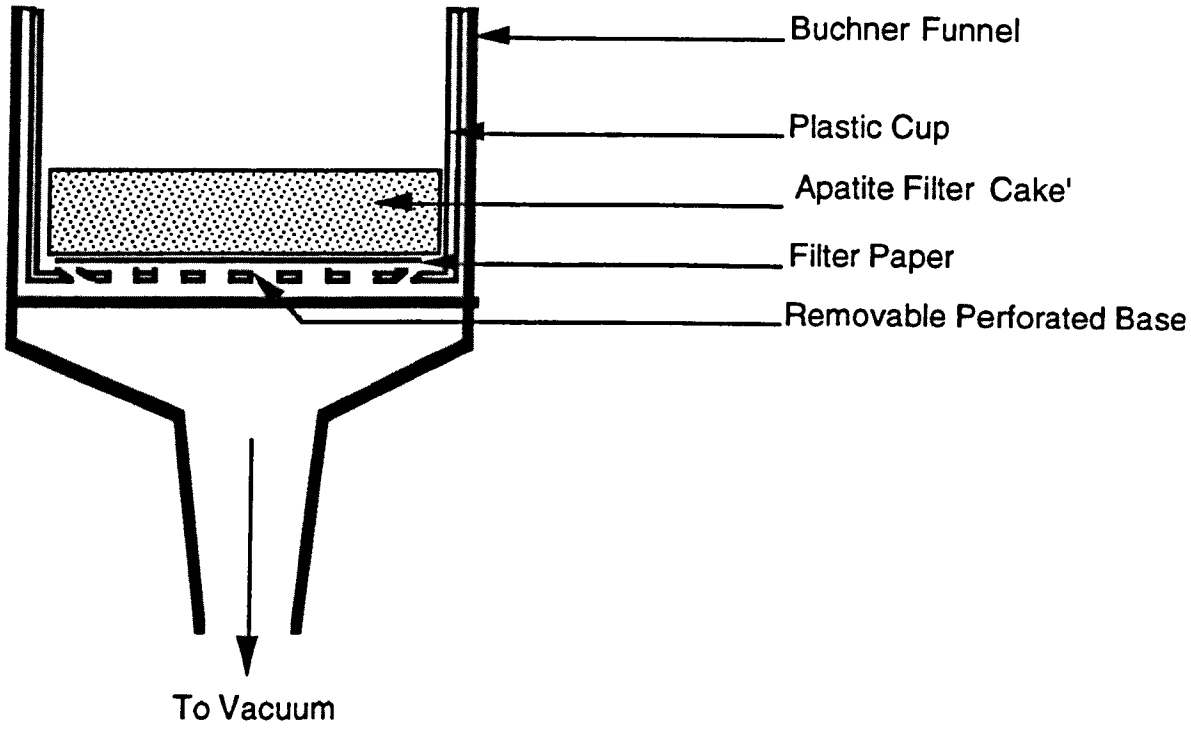

Figure 7.2. Apparatus used for the formation of apatite monoliths.

7.3.2 .Monolith Formation

The solid volume fraction of the 3C9M suspension was determined by weighing a 100ml measuring cylinder both empty and full. From these measurements the density of the suspension could be calculated, assuming a density of hydroxyapatite of 3.15 Mg m^{-3}, the volume fraction could be obtained. Sol was admitted to the filtration cavity via a burette and the vacuum was applied at constant pressure by means of a water pump and vacuum gauge. Once the rate of filtration was imperceptible (<0.10 ml h^{-1}), the mould cavity was sealed by means of tap A. Tap B was closed to maintain the vacuum in the filtration cavity. The unit was left for 24 hours and filtration was restarted and the process repeated. The monolith was then carefully removed from the mould.

Rate of Filtration

The rate of filtration of 3C9M sol was measured throughout the formation process, by measuring the volume filtered per unit time at a particular time. The applied vacuum was measured to be in the order of 100kPa.

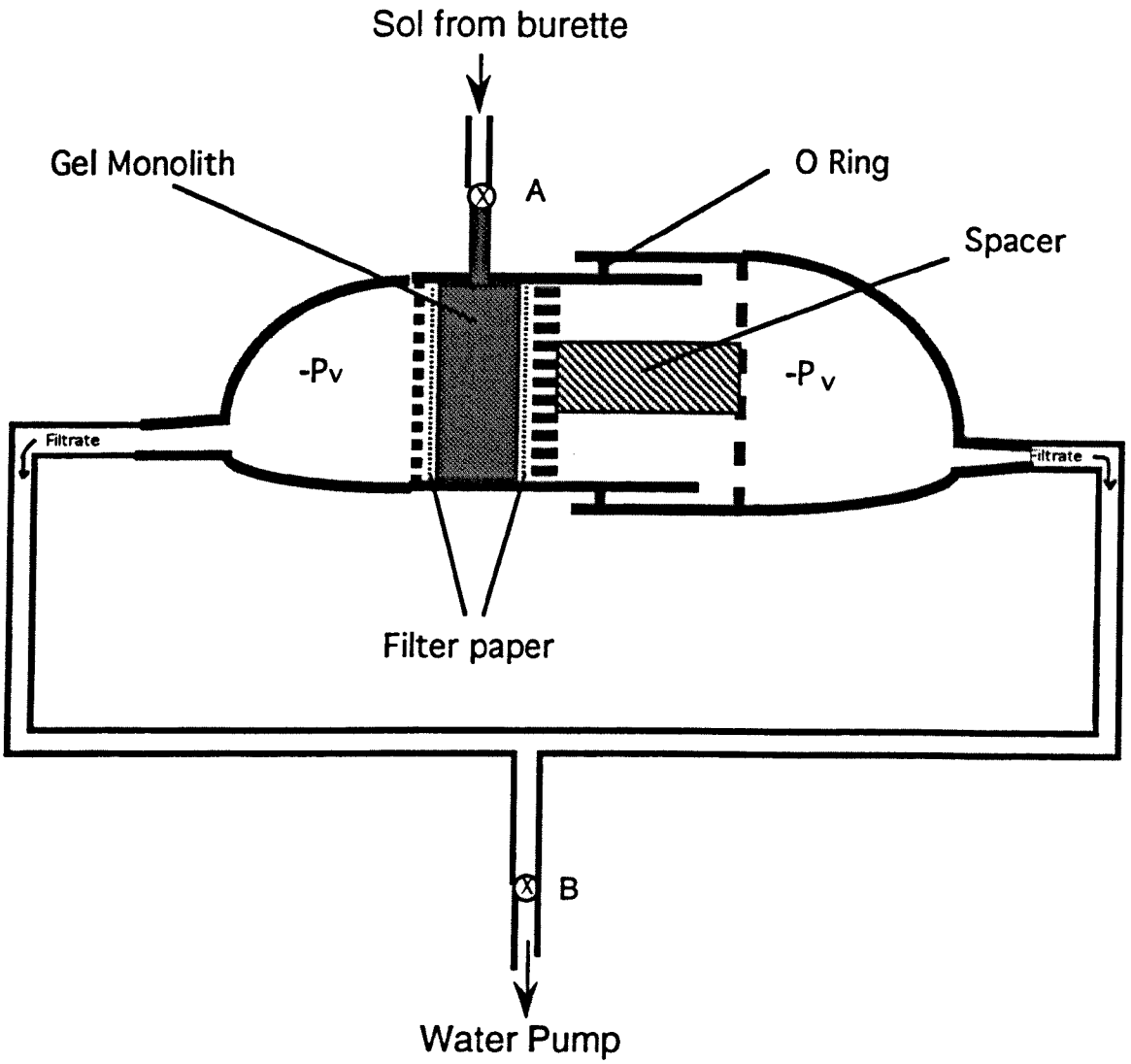

Figure 7.3. Apparatus used for producing biaxially filtered gel monoliths.

7.3.3. Gel Drying Procedure

Gel monoliths were dried slowly in cotton wool at room temperature. This insulating layer was at least 0.25m thick in order to approximate to an infinite layer of insulating still gas.

Drying Rate Measurement

The mass of the green compact was recorded once every 24 hours. When no further mass loss was measured over this time period the nearly dried 'cakes' were placed in an oven at 80°C for 24 hours and any change in mass was

noted. Drying was considered to be complete when no further mass loss was detected.

Gel Density

The diameter and thickness of 3C9M and 3C16M monoliths produced by the biaxial method were measured during drying to enable approximate volumes to be calculated. Once drying was complete, the mass of the apatite was measured and its volume calculated, from this and volume measurements, the solid volume fraction was determined at a given point of drying, by using the following relation:

$$V_d = \frac{V_S}{V_T} \qquad (7.1)$$

where V_d is solid volume fraction, V_S is the mass of the solid and V_T is the total volume.

Gelation Point

From the data obtained in the previous two sections it was possible to calculate the volume percent water in the gel during drying. By plotting this data against the logarithm of the ratio of the volume of the monolith at a given water content to the dry gel volume, the water content at which the particles touch i.e. gelation occurs can be determined, (Cooper, 1987).

7.4 Powder and Gel Characteriation

7.4.1 Density

Initially Archimedes' method was used to measure the density of two gels, 3C0M and 3C9M, however it was found that on contact with water, the gels fragmented. The number of pieces was reduced by hydrating the gel slowly, but this method was inconvenient. Approximate measurements, (±2mm) were made of the diameter and thickness of the monolith. In an attempt to improve

on the accuracy of this method, the surface area of the top and bottom of the cylinder was determined using the Quantimet 570 image analysis system and the average thickness was measured using a micrometer. By measuring the dry weight, the density could be determined.

7.4.2 Gel Green Microstructure

The fracture surface of 3C9M gel was examined using a JEOL 6300 scanning electron microscope. A specimen was mounted on a holder using carbon cement so that the surface to be examined was horizontal. A conductive track of carbon was made from the copper holder to the fracture surface in order to minimize charging, the specimen was then gold coated. An accelerating voltage of 20kV was used at magnifications up to 20,000x.

7.4.3 Powder Morphology

Air dried powders were examined using scanning electron microscopy. Specimens were prepared by folding a short length of carbon adhesive tape back on itself, adhesive side out. One side was attached to a copper holder and a small quantity of powder was sprinkled on the exposed adhesive surface. The holder was tapped to remove any unadhered powder before a gold coating was applied. The powders were then examined using a JEOL 35 JSM at 20kV accelerating voltage.

7.5 Chemical Analysis

The carbonate determination and calcium, phosphorus and sodium determinations were carried out by Medac Ltd. at Brunel University in an F.D.A. inspected laboratory. Acid evolution of carbon dioxide was found to be unreliable as not all the carbon dioxide was evolved and comparisons with standard reference materials yielded erronous results. In addition large quantities of sample were required. Atomic absorption was found to be unsuitable for the accurate determination of calcium contents since phosphorus supresses the signal of the calcium and problems were encountered with reproducability of the results, this was probably due to the large degree of dilution necessary.

7.5.1 Carbonate Determination

Carbonate was determined as carbon using a Control Equipment Corporation Model 240 XA CHN elemental analyser. The samples were dried at 120°C for twenty four hours prior to weighing in order to remove adsorbed water. 2.5 - 3mg of sample was weighed on a CAHN 26 automatic electrobalance, accurate to 0.1µg. This was then sealed in a tin capsule which was then loaded into the machine. A schematic diagram of the analyser is shown in Figure 7.4.

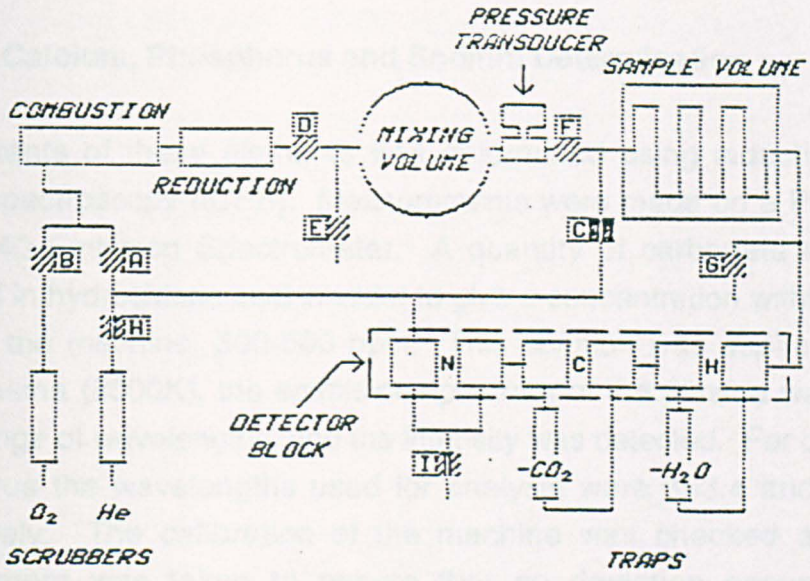

Figure 7.4. Schematic diagram of the Control Equipment Corporation Model 240 XA CHN elemental analyser.

Before sampling, the system was purged with helium, helium was also used as a carrier gas throughout the proceedure. The tin capsule was introduced into the furnace which was held at 1000°C. 30 ml of oxygen was introduced into the furnace four times, each time the position of the sample was moved in order to prevent the formation of a dead or non- oxidizing zone. The tin is burnt and oxidized exothermically at a temperature of 1800°C which was sufficient to decompose the specimen. The gas then passed into a reduction tube which was held at 600°C. The tube was filled with porous copper which reduces any oxides of nitrogen formed in the furnace and a silver scrubber removed any halides present. The gasses then passed to a mixing volume chamber where they homogenise. A volume was sampled and the conductivity was measured, a magnesium perchlorate column removed any

water and the conductivity was measured again and the difference was linearly proportional to the amount of water present. Carbon dioxide was then removed in with sodium hydroxide in the form of Ascarite, again the conductivity was measured. The difference is related to the carbon dioxide content of the gas mixture. Nitrogen was then determined by measuring the difference in thermoconductivity between the helium nitrogen mixture and a pure helium reference. The system was callibrated using three reference materials, acetanalide, cyclohexanone 2,4 dinitrophenolhydrozone and bromo benzoic acid. Duplicate measurements were taken of each sample and the largest difference in values was taken as an indication of the error.

7.5.2 Calcium, Phosphorus and Sodium Determination

The contents of these elements was determined using induction coupled plasma spectroscopy (ICPS). Measurements were made on a Perkin Elmer Plasma 40 Emission Spectrometer. A quantity of carbonate apatite was dissolved in hydrochloric acid in order to give a concentration within the linear range of the machine, 300-500 ppm. This solution was aspirated into an argon plasma (8000K), the emmision spectrum of the plasma was scanned over a range of wavelengths, and the intensity was detected. For calcium and phosphorus the wavelengths used for analysis were 393.4 and 213.6 nm respectively. The calibration of the machine was checked and after a measurement was taken to ensure that no deviation occurred during measurement. The reproducibility of the method was found to be better than 2% of the measured value.

7.5.3 Fourier Transform Infra-Red Spectroscopy

The photoacoustic sampling technique (MTEC Photoacoustic PAC200 system) was used to obtain the infrared spectra of the precipitates and of the dense ceramic sintered at 1250°C in air, carbon dioxide, 'wet' air and 'wet' carbon dioxide. The signal was generated when infrared radiation was absorbed by the sample and converted into heat. This heat diffuses to the sample surface and into the adjacent atmosphere. The thermal expansion of the gas produces the photo acoustic signal. Infrared spectra were recorded on a Nicolet 800 FTIR spectrophotometer. A 680 DSP work station was used to analyse the spectra. A gain of one to four was used depending on the

sample. A four wave number resolution was used and 256 scans were used for data acquisition of the spectra. Helium gas was used to purge the sample chamber. Spectra were obtained between wavenumbers 400 - 4000 cm^{-1}.

7.5.4 X-Ray Diffraction

Diffraction patterns of carbonate hydroxyapatite powders were collected using a Siemens D5000 diffractometer using Cu Kα radiation, λ = 154.18pm with a graphite monochromator. The step size was 0.03° at a count time of 2 seconds per step. The data was analysed on Diffrac AT program. By comparing the patterns with JCPDS standards the phases present could be determined. The lattice parameters of the carbonate apatites were determined by Rietveld analysis of the diffraction profiles using a least squares fitting program (G.S.A.S.). Refinement was continued until the minimum R_{wp} was attained. Diffraction data from selected apatites was collected at the rate of 2θ = 5° to 110 ° with a step size 0.02° and a count time of 12 seconds per step to give high quality data with which Rietveld structure refinement could be carried out.

7.6 Sintering

7.6.1 Tube Furnace Temperature Profile

Sintering was conducted in a Carbolite STF 1600 tube furnace. Temperature was measured using a platinum rhodium type R thermocouple with a Eurotherm Chesel 342 chart recorder. Before sintering the temperature profile of the tube furnace was measured at furnace controller temperatures 1000, 1100, 1200, 1300 and 1400°C. Carbon dioxide was passed through the tube furnace at a flow rate of 1.5 l min^{-1}. The furnace was held at each temperature for one hour to allow thermal equilibrium to be reached. The temperature was measured with the platinum thermocouple. Data from this experiment enabled the temperature displayed on the controller to be calibrated.

7.6.2 Sintering Regimes

Carbonate hydroxyapatites were sintered at temperatures up to 1300°C with a heating and cooling rate of 2.5 °C min^{-1}. This ramp gave rise to thermal histories as displayed in Figure 7.5. Moisture was added to gasses by passing them at a flow rate of 1.5 l min^{-1} through a wash bottle containing 200ml of double distilled water.

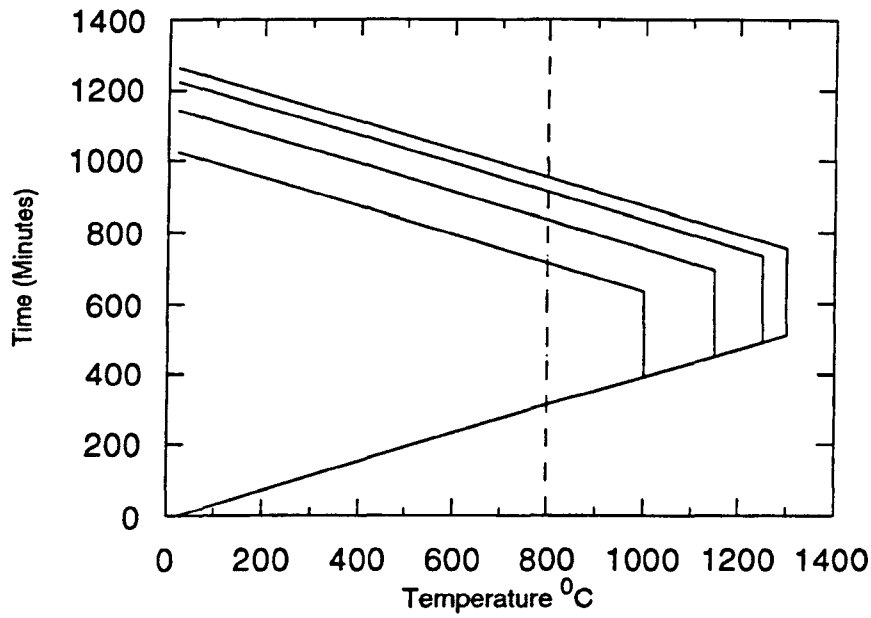

Figure 7.5. Sintering regime used for sintering studies. Sintering commences at ~800°C (Aoki, 1991).

Where wet atmospheres were used the wash bottle was weighed before and after use. The flow rate was maintained at a constant value through each experiment. The gas flow rate and time were recorded and the moisture content of the gas was calculated. From this data an indication of the composition of the gas mixture at various temperatures could be determined using standard thermodynamic relations.

By using the Giauque function Φ and the molar enthalpy the relations (Atkins, 1983) the Gibb's free energy of a particular gaseous reaction at a given temperature and hence the equilibrium constant K could be determined:

$$\frac{\Delta G_m (T)}{T} = \Delta \Phi_0 (T) - \frac{\Delta \{ H_m (298.15K) - H_m(0)\}}{T} + \frac{\Delta H_m(298.15K)}{T} \qquad (7.1)$$

where G (Gibb's free energy) and H (enthalpy) terms refer to standard states, the subscript m indicates the molar value and the number in brackets is the absolute temperature at which the enthalpy value is taken

$$K (T) = \exp \frac{-\Delta G_m}{RT} \qquad (7.2)$$

and where $aZO + bO \Leftrightarrow ZO_2$ is a gaseous reaction:

$$K(T) = \frac{\left(\frac{pZO_2}{p^o}\right)}{\left(\frac{pZO}{p^o}\right)^a \left(\frac{pO}{p^o}\right)^b} \qquad (7.3)$$

where K is the gaseous equilibrium constant, R is the gas constant, T is the absolute temperature, pO is the partial pressure of oxygen and p^o is the total pressure.
It is therefore possible to estimate a probable composition of the furnace atmosphere at a given temperature.

After sintering the densities of the sintered apatites were calculated by means of Archimedes' principle Linear shrinkage (y) .was calculated by pre and post sintering measurements of the apatite sample size:

$$y = \frac{l_o - l}{l_o} \qquad (7.4)$$

where l is the linear measurement after sintering and l_o is the pre-sintered measurement
If the green density (ρ_0)is known the sintered density can be found from linear shrinkage (y), using the relation:

$$\frac{(1-\rho_0)}{(1-y)^3} = \rho_r \qquad (7.5)$$

where ρ_r is the relative sintered density.

However this method provides only a guide to density because of the errors in linear measurements and green density. Pieces of sintered carbonate hydroxyapatite were mounted in epoxy resin, then ground and polished to a one micron finish. Etching was then performed by immersing the polished surface in 10% phosphoric acid for 30 seconds. The acid was washed off in tap water, followed by a final wash in methanol. The polished specimen was examined under a light microscope to check that the microstructure was visible. If necessary the sample was etched for a further 10 seconds and the procedure repeated. The sintered apatites were then gold coated and the microstructure was examined using SEM. From the micrographs obtained, grain size measurements were taken using the linear intercept method. The grain size was deemed to be the mean intercept length using a minimum of 80 grains.

7.6.3 Sintering Studies

Isochronal studies on the effect of sintering atmosphere.

Pieces of 40% dense, 3.2% carbonate hydroxyapatite gel was sintered at temperatures 1000 1150, 1250 and 1300 °C, for four hours in four atmospheres; air, 'wet' air, carbon dioxide and 'wet' carbon dioxide. The physical appearance of the ceramic was noted after sintering. Microstructural and physical characterisation was performed.

Isochronal studies on the effect of carbonate content

In order that the effect of carbonate could be isolated, gels of differing carbonate content and the same green relative density (37%) were used. This was achieved by dividing two pellets of differing carbonate content into small pieces. The carbonate contents of the hydroxyapatites used were 3.2, 5.8 and 7.8 wt%. The gels were sintered at 800, 900, 1000, 1100 and 1250°C, for four hours in wet carbon dioxide.

Isochronal investigations into the effect of green density

5.8 and 7.8 wt% carbonate hydroxyapatite 30, 37 and 40% green relative were sintered at temperatures between 700 and 1300°C for four hours in 'wet' carbon dioxide. The density and linear shrinkage was determined after sintering and the results of materials with different green densities were compared.

Isothermal investigations

Monoliths of 3C9M and 3C16M were produced using the same preparation conditions which resulted in a green density of 37%. These monoliths were divided into small pieces in order to provide specimens with minimal variation, in order to reduce effects brought about by sample to sample variation in green density. The carbonate apatite gels were then sintered in dry and 'wet' carbon dioxide atmospheres at 1000°C for times of ranging between 0 and 1440 minutes. The densities of the sintered apatites were determined and the grain sizes of the materials sintered in wet carbon dioxide were determined.

7.7 Mechanical Characterisation

The effect of sintering conditions on the Vicker's hardness of a 3.2 wt% carbonate apatite that had been sintered in wet and dry carbon dioxide and wet and dry air at temperatures between 1000 and 1300°C for four hours was determined using a Shimadzu microhardness machine. A 1 kg load was applied for 10 seconds. A minimum of six indents were made per sample.

8 Results

8.1 Precipitation

All the reaction conditions used in the precipitation experiments resulted in the formation of white precipitates. When left to stand the precipitate settled out to the bottom of the reaction vessel and the supernatant was clear. It was observed that the time taken for the precipitates to settle varied from approximately 3 hours to 5 days.

8.1.1 Yields

Table 8.1 shows the yield in grams of carbonate hydroxyapatite precipitations at temperatures between 25°C and 70°C, and bicarbonate concentrations up to 560mM.

Table 8.1. The effect of temperature and bicarbonate concentration on precipitate yield (g). (Theoretical yield 0.43g)

T \ $[HCO_3]^-$ (°C)	0	10	40	160	240	320	480
70	0.39	0.41	0.42	0.43	0.42		
60	0.42						
45	0.43		0.43	0.42		0.43	
37			0.41	0.43		0.43	0.39
25	0.39		0.44	0.45		0.45	0.47

8.2 Precipitate Characterisation

8.2.1 Transmission electron microscopy

Crystal size and morphology

Apatite crystals tended to fall into one of two categories; either large (500-700nm long) acicular or smaller (>10nm) spheroidal shaped. These smaller particles are of the size range to expected to exhibit colloidal

behaviour in suspension (Turner, 1991) and are thus referred to as such. The effect of temperature on the morphology of hydroxyapatite crystals was that as reaction temperature decreased, the precipitate size decreased and a more spheroidal habit was observed. Figure 8.1 shows the appearance of the hydroxyapatite crystals precipitated at 3, 25, 37, 45, 60, 70 and 90°C.

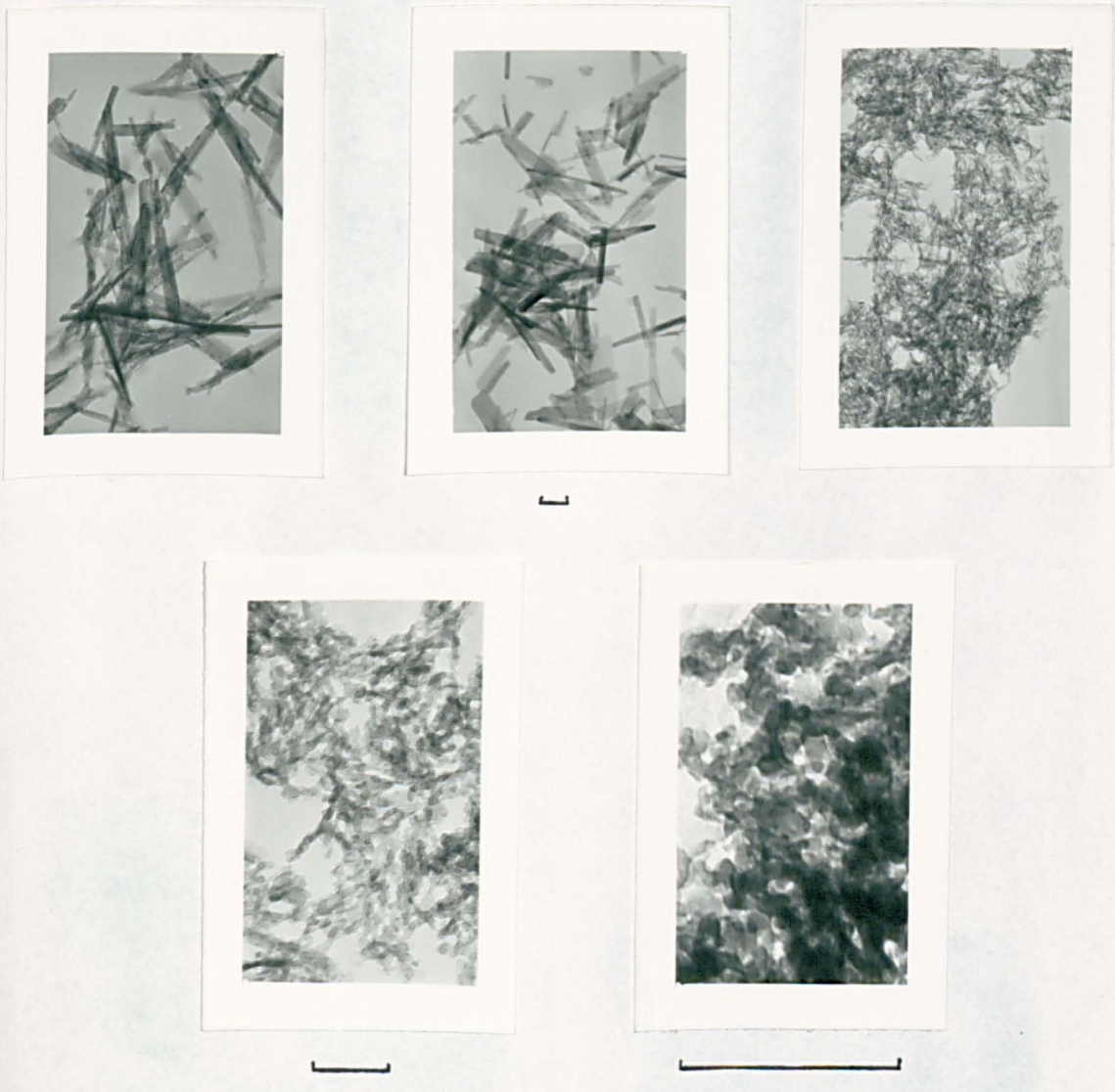

Figure 8.1. The effect of precipitation temperature on the size and morphology of hydroxyapatite precipitates, at a) 3°C, b) 25°C , c) 45°C, d) 70°C and e) 90°C, markers are 100nm.

The effect of increasing bicarbonate concentration was similar to that of decreasing reaction temperature in that precipitate size decreased and more spheroidal shaped crystals were formed. Figure 8.2 illustrates this effect with carbonate hydroxyapatite crystals at 70°C, at concentrations of 10, 40, 160, and 320mM.

a

b

c

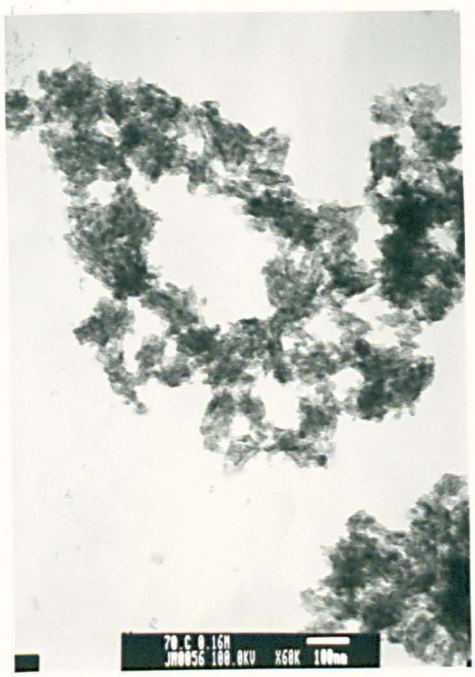

d

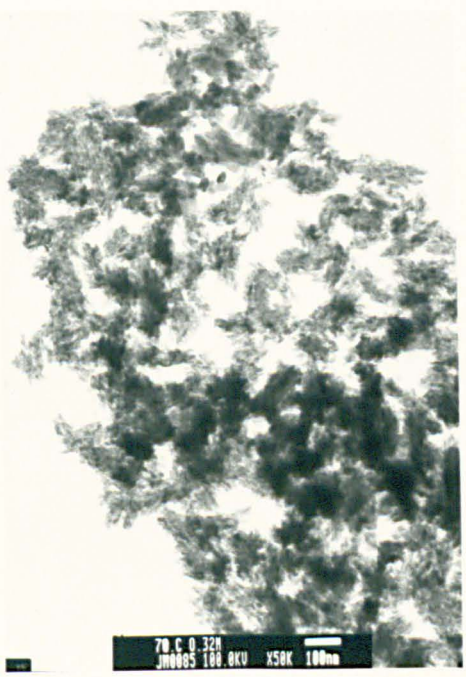

Figure 8.2. The effect of bicarbonate ion concentration on the size and morphology of carbonate hydroxyapatite precipitates at 70°C. a) 10, b) 40, c) 160 mM and d) 320mM.

This effect was observed at all temperatures that were investigated. In cases where hydoxyapatite precipitates were spheroidal, a slight decrease in size was noted with increasing bicarbonate concentration. The effect of reaction condition on the morphology and phase is summarised in Figure 8.3.

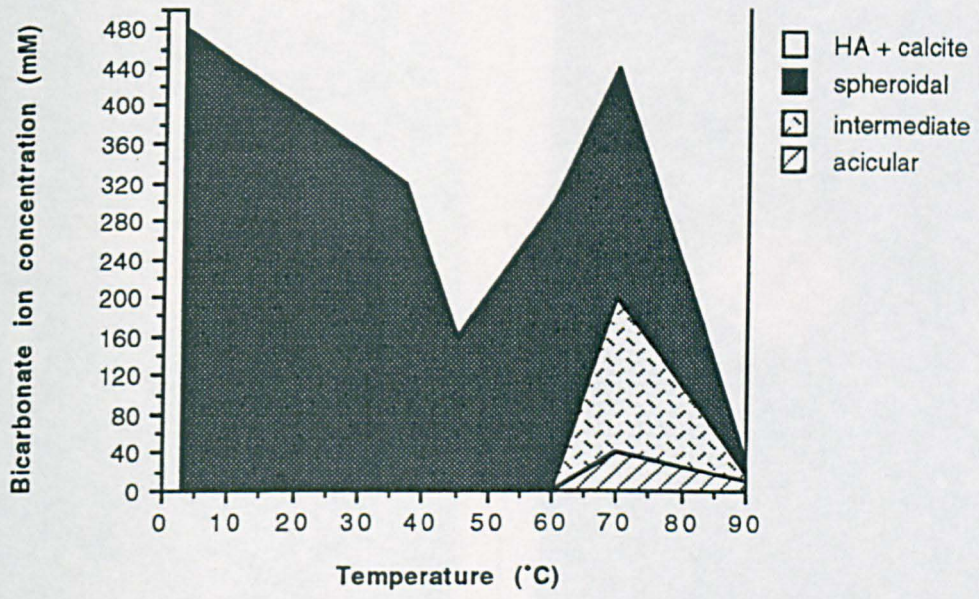

Figure 8.3. Effect of bicarbonate concentration and precipitation temperature on the morphology and phase of apatite crystals.

It can be seen in Figure 8.3 that below 45°C purely spheroidal sol type precipitates were produced. Acicular products were only precipitated at high temperatures and low bicarbonate concentrations. The solubility of carbonate in apatite also appeared to vary with temperature, (Section 8.5.4.).

Electron Diffraction

All the precipitates gave diffraction patterns characteristic of hydroxyapatite. Figure 8.4 shows typical diffraction patterns from a) 90C0M, an acicular hydroxyapatite and b) 3C16M a spheroidal carbonate hydroxyapatite.

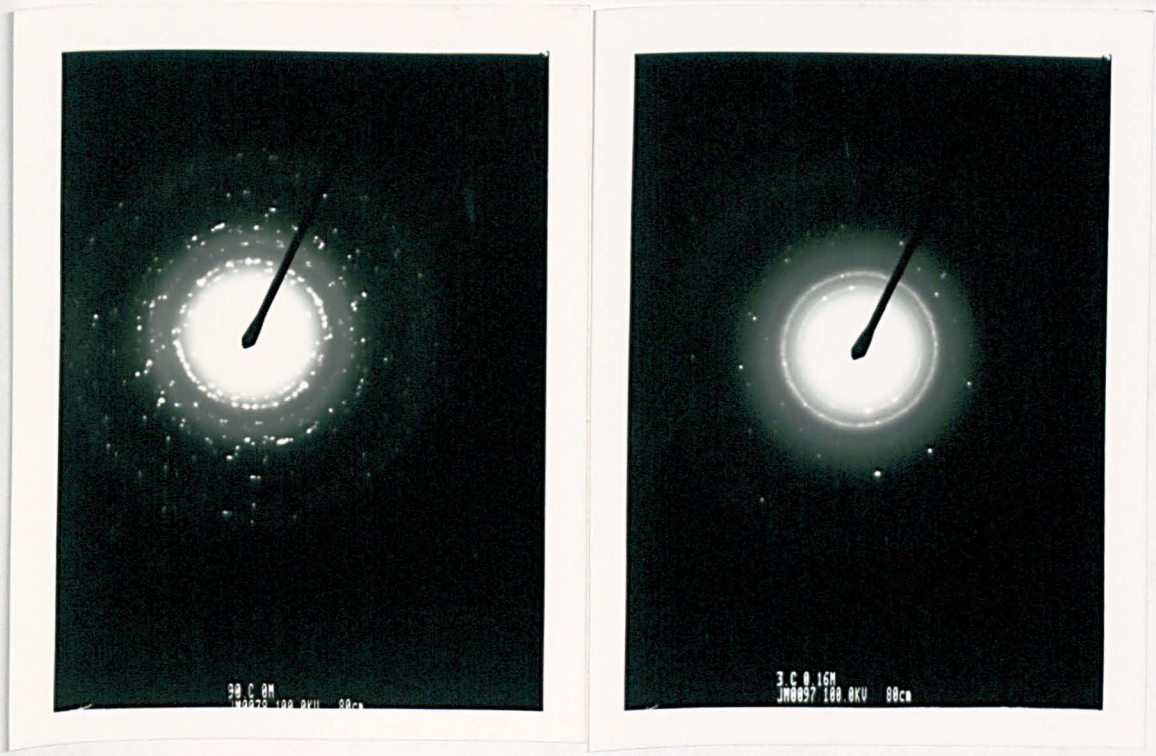

a b

Figure 8.4. Selected area diffraction patterns of a) 90C0M and b) 3C16M.

Figure 8.4.a is spotty due to the diffracted beams coming from a number of individual crystals. Figure 8.4.b is an electron diffraction pattern more characteristic of a polycrystalline material as fewer spots are visible and a more ringed pattern is observed. It was not possible to isolate a single crystal with the aperture used. The planar spacings calculated from the diffraction patterns are compared with the JCPDS values in Table 8.2.

Table 8.2. Planar spacings of hydroxyapatite precipitates calculated from electron diffraction patterns.(±5%)

	d Spacings (pm)							
	d_{002}	d_{210}	d_{211}	d_{112}	d_{202}	d_{311}	d_{222}	d_{213}
HA	**344**	**308**	**281**	**278**	**263**	**215**	**194**	**184**
JCPDS(1987)								
HA-22%CO_3	**346**	**304**	**---**	**278**	**262**	**---**	**193**	**---**
JCPDS(1987)								
90C0M	354	313	283	--	--	--	--	--
90C10M	326	--	--	--	256	--	--	--
90C40M	335	306	--	276	--	--	--	--
70C0M	333	298	--	273	--	--	--	--
70C10M	344	308	--	274	--	--	192	--
70C480M	350	--	--	--	--		--	184
70C640M	334	--	--	--	-	217	--	--
45C0M	322	--	--	--	256	--	--	--
45C320M	337	299	--	--	267	217	--	--	--
45C640M	336	--	--	--	266	218	191	--	--
3C0M		356	317	282	--	--	--	202	
3C160M	335	--	--	--	271	--	--	--	
3C640M	356	--	282	--	--	--	--	188	--

Some spots and rings were not resolvable, hence d spacings could not be determined.

8.2.2 Light Scattering Particle Size Analysis

Both the mode and width of distribution of apatite precipitates decreased with increasing bicarbonate concentration as shown in Table 8.3. For example 70C0M has a particle size distribution with a modal value of 16 μm and a width, within which 90% of the particles lie, of 45μm. At bicarbonate ion concentrations of 160mM the mode became 4μm and the width was 15μm. Above this concentration, at and above which colloidal precipitates were formed, no change in particle size distribution was observed. There is no obvious trend in particle size distribution of hydroxyapatite precipitates with temperature. However, with the exception of 90C04M the mode of size

distribution is approximately the same at and above concentrations of 40mM. The width of distribution at these bicarbonate concentrations is between 11 and 15 μm at 70°C and 15 and 27 μm at 3°C.

Table 8.3. Effect of temperature and bicarbonate concentration on the width and mode of particle size distribution.

	$[HCO_3^{2-}]$ (mM)						
	0	10	40	160	320	480	640
T (°C)	$d_{0.5}$ w	$d_{0.5}$ w	$d_{0.5}$ w	$d_{0.5}$ w	$d_{0.5}$ w	$d_{0.5}$ w	$d_{0.5}$ w
3	18 66	8 14	7 18	6 25	7 27	5 15	6 17
45	8 12						5 26
70	16 45	11 21	8 27	4 15	4 13	5 11	
90	31 70	20 43	16 38				

$d_{0.5}$ mode, w width of distribution ($d_{0.9}$- $d_{0.1}$) (μm).

8.3 Processing

The aim of the processing stage was to produce green compacts suitable for sintering, i.e. a minimal amount of agglomeration, a uniform distribution of porosity and a small particle size. Only gelation was pursued to the sintering stage as other methods appeared unsuitable.

8.3.1 Gelation

It was found from observation and transmission microscopy that precipitates formed at temperatures less than 45°C formed sols. Upon air drying these sols gelled and then dried and cracked into small angular irregular shaped glassy pieces. These pieces were too small to be used for subsequent sintering studies, though Jarcho (1976) reported that hydroxyapatite gels with surface areas up to 100 cm^2 could be formed by this method.

Therefore it was decided to first mould the gels and then dry them to form apatite monoliths. The main causes of cracking during the drying of ceramic - water systems such as clay are: uneven drying rates, large differences in water content in the centre and the surface of the monolith, fast drying rates and friction caused by shrinkage. It was proposed that a layer of cotton wool would prevent uneven drying rates caused by draughts and by not having all the drying surfaces exposed and would provide a support that would offer little resistance to shrinkage. The wool was at least 0.25m thick as it was assumed that this approximated to an infinite layer of cotton wool.

Filtration

The pH of the sols was typically in the range 7.5 - 8.5 irrespective of carbonate content or precipitation temperature. Figure 8.5 shows the filtration rate of 3C09M as a function of filtration time. This suspension was found to have a solid volume fraction of approximately 1%. It can be seen that the rate of filtration decreased with time from an initial value of 0.07 cm^3 min^{-1} to a value of 0.03 cm^3 min^{-1}, within the first two minutes of filtration. The rate then decreased until over the next three hours to a value of 10^{-3} cm^3 min^{-1}. The rate of flow then became almost imperceptible, with approximately 0.1 cm^3 min^{-1} of sol entering the mould over a period of 20hrs. Slip casting theory predicts the time (t) taken for a liquid to flow through a porous medium under capillary action is linearly proportional to the thickness (T) of the medium squared:

$$t^{0.5} \propto T \qquad (8.1)$$

The thickness of the gel is proportional to the volume of slurry entering the mould, assuming a constant concentration in the slurry. The total filtering area is double the area of one circular face due to the biaxial design of the filtration unit. The approxiamte area is therefore:

$$2 \times (2.5^2 \times \pi) = 39.3\ cm^2 \qquad (8.2)$$

A decrease in volume of 39.3 cm^3 is therefore equivalent to a drop of one centimetre in suspension in a uniaxial filtration system of the same area. The volume entering the mould divided by the filtering area (39.3 cm^2),

therefore gives the drop in level h, of a uniaxial filtration system, which is proportional to the increase in thickness of the filter cake as described in Equation 4.12. When the mould is full however, one would expect the total volume of sol admitted into the mould to reach a limiting value, thus Equation 8.1 is only valid during the initial and intermediate stages of filtration. Figure 8.6 is a plot of the slurry volume versus the square root of filtration time.

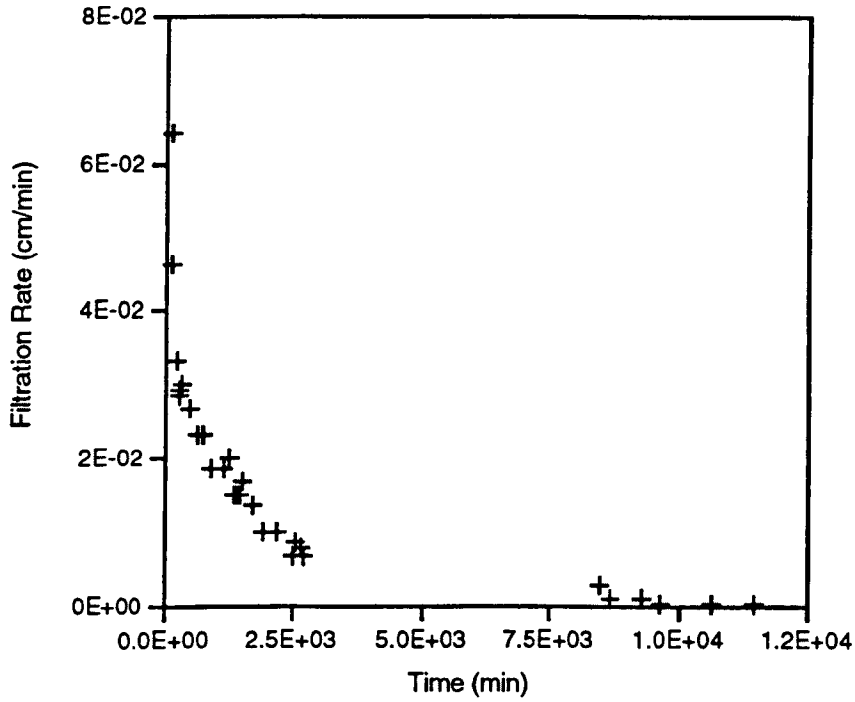

Figure 8.5. Filtration rate of 3C09 M sol with time.

Figure 8.6 clearly shows a linear increase in the gel thickness with the root of filtration time during the initial and intermediate stages of filtration. Therefore it would appear that sol filtration is similar in mechanism to the slip casting. After a time of between one hour and two and a half hours the mould becomes full and the final stage of filtration commences. There appear to be two linear regions. The first corresponding to the filling of the mould and the formation of the filter cake. The second region corresponds to the filling of the central area between the two faces of the filter cake, i.e. an increase in thickness of the filter cakes.

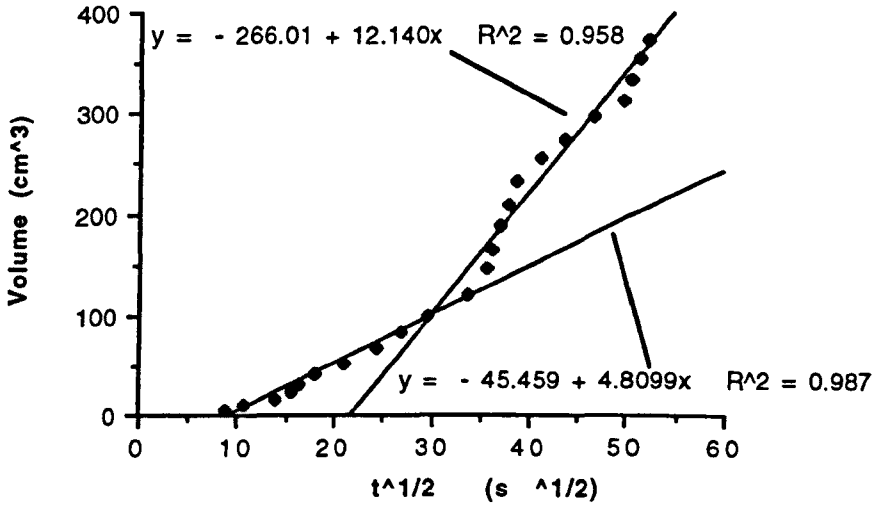

Figure 8.6. The volume of 3C09M sol entering the mould as a function of the square root of filtration time.

8.3.2 Gel Drying

Drying Characteristics

Gels formed by the uniaxial filtration method (Section 7.3.1) tended to curl upon sintering as shown in Figure 8.7. This is due to the decrease in gel density with distance from the filtration surface.

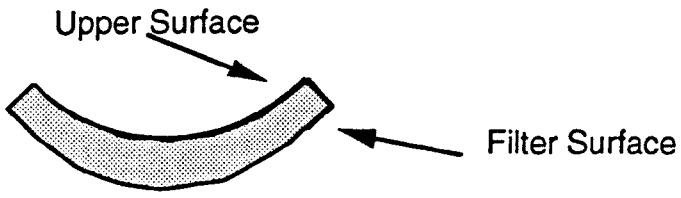

Figure 8.7. The phenomenon of warping during sintering of apatite monoltihs formed by uniaxial filtration, caused by a density decrease with distance from the filtration surface.

Because of the heterogeneous nature of the density of gels formed by this method, the biaxial filter apparatus was devised to eliminate this problem and this method was adopted for further study.

As the drying process was critical for the production of flaw free apatite monoliths the drying time and shrinkage of the gels were investigated. The time taken for the gels to dry was dependent on the size of the monolith. Although a specific relation was not derived, the time required for no further detectable weight loss to occur was of the order of seven days. The surface area to volume ratio of a disc is given by:

$$\frac{2(r+l)}{(r\ l)} \qquad (8.3)$$

Where r is the radius and l is the thickness. When the drying time is normalised with respect to area to volume ratio and mass is normalised it is apparent that all gels followed the same shrinkage behaviour. As Figure 8.8 clearly demonstrates, this behaviour was also independent of carbonate content.

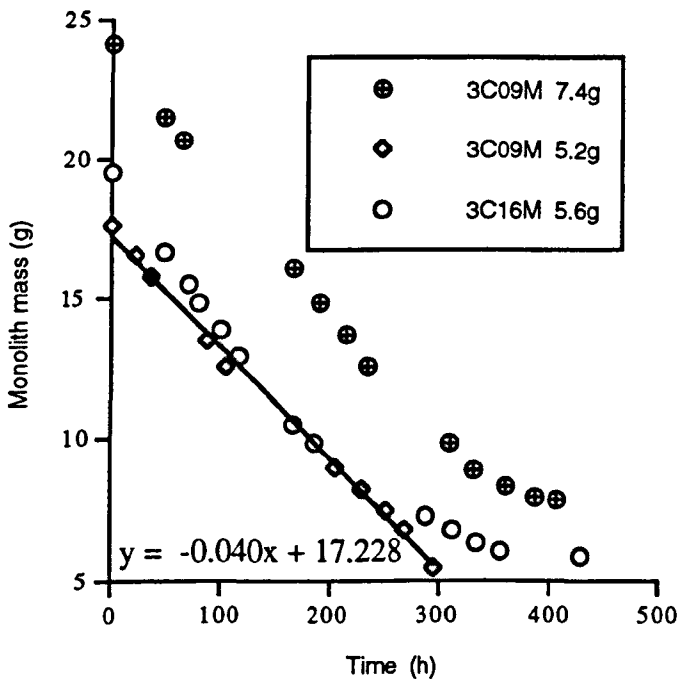

Figure 8.8. The drying characteristics of 3C09M and 3C16M gels of different final masses.

Figure 8.8 shows that the initial water loss rate is independant of carbonate content and size of the gel. The masses in the key of Figure 8.8 refer to the dry weight, since all gels formed monoliths of similar green density. (Section 8.4.1) and, because the radius of each gel is approximately the same, the mass is proportional to the thickness of the monolith. Monoliths

3C09M 7.4g and 3C16M 5.6g show a reduction in rate of water loss after approximately 380 h, this may indicate the onset of a different mechanism of drying.

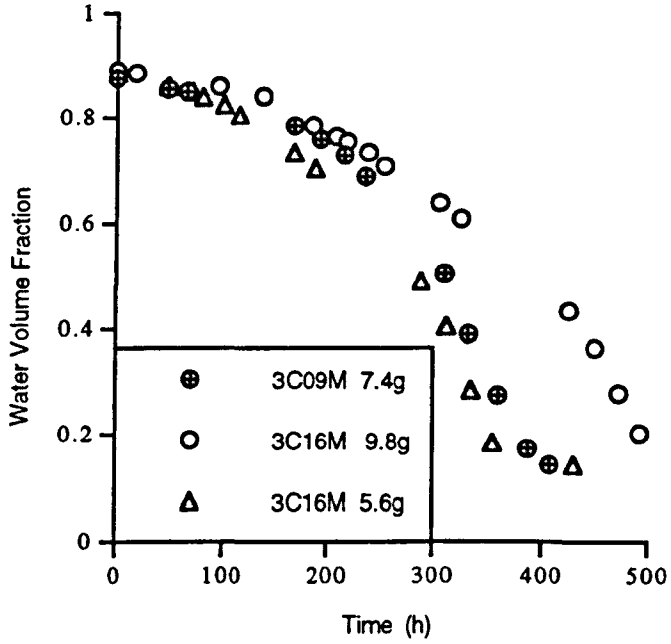

Figure 8.9. Water volume fraction as a function of drying time for 3C09M and 3C16M carbonate apatite monoliths, dry weights as indicated.

Figure 8.9 shows the change in water volume fraction with time. It can be seen that the time taken for a given volume fraction to be attained increases with monolith mass (thickness). Monoliths 3C09M 7.4g and 3C16M 5.6g show a decrease in the rate of water volume fraction. This occurs at approximately the same water volume fraction in both specimens, ~15 %.

Gel Shrinkage During Drying

The solid volume fraction of the gels increased as shrinkage occurred, from 10% at gelation to ~40 % at drying. The drying data showed that at completion of filtration 90% of the cast volume was water. Figure 8.10 shows the change in solid volume fraction with time normalised with respect to surface area to volume ratio (see previous section). As shrinkage progresses with time the solid volume fraction increases to a level between 35-40%, thereafter no further increase in density occurred,

i.e. gelation point was reached. The time for this to occur may be inversely related to the surface area to volume ratio, however there is a variation in the time at which no further increase in solid volume fraction is observed.

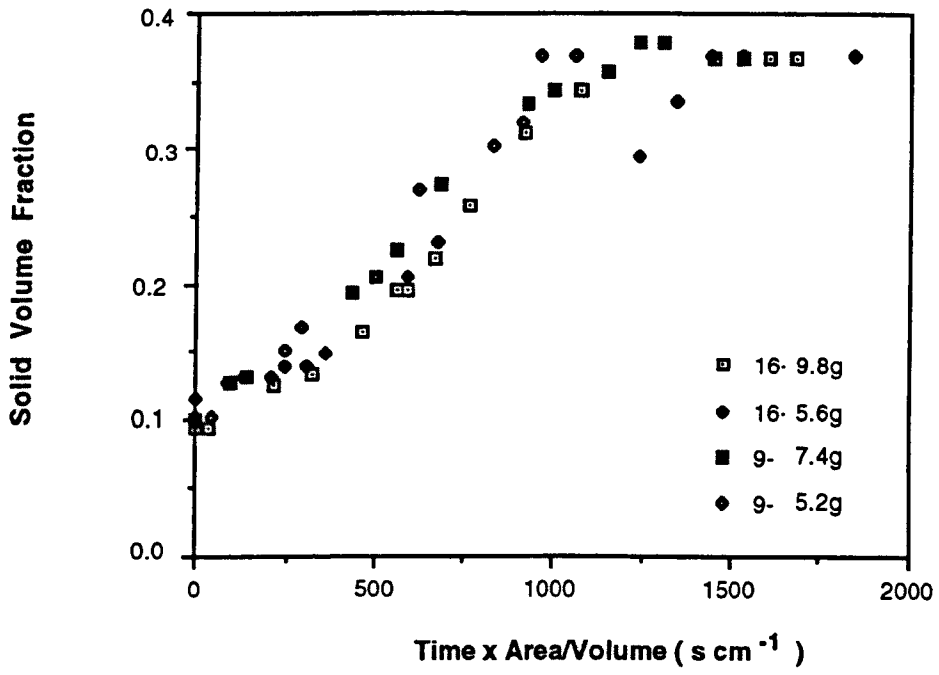

Figure 8.10. Change in solid volume fraction with time during drying of carbonate hydroxyapatite gels.

Gelation point.

Gelation is defined as the point when all particles in the sol are touching. It is unlikely that this occurs homogeneously in the monolith as the water distribution is expected to vary with distance from the surface. By plotting the logarithm of the ratio of monolith volume to dry volume against water content, (Figure 8.11.) gelation point can be determined from the water content at which swelling commences (Cooper, 1987), i.e. at which shrinkage stops.

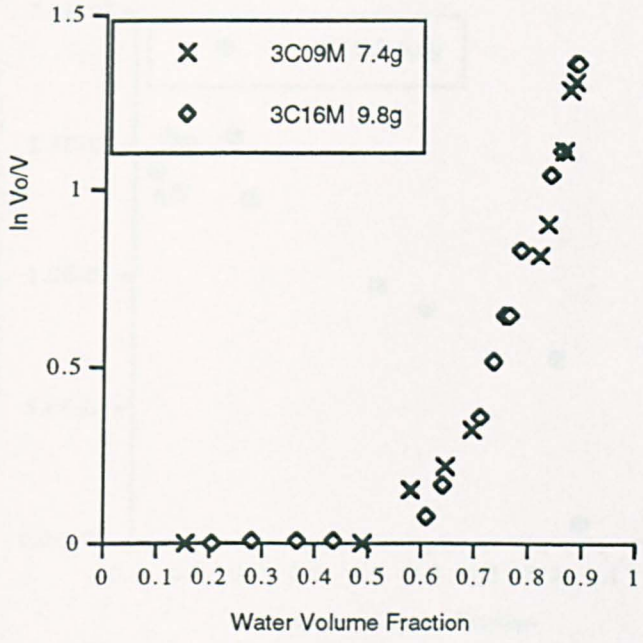

Figure 8.11. Plot of monolith volume against water content, demonstrating shrinkage behaviour during drying.

It can be seen from Figure 8.11 that shrinkage ceases at between 50 and 55% water volume fraction. At this point the solid particles form a rigid network and no further shrinkage occurs. It is interesting to note that the change in water volume fraction loss rate occurred at ~15 % (Figure 8.9). This indicates that the water menisci are inside the gel when the change in water loss rate occurs.

Figure 8.12 shows the change of water loss per unit area per hour with water volume fraction for a 3C16M monolith. Three regions are identifiable. The first represent the values that fluctuate around the rate of 1.5×10^{-3} g cm^{-2} h^{-1} representing the constant rate period. The second rate falling period is seen in the almost linear decrease in loss rate with water volume fraction. The final diffusion controlled region is seen in the rapid decrease in loss rate at low water volume fractions.

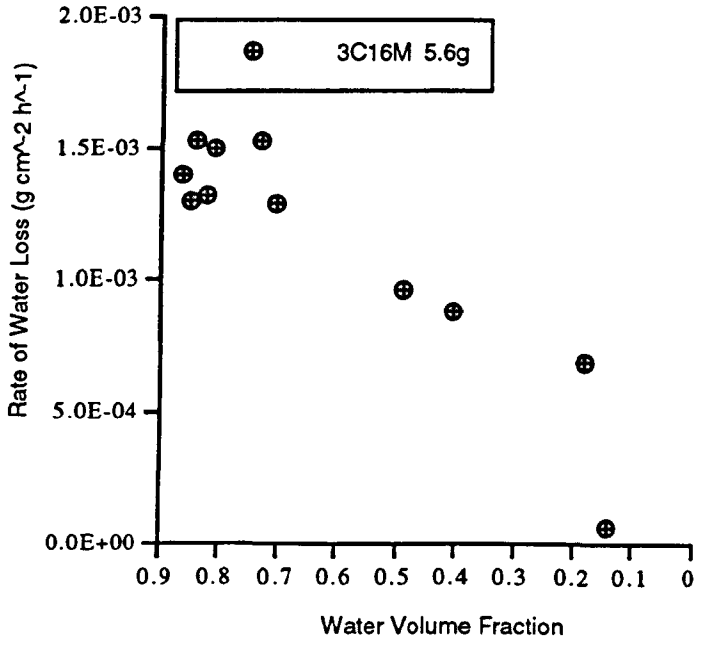

Figure 8.12. Water loss rate as a function of water volume fraction of a 3C9M monolith.

8.4 Powder and Gel Characterisation.

8.4.1 Density

By measuring the surface area of the two approximately parallel surfaces, the average diameter in a fixed plane and by measuring an average thickness, a value for gel volume could be determined. The monoliths formed were ellipsoidal prisms (Figure 8.13) that is the diameter tended to decrease at the centre. Because of this it was necessary to make the assumption that the shape of the cross section normal to the thickness did not change. The mean area was assumed to be related to the square of the mean diameter, d. A constant of proportionality, k, between A_1 and A_2 and the corresponding diameters d_1 and d_2 was determined from:

$$k = \frac{A_1 + A_2}{d_1^2 + d_2^2} \qquad (8.4.)$$

The volume (V), was then calculated from :

$$V = (d^2 * k) * t \qquad (8.5.)$$

Where A_1 and A_2 are the top and bottom areas and t is the average thickness. Table 8.4 shows the green densities of 3C09M and 3C16M gels,

biaxially filtered at a pressure of - 100 kPa. One specimen was filtered uniaxially for comparison.

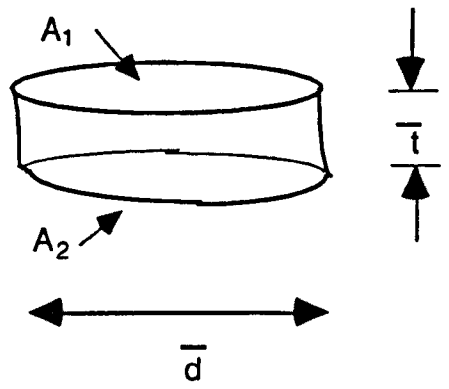

Figure 8.13. The shape of the apatite monoltihs produced and the dimensions measured for density determination.

Table 8.4. The thickness (mm), area (mm^2), volume (mm^3) and relative density of 3C09M and 3C16M gels filtered at 100kPa.

Gel	t	sd	A	sd	V	sd x	Mass(g)	ρ(%)	sd
3C09M	8.24	0.3	564	13	4647	202	5.35	37	1.6
3C09M	10.1	0.6	630	24	6363	449	7.47	37	2.6
3C16M	8.47	0.5	584	21	4943	342	5.72	37	2.5
3C16M	12.7	1.0	682.	24	8661	748	9.93	37	3.2
3C16M*	7.23	0.4	494	50	3572	410	4.74	42	4.3

* Filtered on one side only

x A has a sd of a , B has a sd of b, then sd of (A x B) = $\sqrt{A^2b^2 + B^2a^2}$

Table 8.4. shows that there is a error of up to 11% of the measurement of volume. The largest source of error would appear to be the area measurement, this is in part due to irregularity in shape. However with the exception of the uniaxially filtered monolith, all the gels produced appeared to have a similar relative density and carbonate content did not appear to make a significant difference to the green density.

8.4.2 Gel Green Microstructure.

Scanning electron microscopy revealed the nature of the gel microstructure as shown in Figure 8.14. It is apparent that the gel consisted of agglomerates approximately 100nm in dimension, surrounded by interconnected porosity. There was no evidence of regions of macro porosity and the micostructure appeared homogeneous.

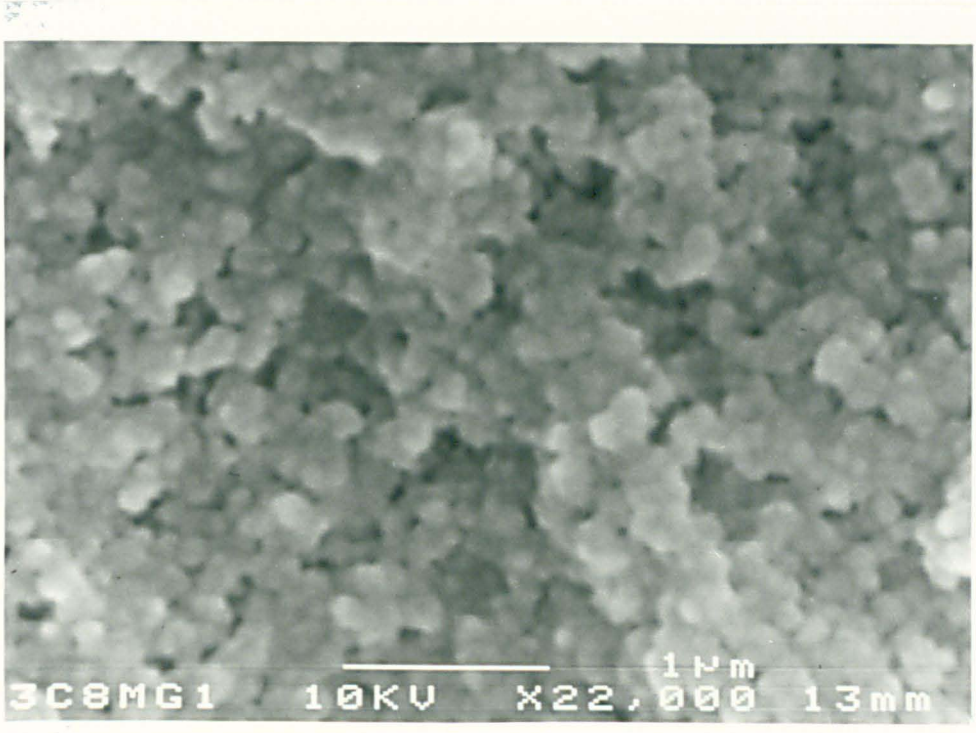

Figure 8.14. Microstructure of 3C9M carbonate hydroxyapatite gel.

8.4.3 Pore Size Distribution

The pore size distributions for a 40% dense 3C16M gel and a pressed (14MPa) powder pellet of commercial hydroxyapatite are shown in Figure 8.15. It can be seen that the distribution of the powder pellet is bimodal about 70nm and 6μm. The gel has a unimodal distribution about 9nm diameter that is very narrow compared to the powder pellet.

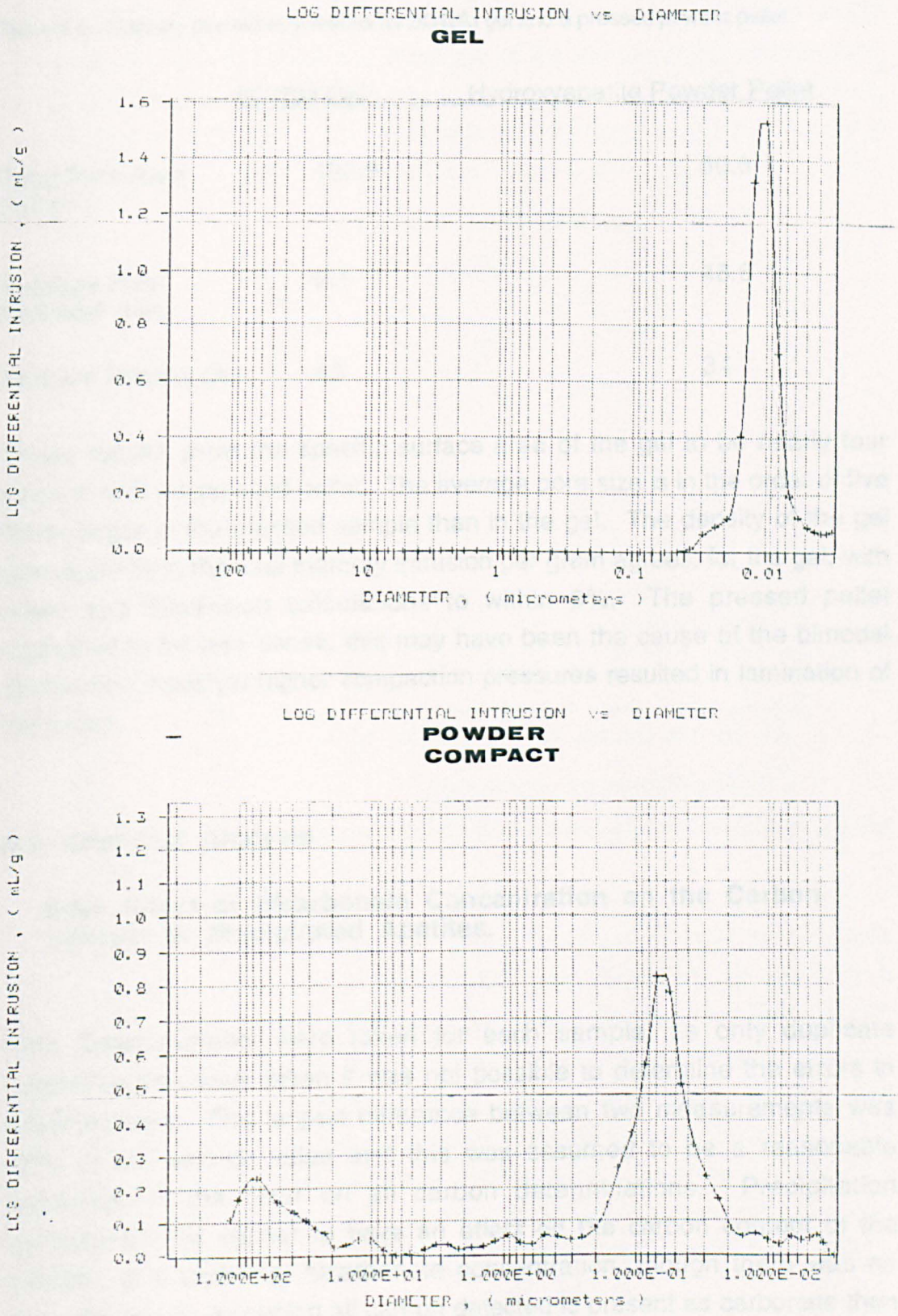

Figure 8.15. Pore diameter distributions of 3C16M gel and a pressed powder pellet.

Table 8.5. shows the results of the mercury porosimetry for the two samples.

Table 8.5. Mercury porosimetry results for 3C16M gel and a pressed powder pellet.

	3C16M Gel	Hydroxyapatite Powder Pellet
Total Pore Area ($m^2 g^{-1}$)	183.9	50.8
Average Pore Diameter (nm)	9.1	48.6
Relative Density (%)	43	34

These results show the specific surface area of the gel to be nearly four times that of the pressed pellet. The average pore size is in the order of five times larger in the pressed sample than in the gel. The density of the gel calculated from the total mercury intrusion per gram agrees, for the gel, with mass and dimension calculations to within 3%. The pressed pellet appeared to be less dense, this may have been the cause of the bimodal distribution, however higher compaction pressures resulted in lamination of the pellet.

8.5 Chemical Analysis

8.5.1 Effect of Bicarbonate Concentration on the Carbon Content of Precipitated Apatites.

Two measurements were taken for each sample, as only duplicate measurements were taken it was not possible to determine the errors in measurement. The largest difference between two measurements was 12% of the smaller value and this was assumed to be a reasonable indication of the error on all carbon determinations. Precipitation temperature did appear to have an effect on the carbon content of the apatites at a particular bicarbonate concentration, though there was no apparent trend. Assuming all carbon detected is present as carbonate then carbon content can be assumed to be a measure of carbonate content. A carbonate ion weighs five times as much as a carbon atom. Figure 8.14

shows the variation in carbon content with bicarbonate ion concentration at precipitation temperatures between 70 and 3°C. At C/P ratios greater than those indicated in Figure 8.16 at a particular temperature a second phase of calcite was formed. With the exception of the series precipitated at 45°C the C/P ratio at which a second phase appears increases with decreasing precipitation temperature. The maximum carbon content observed was 2.8 wt % (14 wt % carbonate). The maximum value at 3°C was lower, 2.3 wt%.

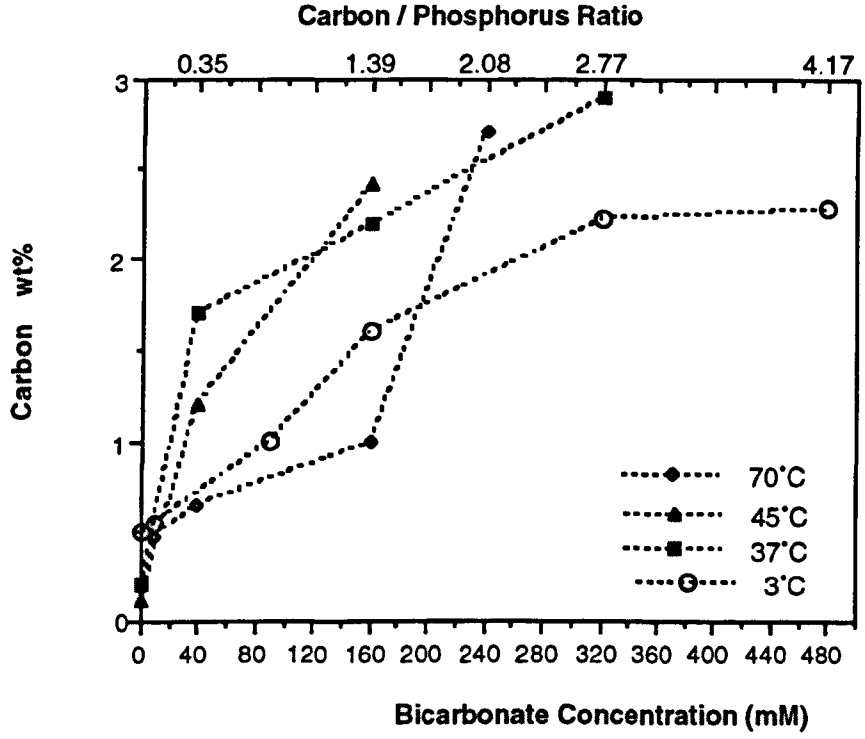

Figure 8.16. Variation in carbon content with bicarbonate concentration of precipitation solutions at temperatures 70 to 3°C.

There was a rapid increase in carbon content at low bicarbonate concentrations (0-10mM). Above this concentration 45 and 37°C precipitates continued to display a rapid increase in carbon content with increasing bicarbonate concentration up to 40mM. The increase in carbon content with bicarbonate concentration then became less marked. The high carbon content of the apatite precipitated at 70°C with 240mM bicarbonate concentration does not fit this trend. At high (>40mM) the carbonate apatite precipitated at 37°C appears to have a higher carbon content at a given bicarbonate concentration than that precipitated at 3°C.

8.5.2 Chemical Analysis of Precipitated Apatites

As some workers (LeGeros, 1967; Nelson and Featherstone, 1982) have reported a $NaCO_3$ for $CaCO_3$ type substitution , the sodium content of a selection of carbonate apatites was measured. It was found that the sodium content of a 4 wt % carbonate apatite was < 0.1 wt% i.e. below the detection level of the apparatus, an 11.5 wt % carbonate apatite contained 1.5wt% sodium. Only single calcium and phosphorus measurements were made, however four repeat measurements were made on a fluorapatite standard reference material the results were: Ca 37.25(0.46), P 17.89 (0.16)

Calcium

The calcium weight percent as a function of carbon weight percent of apatites precipitated at 70, 45,37, 25°C and 3°C is shown in Figure 8.17.

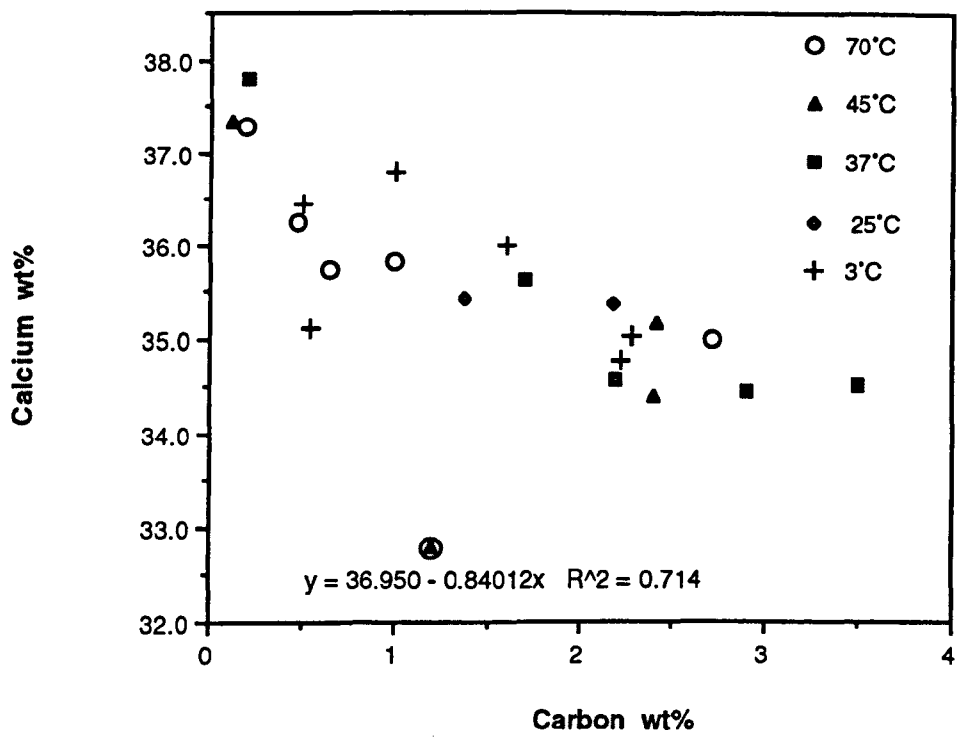

Figure 8.17. Change of calcium content with carbon content of apatites precipitated at 70, 45, 37, 25°C and 3°C.

It would appear that there is a general trend of loss of calcium with increasing carbon content. A clear difference between the precipitation temperatures is not apparent. A least squares fit of all the data except the outlaying point at Ca = 32.5%, circled, gives a gradient of 0.8. The resultant R^2 value was approximately 70%. The intercept of the least squares fit indicates that the precipitated hydroxyapatite is calcium deficient and contains 0.75 calcium vacancies per unit cell.

The change of calcium content with phosphorus content is shown in Figure 8.18. It can be seen that calcium content increases with phosphorus content. No obvious trend between precipitation temperature and calcium and phosphorus ratio is apparent. At low phosphorus contents loss of any linear trend is observed. A linear fit of the data in Figure 8.18 yields a gradient of 0.7.

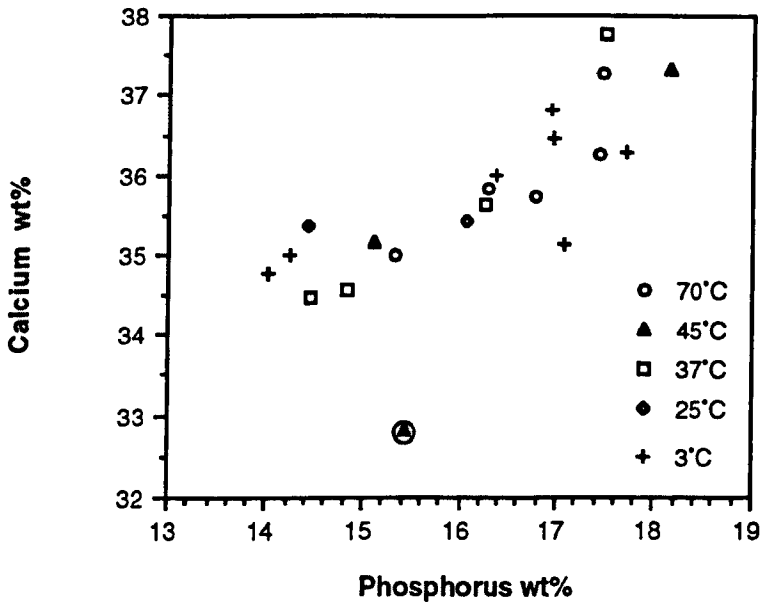

Figure 8.18. Variation of calcium content with phosphorus content of precipitated apatites.

Phosphorus

The change in phosphorus weight percent with carbon content is shown in Figure 8.19. A clear relation exists between the decrease in phosphorus content with the increase in carbon content. This effect would again appear to be independent of precipitation temperature.

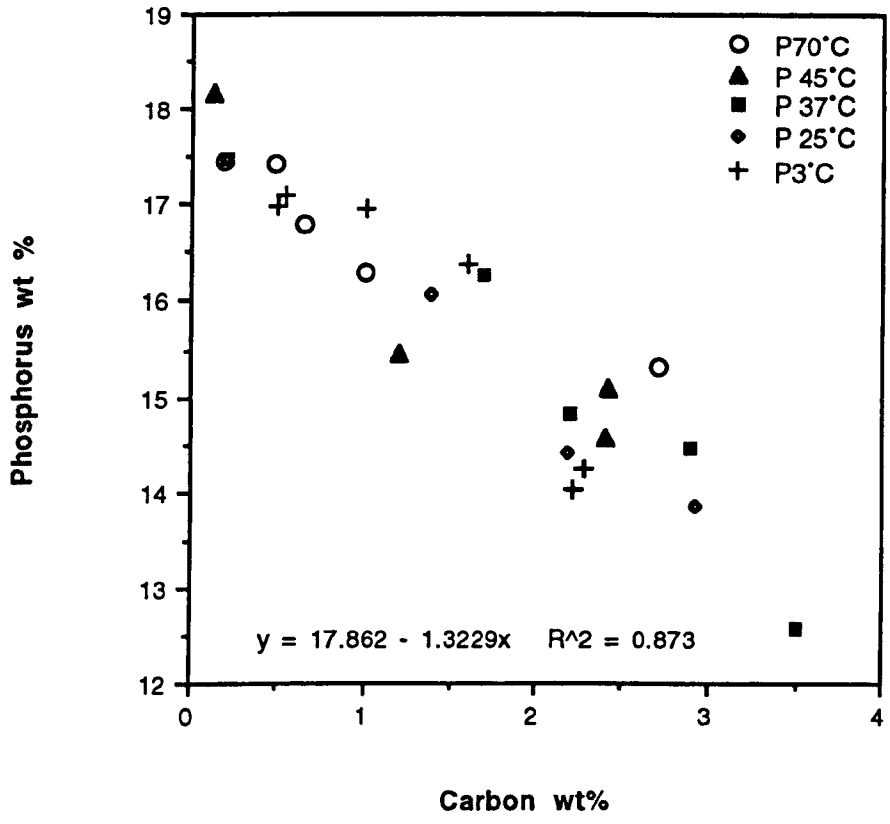

Figure 8.19. Effect of carbon content on phosphorus content of precipitated apatites.

A least squares fit of all the data in Figure 8.19 shows a gradient of -1.32.

Hydrogen

It was found that as the carbon content increased the hydrogen content also increased. Figure 8.20 shows the variation of hydrogen content with carbon content for the apatites precipitated at 70, 45, 37 and 3°C.

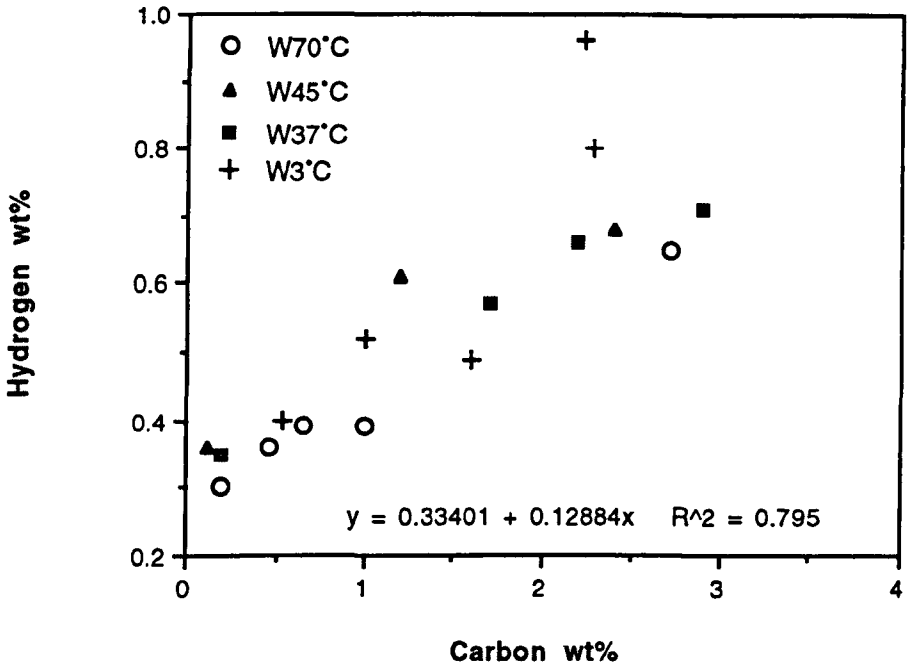

Figure 8.20. Hydrogen content of carbonate apatites as a function of carbon content.

It would appear from Figure 8.20 that a positive correlation exists between the carbon content and the hydrogen content of the precipitates. A least squares fit of all the data except the highest water content of the change in water content with carbon content has a gradient of 0.13. However there is a poor fit for this data as indicated by the low correlation coefficient.

8.5.3 FTIR Spectra of carbonate precipitates

The peak positions of the major carbonate and phosphate peaks of carbonate apatite precipitated at 3, 37, 70 and 90°C are shown in Table 8.6.

Table 8.6. Peak positions of the FTIR spectra of some of the carbonate apatites precipitated at different temperatures and bicarbonate concentrations, compared with reported peak assignments.

Species	CO_3^{2-}	PO_4^{3-}	PO_4^{3-}	CO_3^{2-}
Vibration mode	υ_3	υ_3	υ_1	υ_2
SAMPLE				
3C0M	1574,1557,1534 1488,1454,1420	1086,1059	961	874
3C01M	1557,1456,1418	1084,1041	960	875
3C09M	1557,1539,1419	1063,1048	960	873
3C32M	1505,1489,1473 1457,1434,1419	1050,1008	961	871
3C48M	1505,1488<1473 <1457,1434,1419	1052	960	872
37C0M	1488,1456,1419	1090,1061	961	875
37C04M	1488,1456,1419	1042	961	873
37C16M	1473,1456,1419	1045	961	872
37C32M	1473,1457,1419	1046	961	872
70C0M	1455,1419	1090,1049	962	875
70C01M	1455,1419	1087,1040	961	874
70C04M	1454,1417	1042	961	873
70C16M	1456,1418	1052	961	873
70C24M	1467, 1450<1413	1039	961	873
90C0M	1455,1420	1093,1035	962	875

The hydroxyapatites precipitated in the absence of bicarbonate ions do actually contain carbonate. As the precipitation temperature increases the

carbonate υ_3 bands at higher wave numbers become less prominent and at 70 and 90°C only those at 1455 and 1420 cm^{-1} are observed.

Two phosphate υ_3 bands are present that become further apart as the precipitation temperature increased. The phosphate υ_1 band of the hydroxyapatites prepared in bicarbonte- free conditions appears to be unaffected by precipitation temperature. The υ_2 carbonate bands are observed at 875cm^{-1} in bicarbonate- free conditions at all temperatures (Figure 8.21).

As the bicarbonate concentration of the precipitation media at 3°C was increased, the carbonate υ_3 peak at 1574cm^{-1} then those that at 1557cm^{-1} disappeared. It is not clear whether these peaks are absent or become obscured being shoulders on more intense bands at lower wavenumbers. This effect of increasing bicarbonate concentration is observed at higher temperatures however, as the reaction temperature increases the higher wavenumbers become absent, (Figure8.22). The carbonate υ_2 band was located at wavenumber 875cm^{-1} at all reaction temperatures in bicarbonate free conditions. As the bicarbonate concentration increased the peak position appeared to move slightly to a lower wavenumber (873cm^{-1}). Although the difference is small it was observed in all samples.

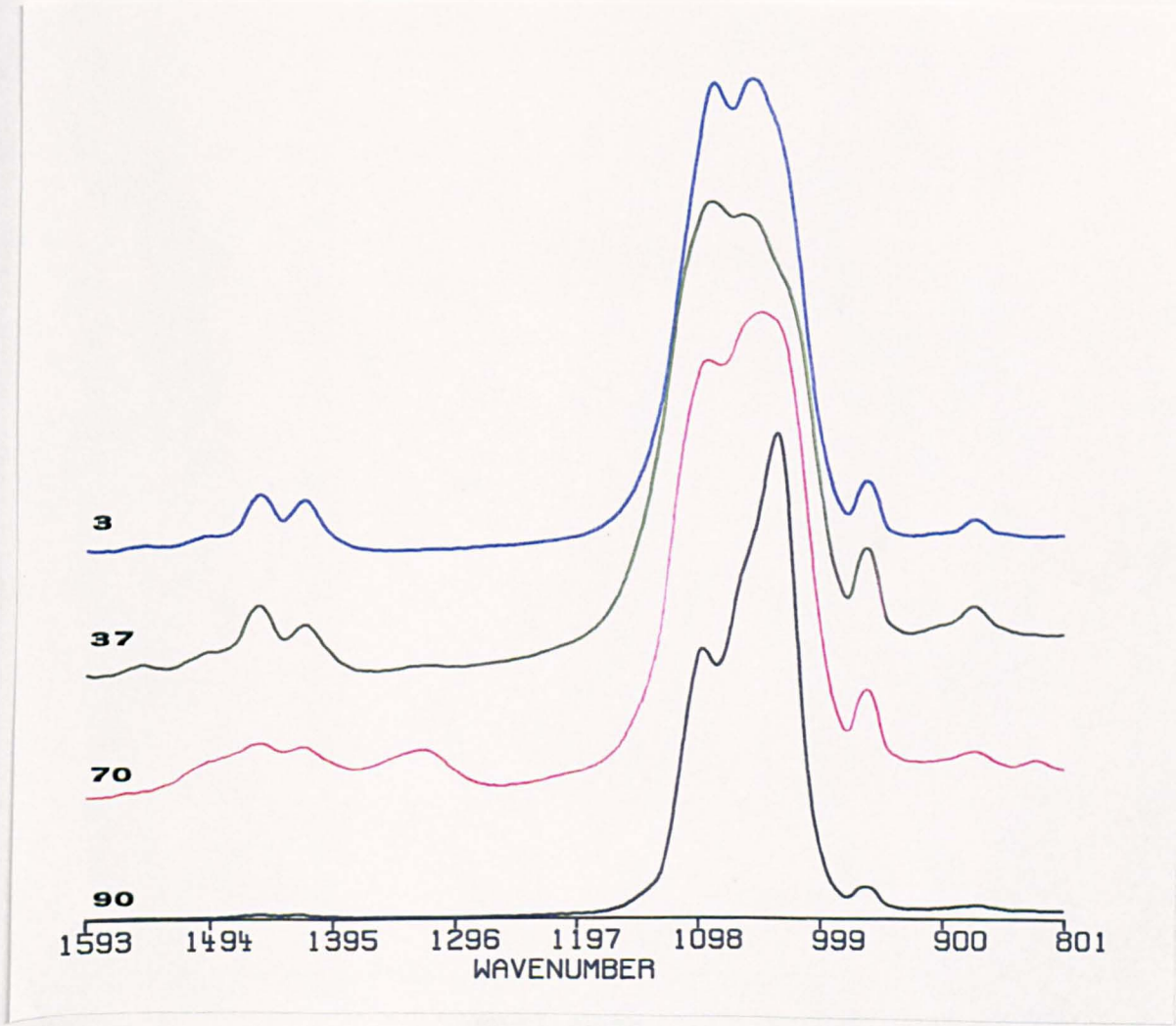

Figure 8.21. Effect of precipitation temperature on the IR carbonate υ_3 and υ_2 and phosphate υ_3 and υ_1 bands.

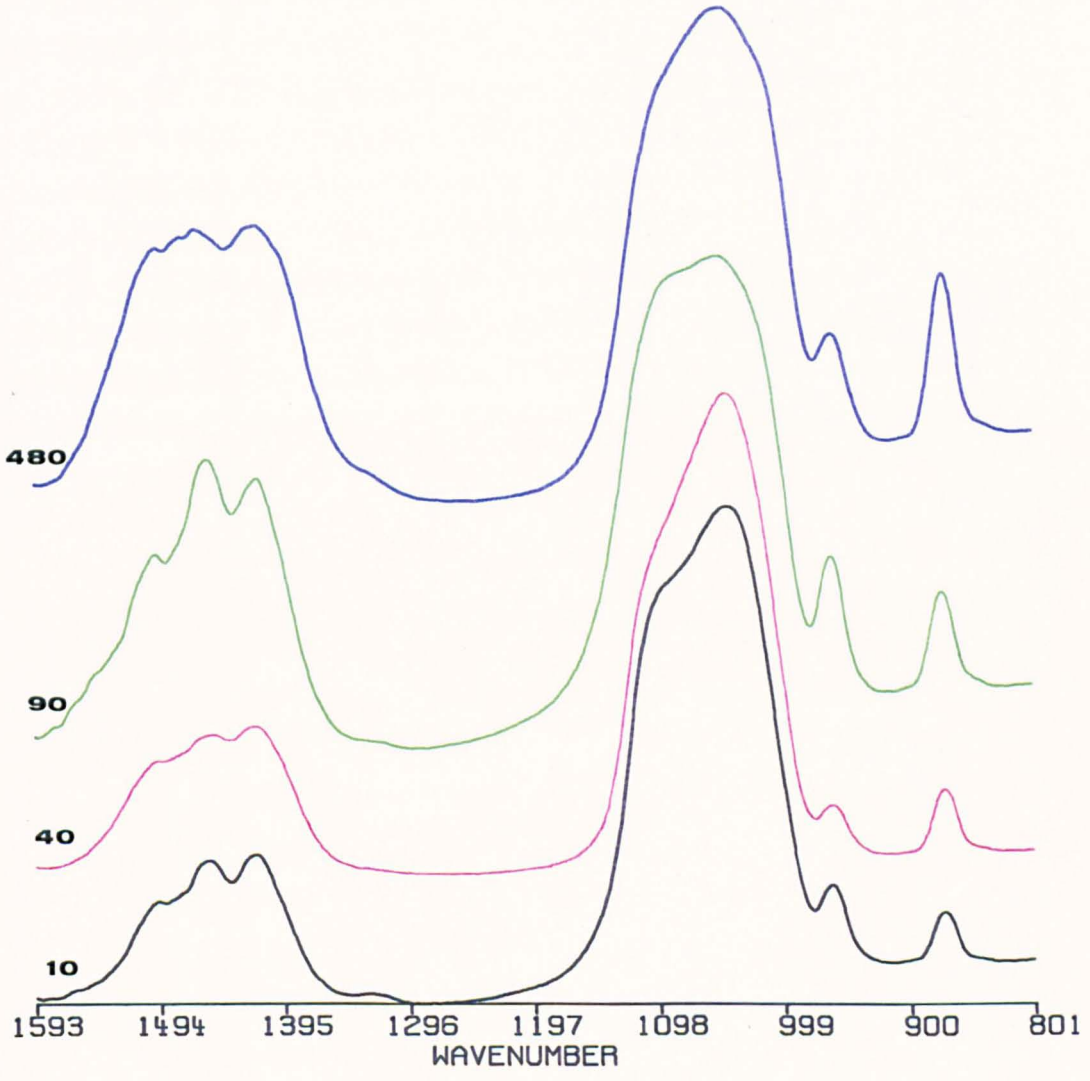

Figure 8.22. Effect of bicarbonate concentration on IR carbonate and phosphate bands of carbonate apatites precipitated at 3°C.

8.5.4 X Ray Diffraction

Phase Determination

The precipitation conditions used were found to produce hydroxyapatite, brushite and calcite phases. At 90°C a unique series of products was formed with increasing bicarbonate concentration: at 0M a single phase of hydroxyapatite precipitated, at 10mM a second phase of brushite is co-precipitated and at the higher bicarbonate concentration of 40mM a mixture of carbonate apatite and calcite was precipitated. At 70°C and below a single phase carbonate apatite was formed, until a limiting bicarbonate concentration was exceeded, whereafter a mixture of calcite and apatite was produced. The relation between temperature and this limiting concentration is somewhat complex and exact values have not been determined. Figure 8.23 is an approximate 'map' of carbonate hydroxyapatite precipitation conditions and products for the system under investigation.

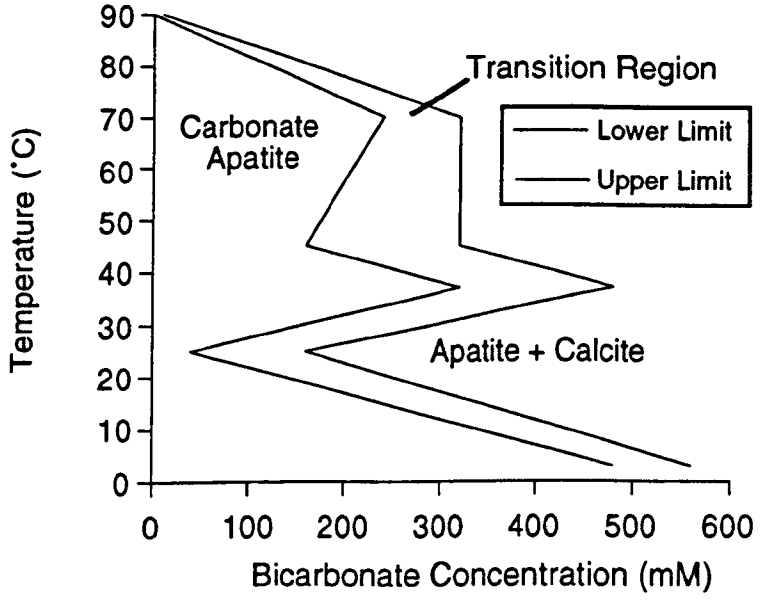

Figure 8.23. Effect of precipitation temperature and bicarbonate concentration on the limiting value of concentration, below which one phase is formed.

Lattice Parameters

At temperatures below 45°C and at high bicarbonate concentrations the crystal dimensions of the precipitate were small (in the order of tens of nanometers). As a consequence, the diffraction patterns of apatites formed under these conditions were typified by broad peaks.

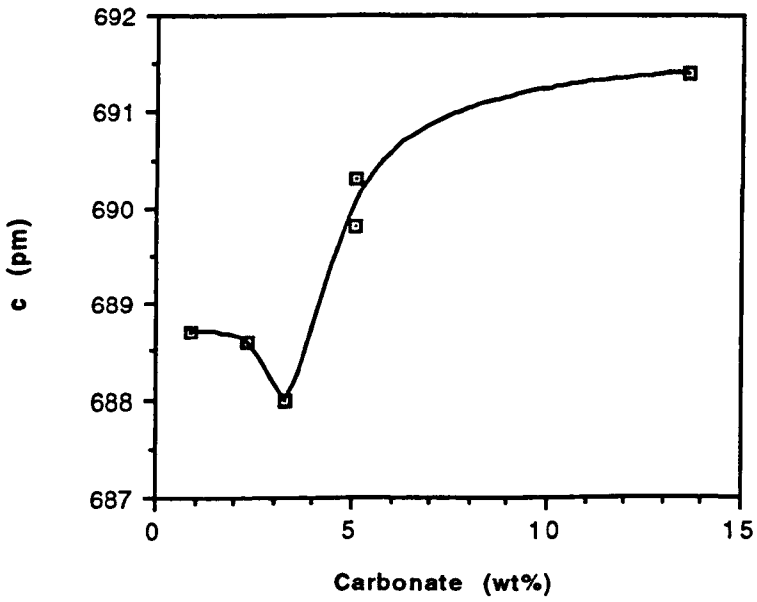

(a)

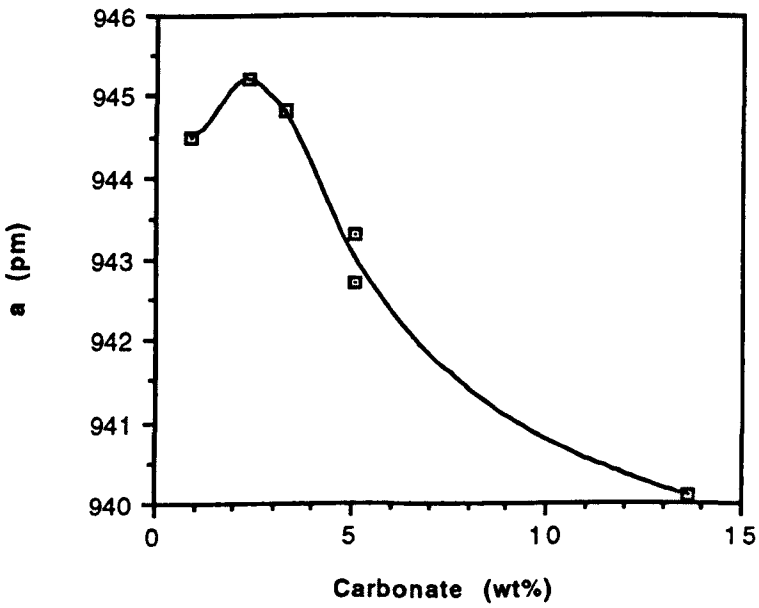

(b)

Figure 8.24. Change in the **c** axis of carbonate apatite precipitated at 70°C with increasing carbonate substitution, b) Change in **a** axis.

Therefore it was not possible to determine the lattice parameters of these apatites with a high level of accuracy. The apatites precipitated at 70°C were of large enough crystal dimensions to give XRD patterns suitable for lattice parameter determination from structure refinement. Figures 8.24 a) and b) show the **c** and **a** axis dimensions as a function of wt % carbonate. It can be seen that the **c** axis decreases slightly and then increases with increasing carbonate substitution. The **a** axis shows the reverse trend, increasing in size as the carbonate content increases up to 4 wt %, thereafter it decreases.

8.6 SINTERING

8.6.1 Temperature Profile

Figure 8.25 shows the furnace temperature profile at controller temperatures between 1000 and 1400°C. Below 1100°C the hot zone temperature is 99% of the controller temperature. From 1100°C to 1400°C the measured hot zone temperature is 98% of the controller temperature. As the furnace temperature increases the length of the hot zone increases from 40mm at 1000°C to 100mm at 1400°C. It can be seen that the hot zone is displaced by approximately one sixth of its length in the direction of gas flow (at a rate of rate 1.5 l min^{-1}).

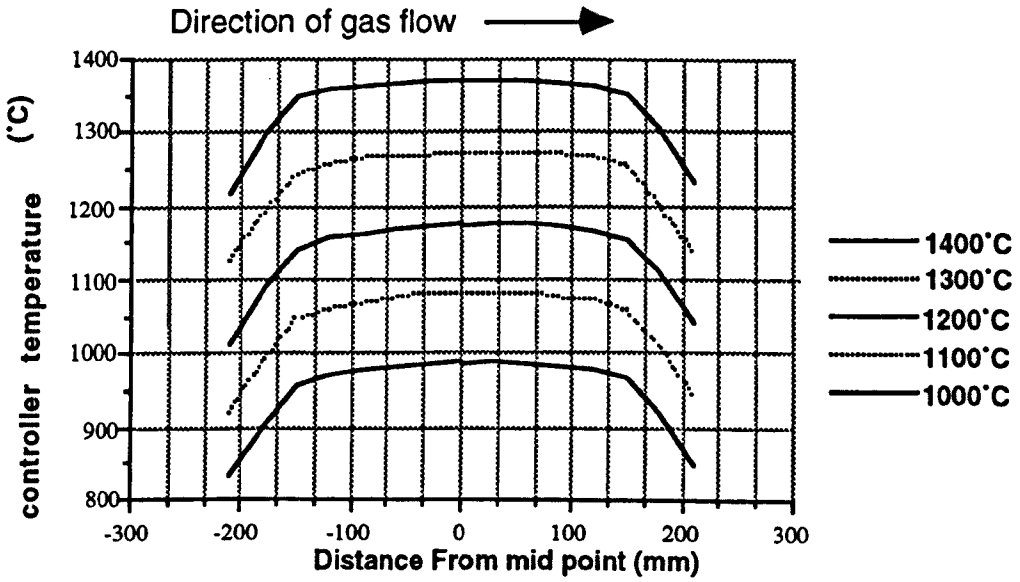

Figure 8.25. Temperature profile of tube furnace at controller temperatures between 1000°C and 1400°C.

8.6.2. Moisture Content of 'Wet' Gasses

The water content of the carbon dioxide gas was measured for 13 experiments. It was found to be 15.2 mg l^{-1} (s.d. 2.4). Assuming a molar volume of 24l at room temperature and a pressure in the furnace of 100kPa, this moisture content corresponded to a partial pressure of 3.04 kPa (s.d. = 0.48 kPa).

Figure 8.26 shows the calculated values of log K for various possible reactions at 500, 1000, 1500 and 2000K.

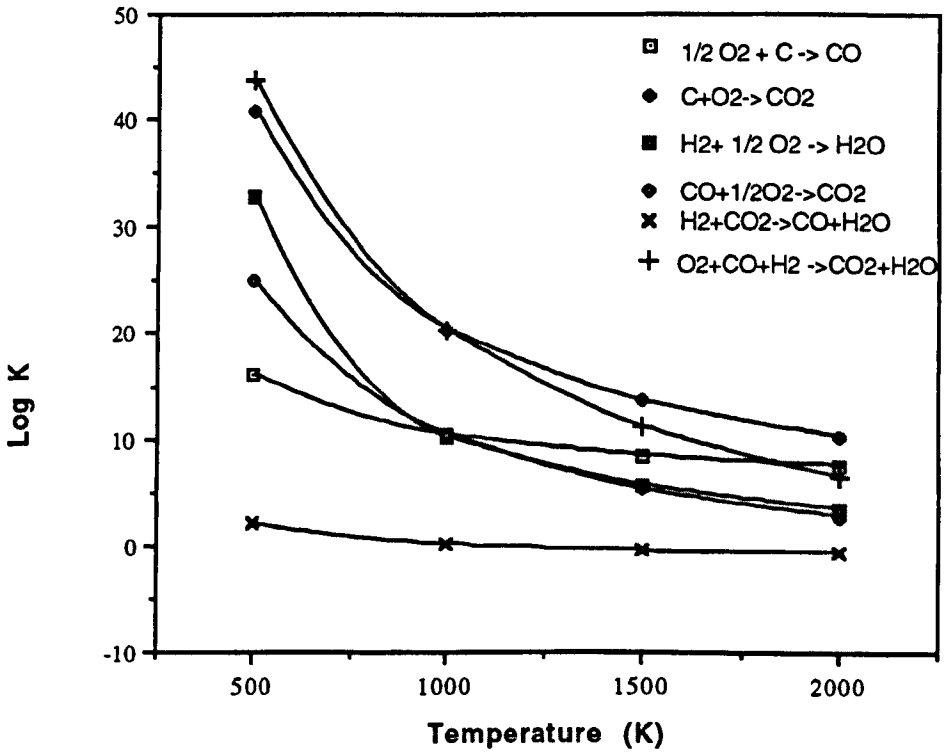

Figure 8.26. The variation of Log K for various possible reactions, (equations shown in legend), at temperatures between 500 and 2000K.

The partial pressure of oxygen in wet and dry carbon dioxide at furnace Temperatures from 500 - 1500°C is shown in Figure 8.27. The values were derived using calculated values for Kp as shown in Appendices 1a and b.

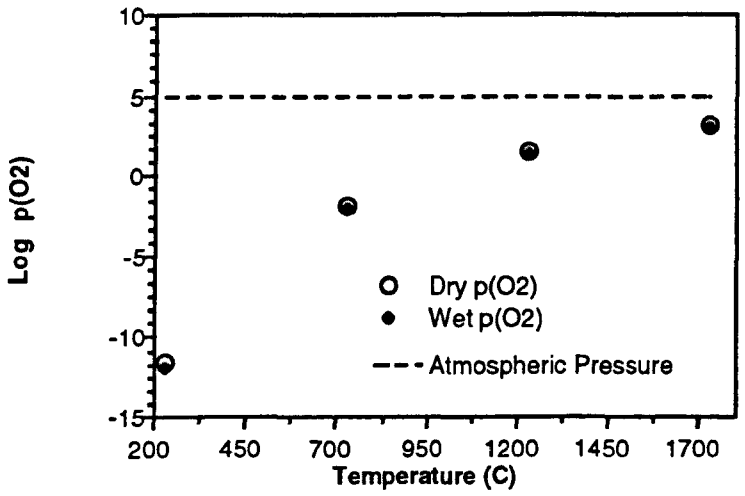

Figure 8.27. The effect of temperature on the partial pressure of oxygen in wet and dry carbon dioxide atmospheres.

Table 8.7. Partial pressure of oxygen (Pa) in wet and dry carbon dioxide atmospheres.

Temperature (°C)	Dry Carbon Dioxide	Wet Carbon Dioxide
227	2.6×10^{-12}	1.3×10^{-12}
727	1.4×10^{-2}	6.8×10^{-2}
1227	3.6×10^{1}	1.9×10^{1}
1727	1.5×10^{3}	7.9×10^{2}

It can be seen from Table 8.7 that the effect of 3% water is to decrease the partial pressure of oxygen in the atmosphere. Measurements show this decrease to be of the order of a half. Despite this, the ratio of partial pressures of water to carbon dioxide remains relatively constant at 3.09×10^{-2} up to 1227°C and reduces only by 3% from this value at 1727°C.

8.7 Sintering Studies

Investigations were carried out in order to determine the effect of carbonate content, green density, temperature, time and atmosphere on the sintering behaviour of carbonate apatites precipitated at 3°C. These precipitates were formed into disc shaped monoliths by filtration. These discs were in some cases broken into small (~5x5x5 mm) fragments in order to increase the number of tests possible from a single monolith.

8.7.1 Isochronal studies on the effect of sintering atmosphere

Appearance

Carbonate apatite (3.2 wt%, 40% green density), sintered in air, wet air and dry carbon dioxide was white and opaque in appearance, when sintered at temperatures between 1000 and 1300°C. Whereas apatite sintered in wet carbon dioxide at 1150 to 1300°C was translucent (Figure 8.28). At 1000°C a white opaque ceramic was formed.

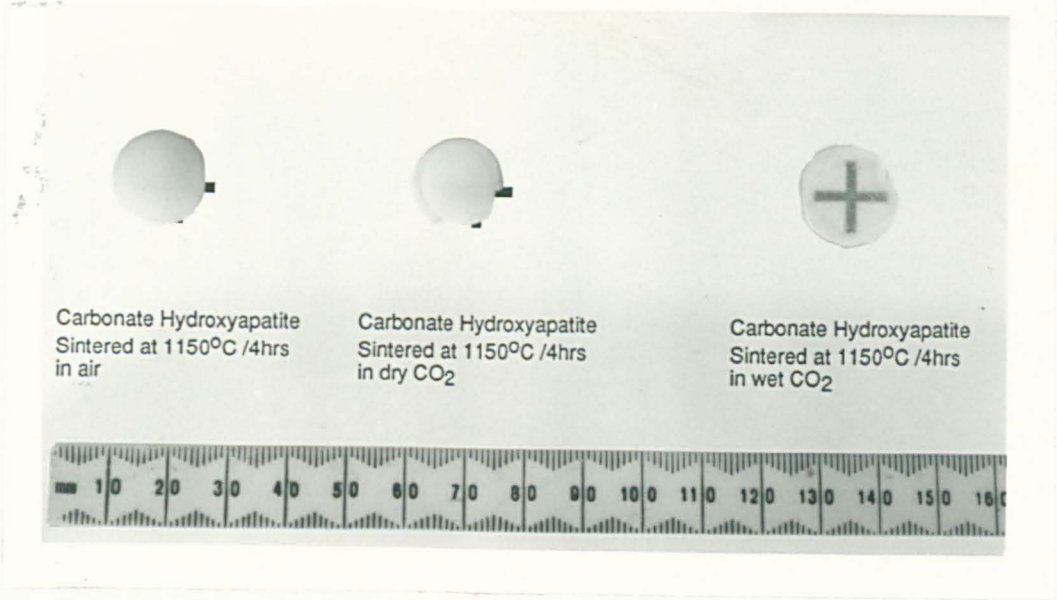

Figure8.28. Appearance of 3.2 wt% carbonate apatite after sintering in air, carbon dioxide and wet carbon dioxide at 1250°C for four hours.

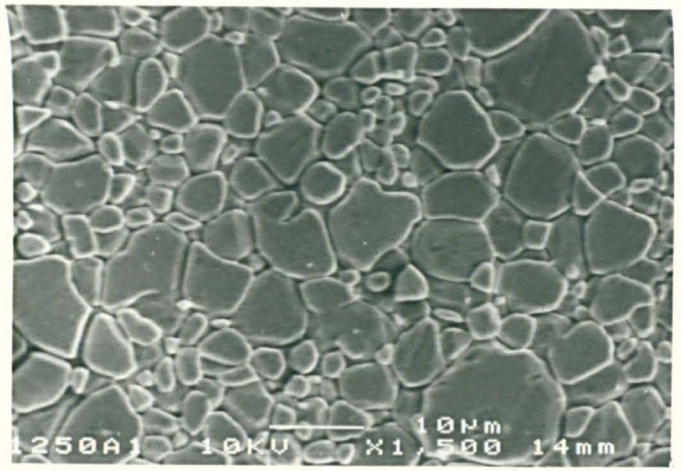

a

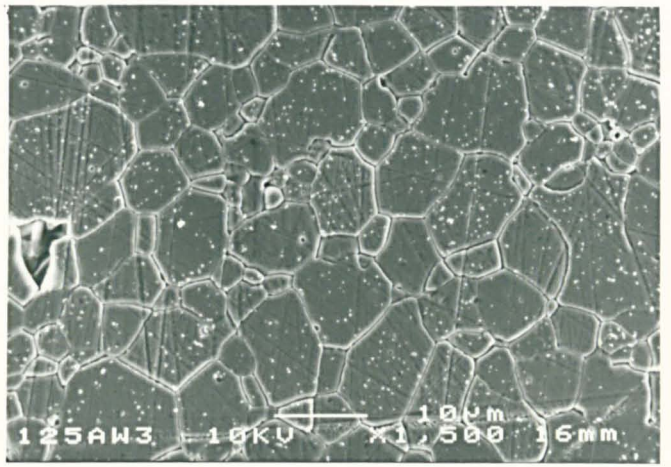

b

c

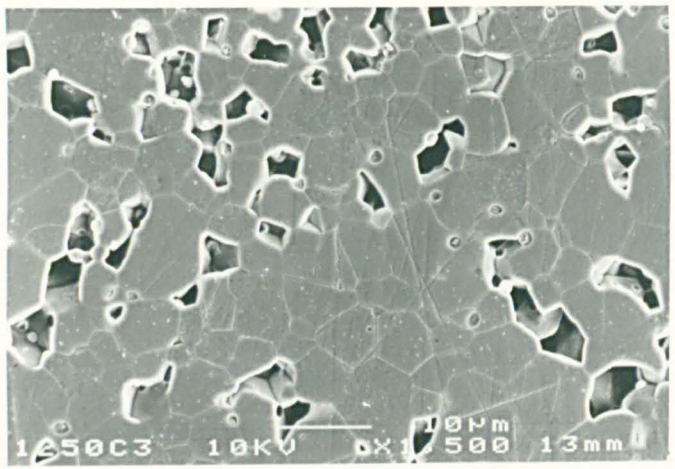

d

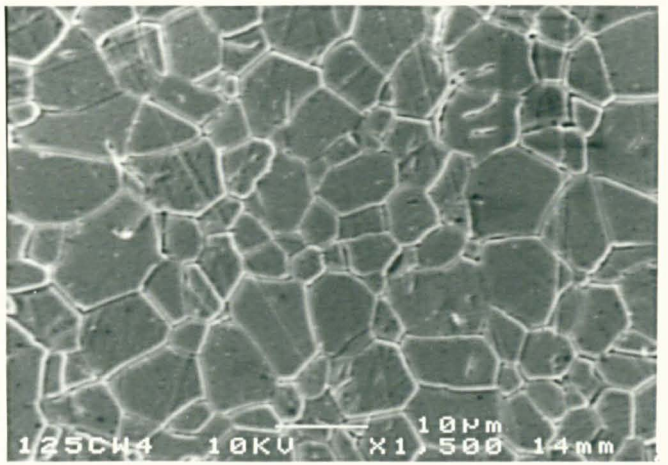

Figure 8.29. Microstructures of 3.2wt% carbonate apatites after sintering in a) air, b) wet air, c) carbon dioxide and d) wet carbon dioxide.

Microstructure

Figure 8.29 shows the microstructures of a 3.2 wt% carbonate apatite sintered at 1250°C in the different atmospheres. All the samples appeared free from large pores above 1150°C, except those sintered in dry carbon dioxide. In this atmosphere, ~8% porosity was observed at 1150°C, further densification did not occur at higher temperatures and agglomeration of pores was noted. Intergranular porosity was evident in carbonate apatite sintered in wet air.

Linear shrinkage

Figure 8.30 shows the linear shrinkage of 3.2% carbonate apatite after isochronal sintering for four hours in the various atmospheres.

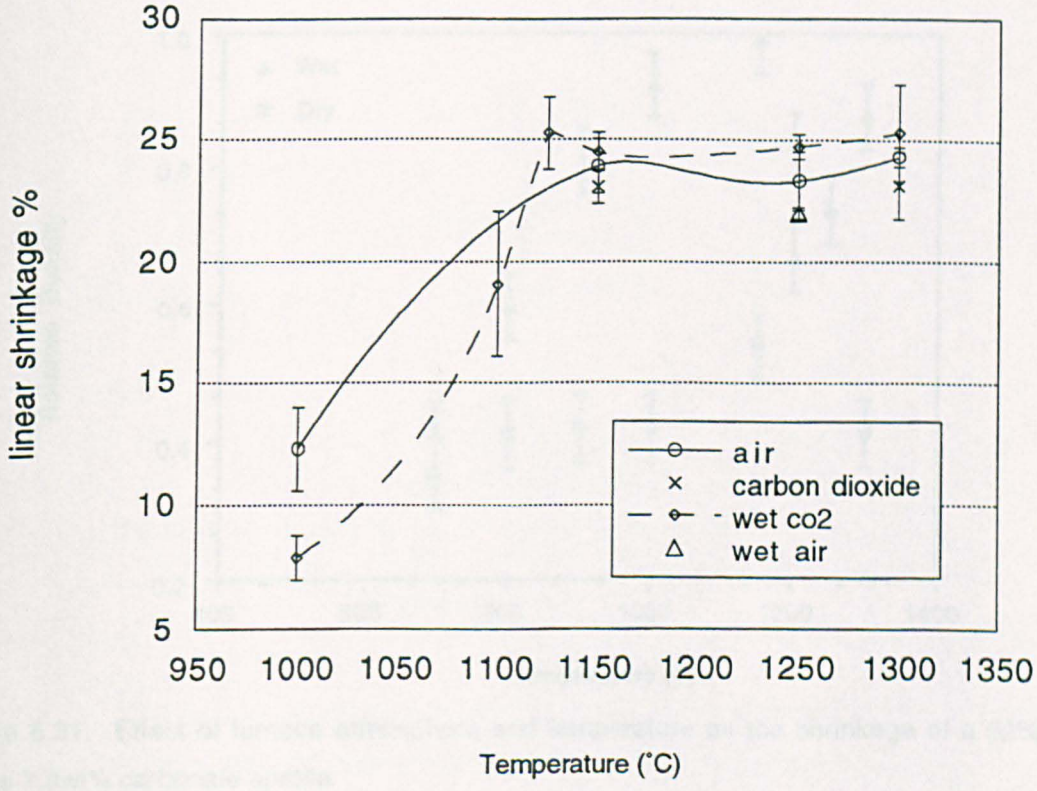

Figure 8.30. Effect of temperature and atmosphere on the isochronal, (4 hours), linear shrinkage during sintering of 40% dense 3.2 wt% carbonate apatite.

It can be seen from the linear shrinkage data that near full density was attained at temperatures above 1150°C. (A linear shrinkage of 25% corresponds to a volume shrinkage of 62%.) Due to the small size of the samples the errors in measurement prevent any conclusions as to the effect of atmosphere being drawn. The only significantly different in shrinkage is observed at 1000°C, where it would appear that the carbonate apatite sintered in air shrunk by 12% and that sintered in wet carbon dioxide shrunk by 8%.

Sintering studies on a low density gel (68% porosity), in wet and dry carbon dioxide atmospheres showed a clearer difference in the shrinkage behaviour in the two atmospheres, as shown in Figure 8.31. Relative density has been calculated from linear shrinkage by Equation 7.5.

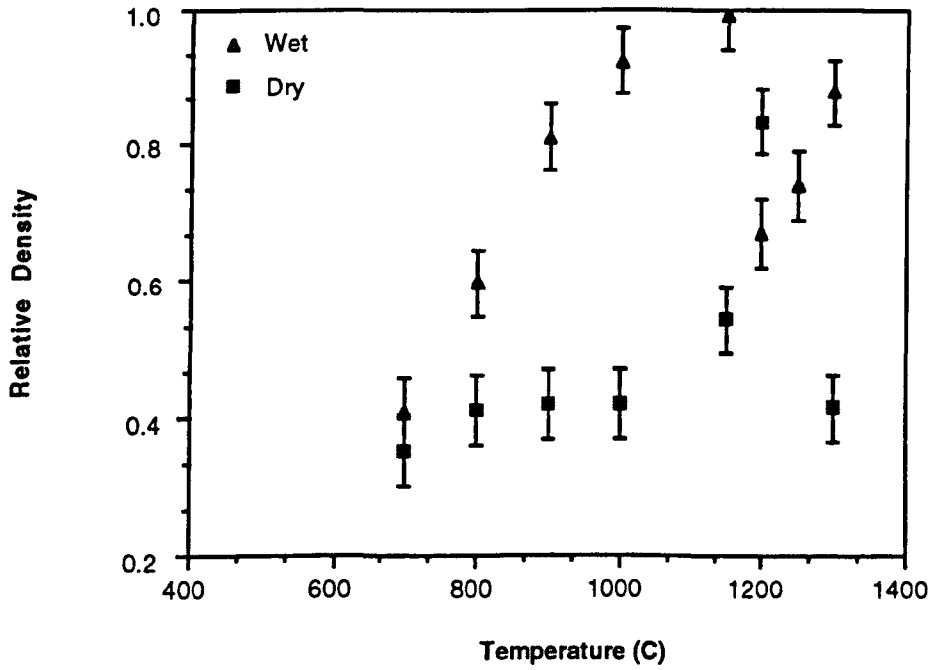

Figure 8.31. Effect of furnace atmosphere and temperature on the shrinkage of a 32% dense 7.8wt% carbonate apatite.

Figure 8.31 shows that at the intermediate stage of sintering the specimen sintered in dry carbon dioxide appeared to reach a limiting density of approximately 45%, whereas that sintered in the wet atmosphere approached full density at 900°C. At 1150°C the apatite sintered in wet gas

attains full density and appears to bloat at 1200°C. It is interesting to note that it is at this point that the specimen sintered in dry gas attained maximum density, (~80%). At higher temperatures, the apatite sintered in wet gas recommenced densification and that sintered in dry gas shows dramatic bloating, as indicated by the large decrease in measured shrinkage.

8.7.2 Effect of atmosphere on the density of carbonate hydroxyapatite

The density of carbonate hydroxyapatite sintered in the different test atmospheres at temperatures between 1000 and 1300°C for four hours is shown in Figure 8.32 It can be seen that the limiting density varies with atmosphere.

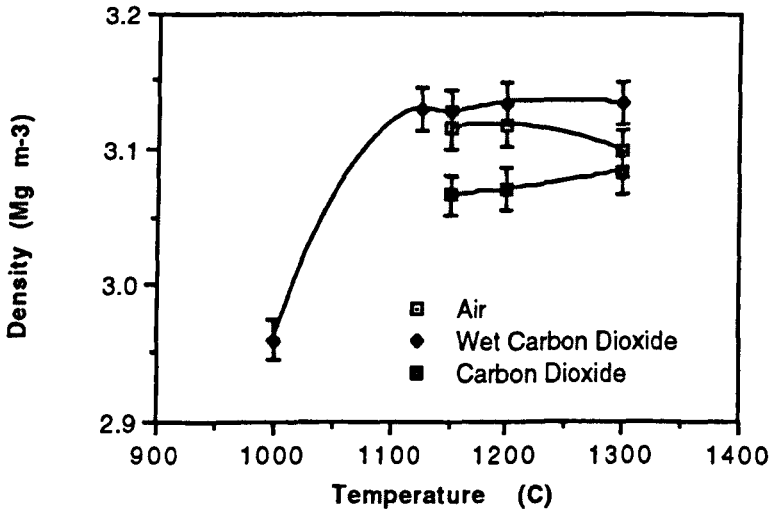

Figure 8.32. Variation in density of 3.2% carbonate apatite, green density 40%, during isochronal sintering, at different temperatures in different furnace atmospheres.

It can be seen that at approximately 1100°C, a limiting density is reached. For wet carbon dioxide atmospheres this is approximately 100%, 99% in air and 98% in carbon dioxide. It can be seen that the apatite sintered in air displays bloating at 1300°C.

Density measurements of a 5.8 wt % carbonate apatite of 30% green density sintered for four hours at temperatures between 700 and 1300°C are shown in Figure 8.33. It can be seen that the apatite sintered in wet carbon dioxide attains full density at between 800 and 900°C. Thereafter a decrease in density is observed. The apatite sintered in dry carbon dioxide shows an increase in density with sintering temperature up to 1150°C whereafter a limiting density (98%) is reached.

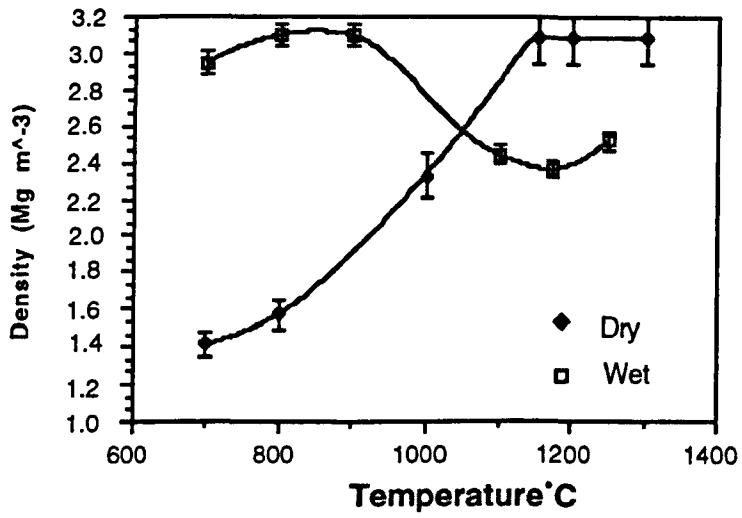

Figure 8.33. Effect of sintering atmosphere on the density of 5.8 wt% carbonate apatite 30% green density.

Grain Size measurement

The average grain size measurement was determined by the linear intercept method for a 3.2 wt% carbonate apatite for temperatures between 1150 and 1300°C, from a minimum of 30 measurements. The values obtained are shown in Table 8.8.

Table 8.8. Mean grain size (μm) of 3.2 wt% carbonate hydroxyapatite sintered for four hours in different atmospheres.

	Air		Carbon Dioxide Wet		Carbon Dioxide	
	$\bar{x}$	s.d.	$\bar{x}$	s.d.	$\bar{x}$	s.d.
1150°C	0.49	0.05	1.14	0.12	0.67	0.07
1250°C	3.18	0.10	6.15	0.84	5.05	0.63
1300°C	3.65	0.68	10.85	1.31	8.20	0.94

Grain growth of hydroxyapatite shows Arrhenius behaviour, a plot of log grain size against the inverse of temperature gives an indication as to the activation energy for grain growth, as shown in Figure 8.34.

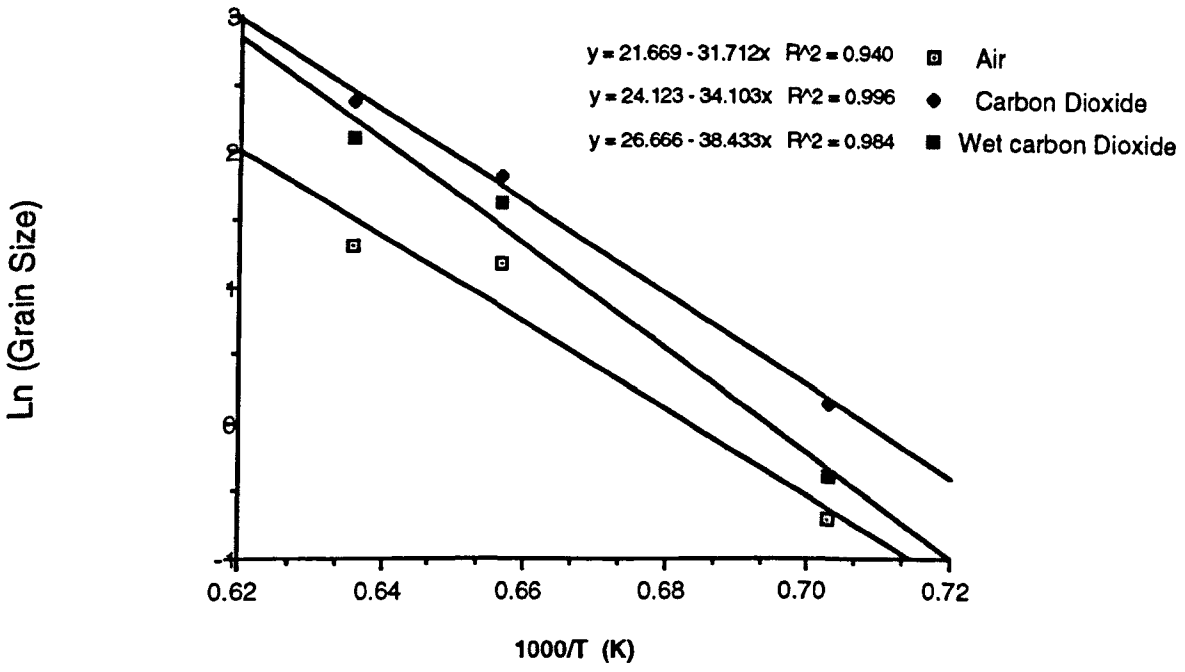

Figure 8.34. Arrhenius plot of grain sizes of 3.2 wt % carbonate apatite isochronally sintered in different atmospheres.

This would indicate that the activation energy for grain growth in carbon dioxide 263.65 kJ mol $^{-1}$, in air is 283.5 kJ mol $^{-1}$ and wet carbon dioxide atmospheres is 319.5 kJ mol $^{-1}$. However there are not enough data points to determine accurate values, as is reflected by the low correlation coefficients for the air and wet carbon dioxide atmospheres.

Figure 8.35 shows an Arrhenius plot for an 11.5 wt% carbonate apatite sintered in wet and dry carbon dioxide.

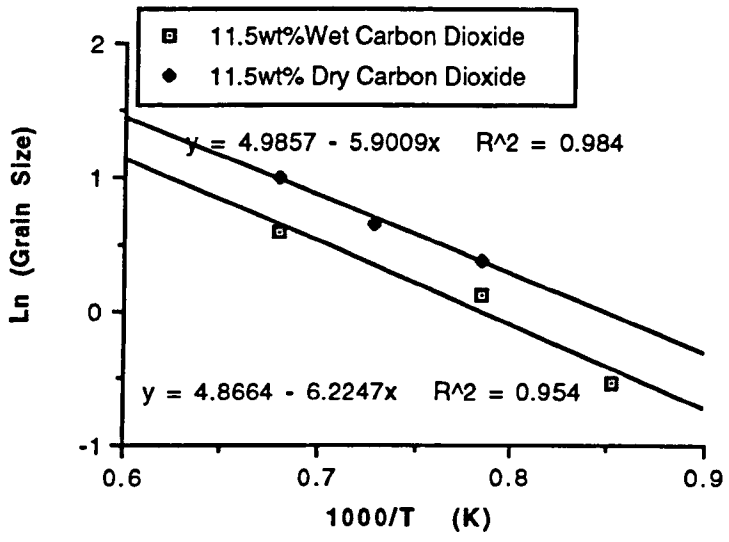

Figure 8.35. Arrhenius plot of grain sizes of 11.5 wt% carbonate apatite isochronally sintered in different atmospheres.

The activation energy for 11.5 wt% carbonate apatite appears to be 49kJ mol^{-1}, in dry carbon dioxide and 52kJ in wet carbon dioxide. This is substantially less than that calculated for a 3.2 wt% carbonate apatite.

Effect of Carbonate On Grain Size

Figure 8.36 shows the grain size of various carbonate apatites sintered at 1000°C for four hours in wet carbon dioxide. It can be seen that as the carbonate content increases the grain size decreases at this temperature. Figures 8.34 and 8.35 show that the carbonate content affects the activation energy of grain growth. This may be due to grain growth being effected by different mechanisms. Figure 8.37 shows that at 1000°C the low carbonate mechanism is predominant. At 1200°C there appears to be change in grain growth mechanism. Therefore at 1000°C the low carbonate content mechanism is dominant. A larger grain size is observed in lower carbonate content apatite ceramics under isochronal conditions as shown in Figure 8.36.

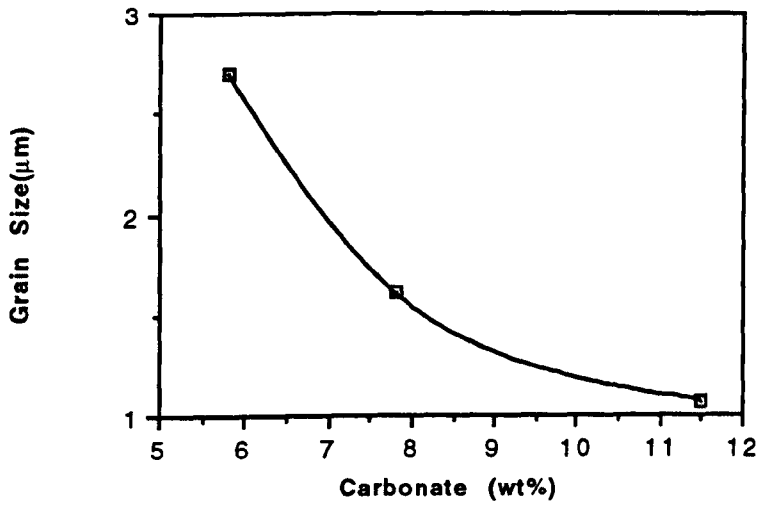

Figure 8.36. The effect of carbonate on the grain size of carbonate apatites sintered in wet carbon dioxide for four hours at 1000°C. The line joining the points is merely a visual aid and does not represent the experimental data as there are insufficient data points.

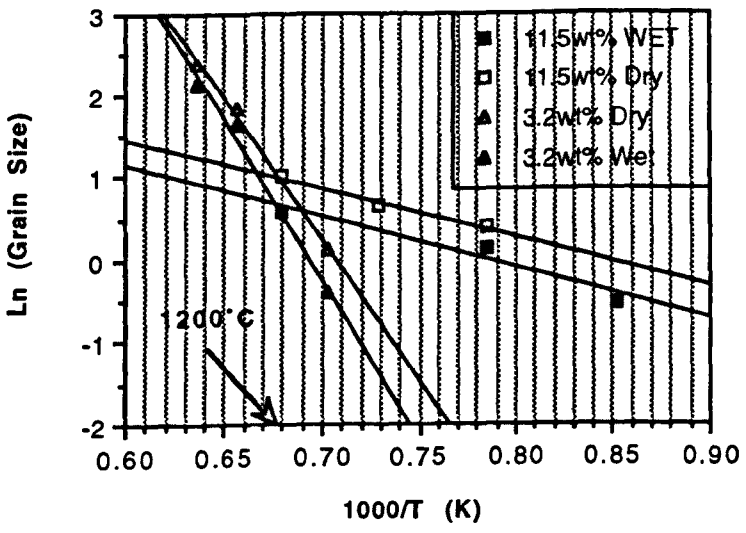

Figure8.37. Transition from high to low carbonate content grain growth mechanisms.

FTIR Spectra of sintered carbonate apatite

The FTIR spectra of samples sintered in air, carbon dioxide, wet air and wet carbon dioxide revealed the presence of the volatile hydroxyl and carbonate groups at 1250°C.

Table 8.9. Positions of the υ_3 carbonate peaks of 3.2 wt% carbonate apatite sintered at 1250°C in wet and dry carbon dioxide.

Atmosphere/ Carbonate	Temp Time	Wavenumber (cm^{-1})	
		υ_3	υ_2
Wet Carbon Dioxide 3.2 wt%	1250°C 4h	1544 1458 (strong) / 1505 1419 (weak)	879
" 5.8 wt%	1000°C 24h	1539(medium),1471,1457, 1418 (strong)	878
Dry Carbon Dioxide 3.2 wt%	1250°C 4h	1539 1457 (strong) / 1525, 1505, 1470(shoulder) 1415(weak)	879
" 5.8 wt%	1000°C 24h	1542,1472,1457, (1417)/(strong)	878
Nelson and Featherstone (1982) A Type (From heating Btype in CO_2) 8 wt%	900°C	1500,1469,1454,1415	879, 873
Le Geros et al. (1969) A type		1550,1525,1460	877
Nadal et al. (1970) A type		1534,1465	884
B type(Fluorapatite heated on CO2)		1455,1430	864

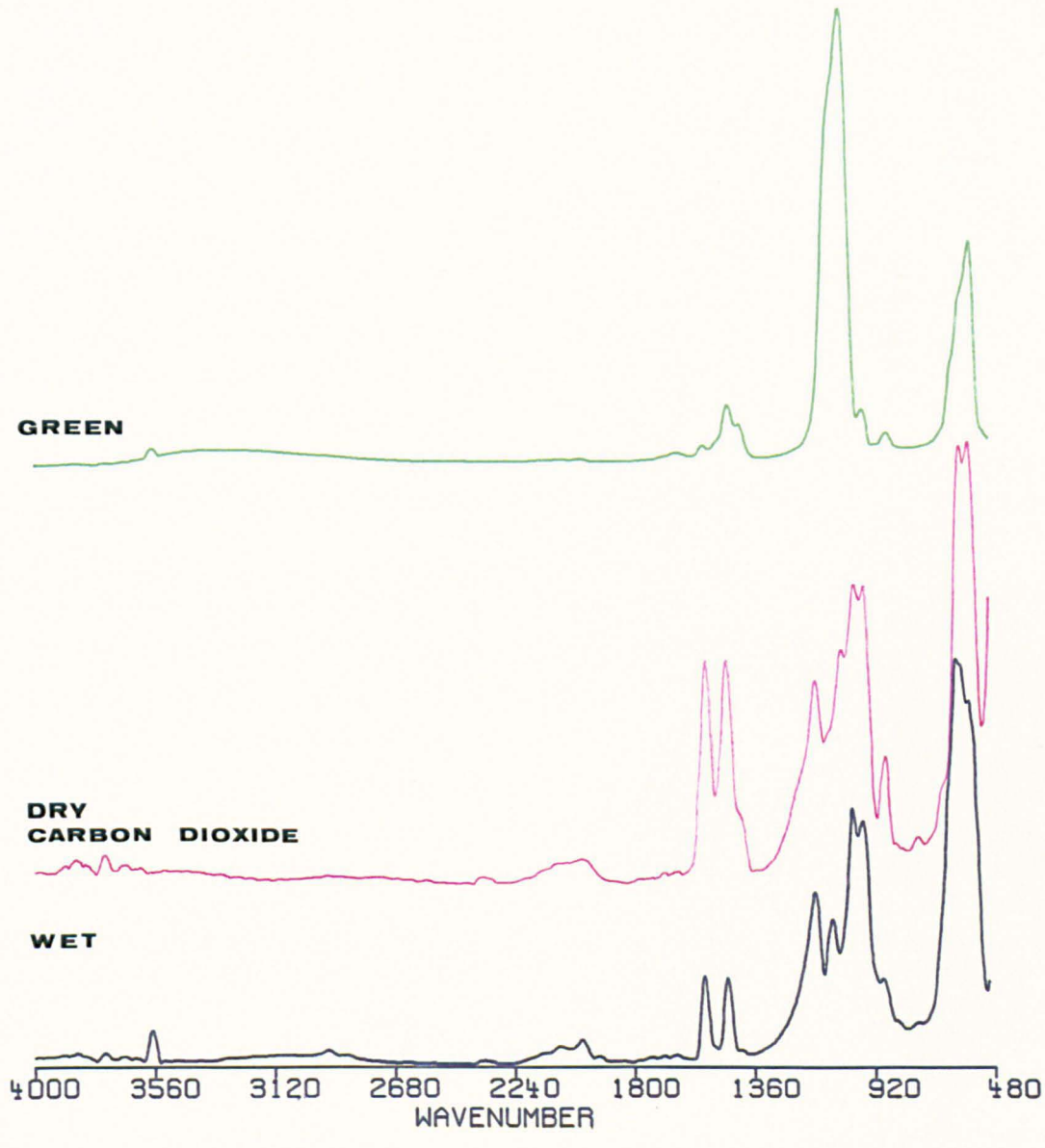

Figure 8.38. FTIR peaks in the range 4000-400 cm^{-1} for a 3.2 wt% carbonate apatite sintered in wet and dry carbon dioxide for four hours at 1250°C and the green material.

Carbonate apatite sintered for four hours in dry carbon dioxide lost the characteristic hydroxyl peak at 3510cm^{-1}. Carbonate peaks at 1415-1570cm^{-1} were observed in apatite sintered in carbon dioxide atmospheres (Figure 8.38). Table 8.9 shows the positions of the υ_3 carbonate peaks. It can be seen that the major carbonate peaks of the sintered carbonate apatite are in the same position in both atmospheres. It would appear that the apatite sintered in both wet and dry carbon dioxide contains carbonate both in the A and B sites, however only υ_2 bands at 883 were observed in both specimens. The material sintered in dry carbon dioxide has shoulders on both of the major peaks. Carbonate bands were only observed in spectra obtained only from carbonate hydroxyapatite sintered in carbon dioxide atmospheres and so were considered to be carbonate hydroxyapatite after sintering. For this reason the carbon dioxide atmospheres were singled out for further investigation.

X Ray Powder Diffraction

The X ray diffraction pattern for carbonate hydroxyapatite sintered in wet carbon dioxide at 1300°C for four hours was compared with the JCPDS standard. It was found that the sintered material was a single apatitic phase. Therefore it was assumed that at temperatures below 1300°C no decomposition took place in wet carbon dioxide. However in dry carbon dioxide partial decomposition into TCP occurred at 1150°C and above in dry carbon dioxide.

Vicker's Hardness

The Vickers hardness appeared to be dependent on grain size and density. The effect of atmosphere and sintering temperature on the hardness is shown in Figure 8.39. The maximum hardness measured was 580 Hv. This was for the apatite sintered in wet carbon dioxide and corresponded to the microstructural situation of minimum grain size and maximum density at ~1150°C. The apatite sintered in carbon dioxide shows a similar change in hardness with sintering temperature, though the hardness is lower. This is presumably due to the increased porosity in this specimen.

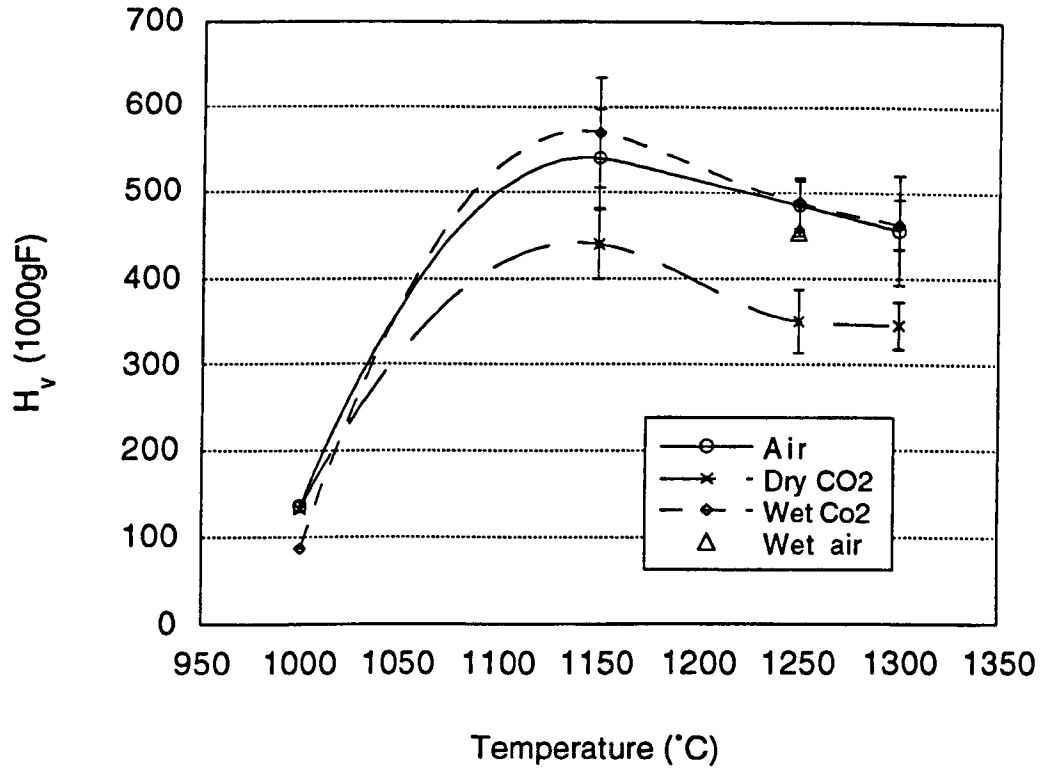

Figure 8.39. Effect of sintering atmosphere and temperature on the Vicker's hardness of 3.2% carbonate apatite.

8.7.3 Isochronal Studies on the effect of carbonate content

Linear Shrinkage

Figure 8.40 shows the variation of linear shrinkage with temperature and carbonate content. A 40% dense 5.8 wt% carbonate and a 35% dense 11.5 wt% carbonate apatite are compared. Filled points indicate that at these sintering conditions translucent ceramics were formed.

It can be seen that the temperature at which maximum density is attained is lower at the higher carbonate content, though the range of temperatures at which this behaviour is observed is smaller. In Figure 8.41 the linear shrinkage of carbonate apatites with carbonate contents of 5.8 and 7.8wt% with green densities of 37% sintered at between 800°C and 1250°C in wet and dry carbon dioxide atmospheres are compared.

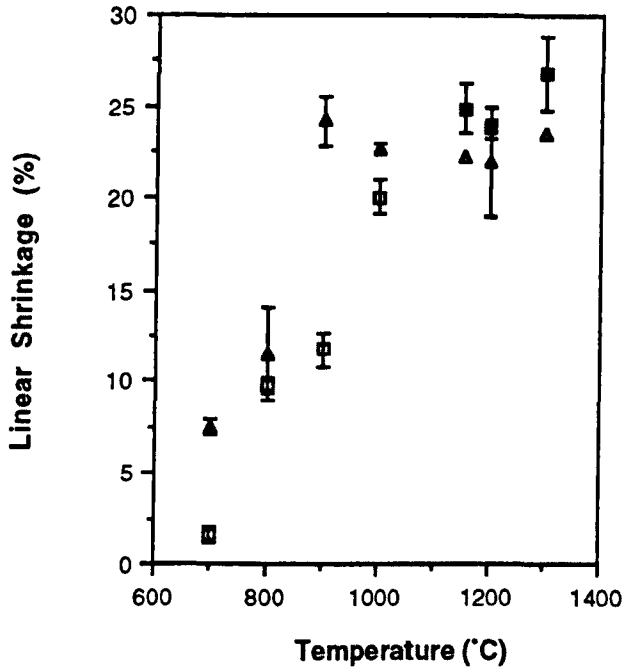

Figure 8.40. Effect of carbonate on the sintering characteristics of carbonate apatite. Triangles refer to 11.5 wt% (green density 35%), squares to 5.8 wt % (green density (40%) and filled points refer to translucent ceramic formation.

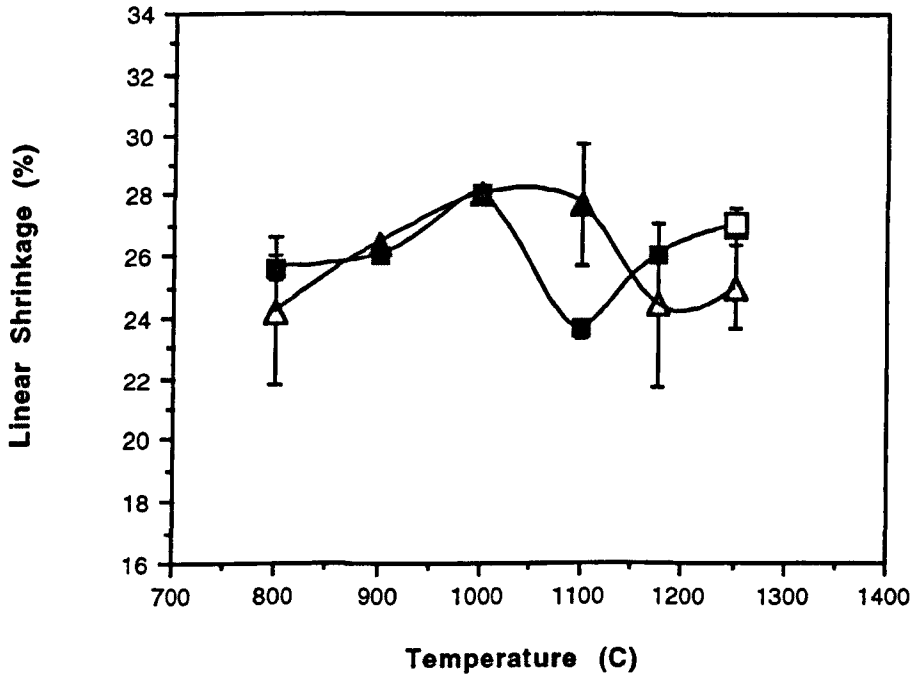

Figure 8.41. Effect of carbonate content on linear shrinkage of 37% dense carbonate apatite gels. (Squares correspond to 5.8 wt% carbonate, triangles to 7.8wt% carbonate, filled points indicate a translucent ceramic is formed.)

Density measurements of gels of the same density (30%) and of different carbonate contents, (9M - 5.8 wt%, and 16M - 7.8 wt%), showed similar trends to the linear shrinkage results. Figure 8.42 shows the effect of temperature on the sintered density.

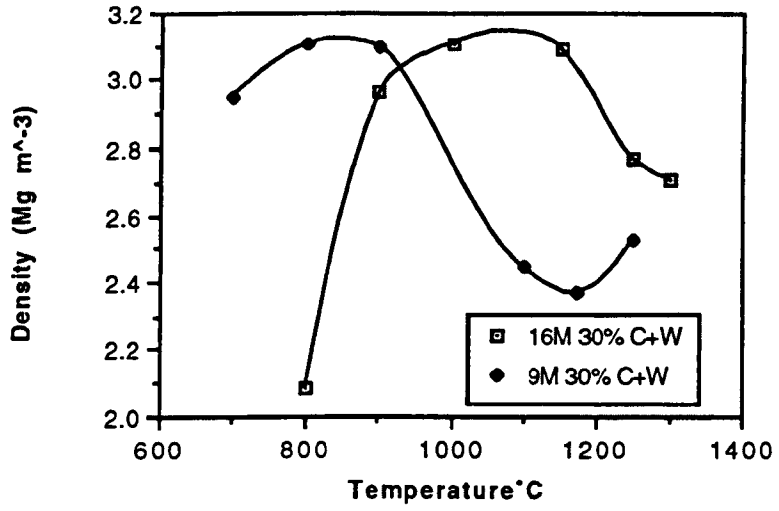

Figure 8.42. Effect of carbonate on the sintered density of 5.8 and 7.8 wt% carbonate apatite.

8.7.4 Isochronal investigations into the effect of green density

7.8 wt% carbonate apatite with green densities of 40, 37, and 30 % of the theoretical density were sintered in wet carbon dioxide at temperatures between 700 and 1300°C for four hours. The results obtained from linear shrinkage measurements are shown graphically in Figure 8.43.

The dotted lines in Figure 8.43 indicate the maximum theoretical shrinkages for a given green density. Common to all samples is the bloating followed by an increase in density at higher temperatures in the temperature range 1100°C to 1300 °C. It appears that as the green density increases the temperature decreases and the range of temperatures increases at and over which maximum densification occurs. On the basis of the limited data presented in Figure 8.43 it is possible to predict an approximate region which shows the temperature range over which a given maximum densification will occur for 7.8 wt % carbonate apatite. Density measurements of the same system at 40 and 30% green density, as shown in Figure 8.44 reveal a similar trend in that as the green density increases,

the temperature at which maximum densification occur decreases. This reduction in temperature is of the order of 100°C for a 10% increase in green density.

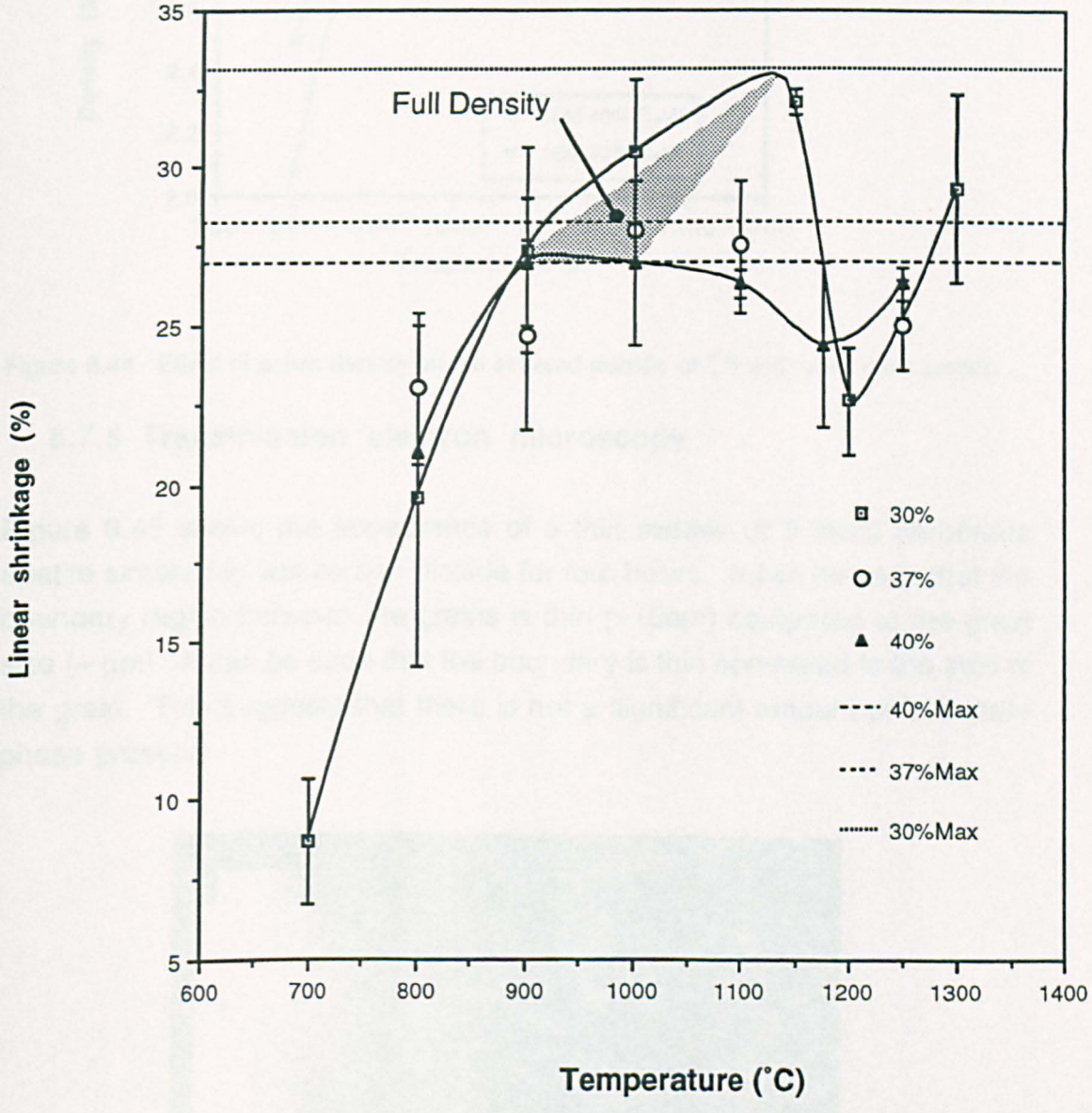

Figure 8.43. The effect of green density on the linear shrinkage of 7.8 wt% carbonate apatite. The shaded region indicates an approximate temperature range over which a maximum linear shrinkage may occur.

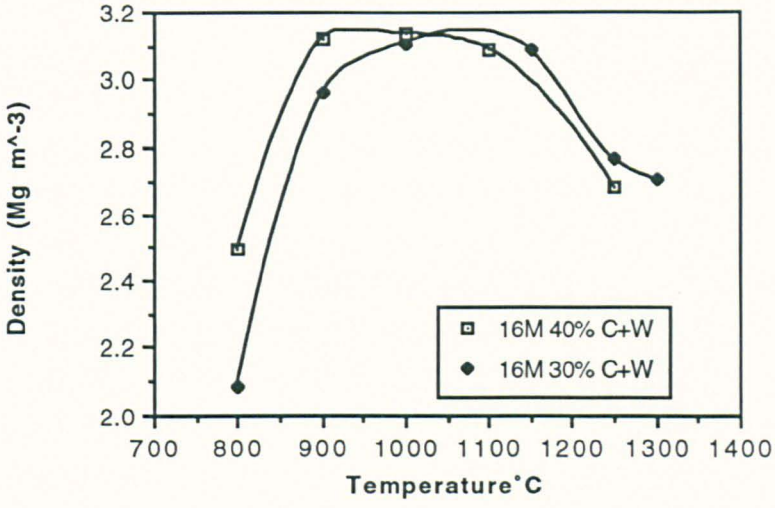

Figure 8.44. Effect of green density on the sintered density of 7.8 wt% carbonate apatite.

8.7.5 Transmission electron microscopy

Figure 8.45 shows the appearance of a thin section of 5.8wt% carbonate apatite sintered in wet carbon dioxide for four hours. It can be seen that the boundary region between the grains is thin (>10nm) compared to the grain size (~ μm). It can be seen that the boundary is thin compared to the size of the grain. This suggests that there is not a significant amount of boundary phase present.

Figure 8.45. Transmission electron micrograph of a thinned section of 5.8wt% carbonate apatite sintered for four hours at 1300°C, (marker is 500nm).

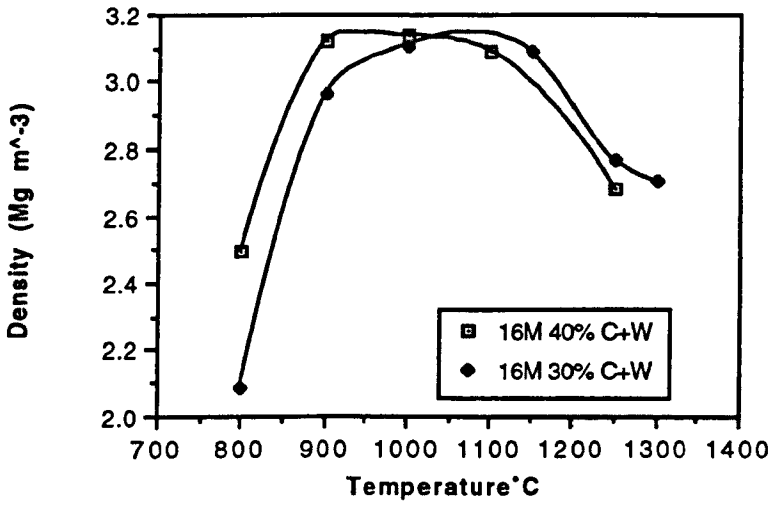

Figure 8.44. Effect of green density on the sintered density of 7.8 wt% carbonate apatite.

8.7.5 Transmission electron microscopy

Figure 8.45 shows the appearance of a thin section of 5.8wt% carbonate apatite sintered in wet carbon dioxide for four hours. It can be seen that the boundary region between the grains is thin (>10nm) compared to the grain size (~ μm). It can be seen that the boundary is thin compared to the size of the grain. This suggests that there is not a significant amount of boundary phase present.

Figure8.45. Transmission electron micrograph of a thinned section of 5.8wt% carbonate apatite sintered for four hours at 1300°C.

8.8 Isothermal Sintering Experiments

8.8.1 Microstructure

The micrographs in Figure 8.46 show the development of the microstructure of the 3C16M carbonate material during isothermal sintering in dry carbon dioxide at 1000°C. At time t=0 (Figure 8.46a) the microstructure consists of an irregular connected solid network. Individual grains are not visible and the thickness of the struts is approximately 200nm. After 45 minutes a change of geometry has occurred and the network appears to have coarsened (Figure 8.46b), this coarsening appears to continue until a time of 240 minutes. At this time, the micrograph (Figure 8.46c) suggests that some densification has occurred. Figure 8.51 indicates that this is not the case and the structure and depth of field may just create this impression. After isothermal heating for twenty four hours a dramatic change in microstructure has occurred, (Figure 8.46d). Individual elongated grains, approximately 1μm in length, connected in an open network are visible. The coordination number of the grains is hard to determine, but a grain with a coordination number of at least five can be seen in the micrograph.

Figure 8.47a shows the development of the microstructure of the 3C16M material during isothermal sintering in wet carbon dioxide. With the exception of the micrograph taken at 1440 minutes, which is an etched fracture surface, all the micrographs are polished and etched sample surfaces. It can be seen that during the first hour some coarsening occurs. It is not clear if the apparent porosity evident in the material heated at time of 0 minutes (Figure 8.47a) is an artefact due to over etching. After a time of 60 minutes some grain growth has occurred and little porosity is apparent (Figure 8.47b). At a time of t=240 minutes, considerable coarsening has occurred (Figure 8.47c), inter and intra granular porosity is evident. Some of the grains appear to be cracked though this may have occurred during polishing. After 1440 minutes considerable grain growth had occurred and no intergranular porosity is evident, though elongated pores are visible along some grain edges (Figure 8.47d). The mode of fracture appears to be transgranular for large grains (~>5μm) and intergranular around smaller grains.

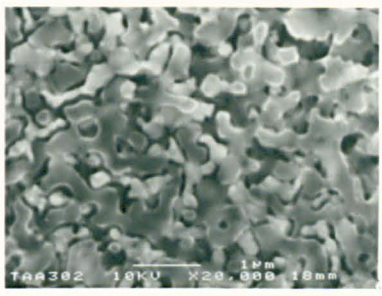

a

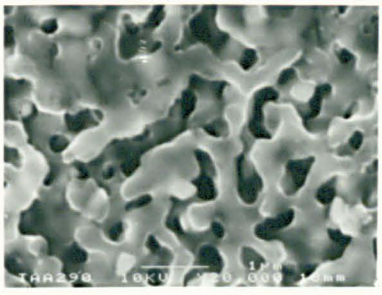

b

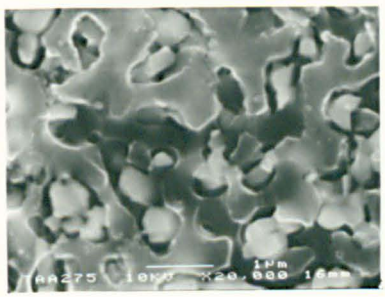

c

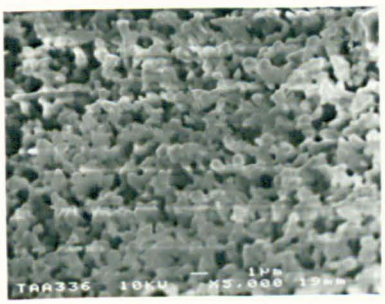

d

Figure 8.46. Development of sintered microstructure of 3C16M in dry carbon dioxide at times of a) 0, b) 45, c) 240 and d) 1440 minutes.

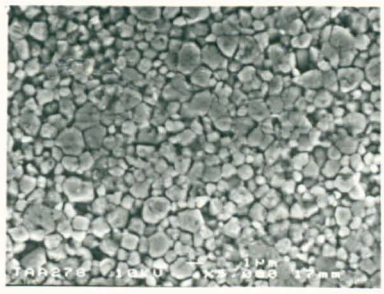

a

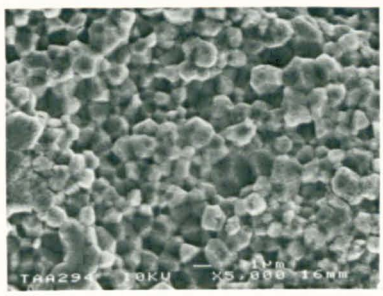

b

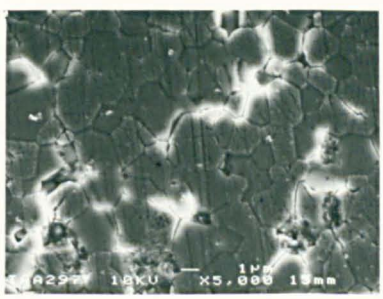

c

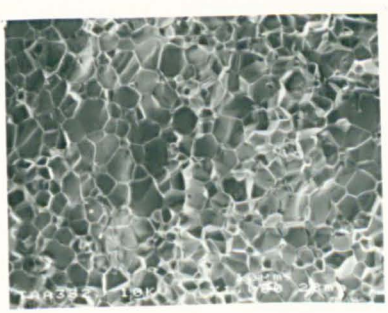

d

Figure 8.47. Development of sintered microstructure of 3C16M in wet carbon dioxide at times of a) 0, b) 60, c) 240 and d) 1440 minutes.

8.8.2 Isothermal Grain Sizes

The average grain size as a function of sintering time in the wet carbion dioxide atmosphere is shown in Figure 8.48.

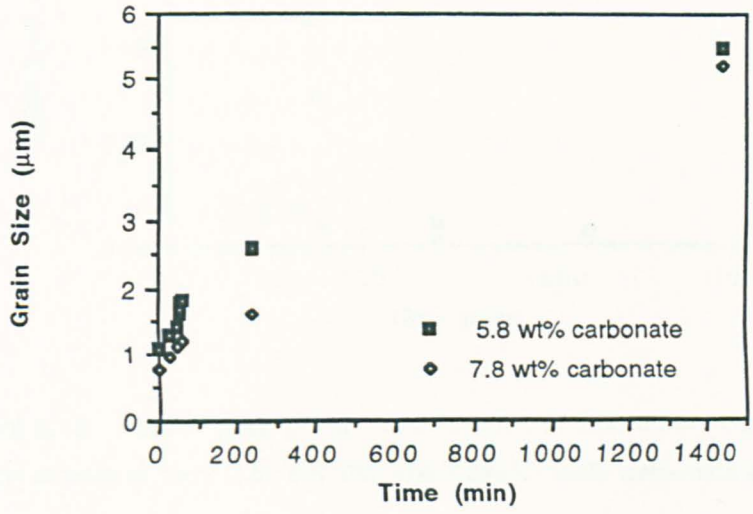

Figure 8.48. Variation of grain size of carbonate apatite with time during isothermal sintering experiments in wet carbon dioxide atmosphere at 1000°C.

It can be seen that the higher carbonate conent material has a smaller grain size than the lower carbonate content apatite. However the increase in grain size with time appears to be similar for both carbonate levels.

The rate of grain growth with time was found to increase dramatically with time and then decrease (Figure8.49) . A comparison with Figures 8.41 and 8.42 shows that the rate of grain growth increases and decreases with the density of the specimen.

A plot of log grain size against log time (Figure 8.50), yields slopes of 0.36 and 0.41 for 5.8 and 7.8 wt% carbonate apaite respectively. The 7.8 wt% carbonate apatite appears to exhibit discontinuous grain growth as indicated by the deviation from linearity. This behaviour at 1440 minutes is responsible for the increased gradient of this graph. Therefore it appears that the time dependence of grain growth is to the cube root of time for both carbonate apatites at 1000°C, during normal grain growth.

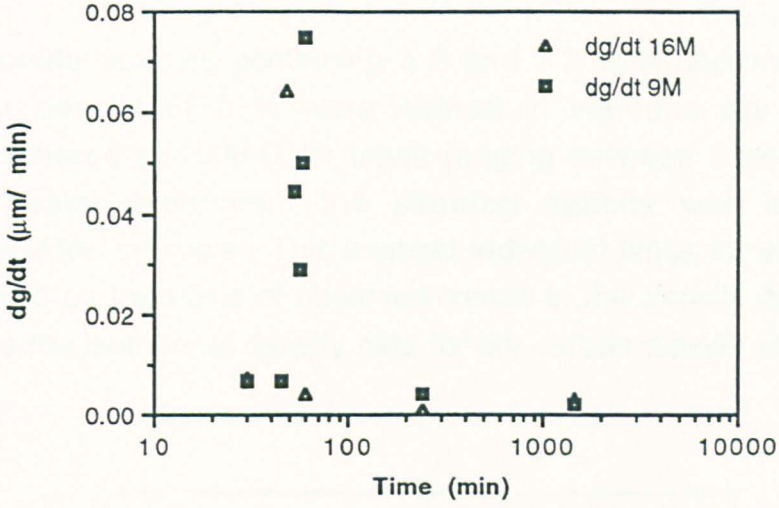

Figure 8.49. Rate of grain growth as a function of time during isothermal sintering in wet carbon dioxide at 1000°C for 5.8 (9M) and 7.8wt% (16M) carbonate apatites.

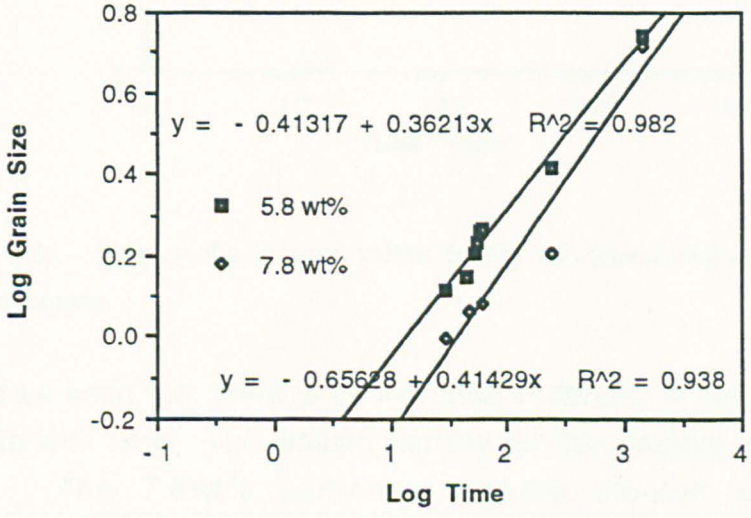

Figure 8.50. Log grain size of 5.8 and 7.8 wt% carbonate apatite in wet carbon dioxide at 1000°C as a function of log time.

8.8.3 Effect of sintering time on the density of carbonate apatites.

Carbonate apatites containing 5.8 and 7.8 wt% carbonate, both with a green density of 37% were heated in wet and dry carbon dioxide atmospheres at 1000°C for times ranging between 0 and 1440 minutes. After each experiment the sintered density was measured using Archimedes' principle. This enabled individual times for each apatite to be selected on the basis of observed trends in the density data. Figure 8.51 shows the isothermal density data for dry carbon dioxide atmosphere.

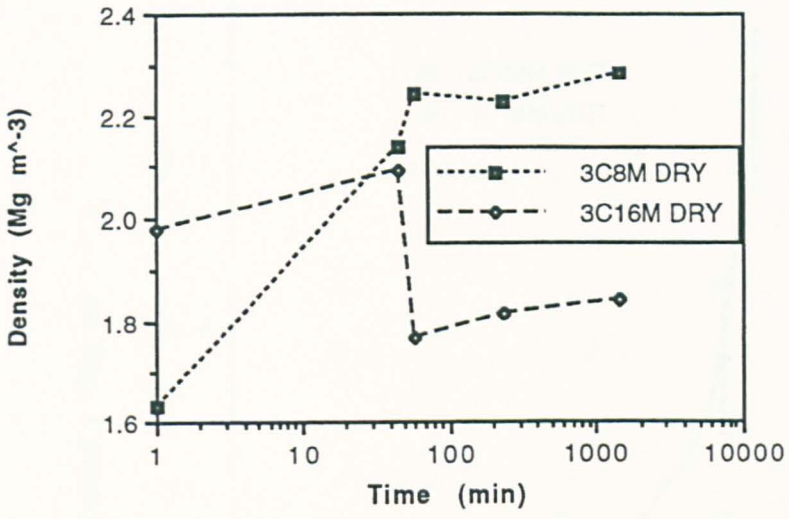

Figure 8.51. Variation of carbonate apatite density with time during sintering at 1000°C in dry carbon dioxide.

It can be seen that there is an increase in density in the 5.8 wt% carbonate apatite with time. The limiting density for this sample would appear to be 73%. The 7.8wt% carbonate apatite bloated after 45 minutes. Densification then continued at a rate that decreased with time. The limiting density was around 60% density.

In wet carbon dioxide, both the 5.8 and 7.8 wt% carbonate apatites demonstrated an increase in density from 98% relative density to a density of 99.8 wt%, as shown in Figure 8.52.

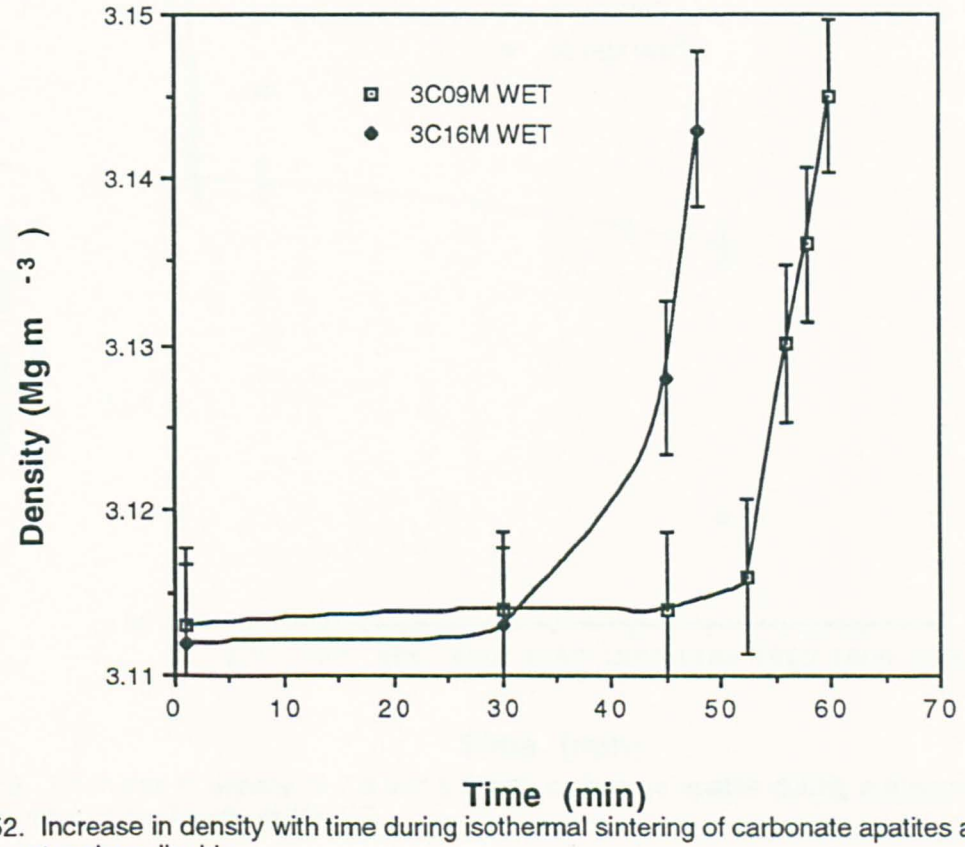

Figure 8.52. Increase in density with time during isothermal sintering of carbonate apatites at 1000°C in wet carbon dioxide.

However shortly after full density is attained, bloating occurs resulting in a rapid decrease in density, to 98% and 96% relative density for 7.8 wt% and 5.8 wt% carbonate respectively. Further densification does not appear to occur (Figure 8.53).

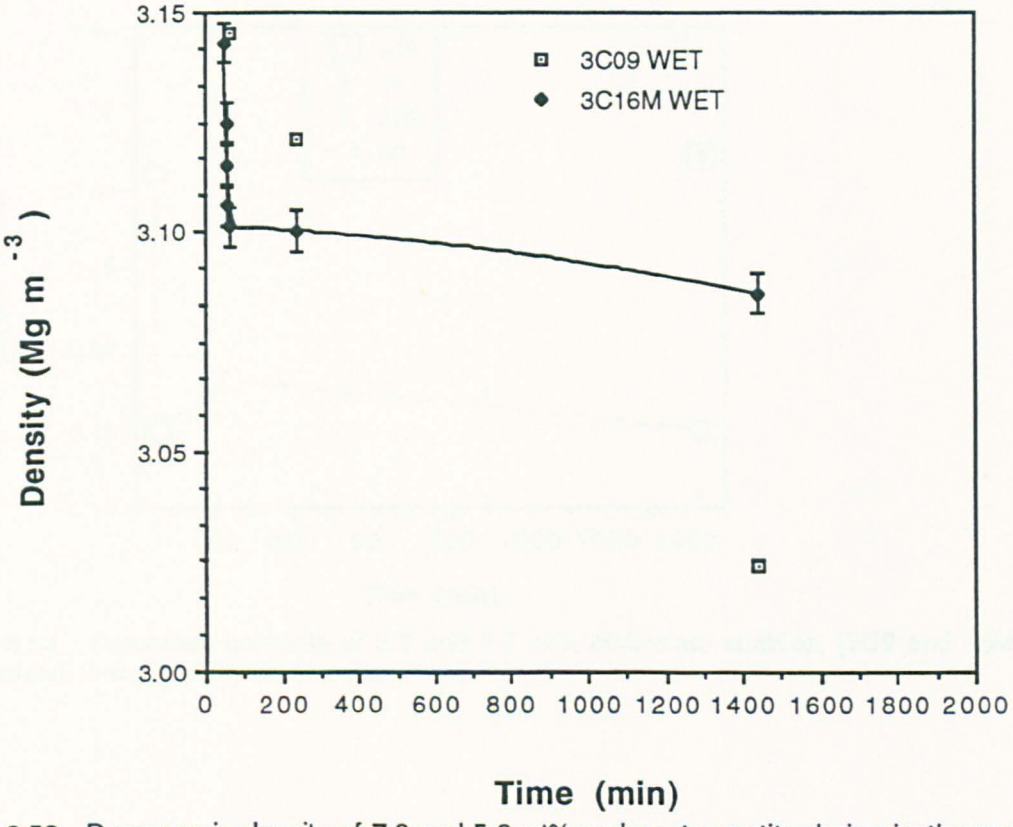

Figure 8.53. Decrease in density of 7.8 and 5.8 wt% carbonate apatite during isothermal sintering in wet carbon dioxide at 1000°C.

The carbon contents of the 5.8 and 7.8 wt% carbonate apatites after sintering at various times at 1000°C in wet and dry carbon dioxide atmospheres is shown in Figure 8.54. There are not enough data points for the material sintered in the dry atmospheres to comment on how the carbonate content varied with time. During sintering experiments in dry carbon dioxide, only the 3C16M material (7.8wt%) displayed any appreciable bloating behaviour, this occured after a time of 45 minutes.

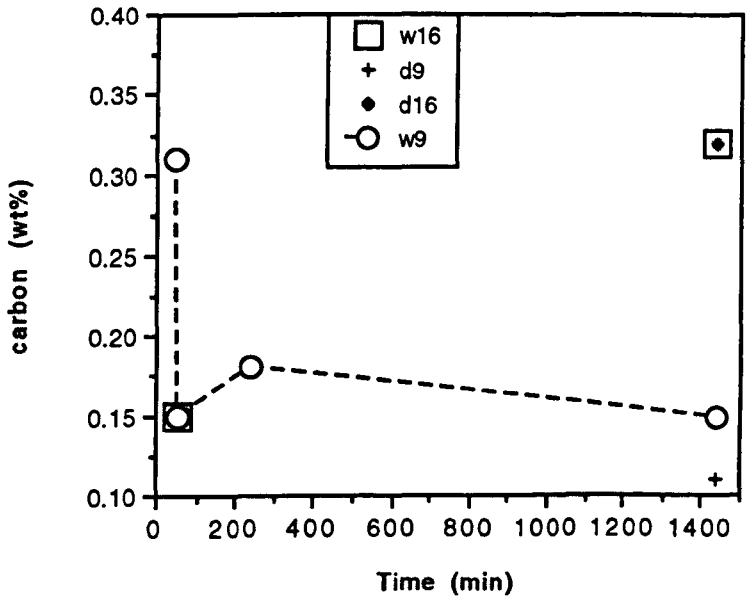

Figure 8.54. Carbonate contents of 5.8 and 7.8 wt% carbonate apatites, (3C9 and 16M respectively), in wet and dry (w and d) atmospheres.

The 3C9M material sintered in the wet carbon dioxide demonstrated a rapid decrease in carbonate content in the order of fifty percent between times of 45 and 58 minutes. Thereafter a fairly constant carbon content was observed. The 3C16M sample appeared to demonstrate an increase in carbonate content with time following bloating, which occurred after a time of 48 minutes (Figure 8.52) in wet carbon dioxide. The final carbonate content of the apatites would appear to depend on the initial carbonate contents rather than than the sintering atmosphere.

9 Discussion

9.1 Precipitation

The mechanism of *in vivo* mineralisation and the nature of the carbonate substitution in apatite have been two of the major driving forces behind *in vitro* hydroxyapatite precipitation studies. As a consequence of the need for an easily characterised product, most precipitation studies reported in the literature were performed at elevated temperatures. These reaction conditions produced highly crystalline products which lent themselves to XRD studies, e.g.(LeGeros, 1965; 1967; Bonel, 1971; Labarthe, 1973; Nelson and Featherstone, 1982 and Shimoda *et al.*, 1990). The bulk of the precipitations performed in this study were conducted below this temperature and consequently little comparative work exists in the literature.

9.1.1 Size and morphology

The results indicate that both the size and shape of the crystals could be controlled by altering both the precipitation temperature and the bicarbonate ion concentration. Selected area electron diffraction patterns showed that hydroxyapatite was formed under all the conditions investigated. Even precipitates that gave 'amorphous' type XRD patterns produced ringed electron diffraction patterns characteristic of a polycrystalline material.

Effect of temperature

The effect of precipitation temperature was most clearly visible in the series of precipitates to which no bicarbonate ions were added. As the temperature increased there was a general trend of increasing crystallinity. As shown in Figure 8.1, at 90°C acicular crystals ~ 700 nm in length were formed, whereas at 3°C smaller (~10nm) more spheroidal particles were formed. This effect may have been due to the increase in supersaturation that would have accompanied a reduction in temperature, as described by Equation 3.4. As the degree of supersaturation increased, the nucleation rate was increased, which in turn reduced the growth rate of the apatite and resulted in much smaller crystals. The effect of temperature and carbonate on crystal size has

been previously observed, if indirectly, by many investigators. Most simply reported a broadening of the XRD patterns at temperatures below 80°C or at high carbonate contents (e.g. LeGeros *et al.*, 1967; Labarthe *et al.*, 1973; Vignoles, 1973). LeGeros *et al.* (1967) found that at 90°C and 70°C 0.5 wt% carbonate apatite formed as acicular crystals approximately one micron long.

Effect of Bicarbonate Concentration

The effect of bicarbonate ion concentration was clearly observed at 70°C. As the bicarbonate ion concentration increased, the morphology of the precipitates changed from acicular to spheroidal. Simultaneously the size of the crystal decreased from 700 nm in length to ~ 10 nm in diameter. The effect of reducing particle size was also present to some degree at 3°C, as the observed broadening of the peaks of the XRD patterns demonstrated.

LeGeros *et al.* (1967) found that at 90°C, 15 - 22 wt% carbonate apatite precipitated as clusters of equiaxed crystals in the order of 10nm diameter. With a more intermediate carbonate content (5 wt %) rod-like crystals were formed which were 100nm in length. These precipitates are not directly comparable with those formed in the present study, as they were produced at a higher temperature (100°C), using the Direct Method and different reagents at different concentrations to those used here. Nelson and Featherstone (1982) stated that the size of precipitated apatites, calculated from TEM measurements, made in the same manner as those of this study, at 85 - 90°C, Ca / P = 0.5 was 0.2 x 0.05 x 0.05μm. and were very similar to those produced at 70°C 160 mM (Ca/P = 1.39) reported here. No other conditions were reported by Nelson *et al.* (1982). Shimoda *et al.* (1990) found that an increase in concentration (supersaturation) decreased the crystal size and hypothesised that this was due to an increase in the number of nuclei. A decrease in temperature is equivalent to increasing the supersaturation and the decrease in crystal size observed at lower (<70°C) temperatures is attributed to this phenomenon. LeGeros *et al.* (1967) proposed that the change in morphology observed with increasing carbonate content was due to the inhibition of crystal growth in the **c** direction. Nelson (1981) and Nelson and Featherstone (1982)reported that carbonate introduced disorder into the apatite lattice and caused the formation of a domain structure in the order of 40nm in size. However, it was not clear that what they were looking at was not in fact an agglomerate of crystals, which is more similar to that observed

here and by LeGeros *et al.* (1967). The results reported in the present study show that carbonate was found to change the morphology of acicular precipitates to smaller more equiaxed crystals which resembled those formed at lower temperatures. The carbonate substitution also decreased the size of spheroidal crystals formed at lower temperatures. It is possible that carbonate disrupts long range order in the crystal as the ion is smaller than the phosphate group it replaces. Another feasible explanation is that the presence of bicarbonate also increases the supersaturation of the precipitation solutions relative to carbonate apatite. In this study and in others e.g. Nelson and Featherstone (1982), Shimoda *et al.* (1990) the carbonate was added together with the phosphate solution so the concentration of phosphate and carbonate combined is much higher than the concentration of the phosphate solution alone.

9.2 FTIR investigations

9.2.1 Precipitates

It was observed that higher wavenumber υ_3 carbonate bands disappeared as the carbonate content increased, (Table 8.10). At 3°C a band was observed at 1574 cm^{-1}, as the bicarbonate concentration of the precipitation medium increased this band was no longer observed. At 37°C bands at 1555 and 1505 cm^{-1} were not observed, as the bicarbonate concentration was increased the band at 1488 $cm^{-1}$was then observed at 1473cm^{-1}. At 70 and 90°C the peaks at 1488 cm^{-1} and 1473cm^{-1} were not observed and only those at 1450 and 1420 cm^{-1} were apparent. The υ_3 carbonate bands were found at 871-875 cm^{-1} at all temperatures and all bicarbonate concentrations. Table 3.3 shows that there is some disagreement as to the carbonate peak positions.

Bonel (1972a), attributed bands at 883, 1465 and 1534 cm^{-1} to A type carbonate apatite, Bonel (1972b) 864, 1430 and 1455 cm^{-1} to B type carbonate apatite, whereas Doi *et al.* (1982) attributed 878, 1450 and 1550 cm^{-1} to A type and 875, 1410 and 1460 cm^{-1} to B type carbonate apatites. Of particular interest are the findings of Nelson and Featherstone (1982) who

prepared B type apatites at 90°C and found that low carbonate content apatites (2 wt%) had υ_3 carbonate bands at 1550, 1500, 1469, 1454 and 1415 cm^{-1} and υ_2 carbonate bands at 879 and 873cm^{-1}. Vignoles attributed the presence of additional carbonate bands at low carbonate contents in alkali deficient conditions at 80°C at 1542 and 882 cm^{-1} to the lack of hydroxyl groups to fill the A site resulting in A type carbonate substitution. Shimoda *et al.* (1990) found differences in the υ_3 carbonate bands of apatites precipitated in alkaline and neutral conditions at 80°C. Neutral precipitation media resulted in additional peaks at 1546, 1471 cm^{-1} which were attributed to A type substitution. This result is in agreement with the findings of Vignoles *et al.* (1988).

Nelson and Featherstone (1982) conducted their precipitation at pH 8.5-9, whereas precipitation in this study was carried out at pH>11. This may explain why the precipitates produced at 70 and 90°C (most similar to those reported) in this study did not display what have been described as A type carbonate bands. No other work has been carried out that characterises apatite precipitates formed at lower temperatures. Although it is tempting to attribute the additional υ_3 carbonate bands observed at lower precipitation temperatures to the A type substitution, the absence of peaks at 882 cm^{-1} casts doubt over this hypothesis.

9.2.2 Heat treated apatites

The FTIR spectra of 3.2 wt% carbonate apatite sintered in wet carbon dioxide for four hours at 1250°C showed little difference to that sintered in dry carbon dioxide with the exception of the absence of shoulders at 1525 and 1470cm^{-1}. The spectra of 5.8 wt% carbonate sintered at 1000°C in wet and dry carbon dioxide for twenty four hours were similar to one another and to the spectra of the 3.2 wt% carbonate apatite. It can be seen in Figure 8.38 that carbonate apatite sintered in wet carbon dioxide contains hydroxyl groups as indicated by the 3570 cm^{-1} and so is still a hydroxyapatite, whereas the material sintered in dry carbon dioxide appears to be completely dehydroxylated.

Comparisons between Tables 8.7 and 8.9 indicate that on heating to 1000°C the 3C9M material (5.8 wt% carbonate) peaks at 1557 cm^{-1} was no longer observed and peaks at 1458 and 1505 cm^{-1} become apparent. The υ_2 peak

at 873 cm^{-1} shifts to the higher wavenumber at 878 cm^{-1}. Table 8.10 shows that these carbonate peak positions do not directly agree with any previous reports. Nelson and Featherstone (1982) reported an extra υ_2 peak at 873 which was attributed to a B type substitution, the υ_3 peak previously assigned to an A type carbonate substitution (Section 3.5.3) was not reported by these workers. LeGeros (1969) reported similar υ_3 carbonate peaks to those found in this study however the peak at 1415 cm^{-1} was not reported. Peaks that have been attributed to carbonate in both A and B locations were observed in carbonate apatites heated in both wet and dry carbon dioxide atmospheres. This suggests that the sintered material may have been what has been termed an AB type carbonate apatite.

9.3 Lattice parameters of carbonate apatite precipitated at 70°C.

The XRD refinement data clearly showed an increase in **a** axis at carbonate contents up to 4wt% (Figure 8.24) a decrease was observed thereafter. The opposite trend was observed in the **c** axis. A type substitutions have been reported as expanding the **a** axis, e.g. Bonel (1972a) and LeGeros (1965) and B type substitutions contract the **a** axis, e.g. Bonel (1972b), Labarthe (1973) and Doi *et al.* (1982).

Nelson and Featherstone (1982) reported an **a** axis expansion at low carbonate content followed by a contraction at higher carbonate content, this effect was attributed to the incorporation of water in the structure. However Vignoles *et al.* (1987) found that for aqueous carbonate apatite to which no ammonia was added there was an increase in the **a** axis up to 4wt% carbonate with a decrease thereafter. This trend was not observed in alkaline precipitation conditions using ammonia, however data was not presented in the range 0 - 5 wt% carbonate. They associated this phenomenon in conjunction with the FTIR data (Section 9.2) as being due to A type substitution at low carbonate contents in alkali free conditions. Shimoda *et al.* (1990) prepared carbonate apatites in a method similar to that used in this study, except the concentrations of calcium and phosphorus were approximately three times more dilute. Alkaline precipitation conditions were found to give carbonate apatites whose **a** axes decreased with increasing carbonate content. Neutral conditions produced carbonate apatites whose **a** axes increased with increasing carbonate content. They concluded that

neutral conditions gave rise to an AB type substitution. The degree of supersaturation in this study was likely to be higher than that used here and this may be a reason why this phenomenon was not observed at either 70 or 90°C here. Comparisons with previous work tend to suggest that the **a** axis expansion observed at low carbonate contents may be due to an A type substitution. However the absence of carbonate υ_3 and υ_2 bands at 1550 and 883 cm^{-1} in precipitates formed at 90 and 70°C and the fact that the precipitations reported here did not occur in alkaline deficient conditions do raise doubt over this hypothesis, however comparisons with other work may be invalid if supersaturation effects affect the position of various IR carbonate bands. It may well be that the 'A type' carbonate peaks are present but are obscured by the more prominent 'B type' peaks (Figure 8.23a).

9.4Chemical Analysis

There was some evidence of sodium being present in the apatites of higher carbonate content. At low carbonate content (~4 wt%) no sodium was found in the material precipitated at 3°C, whereas a more substituted carbonate apatite (11.5 wt%) precipitated at the same temperature was found to contain 1.5 wt % sodium. This would imply that either two mechanisms of substitution are active or that sodium is included as an impurity second phase since the sodium was used in the reaction as sodium bicarbonate. LeGeros (1967) reported sodium contents of 2.4 wt % for a 4 wt % precipitated carbonate apatite. Nelson and Featherstone (1982) reported sodium contents of between 0.4 and 0.7 for a similar wt % carbonate. LeGeros used the Direct Method which requires much higher carbonate concentrations than the Inverse Method to achieve a given degree of carbonate substitution. This means that the reaction mixtures of LeGeros contained much higher levels of sodium. This may account for the higher sodium levels reported by LeGeros compared with Nelson and Featherstone (1982) and this study. A large variation in sodium content was reported at other carbonate contents by Nelson and Featherstone (1982) and so would tend to cast doubt on a clear relation between carbonate and sodium in their samples.

The observed bicarbonate concentrations, at which a second phase was formed, were highest at 3°C and 37°C, (560 and 480mM), lower at 70°C and 45°C, (320mM), 25°C, (160mM) and lowest at 90°C, (<10mM). This

behaviour did not appear to follow any obvious trend. Presumably this is related to a non linear change in solubility product for carbonate apatite with temperature. A similar trend was observed by McDowell *et al.* (1977), however the effect was not investigated further in this study.

Figure 8.16 would seem to indicate that a given degree of carbonate substitution is effected at lower bicarbonate concentrations at 37 and 45°C than at higher or lower temperatures. This may have some relevance to the mineralisation process and the incorporation of carbonate in biological mineral, though there is not enough data to confirm this trend. Labarthe *et al.* (1973) precipitated carbonate apatites at 20, 40, 60, 80°C and boiling point, by the Inverse Method at a carbon phosphorus ratio of 0.8. They found using XRD and IR that the crystallinity increased with temperature and the intensity of the carbonate IR bands also increased with temperature. This suggested that the degree of carbonation increased with temperature. However this may have been an effect associated with the change in crystal size. A similar effect was not observed in this study, the carbonate content at a fixed concentration generally increased with precipitation temperature to a maximum at 37°C and then decreased with temperature. Labarthe *et al.* (1973) found that the Direct Method gave very weak carbonation at 45°C and very strong carbonation at 20°C, they could offer no explanation for the phenomenon. The precipitates produced in this study were boiled to help remove soluble salts. Nelson and Featherstone (1982) found that carbonate content that the carbonate content of a precipitated carbonate apatite decreased by 50% after refluxing for two days. However the short time periods (up to 2 hours), used in the procedure here was unlikely to alter the carbonate content significantly. The effect reported by Nelson and Featherstone (1982) does imply that carbonate apatite has a tendency to lose carbonate at 100°C and may be related to the observation in this study that less carbonate is substituted into the apatite at a given bicarbonate concentration as the formation temperature approaches 100°C, in the range over and above 37°C.

Figure 8.19 clearly demonstrated a negative correlation between the carbon and phosphorus contents of the hydroxyapatites precipitated at all the temperatures investigated. This suggests that a carbon for phosphorus type substitution was operative. The precipitation method used in this study was based on that reported by Nelson and Featherstone (1982). These workers

proposed a substitution mechanism whereby four carbonate atoms replace three phosphate atoms, the charge balance being maintained by the addition of sodium. Nelson and Featherstone (1982) reported that their results showed a very strong (R^2 = 0.93) negative correlation of phosphorus content with carbonate content, Figure 9.1.

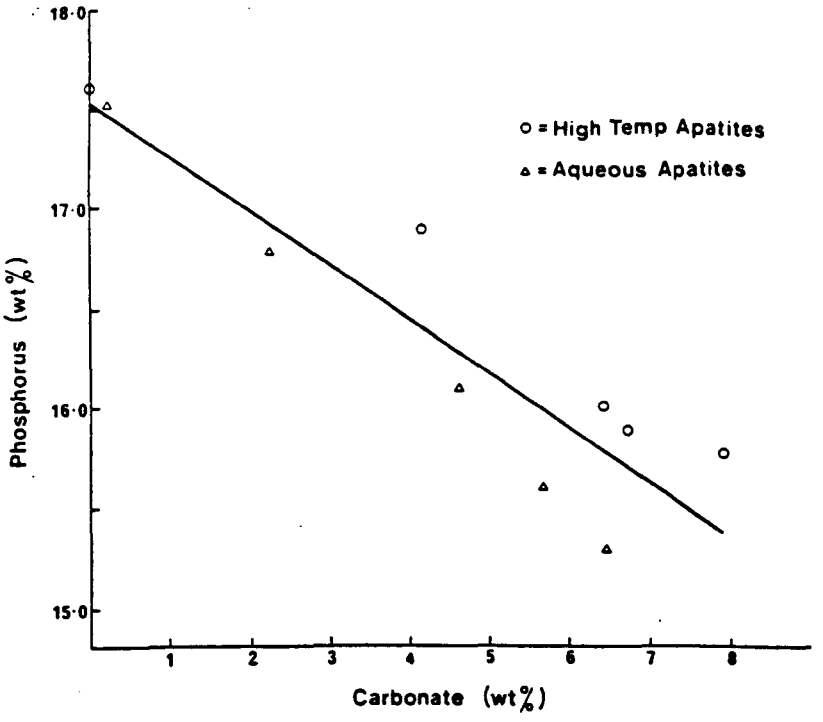

Figure 9.1. Phosphorus content as a function of carbonate content as reported by Nelson and Featherstone (1982). (Reproduced from Nelson and Featherstone, 1982)

The gradient of 0.27 in Figure 9.1 corresponds to a change of phosphorus wt% with carbon of 1.35, which is similar to the result obtained in this work, Figure 8.19. It would appear that the carbonate in apatites precipitated in this study at temperatures between 70 and 3°C replace phosphorus in the same manner as that of Nelson and Featherstone (1982). This is to be expected since the preparation method is essentially the same, precipitation temperature does not appear to affect the mechanism of substitution.

However there appeared to be an anomaly in the conclusion of the report of Nelson and Featherstone (1982). The possibility of an A type substitution was discounted as IR peaks at 1463cm^{-1} and 1528cm^{-1} were reported not to have been observed. However, in the results section, the workers reported the presence of an extra peak at 1550 cm^{-1} in precipitated carbonate apatites. This peak had previously been assigned to A type carbonate by LeGeros *et*

al. (1969). Nelson and Featherstone (1982) also reported that precipitated carbonate apatites with low carbonate contents displayed an increase in **a** axis dimensions, which is indicative of an A type substitution e.g. Elliott (1963), Nadel (1970).

Other reports on precipitated carbonate apatite suggest a mechanism of the type of Kühl and Nebergal (1963) and Labarthe *et al.* (1973). The model proposed by Vignoles (1984) and Vignoles *et al.* (1988) assumed the substitution of one phosphate ion by either a carbonate ion in direct precipitation procedures or a $(CO_3\ OH)^-$ ion in the inverse case as in this study. Figure 8.20 shows that the amount of hydrogen increases with the carbonate content which would appear to be in agreement with this previous work. Vignoles (1984) found that for carbonate apatites precipitated by the Inverse Method in the presence of ammonia, the coefficient **y** in the formula for the apatite given in Equation 9.1 is 0.

$$Ca_{10-x+y}(CO_3)_x(PO_4)_{6-x}(OH)_{2-x+2y} \qquad (9.1)$$

Where: $0 \leq x \leq 2$, $2y \leq x$.

Using Equation 9.1 it is possible to calculate the variations of carbonate hydroxyapatite apatite composition predicted by the Kühl and Nebergal (1963) model. By plotting graphs where y=0 and y= x/2 for values of x giving carbonate contents over the range reported in this study, the entire range of compositions described by Equation 9.1 is described by the area between these two limits of y. Therefore it is possible to determine if the mechanism of carbonate substitution of precipitates produced in this study can be described by the Kühl and Nebergal (1963) mechanism by comparing calculated weight percentages of calcium, phosphorus and carbon with Figures 9.2 a, b and c. It can be seen in Table 9.1 that this mechanism only fits the experimental results when y = 0 in the case of the prediction of the change of phosphorus with carbon.

The FTIR and XRD data (Sections 8.5.3 and 8.5.4) showed evidence of an A type substitution at low carbonate contents. This is in agreement with observations made by Vignoles (1984) and Vignoles *et al.* (1988). Vignoles (1984) reported that the **a** axis increase reached a maximum at 4 wt% CO_3^{2-}. She proposed that once the A site was filled with carbonate, B type substitution occurred. A site substitution was then inhibited by the presence of B type carbonate around the A site channels. Since the effects of the A

type substitution only were apparent at quite low carbonate contents, Vignoles (1984) did not take it into account and assumed A type substitution to be an impurity.

Another explanation for the A type substitution occurring at low carbonate contents and then apparently disappearing is that the B site can accommodate a greater wt% of carbonate than the A site. There are two reasons for this. Firstly a B type substitution reduces the unit cell mass whereas an A type substitution increases it, thus the substitution of a given number of carbonate ions per unit cell will give a smaller wt% of carbonate in an A site than in a B site. Secondly there are more B sites than A sites. Therefore it is likely that the presence of A type carbonate is masked at high carbonate contents by the more prevalent B type substitution.

A model was devised that could describe the simultaneous substitution of the A and B sites. This was assumed to be a two stage process. Firstly, both the A and B sites were filled in equal proportions until half the A sites were filled, (since FTIR spectra showed the hydroxyl ion to be present even in highly carbonated apatites). Secondly, further substitution occurred only in the B site by the mechanism of Kühl and Nebergal (1963).

The first mechanism can be described by:

$$Ca_{9.25-p}\ (PO_4)_{6-p}\ (CO_3, OH)_p\ (OH)_{2-p}\ (CO_3)_p \qquad (9.2)$$

where p is the number of carbonate ions in the A and B sites. Note the calcium deficiency observed in the results of the present study are taken into account. Where charge balance is maintained by the formation of vacancies and / or the substitution of water in the hydroxyl site. Once a limiting value of carbonate occupancy in the A site is reached . Further substitution may occur in the B site by the mechanism of Kühl and Nebergal (1963), i.e.:

$$Ca_{d-x+y}\ (CO_3)_{e+x}\ (PO_4)_{f-x}\ (OH)_{g-x+2y} \qquad (9.3)$$

Where d, e, f and g are the molar ratios of calcium, phosphate, carbonate and hydroxide described in Equation 9.2 when the A site is full and $0 \leq x \leq 2$, $2y \leq x$. This method is subsequently referred to as the AB mechanism.

Figures 9.2 a, b and c show the calculated variations of calcium with carbon, phosphorus with carbon and calcium with phosphorus respectively for the

Kühl and Nebergal (1963) and AB mechanisms up to carbon contents observed experimentally.

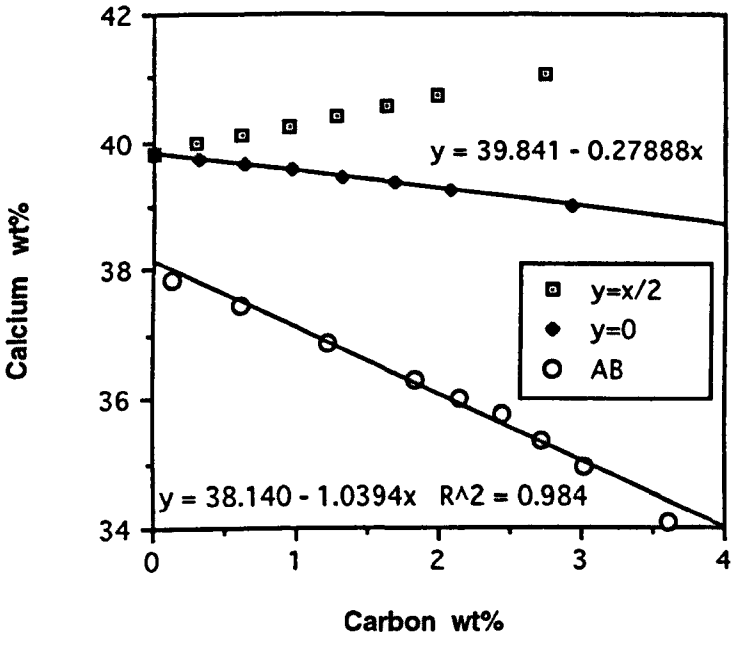

Figure 9.2 a). Calcium weight percent of hydroxyapatite as a function of carbon content as predicted by Kühl and Nebergal (1963) and the AB mechanism of this work.

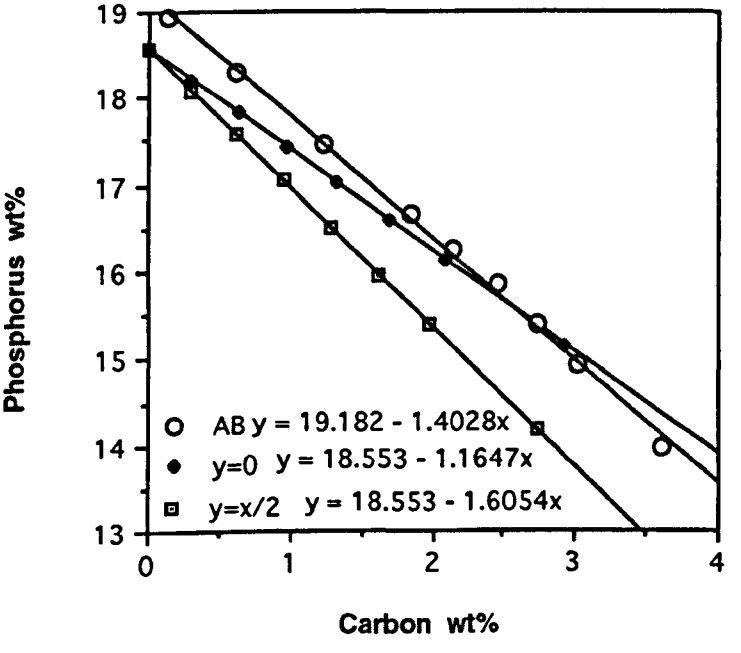

Figure 9.2 b). Phosphorus weight percent of hydroxyapatite as a function of carbon content.

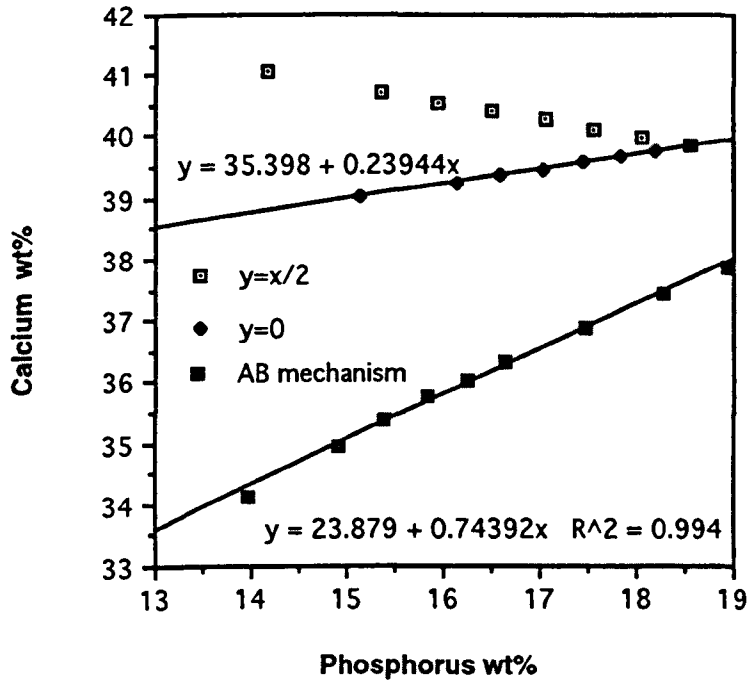

Figure 9.2c). Graphs of variation of calcium and phosphorus with carbon and calcium with phosphorus as predicted by the two extremes of the mechanism of Kühl and Nebergal (1963) and an AB mechanism whereby the carbonate occupies both the A and B sites until half the A sites are filled (2.45%C), the B sites only being filled thereafter. The experimental values are 0.8, 1.3 and 0.7 respectively.

By comparison with Figures 8.17, 8.18 and 8.19, it can be seen that the Kühl and Nebergal (1963) model most closely agrees with the experimental data of the present study when y = 0. The AB mechanism however shows a more impressive description of the experimentally determined values.

Table 9.1 is a comparison of the gradients of graphs of apatite composition with varying carbonate content reported here and predicted by the Kühl and Nebergal (1963) and AB model. In the case of the Ca /C and the Ca / P graph gradients, the Kühl and Nebergal (1963) model shows large deviations from the observed values. On the basis of this evidence, the AB mechanism would seem to better describe the composition of the carbonate apatites precipitated in this study, than the widely accepted Kühl and Nebergal (1963) model.

Table 9.1. Comparison of the gradients of composition graphs determined experimentally, predicted by the Kühl and Nebergal (1963) model and the AB mechanism.

Gradient	Experimental	Kühl and Nebergal (1963). y=0	Kühl and Nebergal (1963). y=x/2	AB mechanism
Ca / C	-0.8	-0.3	POSITIVE	-1
P / C	-1.3	-1.2	-1.6	1.4
Ca / P	~0.7	0.2	NEGATIVE	0.7

9.5 Processing

9.5.1 Filtration

It is hard to predict whether the pH measured for the slurries represented a dispersed or agglomerated state. There is a general disagreement of values for the isoelectric point of hydroxyapatite in the literature, Ducheyne *et al.* (1992) suggested that the zeta potential of hydroxyapatite varied with immersion time. It appears that no workers have published values for the zeta potential of carbonate apatites, therefore it is not clear that any attempt to infer the nature of the dispersion of the slurries from reported values for hydroxyapatite would be valid. It was decided that since one purpose of the study was to determine the effects of carbonate on the sintering behaviour of the apatites, no additives/dispersants would be made. Polymeric deflocculants might have incompletely decomposed in the carbon dioxide atmospheres and interfered with the results. The addition of acids or bases might have altered the chemistry of the apatites or have masked effects of carbonate. As both 3C16M and 3C09M dried to similar green densities (Table 8.5) carbonate content did not appear to affect green density in this carbonate range and so differences in results of sintering studies using these materials were expected to be due entirely to the differing carbonate contents.

The graph of volume of slurry filtered with square root of time (Figure 8.6) shows two linear regions. If the first region at lower filtration times represents the initial period of consolidated layer build up, where the mould slowly fills from bottom to top as a consequence of gravity. The second linear region represents the volume filtered with square root time as the filtering layers increase in thickness.

From the slope of this region, the solid volume fraction at drying time (t =0) i.e. immediately after casting, and assuming ΔP to be 100 kPa, from Equation 4.14 a value for the permeability K of 5 x 10^{-17} m^2 may be obtained. This compares well with the theoretical value obtained by the Carman-Kozeny (1948) relation (Equation 4.16) which predicts a value of 4.6 x 10^{-17} m^2 for particles 10nm diameter. It can be seen that for a given solid volume fraction, the permeability, or ease of flow, increases with the square of particle size. Thus for a given pressure, the time for a given degree of consolidation to occur will increase as a square function of a decrease in particle size. This suggests that although small particles are advantageous for sintering, they are less suitable for filtration casting. However the problem of impractical filtration times can be reduced to some degree by doubling the area of filtration for a given geometry by means of the biaxial filtration system used, which halves the time to consolidate a given thickness of slurry. From the work of Tiller and Tsai (1986) it is hard to deduce anything about the nature of the filter cake from Figure 8.6. The 'two stage' square law behaviour does not appear to have been reported for either pressure or filtration casting, Lange and Miller (1987), Phillipse (1982). Regrettably time did not permit the repeating of this experiment in order to investigate this effect.

9.6 Drying

9.6.1 Shrinkage

It can be seen from Figure 8.8 that the drying rate for all gels is approximately the same, i.e. 40 mg h^{-1}. The 3C09M 7.4g and the 3C16M monoliths show an abrupt decrease in mass loss after approximately 350 hours. This change in water loss rate indicates a change in the mechanism of drying. Dwivedi (1986) observed similar phenomena in drying studies of alumina gels at 80°C. The initial water loss rate was reported as being 180 mg cm^{-3} h^{-1} and he reported extensive cracking of the gels. Macey and Wilde (1944) found the maximum rate of drying of a slab clay 12.7 mm thick without cracking (similar to that of the monoliths in this study) was 50 mg cm^{-3} h^{-1}. Although this rate is not perhaps directly comparable with the carbonate apatite gel system, it is higher than that measured for the apatite monoliths which did not show signs of cracking. Figure 8.10 shows the solid volume fraction as a function of drying time. It can be seen that the time for a given water content to be

attained increases with monolith thickness. 3C09M 7.4g and 3C16M 5.6g monoliths displayed a decrease in the rate of water loss at approximately the same water content (0.18). These results illustrate the constant rate and falling rate periods of drying are influenced by geometrical factors such as the volume occupied by water, air and solid. Figure 8.9 shows that the time for a given degree of water volume fraction to be attained increases with monolith size. One would expect there to be a relation between the time and the surface area to volume ratio. Figure 8.10 shows that the solid volume fraction increases with time in a linear manner until a constant value of 0.37 is reached. This is close to the figure of 0.35 calculated from the data of Nordström *et al.* (1990). Similarities in green density of alumina monoliths are found in the reports of Lange and Miller (1987) and Phil ipse *et al.* (1990). Lange and Miller (1987) report that dispersed alumina slurries have a 68± 2% relative density at low filtration pressures and do not demonstrate shrinkage on drying, whereas flocculated slurries shrank during drying to give 54±1% dense monoliths. These values compare with those of Phillipse *et al.* (1990) who reported relative densities of 65±1% and 56% for comparable states of dispersion. Lange and Miller (1987) found that at filtration pressures greater than 1MPa flocculated slurries did not demonstrate appreciable shrinkage during drying. From this observation they proposed that 1MPa represented the capillary pressures that caused shrinkage. This capillary pressure can be used to determine the capillary radius from Equation 4.9 giving a value of ~140nm. This compares well with the measured pore size of a dried flocculated filter cake of 100nm reported by Phil ipse *et al.* (1990). Since Phil ipse *et al.* (1990) used plaster of Paris to provide the driving force for filtration, which generates pressure differences in the order of 10^5 Pa (Aksay and Schilling, 1984) the combined observations of the two workers would tend to suggest that for the case of alumina slips consolidated at pressures of around 10^5 Pa shrinkage is not observed. This would explain why alumina gels that are dispersed but are dried with no consolidation (e.g. filtration) display shrinkage (e.g.Scherer, 1992).

9.6.2 Gelation

Gelation, or the end of appreciable shrinkage appeared to occur at between 50 and 55 % water volume fraction irrespective of carbonate content. During shrinkage the water remains at the surface, the water loss rate per unit area

would then be expected to be constant. Figure 8.12 shows that the water loss rate is highest at the initial period of drying and fluctuates around a value of 14 mg cm^{-3} h^{-1}, considerably lower than that reported by Macey and Wilde (1944). Once the monolith had formed an interconnected solid network the menisci of the water would change position from being at the gel surface to within the pores. The water would still be in a funicular state and a slight decrease in water rate loss would be expected. Figure 8.12 shows that the rate of water loss per unit area decreases at some volume fraction of water less than 0.7, though there are not enough points to determine the exact value. However this is in general agreement with the gelation point data in Figure 8.11. Dwivedi (1986) found that this behaviour occurred at similar water volume fractions for alumina gels that were dried at a much faster rate at 80°C. This implies that this change in drying mechanism is determined by the relative amounts of water and solid in the gel system. Figure 8.9 suggests that a rapid decrease in the rate of water volume loss occurs at between 0.15 - 0.20 water volume fraction, a rapid decrease in water loss flux is also seen at water volume fraction 0.15 in Figure 8.12. At this point capillary flow is thought (e.g. Dwivedi, 1986; Scherer, 1990) to no longer contribute to water transport as the water becomes pendicular. The flux at this stage was calculated as being 0.1mg cm^{-3} h^{-1}, approximately one tenth of the initial rate. Fick's first law can be expressed in the form:

$$j = D\frac{dc}{dx} \qquad (9.4)$$

Where j is the flux, D is the diffusion coefficient, and $\frac{dc}{dx}$ is the concentration gradient of the diffusing species. The diffusion coefficient depends upon the temperature, the drying mechanism, the specimen geometry and the method of measurement (Cooper, 1987). The concentration gradient depends upon the water concentration in the ambient conditions, the position in the specimen and therefore for the sample as a whole, and the nature of the porosity. Because of all these variables the reported work on the drying of gels giving flux values cannot be compared. However the changes in drying behaviour are common to them and are observed in many different drying systems.

9.6.3 Pore Size

The mercury porosimetry data would appear to indicate that the gel method of processing produces a highly homogenous microstructure with a narrow distribution of pore sizes. Powder pressing appears to have a broad bimodal pore size distribution with a constant population of pore sizes between these two modal values. From a purely qualitative perspective a homogeneous microstructure is desirable from the point of view of sintering since a more uniform densification would be expected. The higher surface area of the gel would be expected to improve the 'sinterability' of the carbonate apatite by increasing the radius of curvature of the particles, assuming that only the particle size affects specific surface area and by increasing the area for gaseous interchange which may occur during sintering.

Mercury porosimetry indicated that the specific surface area of the 3C16M gel was 184 $m^2 g^{-1}$. The average pore diameter of 9nm obtained from Equation 4.17 would be expected, (from Equation 4.9) to give a maximum capillary pressure of 29MPa. The fact that considerable shrinkage took place on drying would seem to indicate that, on the basis of the findings for Lange and Miller (1987), the suspension used to make the monoliths was flocculated. However one cannot be certain in this interpretation since the particle size of the carbonate apatite used in this study was more than forty times smaller than those of Lange and Miller (1987) and Phillipse *et al.* (1990) and their observations were made with alumina. The crystal diameter of this precipitate was determined from TEM micrographs as being approximately 10 nm. Using Equation 4.17 a value of 190 $m^2 g^{-1}$ is derived which is only slightly higher than the value obtained by mercury porosimetry. One would expect a smaller value from mercury intrusion since the particle contact points and incomplete intrusion would decrease the specific surface area and the measured value. This may account for the higher density measured by this technique compared with that obtained by the measurement of the specimen dimensions and mass. The average particle diameter determined from the specific surface area measurement for the powder pellet gives a value of 40nm.

9.6.4 Green Density

Smith *et al.* (1994) reported that green densities lay within the quoted error range for dispersed and flocculated alumina filter cakes, 53±2% and 55±2% respectively. These values are close to the values reported by Lange and Miller (1987) and Phillipse *et al.* (1990) for dispersed filter cakes of the same material. This would suggest that the slurries were in fact both dispersed, or that insufficient differences in dispersion existed between the two slurries for any differences to be apparent or, least likely, that the plaster of Paris mould by these workers provided less pressure difference than that used by Phillipse *et al.* (1990). The particle sizes of the alumina of all three studies was around 500nm. Since Smith *et al.* (1994) provided no information as to the drying procedure it is hard to explain this discrepancy in the results.

It would appear that the state of dispersion is the most important factor in the colloidal processing of ceramics since if dispersion is attained, very small pressures are required to achieve the maximum packing density possible by compression. This in turn eliminates the problem of shrinkage during drying. However for flocculated slurries it seems unlikely any further compaction would yield any large improvement in density since the capillary pressure generated by the pores is so high. The fact that carbonate hydroxyapatite filter cakes that were filtered only one side tended to warp due to differential porosity seems to indicate that the suspension was flocculated to some degree, (Tiller and Tsai, 1986). This did not seem to affect the homogeneity of the microstructure after drying.

9.7 Sintering

9.7.1 Atmosphere

Thermodynamic calculations indicated that the presence of water in the furnace atmosphere reduced the partial pressure of oxygen by approximately 50%. In other words the wet atmosphere was slightly more reducing than the dry atmosphere. However this had a negligible effect on the ratio of pressures of carbonate to water over the sintering temperature range investigated and it remained at the nearly constant value of 0.32.

There is little data concerning the decomposition pressures of carbonate apatites. Figure 9.3 shows the decomposition behaviour of calcium carbonate for which accurate data exists.

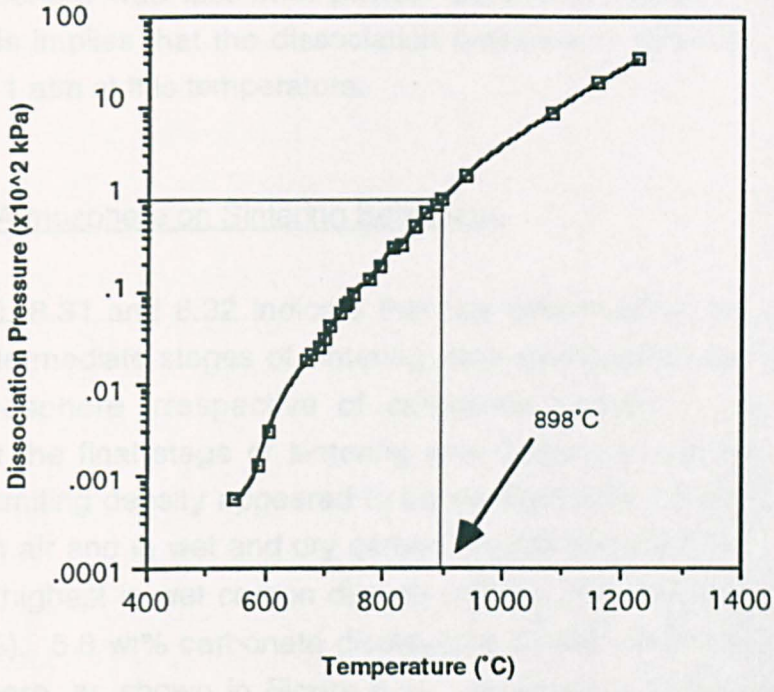

Figure 9.3. Effect of temperature on the dissociation pressure of calcium carbonate, replotted data from Weast (1966).

Figure 9.3 shows that in an atmosphere of carbon dioxide at 100kPa no dissociation of calcium carbonate would occur at temperatures below 898°C. Although the behaviour of hydroxyapatite is likely to be different, the data for calcium carbonate gives an indication of a possible type of decomposition behaviour for carbonate apatite. One can see that in an atmosphere of air (~30Pa carbon dioxide) dissociation would be expected to commence below ~500°C by extrapolation. Sintering carbonate hydroxyapatite in any atmosphere other than carbon dioxide would be expected to yield a carbonate free material unless sintering times were short enough to prevent substantial loss. If carbonate hydroxyapatite behaved in a same manner to that of Figure 9.3, no carbonate would remain in the apatite at equilibrium in an atmosphere of carbon dioxide at temperatures of 898°C and above. However the infra red spectra of 3C09M sintered in wet and dry carbon dioxide for four hours (Figure 8.38) clearly demonstrates that this is not the case for precipitated carbonate apatites, though the position of the carbonate appeared to have changed from the B to the A site during heating.

The data of Doi *et al.* (1993) and of Suwa *et al.* (1993) show that carbonate loss had occurred in carbonate apatites heated in dry argon and what is presumed to be air. Ellies *et al.* (1988) showed that in wet carbon dioxide 14% of carbonate was lost from powder pellets at 825°C in wet carbon dioxide. This implies that the dissociation pressure of carbonate apatite is greater than 1 atm at this temperature.

Effect of Atmosphere on Sintering Behaviour.

Figures 8.30, 8.31 and 8.32 indicate that the densification rate during the initial and intermediate stages of sintering were increased in the wet carbon dioxide atmosphere irrespective of carbonate content. The sintering behaviour at the final stage of sintering was dependent on the carbonate content. A limiting density appeared to be reached with 3.2 wt% carbonate apatite the in air and in wet and dry carbon dioxide (Figure 8.30). This final density was highest in wet carbon dioxide (>99%) and lowest in dry carbon dioxide (98%). 5.8 wt% carbonate displayed a similar limiting density n the dry atmosphere, as shown in Figure 8.33. However at some temperature between 900 and 1100°C the material sintered in wet carbon dioxide decreased in density from nearly full density to ~75% and sintering appeared to recommence at higher temperatures. Carbonate apatite with a higher carbonate content (7.8wt%) only attained 80% relative density in the final stage of sintering in a dry carbon dioxide atmosphere and the density then decreased with a further increase in temperature (Figure 8.31). In a wet atmosphere however nearly full density was attained, at higher sintering temperatures a decrease in density was observed followed by an apparent recommencing of sintering. Figure 8.29 shows that 3.2 wt% carbonate apatite sintered in dry carbon dioxide at 1250°C for four hours contains a significant degree of intragranular porosity which was a few microns in size. The same material sintered under the same conditions in air appeared to contain porosity along the grain boundaries. When sintered in wet air intragranular porosity was less evident but intergranular porosity was observed in practically every grain. The material sintered in wet carbon dioxide contained isolated areas of intergranular porosity but was substantially pore free. Figure 8.28 showed this material to be translucent whereas carbonate apatite sintered in these conditions in other atmospheres were opaque. This suggests that the pores in the material sintered in air, wet air and carbon dioxide were either of

a size or quantity to have caused scattering sufficient to prevent optical transmission.

From the results it appears that bloating behaviour is dependent on both the atmosphere and the carbonate content. The degree of expansion seems to increase with carbonate content, but at low carbonate contents this effect was not observed. At 5.8 wt% carbonate it was observed in the material sintered in the wet atmosphere. At higher carbonate contents, expansion occurred after maximum densification was observed in both wet and dry atmospheres. A comparison of the data of Suwa *et al.* (1993) and Doi *et al.* (1993) (Figure 5.10) shows that dry atmospheres result in a more rapid loss of carbonate than a wet atmosphere. Bloating could be expected to occur when closed porosity is formed before the equilibrium carbonate content at a particular temperature is reached. Since the apatite sintered in the dry atmosphere has a lower densification rate than that sintered in the wet atmosphere this condition is not reached except at high carbonate contents where carbonate loss is incomplete at temperatures sufficient to yield densities high enough to give a significant degree of closed porosity (~80%). As a consequence of the rapid densification rate of carbonate apatite sintered in wet carbon dioxide bloating is observed except at low carbonate contents. It is feasible that the loss of water from the structure may contribute to bloating behaviour.

The reason why the wet carbon dioxide enhanced the sintering rate of carbonate apatites is relative to a dry atmosphere has not been revealed by the present investigation. Reducing atmospheres have been implicated in the prevention of pore / boundary breakaway (Mocellin and Kingery, 1973), the increase in the rate of grain growth, (Quadir *et al.*, 1989; Thompson and Harmer, 1993). However what could be termed a reducing atmosphere was dry hydrogen, which was made more oxidising by the addition of water. It is possible that any differences in behaviour were due simply to the presence of water. Water has been implicated in the increase in densification rate observed in a number of systems, (Aitken, 1960; Dollimore and Spooner, 1971; Yasumoto, 1984; Vila *et al.*, 1994). Although speculative mechanisms were proposed for the role of water, little if any evidence was presented for the hypotheses.

Effect of atmosphere on grain growth.

The data in Table 8.9 shows that 3.2 wt% apatite sintered in carbon dioxide atmospheres had a much larger grain size than that sintered in air. It might be deduced that the material sintered in air contained less carbonate than those sintered in carbon dioxide. The material sintered in dry carbon dioxide had larger grain sizes than those sintered in wet carbon dioxide, but Figures 8.34 and 8.35 would tend to suggest that the grain growth activation energy is relatively insensitive to sintering atmosphere. Thompson and Harmer (1993) found that the mechanism of grain growth of alumina was unaffected by sintering in wet or dry hydrogen, but a reduction in oxygen partial pressure, effected by the absence of water, resulted in an increase in coarsening / densification rate of 250%.

9.7.2 Effect of Carbonate on Grain Size

The level of carbonate in the apatite before sintering appears to have a dramatic effect upon the temperature dependence of grain size as shown in Figure 8.36. It appears that as the carbonate content of the apatite decreases then the activation energy for grain growth increases, from ~50 to 280 $kJmol^{-1}$ for carbonate contents of 11.5 to 3.2 wt% respectively. Figure 8.36 shows that, assuming the different activation energies of grain growth are due to the operation of different mechanisms, at 1000°C, the low carbonate mechanism is dominant. However it is likely that the addition of carbonate to hydroxyapatite is accompanied by the formation of vacancies due to the difference in charge between the carbonate and phosphate ions. As the extrinsic concentration of vacancies increases then diffusion of the deficient species would become easier. This increase in vacancy concentration may be responsible for the decrease in activation energy of grain growth. The average value for the activation energy reported by DeWith *et al.* (1981), Kijima and Tsutsumi (1979), Wakai *et al.* (1990) and Jarcho *et al.* (1976) was 132 ± 5 kJ mol^{-1}. This is between the values obtained for 5.8 wt% and 7.8wt% carbonate apatite. This implies that the addition of carbonate to the apatite structure alters grain growth behaviour depending upon the quantity substituted.

9.7.3 Effect of Carbonate Content on Isochronal Sintering Behaviour.

The temperature at which maximum density was attained seemed to be highly dependent on the carbonate content of the apatite. Table 9.2 summarises the results for materials of green density between 35-40%.

Table 9.2 Temperature at which maximum densification was attained for hydroxyapatites of green carbonate contents of between 3.2 and 11.5 wt%.

Carbonate (wt%)	Temperature of Maximum Densification (°C)
3.2	1125
5.8	1000-1100
7.8	1000
11.5	800-900

It can be seen that in this green density range an increase in the carbonate content has the effect of reducing the temperature at which maximum densification is attained. Figure 8.42 shows the reverse trend for 5.8 and 7.8 wt% carbonate apatites of 30% green density. It is possible that the difference in green density is the reason for this behaviour (Section 9.6.4).

This trend is the same as that reported by Ellies *et al.* (1988), Doi *et al.* (1993) and Suwa *et al.* (1993) but the temperatures of maximum densification reported here are generally higher than those reported. However their data related to pressed powder pellets that were of higher green density. Ellies *et al.* (1988) determined the "sintering temperature" by assessing the ease with which pellets could be broken in the fingers. The other workers took it as the temperature at which maximum linear shrinkage occurred, the degree of shrinkage decreased with increasing carbonate content, presumably as a consequence of the bloating effect being more pronounced in these ceramics. However full density (>99.5%) was not achieved by any of these workers, and this may account for the lower temperatures recorded. Suwa *et al.* (1993) reported that sodium enhanced the densification of carbonate apatite. However data was only provided for one sodium-free specimen that contained nearly 10% more carbonate than the sodium containing materials. The lack of any comparative data makes it difficult to confirm the claim of these authors. The materials used in this study contained less sodium than that reported by Doi *et al.* (1993) and Suwa *et al.* (1993) and this may have had some influence on the densification behaviour observed here.

9.7.4 Effect of green density

Figures 8.43 and 8.44 show that increasing the green density had the effect of reducing the temperature at which full density is attained. A 10% increase in green density reduces the temperature at which full density is attained by more than 100°C. It appears that the densification rate is fairly insensitive to green density during the intermediate sintering stage and has a value between 6 and 9 kg m^{-3} $°K^{-1}$, for 7.8 wt % carbonate and four hour heating time, as measured from the graphs. This effect of green density is similar to that reported by Agrawal (1992) and Fang (1994).

Green density is likely to affect the sintering of carbonate apatites, in particular by varying the area over which gaseous exchange may take place. Carbonate determinations have shown that at 1000°C up to 97% of carbonate was lost (Figure 8.54). Data from Doi *et al.* (1993) indicated that carbonate loss occurred at temperatures less than 600°C. It is feasible that two carbonate apatites of different carbonate contents P and Q, (where P>Q) and different green densities X and Y respectively, (where X<Y) may at some point during the heating process reach the stage where P≤Q. This may in turn affect the densification behaviour of the material. However this does not explain the anomalous behaviour demonstrated in Figure 8.42, where the lower carbonate content material had attained ~99% density at 800°C and the higher carbonate content apatite has attained less than 70% relative density. A possible explanation is the lower green density enabled the lower carbonate content apatite to lose a large proportion of the carbonate. This in turn inhibited any bloating and enabled a more rapid densification than was observed in the higher carbonate content material. Hench *et al.* (1992) produced 20% dense green silica bodies for this reason. This suggests that bloating and sintering processes may occur simultaneously. A high carbonate content favours a high densification rate, yet this in turn will cause bloating. A high green density will reduce the required sintering temperature but may inhibit loss of carbon dioxide.

9.8 Isothermal sintering

Isochronal investigations showed that after four hours at 1000°C nearly full density was obtained in both 3C16 and 3C9M apatites in wet carbon dioxide. In dry carbon dioxide incomplete densification was observed, ~70% relative density for 3C9M. It was envisaged that isothermal investigations at 1000°C would give information on the final stage of sintering for both atmospheres whilst providing a direct comparison between the effects of the two atmospheres.

Figure 8.46 shows that at 1000°C at time t =0 some degree of sintering had occurred in dry carbon dioxide to produce what appears to be a continuous porous solid network. At t= 45 minutes, rearrangement and some degree of coarsening seems to have occurred, however after a further twenty three hours discrete barrel shaped grains are seen that form a porous network, little densification occurred. Figure 8.47 shows that in wet carbon dioxide at time t=0, the microstructure consisted of substantially dense grains. There was some evidence of intergranular porosity however over etching cannot be eliminated as a possible cause. After one hour this porosity is largely absent. Figure 5.23 would suggest that some 1% increase in volume had occurred, though evidence for this is not visible in this micrograph. After four hours sintering however, large crack- like pores are clearly visible. These pores appear to still be present along grain edges after sintering for twenty four hours. Over this time period an increase in linear grain size of approximately ten fold occurred, this corresponds to an increase in volume of one thousand times. These micrographs suggest that water is necessary for both the densification and coarsening of carbonate apatite in carbon dioxide sintering atmospheres.

Figure 8.51 shows the apatites sintered in the dry atmosphere did not appear to densify beyond 73% density. The 5.8 wt% carbonate apatite attained a higher density than the 7.8 wt% carbonate apatite. It is presumed that this is due to the higher carbonate content giving rise to bloating. It can be seen that the density of the 7.8 wt% material is approximately 10% higher than the 5.8 wt% material. This is due to the higher densification rate of the material with higher carbonate content.

In a wet atmosphere however the initial density at time t=0 was 98.8wt% for both carbonate contents (Figure 8.52). No change in density occurred for 30

minutes for the 7.8wt% and for 45 minutes for the 5.8wt% carbonate apatite. Rapid densification then occurred in a matter of a few minutes. The rate of densification appeared to increase with time for both apatites, bloating then reduced the density of the ceramics to 98.4% after a few minutes. The 7.8wt% material showed only slight decrease in density over the following twenty three hours. The 5.8 wt% material continued to decrease in density with time to 96% after twenty four hours.

Sintering models predict that the rate of densification will decrease as the number of pores decreases (e.g. Coble, 1961; Thompson and Harmer, 1993). However Figures 8.52 and 8.53 clearly show that prior to bloating in the wet atmosphere, there was a rapid increase in the densification rate over a short period of time. The reason for this behaviour is not clear though there are two possible explanations. Firstly, the original model of Coble (1961), subsequently modified by other workers, assumes a constant rate process on an atomic level that is influenced by diffusion mechanism, path and geometry. However, if for some reason, possibly the loss of carbonate, the rate of diffusion is increasing with time, for example by the creation of vacancies increasing the diffusion coefficient, then this effect may predominate over the effect of the reduction in the number of pores per unit of grain boundary area. Secondly, the substitution of carbonate of relative mass 60 in the A site replacing a hydroxyl ion of relative mass 17 has the effect of increasing the density of the apatite. However this would only increase the density if the substitution was effected by carbon dioxide entering the lattice and not by the B-> A -> vapour mechanism proposed by Young and Holcombe (1980).

Figure 8.49 shows that the grain size increases with time and the rate of increase generally decreases with time. The lower carbonate content material had a larger grain size at all times, which was to be expected following the findings shown in Figure 8.36. Figure 8.49 shows that the rate of grain growth increased and decreased with density fluctuation. Figure 8.50 suggests that the grain size increased as the cube root of time for both carbonate contents though the data of the 7.8 wt% apatite displayed a poor fit for this behaviour. This relation implies that grain growth was pore drag controlled in these ceramics at these temperatures. At nearly all times at this temperature the ceramics were between 98 and 99% dense, which indicates that porosity was always present. This relation is different to that found by Lopes *et al.* (1990) who found that grain size increased as the fourth root of time and concluded that grain growth of hydroxyapatite in wet carbon dioxide

at 1050°C occurred by surface diffusion. These workers based this hypothesis on only three data points. However similar gradients were found for all sintering conditions employed. The number of pores per grain was not measured and so the model of Brook (1968) (Equation 5.31) could not be applied directly. However, by plotting the rate of grain growth against the products of grain size and density raised to the power relevant to the particular mechanism and assuming the number of pores per grain is constant then the experimental data can be fitted to the possible mechanisms. Liquid phase sintering has been reported as a possible mechanism for the sintering of carbonate apatites (Suwa *et al.*, 1993), however Figure 8.45 would tend to suggest that little if any intergranular phase is present in carbonate apatites sintered in wet carbon dioxide. Table 9.3 shows the value of the slope and intercepts of the various mechanisms, for the data where densification occurred and for the whole data range for the 3C9M material.

Table 9.3. Linear regression analysis of plots of rate of grain growth vs the product of grain size and (1-ρ) raised to the relevant powers as described by the model of Brook (1968).

Data Range	Mechanism	Intercept	Correlation Coefficient (%)
Whole	Evaporation/ Condensation	$1x\ 10^{-8}$	71
	Lattice /Vapour Diffusion	$4x10^{-9}$	68
	Surface Diffusion	$6x10^{-9}$	64
Densifying Region (4 data points)	Evaporation/ Condensation	$1 x\ 10^{-7}$	97
	Lattice /Vapour Diffusion	$-8x10^{-8}$	88
	Surface Diffusion	$-6x10^{-8}$	77

By considering the mechanism with the intercept closest to zero and the highest correlation coefficient it is impossible to conclude that any particular mechanism is operative, though surface diffusion gives the worst fit for the data. This differs from the findings of Lopes *et al.* (1990) which were inconclusive. From the data presented here there is tentative evidence that the mechanism of grain growth in hydroxyapatite is different to that in carbonate apatite as determined from the difference in the activation energies determined from isochronal experiments and isothermal grain size and grain growth rate studies.

The change in carbonate contents shown in Figure 8.54 indicates that the expansion observed during sintering carbonate apatites is due to the loss of carbon dioxide from the dense material. It is interesting to note that 3C9M and 3C16M have the same carbonate content in wet carbon dioxide atmosphere after 58 minutes. Sample 3C9M then remains at that carbonate content and 3C16M increases its carbonate content with time. The final carbonate content appears to be dependent on the initial carbonate content and not on the sintering atmosphere. If the carbonate is assumed to initially be situated predominantly on the B site, then as carbon dioxide is lost vacant B sites are formed. It is reasonable to assume that there is a maximum proportion of vacant sites that can be tolerated by the structure before decomposition occurs.

By taking the mechanism of Kühl and Nebergal (1963), where y=0, to be approximately valid for the carbonate apatites in this investigation, it is found that the number of vacant sites for the 5.8 and 7.8 wt% apatites are approximately 0.5 and 1 respectively assuming all B type carbonate is lost. The carbonate contents of the apatites after 24 hours indicate that there are approximately 0.1 and 0.2 carbon atoms per unit cell for the 5.8 and 7.8 wt% apatites respectively. These carbon atoms are thought to be in the A site, on the basis of FTIR data, (Table 8.10 and Section 3.53). The mechanism of Driessens *et al.* (1983b) does not appear to describe the behaviour reported here in that the partial pressure ratio of the carbon dioxide and water did not influence the carbonate contents of the apatites. These workers prepared their material by solid state reaction and in that way differ from the materials studied here.

PAGE NUMBERING AS ORIGINAL

10 Conclusions

From the results of the work reported in this study the following conclusions can be drawn:

10.1 Precipitation

The size and shape of hydroxyapatite crystals could be altered by varying the precipitation temperature. Precipitation temperatures of 90°C gave an acicular crystal shape approximately 700nm long whereas reactions at 3°C yielded a more spheroidal precipitate approximately two orders of magnitude smaller in size.

Increasing the bicarbonate concentration of the precipitation medium had a similar effect on the crystal size and shape to decreasing the precipitation temperature. It is feasible that both the temperature and bicarbonate ion concentration effects were as a result of the change in supersaturation that occurred.

At low carbonate contents at low precipitation temperatures additional υ_3 carbonate bands were observed in FTIR spectra at 1574 and 1555 cm^{-1}. At higher temperatures or bicarbonate concentrations the intensity of these peaks diminished. These peaks may have been due to some degree of A type substitution. Although the expanded **a** axis observed in these precipitates reinforced this idea, the lack of a υ_2 carbonate band at 883 cm^{-1} suggests that a more complex phenomenon may be operating.

A substitution mechanism whereby A type then B type substitution occurs, as suggested by XRD and FTIR data, fitted the experimental chemical analysis data better than a purely B type substitution model as originally proposed by Kühl and Nebergal (1963).

10.2 Processing

The nanoscale precipitates obtained by increasing the supersaturation of the precipitation medium produced a material that was suitable for colloidal

processing. A biaxial filtration method was devised that was suitable for the production of large monoliths.

Carbonate content did not appear to affect the green density of the monoliths produced.

The filtration processing route formed a homogeneous green microstructure of unimodal pore size distribution.

10.3 Sintering

Sintering atmosphere was shown to have a dramatic effect upon the sintering behaviour of carbonate apatite. Only carbon dioxide atmospheres resulted in a carbonate apatite ceramic.

The presence of moisture in carbon dioxide sintering atmosphere was found to increase the degree of densification during the initial and intermediate stages of sintering at a particular temperature, compared with a dry carbon dioxide atmosphere.

Bloating was observed in both wet and dry carbon dioxide atmospheres after maximum densification was attained. This was attributed to the loss of gas, probably carbon dioxide or possibly water from the crystal structure.

Carbonate in the apatite structure was found to affect grain growth mechanisms. At 1000°C low carbonate content material displayed a larger degree of grain growth than apatite with a higher carbonate content.

In the green relative density range 35-40% the temperature at which maximum densification occurred decreased with carbonate content.

The sintered microstructure of carbonate apatite was sensitive to carbonate content, green density, sintering time and temperature. Bloating and densification are thought to be competing process that can occur simultaneously.

Normal grain growth of carbonate apatite appeared to proceed as a function of the cube root of time, implying that grain growth was pore drag controlled.

The partial pressure of water did not appear to affect the carbonate content of the sintered apatite.

Bibliography

Ackerman U. "The essentials of human physiology," Mosby Year Book (1992).

Adamson A.W., Physical Chemistry of Surfaces, Wiley, New York (1982).

Agrawal D.K., Fang Y., Roy D.M. and Roy R., "Fabrication of hydroxyapatite ceramics by microwave processing,"Mat. Res. Symp. Proc. 269, 231-6 (1992).

Aitken E.A., "Initial sintering kinetics of beryllium oxide," J. Am. Ceram. Soc., 43, 627-33 (1960).

Akao M., Aoki H. and Kato K., "Mechanical properties of sintered hydroxyapatite for prosthetic applications," J. Mater. Sci.,16, 809-12 (1981).

Akao M., Miura N. and Aoki H., "Fracture toughness of sintered hydroxyapatite and β-Tricalcium Phosphate," Yogyo-Kyokai-Shi, 92 (11), 672-4 (1984).

Aksay I.A. and Schilling C.H., "Colloidal filtration route to uniform microstructure," in Ultrastructure Processing of Ceramics, Glasses and Composites, Ed. Hench L.L. and Ulrich D.R., Wiley, New York, 483-91 (1984).

Alder H.H. and Kerr P.F., "Infrared study of aragonite and calcite," Am. Mineral, 47, 700-17 (1962).

Alder H.H., "Infrared spectra of phosphate minerals: symmetry and substitutional effects," Am. Mineral, 49, 1002- 15 (1964).

Alexander K.B., Becher P.F., Waters S.B. and Bleier A., "Grain growth kinetics in alumina-zirconia (CeZTA) composites," J. Am. Ceram. Soc., 77 (4), 939-46 (1994).

Amato I.and Colombo R.L., "The influence of organic additions on the solarization and grain growth of sintered UO_2," J. Nucl. Mater., 11, 348 (1964).

Ames L.L., "The genesis of carbonate apatites," Econ. Geol., 54, 841-929 (1959).

Ando J. "Tricalcium phosphate and its variations" Bull. Chem. Soc. Japan, 31, 196-20 (1958).

Andrievski R.A., "Compaction and sintering of ultrafine powders," The International Journal of Powder Metallurgy, 30 (1), 59-66 (1994).

Aoki H "Science and medical application of hydroxyapatite," Japanese Association Of Apatite Science, (1991).

Aoki H., Akao M., Miura N., Ibo A., Shimizukawa Y. Nakamura S. and Otsuka R., "Crystal structure of carbonate bearing hydroxyapatite from Durango Mexico," Reports of the Institute for Medical and Dental Engineering, 19, 15-20 (1985).

Aoki H., Akao M., Nakamura V. Ito A., Fujii O. and Yoshizawa K., "Bone tissue reactions of carbonate-containing hydroxyapatite single crystals," in Bioceramics Vol 2, Proc. of the 2nd Int. Symp. on Ceramics in Med., Heidelberg, Germany (1989).

Aoki H., Kato K. and Sokawa T., "Development of a handy hot press and its application," Reports of Institute for Medical and Dental Engineering, 7, 113-18 (1973).

Arsenault A.L., Frankland B.W. and Ottensmeyer F.P., "Vectorial sequence of mineralization in the turkey leg tendon determined by electron microscopic imaging," Calcif Tiss. Int., 48, 46-55 (1991).

Atkins P.W., "Physical Chemistry," Oxford University Press, Oxford (1978).

Babushkin O., Lindback T., Holmgren A.,Li J. and Hermansson L., "Thermal expansion of hot isostatically pressed hydroxyapatite," J. Mater. Chem., 4 (3), 413-15 (1994).

Baddiel C.B. and Berry E.E., "Spectra structure correlations in hydroxy and fluorapatite," Spectrochimica Acta, 22, 1407-16 (1966).

Barsa J.J., Farris E.T. and Lagow R., U.S. patent №. 4046858 (1977).

Beck P.A., Kremer J.C. Demer L.J. and Holzwort M.L.,Trans AIME, 175 327 (1948).

Belov N.V. "On some isomorphic substitutions in the apatite group" Doklady. Akad. Naul. SSSR 22, 89-92 (1939).

Bennison S.J. and Harmer M.P. "Swelling of hot-pressed Al_2O_3" J. Am. Ceram. Soc., 68, (11) 591-7 (1985).

Best S.M. "Characterisation, sintering and mechanical behaviour of hydroxyapatite," Ph.D. Thesis University Of London, (1990).

Blumenthall N.C., Posner A.S., Silverman L.D. and Rosenburg L.C., "Effect of proteoglycans on *in vitro* hydroxyapatite formation," Calcif. Tiss. Int. 27, 75-82 (1979).

Bocchi G. and Valdre G. "Physical, chemical and mineralogical characterizarion of carbonate apatite concretions of the human pineal gland," J. Inorg. Biochem., 49, 209-20 (1993).

Boistelle R. and Lope-Valero I., "Growth Units and Nucleation: The case of calcium phosphates," Proc. of the Int. Meeting Geochemistry of Earth Surface and Processes of Mineral Formaion, Spain, March (1966).

Bonel G., "Contrbution à I étude de la carbonation des apatites: I Synthèse et étude des propriétés physico-chimiques des apatites carbonatées du type A," Ann. Chim. 147, 65-88 (1972a).

Bonel G., "Contrbution à I étude de la carbonation des apatites: II Synthèse et étude des propriétés physico-chimiques des apatites carbonatées de type B: III Synthèse et étude des propriétés physico-chimiques des apatites carbonatés dans deux types de sites. Evolution des spectres infrarouge en fonction de la composition des apatites," Ann. Chim., 147, 127-44 (1972b).

Bonel G., Heughebeart J.C., Heughebeart M., Lacout J.L. and lebugle A., "Apatitic calcium orthophosphates and related compounds for biomaterials preparation," Ann. N.Y. Acad. Sci., 115, (1987).

Bonfield W. and Datta P.K. "Impact fracture of compact bone in a shock tube," J. Mater. Sci., 9, 1609 (1974).

Bonfield W. and Tully A.E., "Ultrasonic analysis of the Young's modulus of cortical bone," J. Biomed. Eng., 4, 23-7 (1982).

Bonucci E. "Fine Structures of Early Cartilage Calcification," J. Ultrasonic Res., 20, 33-50 (1967).

Bonucci E., "The locus of initial calcification in cartilage and bone," Clin. Orthop. Rel. Res., 78, 108-39 (1971).

Borneman-Starinkevitch, I.V., "On Some Isomorphous Substitutions in Apatite," Compt. Rend. Acad. Sci. URSS, 22, 113 (1939).

Brecher C., Wei G.C. and Rhodes W.H., "Point deffects in optical ceramics: High-temperature absorption processes in lanthana-strengthened yttria," J. Am. Ceram. Soc., 73 (6), 1473-88 (1990).

Bredig M.A., Frank H.H. and Fuldner H., "Beiträge zur Kenntis der Kalk-Phosphor-säure- Verbindungen II, " Z. Elektrochem. 39, 959-69 (1932).

Brook R.J., "The impurity-drag effect and grain growth kinetics," Scipta Metall., 2, 375-78 (1968).

Brown W. E., Lehr J. R., Smith J. P. and Frazier A. W., "Crystallography of octacalcium phosphate," J. Am. Chem. Soc., 79, 531-8 (1957).

Brown W.E., "Crystal Growth of Bone Mineral," Clin. Orthop., 44, 205-20 (1966).

Brown W.E., Smith J.P Lehr J.R, and Frazier A.W., "Octacalcium phosphate and hydroxyapatite," Nature, 196, 1048-5544.(1962).

Burke J.E. and Turnbull D., in "Progress in metal physics, Vol. III B, Chalmers ed. N.Y. Pergamon Press 220 (1952).

Cant N.W., Bett J.A.S., Wilson G.R., Hall W.K., "The vibrational spectrum of hydroxyl groups in hydroxyapatites," Spectrochimica Acta, 27A, 425-39 (1971).

Carlström D., "Microhardness measurements on single haversian systems in bone," Experimentia, 10, 171 (1954).

Carlström D., "X-Ray crystallographic studies on apatites and calcified structures," Acta Radio Supp., 121 (1955).

Carman P.C., "Some physical aspects of water flow in porous media," Discuss. Faraday Soc., 3, 72 (1948).

Charalambides B. "Comparison of fracture in cortical bone and analogue composites," Ph.D. Thesis, University Of London (1988).

Chickerur N.S., Tung M.S., and Brown W.E. "A mechanism for incorporation of carbonate into apatite," Calcif. Tiss. Int., 32, 55-62 (1980).

Chu Y., Rahaman M.N. and De Jonghe L.C., "Effect of heating rate on sintering and coarsening," J. Am. Ceram. Soc., 74 (6), 1217-25 (1991).

Clasen R., "Preparation and sintering of high-density green bodies to high-purity silica glass," J. Non-Cryst. Solids 89, 335-344 (1987).

Coble R.L, "Sintering crystalline solids.:I Intermediate and final state diffusion models, II. Experimental test of diffusion models in powder compacts," J. of App. Phys., 32 (5), 787-99 (1961).

Coble R.L. and Burke J.E.," Sintering in ceramics," Prog. Cer. Sci. 3, 197-251 (1963).

Coble R.L.,"Transparent alumina and method of preparation," U.S. Patent 3026210, (1962a).

Coble R.L., "Sintering of alumina: Effect of atmospheres, "J. Am. Ceram. Soc., 45 (3), 123-7 (1962b).

Collin R.L., "Strontium calcium hydroxyapatite solid solutions, preparations and lattice parameter measurements," J. Am. Chem. Soc., 81, 5275, (1959).

Conway E.J., "Micro diffusion analysis and volume error ," 5th Review, ed Crosby, Lockwood (1962).

Cooper A.R., "Quantitive theory of cracking and warping during the drying of clay bodies," in Ceramic processing before firing, Ed. Onoda Y.G. and Hench L.L., John Wiley and Sons, New York, 261-76 (1987).

Cooper R.R., Milgram J.W. and Robinson R.A., "Morphology of the osteon. An electron microscopic study," J. Bone and Joint Surgery, 48A, 1239-71 (1966).

Crank J.," Mathmatics of diffusion," Clarendon Press, Oxford, U.K., (1975).

Crouch A.G. and Pascoe R.T., "Density changes during the heat treatment of Fe_2O_3, " Proc.Br. Ceram. Soc., 20, 189 (1972).

Cullity B.D.,"Elements of X-Ray Diffraction," Addison-Wesley, Massachusetts, (1978).

Currey J D ."The effects of drying and re-wetting on some mechanical properties of cortical bone," J. Biomech. 21, 439-41 (1988).

Curtis T.A., Ashrafi S.H. and Weber D.F., "Canalicular communication in the cortices of human long bones," The Anatomical Record, 212, 336-44 (1985).

Cutler I.B. "Active Powders," in Ceramic processing before firing, Ed. Onoda Y.G. and Hench L.L., John Wiley and Sons, New York (1987).

Cutler I.B. and Henrichson R.E., "Effect of particle shape on the kinetics of the sintering of glass," J. Am. Ceram. Soc.,51 (10)., 604-5, (1968).

Daculsi G., LeGeros R.Z., Heughebaert M.and Barbieux I., "Formation of carbonate apatite crystals after implantation of calcium phosphate ceramics," Calcif. Tiss. Int., 46, 20-7, (1990).

Darcy H., "Determination of the laws of flow of water through sand," in Histoires des Fontains de Dijon, 590, (1856). (translated by J.R.Crump).; Fluid/Part. Sep. J., 2, (1), 33 (1989).

de Jong W.F. "Le Sustance Minerale dans le os." Rec Trav Chim. 45, 445-8, (1926).

de With G., Van Dijk H.J.A., Hattu, N. and Prijs K. "Preparation, microstructure and mechanical properties of dense polycrystalline hydroxy apatite," J. Mater. Sci., 16, 1592-8 (1981).

deGroot K., "Ceramics of calcium phosphates: preparation and properties," in Bioceramics of calcium phosphates," Ed. de Groot K., CRC press, 99- 114 (1983).

Dennissen H.W. deGroot K., Makkes P.Ch. van den Hoof and Klopper P.J., "Tissue response to dense apatite implants in rats," J. Biomed. Mat. Res., 5, 713-21 (1980).

Doi Y., Koda T., Wakamatsu N., Goto T., Kamemizu H., Moriwaki Y., Adachi M. and Suwa Y., "Influence of carbonate on sintering of apatites," J. Dent. Res., 72 (9), 1281-86 (1993).

Doi Y., Moriwaki Y., Aoba T., Okazaki M., Takahashi J. and Joshin K. "Carbonate apatites from aqueous and non aqueous media studied by esr, IR, and X-ray diffraction: Effect of NH_4^+ ions on crystallographic parameters," J. Dent. Res., 61, 429-34, (1982).

Dollimore D. and Spooner P., Trans. Faraday Soc., 67, 2750 (1971).

Doss S.K., "Surface properties of hydroxyapatite:I. The effect of various inorganic ions on the electrophoretic behaviour," J. Dent. Res. 75 (6), 1067-75 (1976).

Dowker S.E.P. and Elliott J.C., " Infrared absorption bands from NCO^- and NCN^{2-} in heated carbonate- containing apatites prepared in the presence of NH_4^+ ions," Calcif. Tiss. Int., 29, 177-8 (1979).

Dowker S.E.P. and Elliott J.C., "Infrared study of trapped carbon dioxide in thermally treated apatites," J. Solid State Chem., 47, 164-73 (1983).

Dowker S.E.P. and Elliott J.C., "Infrared study of the formation, loss and location of cyanate and cyanamide in thermally treated apatites," J. Solid State Chem., 49, 334-40, (1983).

Driessens F.C.M. "Formation and stability of calcium phosphates in relation to the phase composition of the mineral in calcified tissue" in Bioceramics of Calcium Phosphates, Editor DeGroot K., CRC Press, Bocca Raton (1983).

Driessens F.C.M., Verbeeck R.M.H. and Kiekens P. "Mechanism of substitution in carbonated apatites" Z. Anorg. Allg. Chemie, 504, 195-200, (1983a).

Driessens F.C.M., Verbeeck R.M.H. and Heijligers "Some physical properties of Na^+ and CO_3^- containing apatites synthesized at high temperatures," Inorganica Chimica Acta, 80 19-23 (1983b).

Ducheyne P., Kim C.S. and Pollack S.R., "The effects of phase differences on the time-dependent variation of the zeta potential of hydroxyapatite," J. Biomed. Mats. Res. 26, 147-68 (1992).

Dwivedi R.K., "Drying behaviour of alumina gels," J. Mater. Sci. Lett., 5, 373-6 (1986).

Eanes E.D. "Crystal growth of mineral phases in skeletal tissue" Prog Cryst. Growth Characterisatics, 3, Pergamon Press Ltd, 3-15 (1980).

Eastoe J.E. and Eastoe B., " The inorganic constituents of mammalian compact bone," Biochem. J., 57, 453-9 (1954).

Eitel W.,"Uber Karbonatphosphate der Apatitgruppe," Schriften konigsberg gelehrten Ges. Naturw., 1 159 (1924).

El Feki H., Rey C. and Vignoles M., "Carbonate ions in apatites: Infrared investigations in the υ4 CO_3 domain," Calcif. Tiss. Int., 49, 269-74 (1991).

Ellies L.G., Nelson D.G.A., Featherstone J.D.B.,"Crystallographic structure and surface morphology of sintered carbonated apatites," J. Biomed. Mats. Res., 22, 541-53 (1988).

Elliot J.C., "The crystallographic structure of dental enamel and related apatites," Ph.D.. Thesis, University Of London, (1964).

Elliot J.C., Bonel G. and Trombe J.C., " Space group and lattice constants of $Ca_{10}(PO4)_6CO_3$" J. Appl. Cryst., 13, 618-21 (1980).

Elliot J.C., "Monoclinic space group of hydroxyapatite," Nature Phys., Sc. 72, 230 (1971).

Emerson W.H., and Fischer E.E., "The infrared spectra of carbonate in calcified tissues," Arch. Oral Biol., 7, 671-83 (1962).

Evans G.P. "Deformation and Fracture of Bone in Thoroughbred Race Horses," Ph.D.. Thesis, University Of London, (1989).

Evans G.P., Beheri J.C. and Bonfield W., Microhardness, Young's modulus and mineral content in bone and a bone analogue., In: Implant Materials in Biofunction, Advances in Bioceramics 8, ed dePutter C.,deLange G.L., deGroot K and Lee A.J.C., Elsevier Science Publishers, Amsterdam, N.L., 311-5 (1988).

Fang Y., Agrawal D.K., Roy D.M. and Roy R., "Fabrication of porous hydroxyapatite ceramics by microwave processing," J. Mater. Res.,7 (3) 490-4 (1992).

Fang Y., Agrawal D.K., Roy D.M. and Roy R., "Microwave sintering of hydroxyapatite ceramics," J. Mater. Res., 9 (1), 180-7 (1994).

Fang Y., Agrawal D.K., Roy D.M. and Roy R., "Rapid sintering of hydroxyapatite ceramics by microwave processing," Ceramics Transactions, 21, 349-56 (1991).

Fang Y., Agrawl D.K., Roy D.M., and Roy R. "Microwave sintering of hydroxyapatite ceramics," J. Mater. Res., 9, 180-7 (1994).

Fang Y., "Personal communication", 14th July (1994).

Feenstra L. and de Groot K., "Medical uses of calcium phosphate ceramics," in Bioceramics of calcium phosphates," Ed. de Groot K., CRC press, 131- 41, (1983).

Fernandez-Moran H. and Engsrom A., "Electron microscopy and X-ray diffraction of bone," Biochim. Biophys. Acta., 23, 260-4, (1957).

Fischer G.R., Bardhan P. and Geiger J.E., "The lattice thermal expansion of hydroxyapatite," J. Mater. Science Letters, 2, 577-8 (1983).

Fisher J.C. and Fullman R., in "Progress in metal physics IIIB," Chalmers ed., N.Y. Pergamon press, 271(1952).

Ford R.W."Ceramics Drying" Pergamon Press (1986).

Fowler B.O., "Infrared studies of apatites: II. Preparation of normal and isotopically substituted calcium, stontium and barium hydroxyapatites and specta-structure correlations," Inorg. Chem. 13, 207, (1974).

Francois B. and Kingery W.D., "The Sintering of Crystalline Oxides.II. Densification and Microstructure Development in UO_2"; in Proceedings of the Second Conference on Sintering and Related Phenomena. Edited by Kuczynski G.C., Hooten N.A., and Gibbon C.F.. Gordon and Breach, New York, 499, (1967).

Frondel C., "Whitlockite A New Phosphate $Ca_3(PO_4)_2$," Amer. Mineral, 26, 145-52, (1941).

Galante J., Rosterhen W. and Ray R. D. "Physical properties of trabecular bone," Calcif. Tis. Res., 5, 236-46, (1970).

Glimcher M.J., Brickley Passons D. and Kossiva D. "Phosphopeptides and g-carboglutamic acid-containing peptides in calcified turkey tendon: Their absence in uncalcified tendon," Calcif. Tiss. Int., 27, 281-84, (1979).

Greenwood G.W. and Boltax A.," Role of fission gas re-solution during post-irradiation heat treatment," J. Nucl. Mater., 5, 234-40 (1962).

Greskovich C., "Effect of green density on the initial sintering of alumina ," Phys. Sintering, 4(1), 33-46 (1972).

Gron P., Spinelli M., Trauntz O., and Brudevold F. "The effect of carbonate on the solubility of hydroxylapatite," Arch. Oral Biol., 8, 251-63 (1963).

Gruner J.W. and McConnel D., "The problem of carbonate apatites," Z. Krist., 97 208 (1937).

Gurkovich S.R. and Blim J., "Preparation of monolithic lead titanate by a sol gel process," in Ultrastructure processing of ceramics, glasses and composites, Ed. Hench L.L. and Ulrich D.R., John Wiley and Sons, New York, 152-159 (1982).

Hagen AR., "Structural features of biologically involved phosphates" Acta Odont. Scand., 31, 149-73 (1973).

Hattori T.,Iwadate Y. and Kato T., "Hydrothermal synthesis of hydroxyapatite from calcium acetate and triethyl phosphate," Adv. Ceram. Mat., 3, 426-28 (1988).

Hayeck E. and Newesely H., 'Pentacalcium monohydroxyorthophosphate," Inorganic Synthesis 7, 63 (1963).

Heimke G. and Griss P., "Tissue interactions to bone replacement materials," in Bioceramics of calcium phosphates," Ed. de Groot K., CRC press, 79-97 (1983).

Hench L.L. in "Science of ceramic chemical processing," Ed. Hench L.L. and Ulrich D.R., Wiley, New York (1986).

Hench L.L., "Ceramics implants for humans," Adv. Ceram. Mats., 1 (4), 306-24, (1988).

Hench L.L., Wilson M.J.R., Balaban C. and Nogues J.L., "Sol-gel processing of large silica optics," in Ultrastructure processing of advanced materials, Ed. Uhlmann D.R. and Ulrich D.R., John Wiley and Sons, New York, 159-77, (1992).

Hendricks, A. and Hills, S.E. "The nature of bone and phosphate rock," Trans Macy Conference on Metabol. Interrel., 3, 1951 (1973).

Herring C.,"Effect of change of scale on sintering phenomena," J. Appl. Phys. 21, 301-3 (1950).

Herzburg G., "Infrared and raman spectra of polyatomic molecules," Volume 2D,. van Nostrand Co., Inc. New York, (1945).

Hodge A.J. and Petruska J.A., "Recent studies on the electron microscope on the ordered aggregates of the tropocollagen macromolecule" in Aspects of Protein Structure, Ed. Ramachandran G. N., Academic Press, New York 289-300, (1963).

Hodgskinson R.A.G., "High resolution imaging of the apatite phase in bone tissue" Ph.D.Thesis, University Of London, (1991).

Howlett S.P. and Brook J.P. , "Density loss in sintered cobalt oxide"; presented at the 2d Irish Durability Congress, N.I.H.E., Limerick, Ireland, March, (1984).

Huaxia J. and Marquis P.M., "Effect of heat treatment on the microstructure of plasma-sprayed hydroxyapatite coating," Biomaterials 14 (1), 64-8 (1993).

Huaxia J. and Marquis P.M., "Sintering behaviour of hydroxyapatite reinforced with 20 wt % Al_2O_3," J. Mater. Sci., 28, 1941-5 (1993).

Hulbert S.F., Bokros J.C., Wilson J. and Heinke G., "Ceramics in clinical applications: Past future and present," in High Tech. Ceramics, Ed. Vincenzini P., Elsevier, Amsterdam, Netherlands 189-213 (1987).

Hunt J.M., Wisher M.P., and Bonham L.C., "Infrared absorption spectra of mineral and other inorganic compounds," Anal. Chem., 22, 1478-97 (1960).

Hutchinson J.L., "Seeing atoms in and around crystals," Microscopy and Analysis, 3, 11-4 (1994).

Ikegami T. and Moriyoshi Y., "Evaluation of grain-growth parameters," J. Am. Ceram. Soc., 68 (11), 597-603 (1985).

Ioku K., Yoshimura M. and Somiya S., "Microstructure and mechanical properties of hydroxyapatite ceramics with zirconia dispersion prepared by post-sintering," Biomaterials ,11, 57-61 (1990).

Irvine G.D., "Synthetic bone ash," British patent №. 1586915 (1981).

Irving J.T., Arch. Oral Biol. 8, 735 (1963).

Ishikawa K., Ducheyne P. and Radin S., "Determination of the Ca/P ratio in calcium deficient hydroxyapatite using X-ray diffraction analysis," J. Mater. Sci.: Mats. in Medicine, 4, 165-68, (1993).

Isrealachvili J.N., "Intermolecular and Surface Forces," Academic Press, New York (1985).

Jackson S.A., Cartwright A.G. and Lewis D. "The morphology of bone mineral crystals," Calcif. Tiss. Res., 25, 217-22 (1978).

Jaffe, H.L., "The structure of bone with particular reference to its fibrillar nature and the relation of function to internal architecture," Archives of Surgery, 19, 24-52 (1929).

Jarcho M., Bolen C.H., Thomas M.B., Bobick J., Kay J.F. and Doremus R.H., "Hydroxylapatite synthesis and characterization in dense polycrystalline form," J. Mater. Sc., 11, 2027-53 (1976).

Jarcho M., "Calcium phosphate ceramics as hard tissue prosthetics," Clin. Orthop. 157, 281-8, (1981).

Jarcho M.B., Bolen O.H., Thomas M.B., Bolick J., Kay J.F. and Doremius R.H., "Hydroxyapatite Synthesis in Dense Polycrystalline Form," J. Mater. Sci.,11, 2027, (1975).

Jarcho M.J., Hydroxylapatite Ceramic, US Patent No.4097935 , (1978).

JCPDS International Centre for Diffraction, Powder Diffraction File (inorganic phases)., Pub. JCPDS, 9-432, (1980).

Jenson A.T., Rowles S. L. " Magnesium whitlockite a major constituent of dental calculus," Acta Orden. Scand., 15, 121-39 (1957).

Johansen E. and Parks H.F., "Electron microscopic observations on the three dimensional morphology of apatite crystallites of human dentine and bone," J. Biophys. and Biochem. Cytol, 7, 743-53, (1960).

Kanazawa T., Umegaki T., Yamashita K., Monma H. and Hiramatsu T., "Effects of additives on sintering and some properties of calcium phosphates with various Ca/P ratios," J. Mater. Sci., 26, 417-22, (1991).

Katz J.L., Akers A.S., Germiller J.A., Obremski S.M. and Singh S., "The elastic properties of apatites and TCP-Calcite Mixtures," Proceedings of 1st. International Symposium on Bioceramics, Kyoto (1989).

Katz J.L., Yoon H.S., Lipsom S., Maharidge R., Meunier A. and Christel P. "The effects of remodelling on the elastic properties of bone," Calcif. Tiss. Int., 36, s31-s36 (1984).

Kay I.M., Young R.A., Posner A.S., "Crystal structure of hydroxyapatite," Nature, 204 (12), 1050-2, (1964).

Kelly P.J. and Peterson L.F.A., "The blood supply of bone," Heart Bulletin 12, 96-99 (1963).

Kijima T. and Tsutsumi M., "Preparation and thermal properties of dense polycrystalline oxyhydroxyapatite," J. Am. Ceram. Soc., 62 (9), 455-61 (1979).

Kingery W.D. and Berg M.J., "Study of the initial stages of sintering solids by viscous flow, evaporation-condensation, and self diffusion," J. Appl. Phys., 26, 1205-12 (1955).

Kingery W.D., Bowen H.K. and Uhlman D.R., "Introduction to ceramics," John Wiley and Sons, New York 2nd Ed. (1976).

Klein C.P., Driessen A.A. and deGroot K., "Relationship between degradation behaviour of calcium phosphate ceramics and their physical-chemical characteristics and ultrastructural geometry," *Biomaterials*, 5, 157-60 (1984).

Klein L.C. and Gamey G.J.,"Monolithic dried gels," J. Non Cryst. Solids, 48, 97-104 (1982).

Knets I.V. , "Mechanics of biological tissues. a review," Mekhanika Polimerov, 13, 434-40, (1978).

Knowles J.C. and Bonfield W., "Development of a glass reinforced hydroxyapatite with enhanced mechanical properties. The effect of glass composition on mechanical properties and its relationship to phase changes," J. of Biomedical Mater. Res., 27, 1591-8 (1993).

Knowles J.C., Abrahams I. and Bonfield W., "Effect of reinforcing glass composition on phase transformation and crystallographic parameters in hydroxyapatite," Bioceramics, 6, 191-6 (1993).

Knudsen F.P., "Dependence of mechanical strength of brittle polycrystalline specimens on porosity and grain size," J. Am Ceram. Soc., 42 (8), 376-87, (1959).

Kuczynski G.C., Abernethy L. and Allan J., "Sintering mechanisms of aluminium oxide," in Kinetics of high temperature processes -Report of Endicott House Conference on Kinetics of High Temperature Processes June 1958, Ed W.D. Kingery, Technology Press of Massachusetts Institute of Technology, Cambridge, and John Wiley and Sons, Inc., New York 163-172 (1959).

Kühl G. von and Nebergal W.H., " Hydrogenphosphat- und carbonat apatat," Z. Anorg. Allg. Chem., 324, 313-20 (1963).

Labarthe J-C., Bonel G. and Montel G. "Sur la structure et les propertes des apatites carbonatées de Type B Phospho-Calciques" Ann. Chim., 7, 289-301, (1973).

Lange F.F. and Miller K.T. "Pressure filtration: Consolidation kinetics and mechanics," Am. Ceram. Soc. Bull., 66 (10), 1498-504 (1987).

Lange F.F., "Powder processing science and technology for increased reliability," J. Am. Ceram. Soc., 72 (1)., 3-15 (1989).

Lange F.F., "Transformation toughened ZrO_2.Correlations between grain size control and composition in the system ZrO_2.and $Y_2.O_3$.," J. Am. Ceram. Soc., 69(3), 240-42 (1986).

Laugier M.T., "New formula for indentation toughness in ceramics," J. Mater. Sci. Lett., 6, 355(1987).

Lee H.W. and Sacks M.D., "Pressureless sintering of SiC whisker reinforced Al_2O_3 composites I: effect of matrix powder surface area," J. Am. Ceram Soc., 73 (7), 1884-93 (1990).

LeGeros R.Z. and Tung M., "Chemical stability of carbonate- and fluoride - containing apatites," Caries Res., 17 ,419-29 (1983).

LeGeros R.Z. "Crystallographic studies of the carbonate substitution in the apatite structure," Ph.D.. Thesis N.Y. Uni. (1967a).

LeGeros R.Z., Trautz O.R. LeGeros J.P. and Klein E., " Apatites: Effects of carbonate on morphology ," Science 155 1409-1411 (1967b).

LeGeros R.Z. Miravite M.A., Quirolgico G.B. and Curzon M.E.J., "Effect of carbonate on the lattice parameters of apatites," Nature, 206, 403-4 (1965).

LeGeros R.Z., Trautz O.R., Klein E and LeGeros J.P., "Two types of carbonate substitution in apatite substitution," Specialia Experimentia 25(1), 5-7 (1969).

Lehr J.R., Brown E.H. Frazier A.W. Smith J.P. and Thrasher R.D." Crystallographic properties of fertilizer compounds," Tenesee Valley Authority, Chem. Eng. Bull., 6 1-166 (1967).

Levitt S.R., Crayton P.H. Monroe E.A. and Condrate R.A., " Forming methods for apatite prosthesis," J. Biomed. Mater. Res., 3, 683 (1969).

Li J. and Hermansson J. L. "Mechanical evaluation of hot isostatically pressed hydroxylapatite," Interceram 39(2), 13-5 (1990).

Liu Y. and Patterson B.R., "Determination of pore mobility during sintering," Metallurgical and Materials Transactions, 25A, 81-7 (1994).

Locardi B., Pazzaglia U.E., Gabbi C. and Profilo B.,"Thermal behaviour of hydroxyapatite intended for medical applications," Biomaterials 14 (6), 437-41 (1993).

Lopes A.B.,Correia R.N. and Fonseca A.T., "Bioceramicos de hidroxiapatite: sinterizacao e propriedades mecanicas," 2nd. Int. Congress on Biomedical Engineering, 1.4.1, (1990).

Louat N.P. and Duesbery M.S., "On the theory of normal grain growth," Philosophical Magazine A, 69 (5), 841-54 (1994).

Luklinska Z. and Bonfield W., "High resolution electron microscopy of bone implant interface," in The bone material interface, Ed. Davies J.E., University of Toronto Press, 89-93, (1991).

Macey H.H. and Wilde F.G., "Experiments on the drying of clay," Trans. Br. Ceram. Soc. 43, 93, (1944).

Maitland M.E. and Arsenault A.L., "A correlation between the distribution of biological apatite and amino acid sequence of type I collagen, "Calcif. Tiss. Int., 48 341-52 (1991).

Martin R.B. and Burr D.B., Structure function and adaptation of compact bone, Raven Press , New York (1989).

Matsui M., Takahashi T. and Oda I., " Influence of MgO vaporization on the final stage sintering of $MgO-Al_2O_3$ spinel," in : structure and properties of MgO and Al_2O_3 ceramics, Ed. W.D. Kingery, Advances in ceramics 10, (1984).

McConnell D., "The crystal chemistry of carbonate apatites and their relation to the composition of calcified tissues," J. Dent. Res., 31, 53-63 (1952).

McDowell H., Gregory T.M. and Brown W.E., "Solubility of $Ca_5(PO_4)_3OH$ in the system $CaOH_2-H_3PO_4-H_2O$ at 5, 15, 25, and 37°C," J. Res. Nat. Bur. Stand., 81A, 272-81, (1977).

Mehmel M., "Uber die Struktur des Apatits," Z. Krist., 75, 323, (1930).

Menton D.N., Simmons D.J., Chang S.L. and Orr B.Y., "From bone lining cell to osteocyte - an SEM study," The Anatomical Record 209, 29-39, (1984).

Merz W. and Schenk R., "A quantitive histological study on bone formation in human cancellous bone," Acta Anatomica, 76, 1-15 (1970).

Milhofer H.F., Hlady V., Baker S.F., Beebe R.A., Wikholm N.W. and Kittelberger J.S.,"Temperature programmed dehydration of hydroxyapatite," J. of Colloid and Interface Science, 70 (1), 1-9 (1979).

Miller S.C., Bowman B.M., Smith J.M. and Jee W.S.S., "Characterisation of endostial bone-lining cells from fatty marrow bone sites in adult beagles," The Anatomical Record, 198 163-73, (1980).

Mizuno T., Nagata H. and Manabe S., "Attempts to avoid cracks during drying," J. Non-Cryst. Solids, 100 236-40 (1988).

Mocellin A. and Kingery W.D., "Microstructural changes during heat treatment of sintered Al_2O_3," J. Am. Ceram. Soc. ,56 (6), 309 - 14 (1973).

Mohamed N. and Rahaman, " Effect of green density on densification and creep during sintering," J. Am. Ceram. Soc. 74(3), 514-9 (1991).

Molnar Z., "Additional observations on bone mineral crystal dimensions," Clin. Orthop. 17, 38-42, (1960).

Monma H. and Kamiya T., "Preparation of hydroxyapatite by the hydrolysis of brushite," J. Mater. Sci., 22, 4247-50, (1987).

Monma H., Ueno S. and Kanazawa T., "Properties of hydroxyapatite prepared by the hydrolysis of tricalcium phosphate," J. Chem. Tech. Biotechnol., 31, 15-24 (1981).

Monroe E.A., Votava W., Bass D.B., McMullen J., "New calcium phosphate ceramic material for bone and tooth implants," J. Dent. Res., 50, 860-1, (1971).

Montel G., "Contribution a l'étude des mechanismes de synthese de la fluorapatit," Annal. Chim., 3, 313-69, (1958).

Morancho R.,Ghommidh J. and Buttazoni B.G., "Constant thin films of several calcium phosphates obtained by chemical spray of aqueous calcium hydrogen phosphate solution: A route to hydroxyapatite films," Proc. of the 8th Int. Conference on Chem. Vap. Deposition. Electrochem. Soc. N.Y. (1981).

Morgan C.S., McCorkle K.H., and Powell G.L., "Pore growth in sintered thoria," J. Am. Ceram. Soc., 59 (3-4), 104-7 (1976).

Mullin J.W., "Crystallization", Butterworths, London, (1961).

Nadal M. Trombe J.C. Bonel G. and Montel G. J., "Etude par spectrométrie d'absorption dans l'infrarouge de quelques substitutions dans les apatites carbonatés," Chim Phys. 67, (1), 1161-7, (1970).

Nagai M., Saeki T. and Nishino T., "Carbon dioxide sensor mechanism of porous hydroxyapatite ceramics," J. Am. Ceram. Soc., 73 (5), 1456-60, (1990).

Naráy -Szabó St., "The structure of apatite, $(CaF).Ca_4(PO_4).3$," Z. Kryst. 75, 387, (1930).

Nash A., "Viscoelasticity and the mineral phase of compact bone", Ph.D. Thesis University Of London, (1980).

Nelson D.G.A, Stokroos I. and Arends J., " Lattice parameters of apatite materials using high- resolution transmission electron microscopy fringe techniques," Caries Res., 21, 117-125 (1987).

Nelson D.G.A. and Featherstone J.D.B. "Preparation analysis and characterization of carbonated apatites," Calcif. Tiss. Int. 34 569-581 (1982).

Nelson D.G.A. Featherstone J.D.B. Duncan J.F. and Cutress T.W. "Paracrystalline disorder of biological and synthetic carbonate substituted apatites,"J. Dent. Res. 61(11), 1274-1281(1981).

Nelson D.G.A., Featherstone J.D.B. Duncan J.F. and Cutress T.W., "Effect of carbonate and fluoride on dissolution behaviour of synthetic apatites", Caries Res. 17 200-211 (1983).

Nelson D.G.A., McLean J.D., and Sanders J.V., "A high resolution electron microscope study of synthetic and biological carbonated apatites," J. Ultrastructure Res., 84, 1-15 (1983).

Nelson D.G.A.," The influence of carbonate on the atomic structure anc reactivity of hydroxyapatite," J. Dent. Res., 60(C)., 1621- 9 (1981).

Neuman M.W. and Neuman W.F., "On the measurement of water compartments, pH and gradients in calcaria," Calcif. Tiss. Int. ,31, 135-145, (1980).

Newman W. F. and Newman M. W. , "The chemical dynamics of bone mineral," University of Chicago Press Chicago, (1969).

Nordsröm E.G. and Karlsson K.J., " Slip cast apatite ceramics," Ceram. Bull., 69, (5), 824-7, (1990).

Nordstôm E.G. and Karlsson K.H. "Carbonate-doped hydroxyapatite," J. Mater. Sci.: Mats in Med. 1, 182-4, (1990).

Norimatsu H.C., Vander Wiel C.J. and Talmage R.V., "Morphological support of a role for cells lining bone surfaces in maintanence of plasma calcium concentrations," Clinical Orthopaedics and Related Research 138, 254-262, (1978).

Occinero M.A. and Halloran J.W., " The influence of green density on sintering," in Mat. Sci. Res. 16 Sintering and Heterogeneous Catalysis, Ed. G.C. Kuczynski, A.E. Miller G.A. Gordon. Plenum Press N.Y. (1984).

Okazaki M., Moriwaki Y., Aoba T., Doi Y. and TakahashiJ., " Dissolution rate behavior of fluoridated apatite pellets," J. Dent. Res., 60, 1907-11 (1981).

Onsagar L., "Reciprocal relations in irreversible processes I.", Phy. Rev., 37 405-26 (1931).

Oonishi H., "Orthopaedic applications of hydroxyapatite," Biomaterials, 12, 171-8, (1991).

Osborn J.F., and Neweseley H., "The materials science of calcium phosphate ceramics", Bioceramics, 1, 108-11, (1980).

Packard R.Q., " Moisture stress in unfired ceramic clay bodies," J. Am. Ceram. Soc., 50 (5), 223-9 (1967).

Palmquist S., "Occurrance of crack formation during Vickers indentation as a measure of toughness of hard metals," Arch. Eisenhuettenwes, 33, 9, 629, (1962)

Parffit G.D., "Dispersion of powders in liquids, with special reference t: pigments", Elsevier Publishing Company Limited, London, (1969).

Parfitt A.M. "The quantitive approach to bone morphology: A critique of current methods and their interpretation. In: Clinical Aspects of Metabolic Bone Disease", Eds Parfitt A.M. and Duncan H., Exerpta Medica, Amsterdam, (1973).

Peelen J.G.J., Rejda B.V. and De Groot K., "Preparation and properties of sintered hydroxylapatite," Ceramurgia International, 4 (2), 71-4 (1976).

Perdikatsis B., "X-ray diffraction study of Francolite by the Reitveld method," Materials Science Forum, 78-82, 809-14, (1991).

Perloff A. and Posner A.S. "Preparation of pure hydroxyapatite crystals," Science, 124, 583 (1956).

Philipse A.P., Bonekamp B.C. and Veringa H.J.," Colloidal Filtration and (simaltaneous) sedimentation of alumina and silica suspensions:Influence of aggregates," J. Am. Ceram. Soc., 73 (9), 2720-7 (1990).

Portigliatti-Barbos M., Bianco P., Ascenzi A. and Boyde A., "Collagen orientation in compact bone II. Distribution of lamellae in the whole of the human femoral shaft with relation to its mechanical properties," Metabolic Bone Disease and Related Research, 5 309-15 (1984).

Posner A.S. and Betts F., "Synthetic amorphous calcium phosphate and Its relation to bone mineral structure," Bone Mineral Structure, Accounts of Chemical Research, 8, 273-81(1975).

Posner A.S. and Duyckaerts G., "Infrared study of the carbonate in bone, tooth and francolite," Experimentia, 10, 424-5 (1954).

Posner A.S., Perloff A and Dionio A.F., "Refined structure of hydroxyapatite," Acta Cryst., 11, 308-9 (1958).

Puajindanetr S. "Characterisation and sintering of precipitated hydroxyapatite" Ph.D.. Thesis, University of London, (1992).

Quadir T. and Readey D.W., " Microstructure development of ZnO in hydrogen," J. Am. Ceram. Soc. 72 (2), 297-302 (1989).

Rahaman M.N., De Jonghe L.C. and Chu Y., "Effect of green density on densification and creep during sintering," J. Am. Ceram. Soc., 74, (3), 514-9 (1991).

Randolph A.D. and Larson M.A., "Theory of particulate processes," Academic Press, New York, (1971).

Rao W.R. and Boehm R.F., "A study of sintered apatites," J. Dent. Res., 53 (6), 1351-4 (1974).

Ratnasmay P., "Electron spectroscopy of molybdenum sulphides," Indian J. Chem. 11, 695-7 (1973).

Ravaglioli A. and Krajewski A., "Bioceramics" Chapman & Hall.(1992).

Reilley D.T.and Burstein A.H., "The elastic and ultimate properties of compact bone tissue," J. Biomechanics, 8, 393 (1975).

Reilly D.T., Burstein A.H. and Frankel V.H. "The elastic modulus for bone," J. Biomechanics 7 271-275 (1974).

Reisner I. and Klee W.E., "Temperature dependence of the υ(OH), bands of hydroxyapatites," Spectrochimica Acta, 38A, 8, 899-902 (1992).

Reitveld H.M., "The structure of some alkaline earth metal uranate of the type M_3UO_6," Acta Cryst., 20, 508-13, (1966),

Rey C., Renugopalakrishnan V., Shimizu M., Collins B. and Glimcher M.J., "A resolution enhanced fourier transform infrared spectroscopic study of the environment of the CO_3^{2-} ion in the mineral phase of enamel during its formation and maturation," Calcif. Tiss. Int. 49, 259-268 (1991a).

Rey C., Renugopalakrishnan V., Shimizu M., Collins B. and Glimcher M.J., "Fourier transform infrared spectroscopic study of the carbonate ions in bone mineral during ageing," Calcif. Tiss. Int. 49, 251-8 (1991b).

Rhines F.N. and DeHoff R.T., in "Channel network decay in sintering," Sintering and Heterogeneous Catalysts, Vol. 16, 49-61,Ed Kuczynski G.C., Miller A.E. and Sargent G.A., Plenum Press, New York (1983).

Rice R. W., "Effect of Gaseous Impurities on the Hot Pressing and Behaviour of MgO, CaO and Al_2O_3 ," Proc. Br. Ceram. Soc., 12, 99 (1969).

Rice R.W., "CaO: I, Fabrication and Characterization, " J. Am. Ceram. Soc., 52 (8), 420-7, (1969).

Roberts J.P., Hutchings J. and Wheeler C., " Sintering and Diffusion Studies in Zinc Oxide," Trans. Brit. Ceram. Soc. 55 (1), 75-81(1956).

Robinson R. A. "An Electron Microscopic Study of the Crystalline Inorganic Matrix "J. Bone Joint Surg., 34, 389-435 (1952).

Robinson R. A., "Observations Regarding Compartments for Tracer Calcium in the Body," In: Bone Biodynamics ed Frost H. M. , Churchhills London, 423-9, (1964).

Romo L.A., "Synthesis of Carbonato-apatite" J. Am. Ceram. Soc., 76 3924-5 (1954).

Rootare H.M. and Craig R.G., "Characterization of hydroxyapatite powders and compacts at room temperature and after sintering at 1200°C," J. of Oral Rehabilitation, 5, 293-307 (1978).

Rootare H.M., Powers J.M. and Craig R.G., "Sintered hydroxyapatite ceramic for wear studies," J. Dent. Res., 57, (7-8), 777-83 (1978).

Royer A., Viguie J.C., Heughebaert M., and Heughebaert J.C., "Stoichiometry of hydroxyapatite: influence on the flexural strength," J. Mater. Sci.:Mats in Med., 4, 76-82 (1993).

Scherer G.W., "Physics of drying," in Ultrastructure Processing of Advanced Materials, Ed. D.R. Uhlmann and Ulrich D.R., Wiley, New York, 179-199, (1992).

Scherer G.W., "Drying gels: VIII. Revision and review," J. Non- Cryst. Solids, 109 171-82 (1989).

Schroeder H.E., "Formation and inhibition of dental calculi," Hans Huber Publishers Berne, Stuttgart, Vienna.(1969).

Sherman M.S., "The nerves of bone," J. Bone and Joint Surgery, 45A, 522-8, (1963).

Shi J.L., Goa J.H., Lin Z.X., and Yan D. S., "Effect of agglommerates in ZrO_2 powder compacts on microstructural development," J. Mater. Sci. 29, 342-8. (1993).

Shijo K., Makiyama T., Sugiura I. and Kondo K., "Clinical application of the hydroxyapatite implants," in Bioceramics 1, Ed. Oonishi H., Aoki H. and Sawai K., Ishiyaku EuroAmerica, Inc. Tokyo 124-32 (1989).

Shimoda S.,Aoba T., Moreno E.C. and Miake Y., "Effect of solution composition on morphological and structural features of carbonated calcium apatites," J. Dent. Res., 69, 1731-40 (1990).

Silverman S.R., Fuyat R.K. and Weiser J.D.,"Quantitative determination of calcite associated with carbonate-bearing apatites," Am. Mineral, 37, 211-2 (1952).

Simkins P.J., Johnson D.W., and Fleming D.A., "Drying behaviour of colloidal silica gels," J. Am. Ceram. Soc., 72 (10), 1816-21 (1989).

Simões L.P., Correia R.N. and Almeida M.M., "Slip casting of hydroxyapatite with differential porosity,"in Bioceramics Volume 4, Proceedings of the 4th International Symposium on Ceramics in Medicine, London, U.K., September (1991)., Ed. Bonfield W.,Hastings G.W. and Tanner K.E., Butterworth Heinemann Ltd (1991).

Slamovich E.B., and Lange F.F., "Densification of large pores: I, Experiments." J. Am. Ceram. Soc. 75 (9), 2498 - 508 (1992).

Smith C.J.E. and Hughes A.N., "The corrosion fatigue behaviour of a titanium 6 w/o aluminium - 6 w/o vanadium alloy, "Engineering in medicine," 7, 158-71 (1966).

Smith P.A., Kerch H., Krueger S., Long G.G., Keller J. and Haber R.A., "Pore sizes and filtration rates from two alumina slip," J. Am. Ceram. Soc., 77 (7)., 1777-82, (1994).

Solomon A.A. and F.Hsu, "Swelling and gas release in ZnO," J. Am. Ceram. Soc.,63 (7-8), 467-74 (1980).

Speckman T.W. and Norris W.P., "Bone crystallites as observed by use of the electron microscope," Science, 126, 753, (1957).

Spengler P.M., Morey E.R., Carter D.R., Turner R.T., Baylink D.J., "Effects of space flight on structural and material strength of growing bone," Proc.of Soc. for Experimental Biology and Medicine, 174, 224-228 (1983).

Sudre O. , Gang B., Fan B., Lange F.F., Evans A.G., "Effect of Inclusions on Densifications: II, Numerical Model." J. Am. Ceram. Soc., 75 (3), 525 - 31 (1992).

Sudre O. and Lange F.F., "Effect of inclusions on densification: I, microstructural development in an Al_2O_3 matrix containing a high volume fraction of ZrO_2 inclusions," J. Am. Ceram. Soc., 75 (3), 519 - 24 (1992).

Sudre O. and Lange F.F., "The effect of inclusions on densification: III, The desintering phenomenon," J. Am. Ceram. Soc., 75 (12), 3241-51 (1992).

Suwa Y., Banno H., Saito H., Doi Y., Koda T., Adachi M. and Moriwaki Y., "Sintering of carbonated hydroxyapatite," Bioceramics 6, Proceedings of the 6th International Symposium on Ceramics in Medicine, London, U.K., November (1993), Butterworth Heinemann Ltd, 381-6 (1993).

Tanahashi M., Kamiya K. Suzuki T. and Nasu H., "Fibrous hydroxyapatite grown in the gel system: effects of pH of the solution on the growth rate and morphology," J. Mater. Sci.: Mats in Med. 3, 48-53 (1992).

Thomas G. and Goringe M.J., "Transmission electron microscopy of materials," John Wiley and Sons., New York, (1979).

Thompson A.M. and Harmer M.P., "Deterioration of a classical final-stage microstructure: A study in alumina," J. Am. Ceram. Soc., 75 (4), 976-80 (1992).

Thompson A.M. and Harmer M.P., "Influence of atmosphere on the final stage sintering of ultra-high purity alumina," J. Am. Ceram. Soc., 76 (9), 2248-56 (1993).

Thomson W. D'Arcy "Bone growth and formation" Cam. Univ. Press, Cambridge (1942).

Tiller F.M. and Tsai C., "Theory of filtration of ceramics: I, Slip casting," J. Am. Ceram. Soc., 69 (12), 882-7 (1986).

Ting J.M., Lin R.Y. and Ko Y.H., "Effect of powder characteristics on microstructure and strength of sintered alumina," Ceramic Bulletin, 70 (7), 1167-72 (1991).

Trautz O.R., "Crystallographic studies of calcium carbonate phosphates," Ann. N.Y. Acad. Sci., 85, 145-60, (1960).

Trautz O.R., "X-ray diffraction of biological and synthetic apatites," Ann. N.Y. Acad. Sci., 60, 696-712 (1955).

Trombe J.C. and Montel G., "Some features of the incorporation of oxygen in different oxidation states in the apatite lattice I," J. Inorg. Nucl. Chem., 40 (1), 15-30 (1978).

Tromel G., "Untersuchingen Uber die Bildun eines Halogenfreien Apatits aus Basichen Calciumphosphaten" Z. Phys. Chem., 158, 422 (1932).

Tsai D.S. and Hsieh C.C., "Controlled gelation and sintering of monolithic gels prepared from y-alumina fume powder," J. Am. Ceram. Soc., 74 (4) 830-6 (1991).

Tucker M.O., "The growth of grain edge porosity in irradiated UO_2," J. Nucl. Mater., 79, 206 (1979).

Turner C.W., "Sol-gel process- principles and applications," Ceramic Bulletin, Vol 70, 9, 1487-90 (1991).

Uematsu K., Takagi M., Honda T., Uchida N., and Saito K., "Transparent hydroxyapatite prepared by hot isostatic pressing of filter cake" J. Am. Ceram. Soc., 72(8), 1476-8 (1989).

Varela J.A. Longo E., Pandolfelli V.C. and Santilli C.V., Ceramica 32 187 (1986).

Vaughan J., "The Physiology of Bone," Clarendon Press, Oxford (1981).

Vignoles C., "Contribution à l'étude de l'influence des ions alcalins sur la carbonation dans les sites de type B des apatites phosphocalciques," Thèse de 3ème cycle - Université paul Sabatier, Toulouse, France, (1973).

Vignoles C., "Contribution à l'étude de l'influence des ions alcalins sur la carbonation dans les sites de type B" Thèse, Toulouse, France, (1984).

Vignoles M., Bonel G. and Young R.A., "Occurrence of nitrogenous species in precipitated B type carbonated hydroxyapatites," Calcif. Tiss.. Int., 40, 64-70, (1987).

Vignoles M., Bonel G., Holcomb D.W. and Young R.A., "Influence of preparation conditions on the composition of type B carbonated hydroxyapatite and on the localisation of the carbonate ions." Calcif. Tiss. Int. 43, 33-40, (1988).

Vila F., Ventura O.N., Varela J.A. and Logo E., "An AM1 semiempirical study of the mechanism of sintering for ZnO in the presence of water and carbon dioxide" J. Molecular Structure (Thermochem), 305, 175-184, (1994).

Vincentelli R. and Evans F.G., "Relations among mechanical properties, collagen fibres and calcification in adult human cortical bone," J. Biomechanics, 18, 201-7, (1971).

Von Smoluchowski, in " Handbuch des electrizitat und des magnetismı Ed. Graetz X., Leipzig, Barth, 2, 366, (1914).

Von Weinmam P.P., Chem Revs 2, 217, (1925).

Wakai F., Kodama Y. and Sakaguchi S., "Superplasticity of hot isostatically pressed hydroxyapatite," J. Am. Ceram. Soc., 73, (2), 457-60, (1990).

Waldron M.B., Daniell B.L., "Sintering " Institution of Chemical Engineers Task Unit on Sintering, Monographs" in powder science and technology. Ed. Goldberg A.S., Heyden and Son, London, (1978).

Wallaeys R., "Etude d'une apatite carbonatée obtenue par synthèse dans l'état solide," in "Silicon, sulphur and phosphorus," IUPAC Colloquium, Weinheim, Verlag Chemie, 183-190, (1954).

Wang H.A. and Kröger F.A., "Pore formation during oxidative annealing of iron doped alumina and slowing of grain growth by precipitates and pores," J. Mater. Sci., 15, 1978, (1980).

Wang P.E. and Chaki T.K. "Sintering behaviour and mechanical properties of hydroxyapatite and dicalcium phosphate" J. Mater. Sci., 150-8, (1993).

Warman M.O. and Budworth B. W., "Residual gas effects on the sintering of alumina," Trans. Br. Ceram. Soc., 66, 265 (1967).

Weast R.C., Ed. "Handbook of chemistry and physics" forty seventh edition, The Chemical Rubber Company, Ohio, U.S.A, F56, (1966).

Weaver D. "The microscopic hardness of bone," J. Bone and Joint Surg., 42A(2), 273, (1966).

Weiner S. and Price P.A. "Disaggregation of bone into crystals," Calcif. Tiss. Int., 39, 365-75 (1986).

White L.R., "Capillary rise in powders," J. Colloid Interface Sci., 90 (2), 536-8, (1982).

Whittlemore O.J. and Varela J.A., "Initial sintering of MgO in several vapor pressures" in :Structure and properties of MgO and Al_2O_3 ceramics," in Advances in ceramics, Ed. Kingery W.D., 10, (1984).

Williams P.L. and Warwick R. Eds "Gray's Anatomy" Chap. 3, 36th edn., Churchill Livingstone (1980).

Wilson J., Pigott G.H., Schoen F.J. and Hench L.L., "Toxicology and biocompatability of bioglass" J. Biomed. Mater. Res., 15, 805, (1981).

Winter M., Griss P. and deGroot K., Tagai H., Heimke G., Vondijk H.J.A. and Sawai K., "Comparative histocompatability testing of seven calcium phosphate ceramics" Biomaterials, 2, 159-60, (1981).

Wroblewski B.M., "15-21 Year results of the Charnley low-friction arthroplasty," Clinical Orthopaedics and Related Research, 211, 30-5 (1986).

Wroblewski B.M., "Wear of high density polyethylene on bone and cartilage," J. Bone and Joint Surgery, 61B, 498-500, (1979).

Wu J.M. and Yeh T.S. "Sintering of hydroxylapatite-zirconia composites materials" J. Mat. Sci. 2, 3771-3777, (1988).

Wu S., Gilbart E. and Brook R.J., "Solid state sintering: the attainment of high density" in : structure and properties of MgO and Al_2O_3 ceramics, Ed. W.D. Kingery, advances in ceramics 10, 575-573, (1984).

Xue L.A. and Brook R.L., "Promotion of densification by grain growth," J. Am. Ceram. Soc., 72 (2), 341-4, (1989).

Yasumoto I., "Addition of water, ammonia and carbon dioxide on ZnO at elevated temperatures," J. Phys. Chem., 88, 4041-4 (1984).

Young R.A. and Elliot J.C., " Atomic scale properties of apatites," Archs. Oral Biol., 11, 699-707, (1966).

Young R.A. and Holcombe D.W., "Variability of hydroxyapatite preparations" Calcif. Tiss. Int., 34, S17-32, (1982).

Young R.A. and Holcombe D.W., "Thermal decomposition of human tooth enamel" Calcif. Tiss. Int., 31, 189-201, (1980).

Young R.A., Bartlett M.L., Spooner S. Mackie P.E. and Bonel G., "Reversible high temperature exchange of carbonate and hydroxyl ions in tooth enamel and synthetic hydroxyapatite" J. Biol. Phys., 9, 1-26, (1981).

Yubao L., Klein C.P.A.T., de Wijn J., Van de Meer S. and de Groot K., "Shape change and phase transformation of needle-like non-stoichiometric apatite crystals" J. Mater. Sci.: Mats. in Med., 5, 263-8 (1994).

Zarzycki J., Prassas M. and Phalippou, "Synthesis of glasses from gels: The problem of monolithic gels," J. Mater. Sci., 17, 3371-9 (1982).

Zhao J. and Harmer M.P., "Sintering kinetics for a model final stage microstructure: A study in Al_2O_3," Philos. Mag. Lett., 63 (1), 7 - 14 (1991).

APPENDICES

1a) Determination of oxygen partial pressure in carbon dioxide furnace atmospheres.

Consider the gaseous reaction:

$$CO_2 \text{-----} > \quad CO + 1/2\ O_2 \qquad \text{(A.1)}$$

The molar quantities being:

$$(1\text{-}x) \qquad x \qquad x/2 \qquad \text{(A.2)}$$

where x is the molar fraction of carbon dioxide reduced.

$\therefore$ At equilibrium the number of moles of each gas is:

CO_2	$(1\text{-}x)$
CO	x
O_2	$\left(\frac{x}{2}\right)$
N_T	$1+\frac{x}{2}$

where N_T is the total number of moles and,

$$_p(Z) = \frac{n(Z)}{(N_T)} P\,, \qquad \text{(A.3)}$$

where $_p(Z)$ is the partial pressure of a gaseous component Z, N(z) is the number of moles of component z and P the total pressure which is in this case 1 atm. The system is not of fixed volume therefore P is a constant:

$$K_1 = \frac{n(CO_2)(N_T)^{0.5}}{n(CO)[n(O_2)]^{0.5}} \qquad \text{(A.4)}$$

$$\Rightarrow \quad K_1 = \frac{(1\text{-}x)(1+\frac{x}{2})^{0.5}}{(x)(\frac{x}{2})^{0.5}} \qquad \text{(A.5)}$$

$$\Rightarrow \quad K_1^2 = \frac{(1\text{-}x)^2(1+\frac{x}{2})}{(x)^2(\frac{x}{2})} \qquad \text{(A.6)}$$

$$\Rightarrow \quad \left(\frac{K_1^2 - 1}{2}\right)x^3 + \frac{3x}{2} - 1 = 0 \qquad \text{(A.7)}$$

where K is the gaseous equilibrium constant.

Estimated values of x were used in the cubic relation, together with the calculated value of K in an Excel spreadsheet. By determining the value of x at which the cubic function changed sign for a given K_1 value, the equilibrium composition was calculated from the Equation (A.3).

1b) Determination of gas partial pressures in 'wet' carbon dioxide atmospheres.

Consider the reactions:

$$\underset{(0.97-x)}{CO_2} \text{-----} > \quad CO + 1/2\ O_2 \qquad \text{(A.8)}$$
$$\qquad\qquad\quad x \qquad x/2$$

$$\underset{(0.03-y)}{H_2O} \text{-----} > \quad H_2 + 1/2O_2 \qquad \text{(A.9)}$$
$$\qquad\qquad\quad y \qquad y/2$$

$\therefore$ At equilibrium the number of moles of each gas is:

$\mathbf{CO_2}$	$(0.97-x)$
$\mathbf{CO}$	x
$\mathbf{O_2}$	$\left(\frac{x+y}{2}\right)$
$\mathbf{H_2}$	y
$\mathbf{H_2O}$	$(0.03-y)$
$\mathbf{N_T}$	$1+\frac{x+y}{2}$

$$K_1 = \frac{n(CO_2)(N_T)^{0.5}}{n(CO)[n(O_2)]^{0.5}} \qquad \text{(A.10)}$$

$$K_2 = \frac{n(H_2O)\ (N_T)^{0.5}}{n(H_2)\ [n(O_2)\ ]^{0.5}} \qquad \text{(A.11)}$$

Dividing A.11 by A.10 gives:

$$K_3 = \frac{n(CO)\ n(H_2O)}{n(H_2)\ n(CO_2)} \qquad \text{(A.12)}$$

$$\therefore \quad K_1 = \frac{(0.97-x)\left(1+\frac{x+y}{2}\right)^{0.5}}{(x)\left(\frac{x+y}{2}\right)^{0.5}} \qquad (A.13)$$

$$K_3 = \frac{(x)(0.03-y)}{(y)(0.97-x)} \qquad (A.14)$$

(by substituting A.8 and A.9.)

x was solved for estimated values of y in A.14 and these values of x and y were substituted in the expression for K_1, until the value obtained equalled the equilibrium constant determined from thermodynamic relations. This was done using an Excel spreadsheet. By using the equilibrium values of x and y at a particular temperature, the partial pressures of each component could be determined in a similar manner to that of the dry atmosphere, (Appendix 1a).

2 Calculation of theoretical density of hydroxyapatite.

Relative atomic weight of unit cell is:
(10 x 40.08)+(6 x 30.97376) + (24 x 15.9994) + (2 x 17.0073) = 1004.6428

$$\text{Mass: } = \frac{\text{R.A.M.}}{6.03 \times 10^{23}} = 1.666 \times 10^{-24} \text{ kg}$$

From JCPDS(1980) data, **a** = 942.3 pm, **c** = 687.5pm

$$\text{Unit cell volume} = \frac{\sqrt{3}}{2} \mathbf{a}^2 \times \mathbf{c} = 5.286 \times 10^{-28} \text{ m}^3.$$

$$\therefore \quad \text{Density} = \frac{\text{mass}}{\text{volume}} = 3.151 \text{ Mgm}^{-3}.$$

Note that the density of a B type hydroxyapatite is expected to be less than this, although it is hard to estimate by how much as the exact substitution mechanism is not known.

APPENDICES

1a) Determination of oxygen partial pressure in carbon dioxide furnace atmospheres.

Consider the gaseous reaction:

$$CO_2 \text{-----}> \quad CO + 1/2\ O_2 \qquad \text{(A.1)}$$

The molar quantities being:

$$(1\text{-}x) \qquad x \qquad x/2 \qquad \text{(A.2)}$$

where x is the molar fraction of carbon dioxide reduced.

$\therefore$ At equilibrium the number of moles of each gas is:

CO_2	$(1\text{-}x)$
CO	x
O_2	$\left(\frac{x}{2}\right)$
N_T	$1+\frac{x}{2}$

where N_T is the total number of moles and,

$$p(Z) = \frac{n(Z)}{(N_T)} P, \qquad \text{(A.3)}$$

where $p(Z)$ is the partial pressure of a gaseous component Z, N(z) is the number of moles of component z and P the total pressure which is in this case 1 atm. The system is not of fixed volume therefore P is a constant:

$$K_1 = \frac{n(CO_2)(N_T)^{0.5}}{n(CO)[n(O_2)]^{0.5}} \qquad \text{(A.4)}$$

$$\Rightarrow \quad K_1 = \frac{(1\text{-}x)(1+\frac{x}{2})^{0.5}}{(x)(\frac{x}{2})^{0.5}} \qquad \text{(A.5)}$$

$$\Rightarrow \quad K_1^2 = \frac{(1\text{-}x)^2(1+\frac{x}{2})}{(x)^2(\frac{x}{2})} \qquad \text{(A.6)}$$

$$\Rightarrow \quad \left(\frac{K_1^2 - 1}{2}\right)x^3 + \frac{3x}{2} - 1 = 0 \qquad \text{(A.7)}$$

where K is the gaseous equilibrium constant.

Estimated values of x were used in the cubic relation, together with the calculated value of K in an Excel spreadsheet. By determining the value of x at which the cubic function changed sign for a given K_1 value, the equilibrium composition was calculated from the Equation (A.3).

1b) Determination of gas partial pressures in 'wet' carbon dioxide atmospheres.

Consider the reactions:

$$\underset{(0.97-x)}{CO_2} \text{-----} > \quad CO + 1/2\, O_2 \qquad \text{(A.8)}$$
$$\qquad\qquad\quad x \qquad x/2$$

$$\underset{(0.03-y)}{H_2O} \text{-----} > \quad H_2 + 1/2 O_2 \qquad \text{(A.9)}$$
$$\qquad\qquad\quad y \qquad y/2$$

$\therefore$ At equilibrium the number of moles of each gas is:

CO_2	$(0.97-x)$
CO	x
O_2	$\left(\frac{x+y}{2}\right)$
H_2	y
H_2O	$(0.03-y)$
N_T	$1+\frac{x+y}{2}$

$$K_1 = \frac{n(CO_2)(N_T)^{0.5}}{n(CO)[n(O_2)]^{0.5}} \qquad \text{(A.10)}$$

$$K_2 = \frac{n(H_2O)\,(N_T)^{0.5}}{n(H_2)\,[n(O_2)\,]^{0.5}} \qquad \text{(A.11)}$$

Dividing A.11 by A.10 gives:

$$K_3 = \frac{n(CO)\,n(H_2O)}{n(H_2)\,n(CO_2)} \qquad \text{(A.12)}$$

$$\therefore \quad K_1 = \frac{(0.97-x)\left(1+\frac{x+y}{2}\right)^{0.5}}{(x)\left(\frac{x+y}{2}\right)^{0.5}} \qquad (A.13)$$

$$K_3 = \frac{(x)(0.03-y)}{(y)(0.97-x)} \qquad (A.14)$$

(by substituting A.8 and A.9.)

x was solved for estimated values of y in A.14 and these values of x and y were substituted in the expression for K_1, until the value obtained equalled the equilibrium constant determined from thermodynamic relations. This was done using an Excel spreadsheet. By using the equilibrium values of x and y at a particular temperature, the partial pressures of each component could be determined in a similar manner to that of the dry atmosphere, (Appendix 1a).

2 Calculation of theoretical density of hydroxyapatite.

Relative atomic weight of unit cell is:
(10 x 40.08)+(6 x 30.97376) + (24 x 15.9994) + (2 x 17.0073) = 1004.6428

$$\text{Mass: } = \frac{\text{R.A.M.}}{6.03 \times 10^{23}} = 1.666 \times 10^{-24} \text{ kg}$$

From JCPDS(1980) data, **a** = 942.3 pm, **c** = 687.5pm

$$\text{Unit cell volume} = \frac{\sqrt{3}}{2} \mathbf{a}^2 \times \mathbf{c} = 5.286 \times 10^{-28} \text{ m}^3.$$

$$\therefore \quad \text{Density} = \frac{\text{mass}}{\text{volume}} = 3.151 \text{ Mgm}^{-3}.$$

Note that the density of a B type hydroxyapatite is expected to be less than this, although it is hard to estimate by how much as the exact substitution mechanism is not known.